Transactions

of the

ASME

APRIL, 1948

VOL. 70, NO. 3

Transactions

of The American Society of Mechanical Engineers

Published on the tenth of every month, except March, June, September, and December

---

Published monthly by The American Society of Mechanical Engineers. Publication office at 20th and Northampton Streets, Easton, Pa. The editorial department is located at the headquarters of the Society, 29 West Thirty-Ninth Street, New York 18, N. Y. Cable address, "Dynamic," New York. Price $1.50 a copy, $12.00 a year; to members and affiliates, $1.00 a copy, $6.00 a year. Changes of address must be received at Society headquarters three weeks before they are to be effective on the mailing list. Please send old as well as new address. . . . By-Law: The Society shall not be responsible for statements or opinions advanced in papers or . . . printed in its publications (B13, Par. 4). . . . Entered as second-class matter March 2, 1928, at the Post Office at Easton, Pa., under the Act of August 24, 1912. . . .

The Influence of Reaction Interface Extension in the Combustion of Gaseous Fuel Constituents

By W. J. WOHLENBERG,[1] NEW HAVEN, CONN.

A burning mixture is in general composed of zones, alled concentration zones, differentiated with respect o their surroundings by differences in concentrations of he several kinds of molecules present in the mixture. ome of these zones are rich in fuel molecules and others n oxygen molecules. This results in diffusion of oxygen nd fuel molecules each from its own concentration zone oward a concentration zone of the other. At the inter- one between the two, fuel and oxygen molecules collide ith each other in such numbers per unit volume that igorous combustion ensues, provided that the tempera- ure is well above the ignition point.

The essential geometrical characteristics of this sys- em to which the energy release rate per unit volume of he mixture is proportional for a given set of conditions therwise, is the extent of the interzone per unit volume f the mixture. It is shown that the extent factor, in his sense, of the interzone is the area of an imaginary nterface within the interzone per unit volume of the ixture.

The foregoing proportionality between extent of reac- on interface and reaction rate per unit of volume applies henever the concentration zones are large compared to olecular dimensions and this proportionality holds nder these conditions independently of the mechanism f the processes by which the fuel and oxygen molecules pproach the interface for a given set of conditions such s pressure, temperature, and composition. The concept f reaction interface extension thus appears to be of a ndamental nature with respect to reaction rate and ombustion progress.

It is shown that inclusion of the co-ordinate reaction nterface extension has an influence on the magnitude f the pressure and temperature effects on the reaction te for compressible mixtures. This follows because the extension of interface in a unit of volume depends, among other things, on the density of the mixture. It is found also that a large part of the macroscopic effects of turbulence on the reaction rate may be accounted for by the increase in reaction interface extension which results because of turbulence. A large part of the effect of eddy diffusion on the reaction rate is thus accounted for in the present analysis by the increase in reaction interface extension which results because of turbulence.

The paper contains the reaction-rate and combustion-progress equations which result when reaction interface extension is included as one of the co-ordinates on which the rate of the reaction per unit volume of the mixture depends. One set of these equations is based on the frequency of effective collisions between fuel and oxygen molecules per unit area of reaction interface. The reaction rate per unit volume of the mixture is the product of the foregoing, times the interface extension per unit volume of the mixture. The combustion-progress equation results by integration of the rate equation over an interval of combustion progress.

The foregoing equations are applied to a mixture containing natural gas as the fuel and with varying air-fuel ratios. The results are shown in both tabular and graphical form.

The equations permit also establishment of the order of magnitude of the maximum possible mean energy release rates over a given combustion progress. These maxima should occur when the molecular distribution in the mixture is uniform. It is shown that with natural gas as the fuel, when burned with 1.2 times theoretical air to within 99 per cent of completion, at one atmosphere furnace pressure, this average maximum over this combustion progress is of the order of 2×10^6 Btu per hour per cu ft of furnace volume.

Nomenclature

The following nomenclature is used in the paper:

Subscripts:

- 1 = fuel (except with φ)
- 2 = oxygen (except with φ)
- A = as subscript = per unit of interface area
- D = as subscript indicates thermal diffusion
- e = entrance plane after initial turbulence
- i = initial conditions
- m = mean conditions; also molecular weight
- o = standard conditions
- r = only in l_r; defined later
- v = partial volume
- χ = interzone

Conditions and co-ordinates (English letters):

- A = extent of reaction interface (ft^2/ft^3)
- $A/1$ = volume diffusance factor
- C = concentration
- D = coefficient of thermal diffusion, $ft^2/sec = \mu/\rho$
- E = energy of activation per lb mole
- f = fraction combustible in fuel gas by volume
- F = collision frequency
- ΔH_{12} = energy release per effective molecular collision

[1] Professor of Mechanical Engineering, Yale School of Engineering, le University. Fellow and Past Vice-President, ASME.

Contributed by the Fuels Division and presented at the Annual eeting, Atlantic City, N. J., December 1–5, 1947, of The American ciety of Mechanical Engineers.

Note: Statements and opinions advanced in papers are to be derstood as individual expressions of their authors and not those the Society. Paper No. 47—A-27.

dH = differential of energy released in reaction, Btu/ft^3
$(dH/d\theta)$ = energy release rate, Btu/(ft^3 × sec), based on effective collision rate
$(dH/d\theta)_D$ = energy release rate, Btu/(ft^3 × sec), based on diffusion rate of oxygen
$(dH/d\theta)_A$ = energy release rate by effective collisions in interzone, Btu/(ft^2 × sec), based on effective collision rate
$(dH/d\theta)_{AD}$ = energy release rate, Btu/(ft^2 × sec), based on diffusion rate of oxygen
k = thermal conductivity of gas, Btu/(ft^2 × sec × deg/ft)
l = distance from interface through thermal diffusion layer
l_D = effective thickness of thermal diffusion layer
$2l_X$ = depth of interzone
$2l_r$ = total normal spacing of interface planes
m = molecular weight
n = number of mean free molecular path lengths
n' = temperature exponent on coefficient of diffusion
n_2 = volume of oxygen required per cu ft of combustible in fuel gas; also number of effective collisions required with oxygen molecules per fuel molecule
N = theoretical air/fuel as supplied
$N_f = N/f$
N_o = Avogadro's number = 2.705 × 10^{19} molecules/cm^3
$N_o' = N_o \times (\text{cm}^3/\text{ft}^3) = 7.65 \times 10^{23}$ molecules/ft^3
P = pressure
Pr = Prandtl number
p = probability fraction (see Equation [1])
Q = calorific content of fuel gas, Btu/ft^3
$Q_{of} = Q_o/f$
q = calorific content of gas mixture, Btu/ft^3
R = universal gas constant per mole = 1.985
Re = Reynolds number
T = temperature, deg R. Without subscript is mean across $2l_r$; otherwise as indicated by subscript
V = volume, cu ft
ΔV = difference in volume between products resulting from complete combustion and fuel-gas plus oxygen entering to form products, expressed as fraction of entering volume of combustible in fuel gas (see Equation [36])
x = fraction burned
$X = \Theta$, see Equations [13] and [11a]
$X_D = \Theta_D$, see Equations [30c] and [30e]
y = actual air/theoretical air
Y = see Equations [10] and [10a]
Z = see Equations [10] and [10b]

Conditions and Co-ordinates (Greek letters):

α = absorptivity of gas contained in one ft^3
$\beta = 1/f(\beta + x \cdot f \cdot \Delta V)$
$\beta_f = (yN_f + 1) = (yN/f + 1)$
$\beta_o = (yN + 1)$
$\gamma = m_1/m_2$
ϵ = emissivity of gas contained in 1 cu ft
$\zeta = l_X/l$ = interzone depth ratio
η = see Equation [9a]
θ = time, sec
$\Theta = X$, see Equations [11a] and [13]
$\Theta_D = X_D$, see Equations [30e] and [30c]
λ = molecular mean free path length
μ = coefficient of viscosity, lb/sec × ft
$\bar{\mu}$ = transfer fraction of released energy
$\bar{\mu}_m$ = fraction released energy absorbed at furnace walls
$\xi = l/l_r$ = interior turbulence space factor
ρ = density, lb/ft^3
φ = function
φ_X = interzone concentration ratio
$\chi = C_{xvD}/C_v = (C_{xv}/C_v)\varphi_X = 1.00$ = concentration ratio
$\psi = A \cdot (2l_X)\chi^2\varphi_X = \zeta\chi^2\xi\varphi_X$ (Dimensionless, see Equation [10g])
$\psi_D = (A_o/l_{oD})\ (1 - \chi)\xi$ Dimension = L^{-2} (see Equation [30f])

Introduction

The theory of the combustion progress for small flames, such, for example, as the Bunsen burner, is included in Jost (6)[2] and in Lewis and von Elbe (10). Inaerated flames have been investigated by Burke and Schumann (1) and the results reported based upon a diffusion mechanism. In the foregoing references the geometry of the flow pattern may be fairly well defined in advance, since turbulence takes no appreciable part in mixing of the constituents. Rummel (2) employs experimental research in the investigation of combustion progress for a series of burner and furnace models. These experiments include the influence of turbulence on the mixing for different cases.

The results represent the influence of an air factor (actual/theoretical air) on the shape and size of the volume occupied by a mixture within which combustion is occurring. This volume is shown as divided into air-rich and fuel-rich zones, the configuration of which is determined by the relation to each other of the air and fuel passages leading to the combustion space. The zones are thus air and fuel zones and the space between them is the reaction zone.

The reported results include correlations between certain of the experimental factors and are, in general, very illuminating, being well worthy of study by anyone interested in the combustion process which occurs in an air-gas mixture following its discharge into the furnace cavity or combustion space. Rummel's experiments were conducted at a constant pressure of 1 atm. A brief review of both Rummel (2) and Burke and Schumann (1) is contained in Jost (6). A more extensive review of Burke and Schumann is contained in Lewis and von Elbe (10).

In its most general aspects the mixture investigated by Rummel may be considered as made up simply of zones, hereafter called concentration zones, differentiated with respect to their surroundings by differences in concentrations of the several kinds of molecules present in the mixture. Some of these zones are high in concentrations of fuel molecules and others in oxygen molecules. These conditions result in diffusion of oxygen and fuel molecules each from its own concentration zone toward a concentration zone of the other. At the interzone between the two, fuel and oxygen molecules come in contact in such proportions per unit of volume that vigorous combustion ensues, provided the temperature is well above the ignition point.

The essential geometrical characteristics of the foregoing system to which the energy release rate per unit volume will be proportional, for any given set of conditions otherwise, is the extent of the reaction interzone per unit of volume of the mixture. In arriving at the proper dimensions of this extent it is first noted that the volume occupied by the interzone may be considered as the product of its spread normal to the direction of diffusion into it from the concentration zones adjacent to it and a thickness or depth factor in the direction of diffusion. The magnitude of the depth of the interzone is then that portion of the molecular journey from concentration zone into interzone during which those molecular collisions occur which result in

[2] Numbers in parentheses refer to the Bibliography at the end of the paper.

reaction. This depth factor is not an extent factor of the zone. Instead it is merely an extension of the molecular transfer path from the concentration zone into the reaction zone. Whatever distance a molecule travels into the interzone before it finally reacts, the amount of energy released per reacting molecule will be the same for a given final product molecule. It follows that the depth of the interzone is not an extent factor of this zone, since the latter is proportional to the energy release rate per unit of volume. The spread alone is such a factor, and this may be thought of as a potential reaction interface between concentration zones. It is thus an area which is represented henceforth by the letter A. It has the following dimensions: Square feet of reaction interface per unit volume of the mixture, i.e. (ft^2/ft^3), and is therefore in one sense the density of the reaction interface in the mixture.

In particular it should be noted that the proportionality between energy release rate per unit of volume and A is independent of the mechanism which controls the reaction rate per unit area of the interface. Hence for any conditions which make it possible to specify the magnitude of A the foregoing statement holds. But in the limiting case of a uniform mixture the concentration zones themselves cease to have any meaning and so A itself becomes meaningless. It follows that the extent A of interface is a co-ordinate of the reaction to which energy release rate per unit volume is proportional so long as the state of mixture contains concentration zones which are large compared to molecular dimensions. Under such conditions the proportionality between energy release rate and extent of A exists.

It will be shown later that the introduction of this concept carries with it important implications as to the influence of pressure, temperature, and turbulence on the reaction rate, and provides for a closer evaluation of the distribution of the released energy. Since the concept expresses the effect on energy release rate of the configurations of concentration zones independently of their detailed geometry, then application of experimental results in equations including the concept specifically

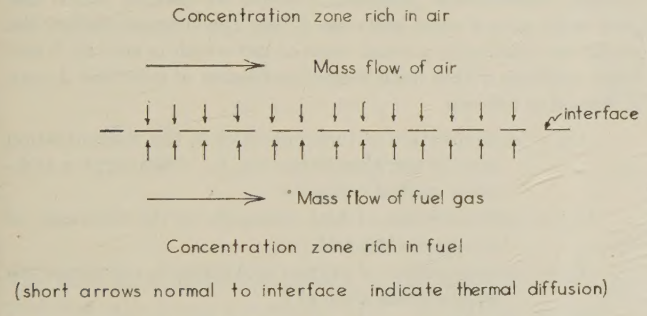

FIG. 1 INTERFACE IN LAMINAR FLOW

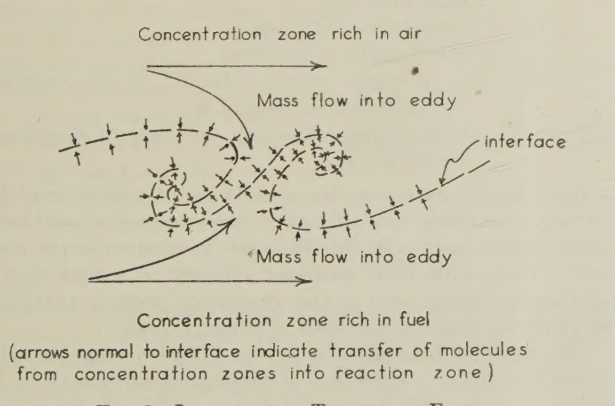

FIG. 2 INTERFACE IN TURBULENT FLOW

lead directly to its magnitude for the given experimental conditions. This is important because it is difficult to see how any reliable definition as to the detailed geometry of these zones may be prescribed when initial turbulence is high.

In order to visualize the effects of turbulence in such respects more fully, refer to Figs. 1 and 2. Comparing the interface extensions in these figures, it is seen that when eddies impinge on the interzone their envelopes or boundaries serve as an extension of the potential reaction interface. At the same time the required distance of travel between concentration zone and interface is diminished to the very short distance from the interior of the eddy to its boundaries for those molecules contained within the volume of the impinging eddy currents. The macroscopic effect of turbulence near the interface, on the energy release rate, is thus accounted for, in a large measure at least, by the increase in A and decrease in l previously noted, or to put it otherwise, turbulence may be considered as a source of increasing the value of the ratio A/l. This at least in part accounts also for the effects of the so-called eddy diffusion (7, 8) which is directed toward the reaction interface. If the decrease in concentration through the thermal diffusion zone bounding the interface is large compared to the decrease in concentration of interior eddy diffusion paths which terminate at the outer boundary of the thermal diffusion layer then the effects of eddy diffusion are almost wholly accounted for by the equations to be stated later. Since eddy diffusion is at the expense of kinetic energy and thus has no direct effect on concentrations, the error involved, because of the omission mentioned, should have but a negligible effect as to the correctness of the form of the resulting equations.

MECHANISM WHICH GOVERNS MOLECULAR MOTIONS AS MOLECULES APPROACH INTERZONE

In order to investigate this question consider first the factors on which the depth of the interzone depends. Under ideal reaction conditions, when every collision between fuel and oxygen molecules results in chemical union of the two, the magnitude of this depth is very small and particularly so if the fuel itself is a solid. This follows from the fact that the fraction p of the total molecules in space about a given fixed point which have their next collisions with that point is represented by the equation

$$p = 1 - e^{-n} \quad \ldots\ldots\ldots\ldots\ldots\ldots [1]$$

Here n is the number of molecular free path lengths λ in the distance $n\lambda$ extending from the point. Referring to Table 1, it is seen that with $n = 5$, fraction p has already increased to 0.99 and so only 1 per cent of those molecules beyond 5λ have their next collisions at this point. Hence 5λ is the collision range for 99 per cent of the total molecules, and so if the fixed point is on the

TABLE 1 VALUES OF p

n	p		n	p	
1	0.63		6	0.997	
2	0.86	Collision	7	0.999	Diffusion
3	0.95	Range	8	0.9997	Range
4	0.98		9	0.9999	
5	0.99		10	0.99995	
			⋮		
			n	0.999999	

surface of a solid fuel then $5\ \lambda$ is the order of magnitude of the depth of the interzone. But λ is of the order of magnitude of 10^{-7} ft, and so the interzone itself has in such cases a depth of less than 10^{-6} ft.

However, the fraction of collisions between oxygen and fuel molecules which result in reaction is exceedingly small (of the order of 10^{-5}) at 3700 R and if the fuel as well as the oxygen is gaseous, then at lower and lower concentration as combustion progresses there will be fewer and fewer molecules of each near an imaginary interface between two concentration zones, one

initially of 100 per cent air and the other initially of fuel molecules. As a result of all of these conditions, the depth of the interzone in a totally gaseous system may be quite large compared to that which might exist at the surface of a burning solid fuel. But it still remains true that wherever an effective collision occurs there will be a sudden reduction of concentration of oxygen and fuel molecules, and this tends to induce thermal diffusion from the surrounding region.

Inspection of Table 1 indicates that the inner boundary of a diffusion layer extends to within 6 to 5 λ of an effective collision. It follows that even if eddies should succeed in penetrating to within, say, 10 or 15 λ of the collision point there would still be a diffusion layer of from 5 to 10 λ in thickness. Available evidence (8) indicates definitely that the scale of turbulence which could result under feasible furnace conditions would be very large compared to 10 λ. It follows that the chance of having furnace turbulence toss molecules directly into the interzone by complete elimination of the thermal diffusion layer is so small as to be negligible. But the layer which is left by turbulence may still be so thin that a very small difference in concentration between that of the concentration and interzone is sufficient to meet the demands of the effective collision rate in the interzone. Under such conditions, activities of the interzone mechanism take over primary control of the reaction rate, and the activities of the thermal diffusion mechanism merely follow along.

Influence of Turbulence and Time on Value of A/l in a Mixture Free of Chemical Reaction

Since the extension A of potential reaction interzone in a volume element is affected so strongly by turbulence, the value of A at any point in space and time depends upon the history of the turbulence to which the volume element has been submitted as well as upon the initial interzone extension within the element. If the volume element is left to itself as in a self-acting process, then A will increase in value. This follows because increase of A implies passing from a less to a more uniform state as to molecular distribution. Hence A, like entropy, always increases with time in a self-acting process.

All three, turbulence, forces of the chemical reaction, and gravity are superimposed on whatever self-acting characteristics the mixing process possesses. But gravity is insignificant compared to the other two and so may be neglected. The influence of the chemical reaction in such respects will be discussed later.

With respect to turbulence and time effects alone, the truth of the following statements should now be fairly obvious:

1 The principal extension of A occurs as the mixture passes through the initial turbulent zone unless subsequent augmentation of tubulence is present.

2 This extension tends to increase even after the initial turbulence dies down. However, as will be seen later, the influences of the chemical-reaction progress are opposite.

3 The normal distance between interface layer varies inversely with A. Hence the change in A/l is proportional to the square in the change of A except for the effects of interior turbulence to be explained later.

Variation of A/l With Change of Pressure and Temperature of Mixture

If the density ρ of the mixture varies, this alone will result in a change of the interface extension A. Thus if A_o represents the value of A when referred to standard pressure and temperature P_o and T_o, respectively, then

$$A = A_o(\rho/\rho_o)^{1/3} = A_o(P/P_o)^{1/3}(T_o/T)^{1/3} \quad \ldots\ldots [2]$$

This follows because the surface-volume ratio of a concentration zone of any shape whatever varies directly with the $^1/_3$ power of the density of its contents. Then assuming the contents to be perfect gases leads to Equation [2]. Thus is seen how introduction of the concept A introduces a portion of the net values of the exponents which are attached to the pressure and temperature co-ordinates in the final equations of the combustion process.

The companion equation to Equation [2] but with respect to the depth factor, l, is

$$l = l_o(\rho_o/\rho)^{1/3} = l_o(P_o/P)^{1/3}(T/T_o)^{1/3} \quad \ldots\ldots [3]$$

This follows because this depth factor, which is approximated by a volume-surface ratio (the inverse of surface-volume ratio employed for A) of a concentration zone of any shape whatever, varies inversely with the $^1/_3$ power of the density of the contents of the zone. Then assuming such contents to be perfect gases leads to Equation [3].

It follows from Equations [1] and [2]

$$A/l = A_o/l_o(P/P_o)^{2/3}\ (T_o/T)^{2/3} \quad \ldots\ldots [4]$$

It should be noted that Equations [2] and [3] and hence also Equation [4] are each true even when the concentration zones are not completely bounded by reaction interface, since, in the development leading to the equations, any arbitrary relation may be inserted between the surface and volume of the concentration zone. Therefore a reduction of the extent of the interface bounding a given concentration zone increases the effective depth of this zone with respect to that interface.

Energy-Release-Rate Equation for Steady State of Firing

Under these conditions the reaction rate has a steady time mean value at any point along the combustion progress curve even through it fluctuates in time about this mean. This time mean rate varies from point to point along the combustion progress curve, rising at first during the heating-up period as the temperature increases and passes through the so-called ignition point, and then falling rapidly as the concentrations of combustible constituents decrease. Hence at time θ, when the gases have passed some distance L into the furnace cavity, the conditions existing in a small mass of gas which is now at L and which contains within itself a small extension of interface A may be defined as follows:

C_{1v} = concentration of fuel molecules in the concentration zone of the mass when at L. (Subscript v indicates partial volume)

C_{1x_v} = concentration of fuel molecules in the interzone of the mass when at L

C_{2v} = concentration of oxygen molecules in concentration zone of mass when at L

C_{2x_v} = concentration of oxygen molecules in interzone of mass when at L

Tx = temperature of interzone

l_x = one-half depth of interzone

$dH/d\theta$ = rate of energy release (Btu/ft^3 $\times$ sec) occurring from within mass when at L

$(dH/d\theta)_A$ = rate of energy release per unit area of interface in mass when at L

For a steady state, the rate of diffusion of oxygen or of fuel through a boundary layer adjacent to the interzone is equal to the rate at which such molecules disappear in reaction in the interzone. Then with both processes referred to a unit area of interface at a given point on the combustion progress path $(dH/d\theta)_A$ may be stated on the basis of either process.

The concentration gradient in the diffusion equation when stated in terms of a difference of concentrations divided by the length l_D of the diffusion path becomes $(C_v - C_{x_v})/l_D$. Here

$(C_v - C_{xv})$ is the drop in concentration through a thermal diffusion layer of thickness l_D. Concentration C_v is a function of the combustion progress only for a given set of initial conditions but concentration C_{xv} depends upon both C_v and the condition in the interzone. It follows that unless C_{xv} is negligible compared to C_v then the diffusion equation by itself is insufficient to represent properly the energy release rate per unit of interface. Investigation shows that C_{xv} is not a negligible term. Therefore use of the interzone equation is not avoided by basing the energy-release-rate formulas upon the rate of diffusion through the diffusion layer. In view of this, the interzone branch of the equilibrium equation (diffusion rate through boundary layer = rate of disappearance of molecules by reaction in interzone) is taken as a starting point in this development.

The energy release rate in the interzone volume per unit area of interface is proportional to the frequency of effective collisions there between fuel and oxygen molecules. On this basis

$$(dH/d\theta)_A = \Delta H_{12} \cdot (2l_\chi)\ (F_{12}) \cdot (e^{-E/RT_\chi})\ \text{Btu/ft}^2 \times \text{sec} \quad [5]$$

Here ΔH_{12} is the energy released per effective collision and $2l_\chi$ is the volume of interzone per unit area of interface A. Factor F_{12} represents the collision frequency per unit volume of the interzone, and the last term on the right is the fraction of these which are effective in reaction. In it E is the energy of activation per mole and R is the universal gas constant per mole.

The equation for the collision frequency F_{12}, as developed by Jeans (3) will be found in the Appendix. This leads, as there shown, to the equation

$$F_{12} = 26.8 \times 10^{31}\, C_{1\chi v} \cdot C_{2\chi_v} \cdot (P/P_o)^2 (T_o/T)^2 \sqrt{\frac{T_\chi\,(\gamma+1)}{\gamma}} \quad [6]$$

where F_{12} is the collision frequency per cu ft.

Concentration product $C_{1\chi v} \cdot C_{2\chi v}$ is a mean of values of the product for the total depth through the interzone. Let $C_{1\chi vD}$ and $C_{2\chi vD}$ represent the concentrations where the interzone meets the diffusion boundary layer. Also let

$$\left.\begin{aligned} C_{1\chi vD} &= \chi_1 C_{1v} \\ C_{2\chi vD} &= \chi_2 C_{2v} \end{aligned}\right\} \quad [6a]$$

$$\varphi_\chi = \frac{C_{1\chi v} \cdot C_{2\chi v}}{C_{1\chi vD} \cdot C_{2\chi vD}} \quad [6b]$$

$$\chi = \sqrt{\chi_1 \cdot \chi_2} \quad [6c]$$

The ratio φ_χ is introduced merely to call attention to the fact that this ratio is not necessarily unity. It approaches unity as a limit. Establishment of the exact form of this function would require an extended analysis. Presumably the concentrations of either fuel or oxygen molecules are near zero at the boundary of this zone opposite that at which either enters. Then, since even at high temperatures only 1 in about 10^5 collisions between fuel and oxygen molecules is effective, it appears as though the decrease in concentration of each with distance traveled across the interzone might vary with this distance in practically the same way as it does in the case of thermal diffusion through a boundary layer. If this should be true then

$$\varphi_\chi \cong 0.5 \times 0.5 = 0.25$$

However, a high rate of energy release within the interzone may disturb the thermal equilibrium necessary for existence of the concentration gradients of diffusion to such an extent that any conclusions based on the assumption of their existence are far from the real facts in the case. If, for example, the reaction induces turbulence within the interzone itself of such an intensity that the rate of distribution of oxygen and fuel molecules within this zone is so high as to eliminate completely the existence of any concentration gradients as to these constituents, then in the limit $C_{xv} = C_{xvD}$ and φ_χ = unity. It appears therefore as though the true value of φ_χ must lie between 0.25 and 1.00. In the present discussion its value will be considered as unity where a specific value must be assigned to it and so the results based on this are limiting values. It is of course dimensionless and so its value should not be affected by variations in the density of the mixture alone. The function φ_χ is henceforth designated as the interzone concentration ratio.

Expressions representing C_{v1} and C_{v2} in terms of the combustion progress are developed in the Appendix with the following results

$$\left.\begin{aligned} C_{1v} &= (1-x)/\beta \\ C_{2v} &= 0.21 N_f (y-x)/\beta \end{aligned}\right\} \quad [6d]$$

where

x = fraction burned
y = actual air/theoretical air
N = theoretical air/fuel as supplied = ft³/ft³
N_f = N/f
f = fraction of combustible in fuel gas by volume
β = $1/f(\beta_o + x \cdot f \cdot \Delta V)$
β_0 = $yN + 1$
ΔV = volume change in reaction referred to volume of entering combustible in fuel gas; see Equation [36]

The energy ΔH_{12}, which is that released per effective collision, may be stated as

$$\Delta H_{12} = Q_{of}/n_2 \cdot N_o' \quad [7]$$

Here Q_{of} is the calorific content, Btu per cu ft, of the combustible portion of the fuel gas when referred to standard conditions, and n_2 the number of effective contacts required by the fuel molecule with oxygen molecules in order to complete the reaction; or n_2 is the number of oxygen molecules required per average fuel molecule.

Noting that

$$N_o' = 7.65 \times 10^{23} \text{ molecules per cu ft} \quad [8]$$

and then substituting relations now available in Equation [5] results in

$$(dH/d\theta)_A = 0.21\,(N_f/n_2) Q_{of} \cdot 2l_\chi \cdot \chi^2 \cdot \varphi_\chi \cdot \eta \cdot \frac{(1-x)\,(y-x)}{\beta^2} \quad [9]$$

where

$$\eta = 0.35 \times 10^9\,(P/P_o)^2\,(T_o/T)^2 \sqrt{T_\chi \frac{\gamma+1}{\gamma}} \cdot e^{-E/RT_\chi} \quad [9a]$$

to which the following additional definitions apply:

P, T = pressure and temperature (degrees Rankine) in furnaces where burned fraction is x
P_o, T_o = standard P, T
γ = m_1/m_2 = ratio of mean molecular weight of fuel molecules to that of oxygen, i.e., $m_2 = 32$
e = base of natural logarithm

Equation [9] leads directly to the result

$$dH/d\theta = A \cdot (dH/d\theta)_A = Y \cdot Z \quad [10]$$

which is the energy release rate on the volume base (Btu/ft³ × sec). Here

$$Y \equiv \frac{Q_{of} \cdot (1-x)\,(y-x)}{\beta^2} \quad [10a]$$

$$Z \equiv 0.21\,(N_f/n_2) \cdot \eta \cdot \psi \quad [10b]$$

where $Q_{of} = Q_o/f$ = calorific content of combustible in fuel-gas (Btu per cu ft) at standard conditions, and

$$\psi = A \cdot (2lx) \chi^2 \cdot \varphi_\chi \quad [10c]$$

Then, since A has dimensions $ft^2/ft^3 = 1/ft$ and χ and φ_χ are both dimensionless, it is seen that ψ is a dimensionless group.

Geometry of an Equivalent Mixture Distribution and Interzone Depth Ratio

Consider the sum total of areas (one side) of plane sections contained in a "unit" cube, all parallel to one face of the cube and separated from each other by the normal distance $2l$, where l is the denominator of the ratio $\zeta = l_X/l$. Since these planes may be considered as large in extent compared* to l, then the diffusion path length of the diffusion layer bounding the interzone of normal depth l_X becomes

$$l_D \cong l - l_X \quad [10d]$$

The unit cube contains $^1/_2\ l$ planes. Each plane represents one unit of area, when counted on one side only, and so the extent of interface in the cube is $A = {}^1/_2 \cdot l$. Then $A \cdot (2 \cdot l_X) = l_X/l = \zeta$ which substituted in Equation [10c] yields

$$\psi = \psi_{\lim} = \zeta \chi^2 \varphi_\chi \quad [10e]$$

The ratio ζ will henceforth be designated as the interzone depth ratio or simply as the depth ratio of the mixture distribution.

Interior Turbulence Space Factor

The foregoing discussion does not include the possible space effect which an interior turbulent core, within a concentration zone, might have on the space assigned to such a zone, when this assignment is in the manner outlined. With any such space effect included, the real normal spacing, $2l_r$, between parallel interface planes in the cube would exceed the normal spacing, $2 \cdot l$, by the mean normal thickness of the turbulent core. It follows that the ratio of the real interface extension $A_r = {}^1/_2 l_r$ is related to the foregoing assigned interface extension $A = {}^1/_2 \cdot l$ by

$$A_r/A = l/l_r = \xi \quad [10f]$$

Thus it is seen that ξ becomes a multiplying factor on $\zeta \chi^2 \varphi_\chi$ in Equation [10e] and so

$$\psi = \zeta \cdot \chi^2 \cdot \varphi_\chi \cdot \xi \quad [10g]$$

With this space effect of interior turbulence included, in addition to the effect on A/l of the eddies impinging on the interzone (Fig. 2), and which effect was formerly incorporated and is present in ζ, the general aspects of the influence of turbulence on the energy release rate have been adequately defined. It is seen these effects are of two kinds, namely, that on A/l and that on ξ. In both cases the energy release rate is directly proportional to the factor. The first one increases with turbulence. The second one (ξ) is the result of volume occupied within the interior of a concentration zone by interior turbulence and decreases with the increase in the fraction of the total volume of a concentration zone which is occupied by an interior turbulent core. This factor will henceforth be designated as the interior-turbulence space factor, or simply as the space factor.

When this factor is unity, the volume effect of interior turbulent cores is nil and ψ is represented by Equation [10e]. Therefore this is the limiting value for any given turbulent state. Hence with the value $\psi = \psi_{\lim} = \zeta \cdot \chi^2 \cdot \varphi_\chi$ in the energy release equation, this equation yields the maximum values of energy release rate which are possible to any given state of turbulence.

It is difficult to see how the factor ξ could ever be very far from unity. It has the best chance of tending to smaller values in large concentration zones with a small part of the interior volume occupied by a turbulent core. But then, even if such conditions could ever be maintained for any length of time, ξ is not far from unity because the volume fraction of the turbulent core is small. As this volume fraction increases, then, at some point in the increase, the turbulence immediately becomes dispersed throughout the total volume of gases in the concentration zone. Under such conditions, ξ might possibly at some time or other attain a lower limiting value of 0.50, but it is difficult to see how a value as low as this could endure for any length of time. It is only with respect to boundary layers at stationary solid surfaces as, for example, flow through a pipe, that the space occupied by the turbulent core can be a large fraction of the total volume. With this in view, such results as will be disclosed later will be based upon $\xi = 1.00$ and will be designated as the "limiting release rate" for the case under consideration.

Combustion Progress Equation

This relates the combustion progress in terms of burned fraction x to time θ in seconds. In developing the equation, $d\theta$ is transferred to the right-hand side of Equation [10] followed eventually by separation of variables and integration of a portion of the equation. The necessary preliminary steps are outlined in the Appendix, and the final result is shown as follows

$$\frac{1}{(f^2 \cdot \beta_f)} [\varphi_1 + \varphi_2 + \varphi_3] = \Theta \quad [11]$$

where

$$\Theta \equiv 0.21 (N_f/n_2) \int_0^\theta \psi (P_o/P)(T/T_o) \eta d\theta \quad [11a]$$

$$\varphi_1 \equiv \beta_o{}^2/(y-1) \log_e \frac{y-x}{y(1-x)} \quad [11b]$$

$$\varphi_2 \equiv \frac{2\,\beta_o \cdot f \cdot \Delta V}{y-1} \left[y \log_e \frac{(y-x)}{y} - \log_e (1-x) \right] \quad [11c]$$

$$\varphi_3 \equiv \frac{(f \cdot \Delta V)^2}{y-1} \left[y^2 \log_e \frac{y-x}{y} + yx - x \log_e (1-x) - x \right] \quad [11d]$$

$$\beta_f = yN_f + 1 \quad [11e]$$

Functions φ_2 and φ_3 correct the combustion progress of the case where $\Delta V = 0$ to that for which $\Delta V \gtrless 0$. The effect of omission of ΔV is considerable for a gas like CO when $y = 1.1$, since $\Delta V = -0.50$ for this gas. However, for CH_4, ΔV = zero, and for a fuel like natural gas where $\Delta V = -0.06$, the effect of its omission is very small.

For convenience let

$$\frac{1}{f^2 \beta_f} [\varphi_1 + \varphi_2 + \varphi_3] \equiv X \quad [12]$$

when Equation [11] may be stated as

$$X = \Theta \quad [13]$$

The left-hand side of Equation [13] represents combustion progress in terms of burned fraction x. The right-hand side is the time integral expressed by Equation [11a] where θ represents time in seconds. The value of X becomes infinite at $x = 1.00$ but as will be seen later the value of y has a powerful influence on X for values of x approaching unity. The equation is applicable throughout the temperature range from entrance to exit of the gases since it contains the effective factor for collisions. For $y = 1.00$ (theoretical air) the value of X is indeterminate. For $y < 1.00$, the result for X assumes that whatever oxygen disappears in reaction completely burns such fuel constituents as

* See Summary at end of main text.

enter the reaction. This of course would prove to be at some considerable variance with the facts in the case when $y << 1.00$. However, should Q_{of} be redefined as the calorific content based on the reaction as it actually occurs and values of N and f accordingly adjusted, then the equation should be generally applicable if the coefficient ψ is experimentally determined. These remarks apply also to Equation [10].

If χ and ζ in the preceding equations should each be unity they would represent either a uniform mixture or the case in which molecules are tossed directly into the interzone without interference by a thermal diffusion boundary layer adjacent the interzone. It is because of the presence of this layer that χ and ζ are each less than unity. Hence if ψ, which includes these factors among others, is solved for, from experiment by application of the preceding equations to experimental results, then the values of ψ and of the factors which it contains include whatever effects this thermal diffusion boundary layer may have had on the reaction rate. Inclusion of this effect specifically in the equations requires the equilibrium equation before mentioned, in which the supply rate of, say, oxygen molecules, through the thermal diffusion layer bounding the interzone is equal to the rate at which they disappear, within the interzone, into chemical reaction. This equation will be presented later. For the present, further clarification is best accomplished by application to a particular fuel; this to be followed by application for a particular fuel to a particular furnace.

Results for Natural Gas

In this case the fuel parameters, as taken from Trinks (4), have the values: $Q_o = 1097$, $N = 10.5$, $f = 0.918$, $V = -0.06$. The combustion is at constant pressure $P = P_o$ with $T_o = 530$ R and $T_m = 6T_o = 3180$ R. Substitution of these conditions in Equations [10] and [11] then leads to the curves shown in Figs. 3, 4, and 5. Values are given in Tables 2 and 3.

sion rate in the interzone and shows the effects of pressure and temperature on combustion progress Δx for a given time interval $\Delta\theta$. If thermal diffusion through the boundary layer takes a prominent part in the reaction rate control then the true pressure and temperature law lies between the foregoing and that indicated later in Equation [30e] which applies when thermal diffusion dominates the reaction rate. The least satisfactory quantity in Equation [15] is the energy of activation E. Unfortunately it occurs where any variation in its value exerts a powerful effect on the influence of temperature on the reaction rate.

The difference $T_X - T$ is discussed in the Appendix and a method for computing it is outlined. In this, T_X is the mean temperature of the interzone and T the mean temperature of the remainder of the concentration zone associated with the interzone. Based upon the results shown there, the mean difference $T_X - T$ is about 30 deg F when the mean energy release rate of the reaction is 36,000 Btu/ft^3 × hr for natural gas with air-fuel ratio 1.2 and mean $T = 3180$ R. This difference, as computed from the equation shown in the Appendix, would increase considerably with increase in energy release rate. It might be considered for a moment that in the high-temperature range the effective value of T_X in e^{-E/RT_X} depends to a greater extent upon the chemical reaction itself than it does on the temperatures which result by use of an equation which is based upon distribution of reaction energy after its release. If this should be the case, then the difference, $T_X - T \cong 30$ deg F, is too low. However, the energy of activation, E, is a property of the molecules which enter into an effective collision prior to that collision and so must it seems, be based upon the distribution of the released energy in the vicinity of the collision. The only conclusion possible from the latter point of view is that the energy-distribution equation shown in the Appendix yields results of the right order of magnitude for $T_X - T$.

TABLE 2 VALUES OF ($X = \Theta$) VERSUS (x, y)

Natural gas, $Q_o = 1097$, $N = 10.5$, $f = 0.918$

	x										
y	0.15	0.30	0.40	0.50	0.60	0.70	0.80	0.90	0.93	0.96	0.99
1.1	2.47	5.42	8.04	11.9	17.9	26.3	40.6	76.0	96.2	160.0	318.0
1.2	2.13	5.17	7.88	11.6	15.9	24.2	38.1	68.2	85.8	120.0	214.0
1.4	2.09	4.93	7.48	10.9	15.4	21.9	32.7	54.7	67.4	88.4	145.0
2.0	2.01	4.66	6.95	9.7	13.5	18.7	26.4	41.2	49.0	61.8	95.0

TABLE 3 VALUES OF Y VERSUS (x, y)

Natural gas, $Q_o = 1097$, $N = 10.5$, $f = 0.918$

	x											
y	0	0.15	0.30	0.40	0.50	0.60	0.70	0.80	0.90	0.93	0.96	0.99
1.1	7.03	5.15	3.58	2.69	1.91	1.28	0.768	0.363	0.128	0.0764	0.0359	0.0071
1.2	6.54	4.85	3.43	2.62	1.91	1.31	0.818	0.435	0.163	0.103	0.0524	0.0114
1.4	5.74	4.35	3.16	2.46	1.84	1.31	0.861	0.493	0.204	0.1351	0.0720	0.0168
2.0	4.17	3.28	2.48	2.00	1.56	1.16	0.812	0.505	0.229	0.1561	0.0866	0.0211

Points where $x = 0.99$, i.e., where the undeveloped energy in the gases has been reduced to 1 per cent, are indicated in the figures.

The abscissas, Θ, of Fig. 3 are proportional to time θ if the group

$$\psi \cdot (P_o/P) \cdot (T/T_o) \cdot \eta \ldots\ldots\ldots\ldots\ldots\ldots [14]$$

under the integral in Equation [11a] is a constant. This then is the scale factor between Θ and real time θ. Hence for those cases where exact comparisons for time intervals along a curve of a given y, or, as between time intervals for corresponding points as between curves of different y, the differences in scale factor must be taken into account. By reference to Equation [9a] it is seen that

$$(P_o/P)(T/T_o)\eta = (P/P_o)(T_o/T)\sqrt{T_X \frac{\gamma + 1}{\gamma}} \cdot e^{-E/RT_X} \ldots [15]$$

This applies when the reaction rate is dominated by the collli-

In Fig. 4 ordinate Y is related to the real energy release rate $dH/d\theta$ by the scale factor

$$Z \equiv 0.21\ (N_f/n_2)\eta \cdot \psi \ldots\ldots\ldots\ldots\ldots [16]$$

where reference to Equation [9a] discloses the pressure temperature effect as

$$(P/P_o)^2\ (T_o/T)^2 \sqrt{\frac{T_X(\gamma + 1)}{\gamma}} \cdot e^{-E/RT_X} \ldots\ldots [17]$$

The limitations on Equation [17] are the same as those before noted for Equation [15]. The powerful influence shown for both pressure and temperature would be considerably reduced where the reaction rate is dominated by the thermal diffusion rate through the boundary layer adjacent to the interzone.

The value of Θ to be associated with any given Y is found by transferring the y, x of a given Y from Fig. 4 to Fig. 3. This procedure leads to the curves shown in Fig. 5 where, because of

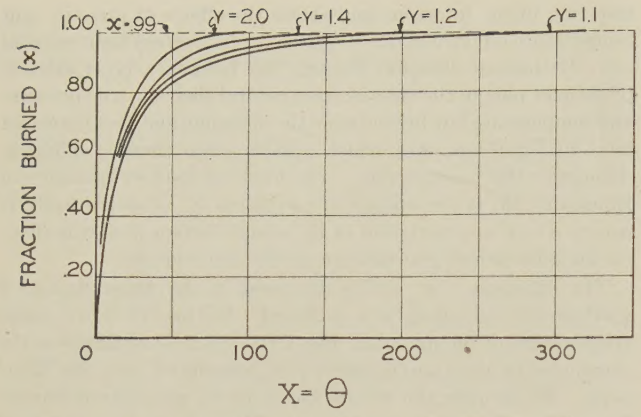

FIG. 3 COMBUSTION PROGRESS VERSUS Θ. NATURAL GAS
(Abscissa $X = \Theta$ is proportional to real time θ when ψ, P, and T each constant.)

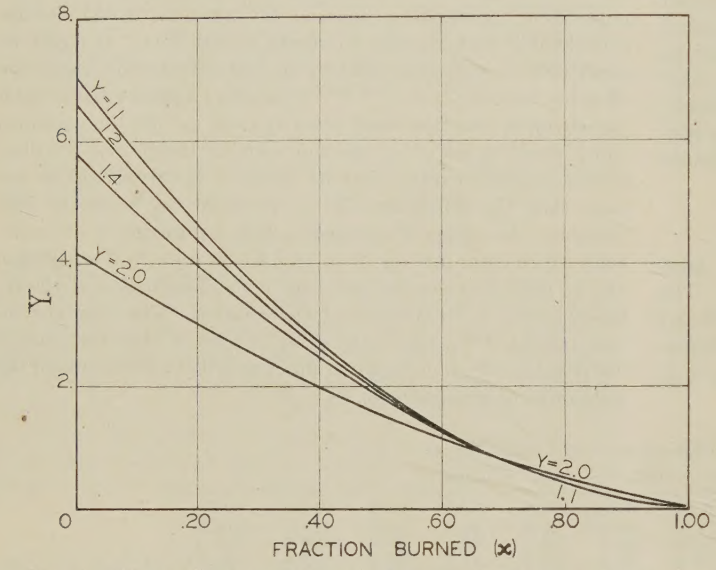

FIG. 4 ENERGY RELEASE RATE FACTOR Y VERSUS x. NATURAL GAS
(Variation of Y proportional to variation in energy release rate when ψ, P, and T each constant.)

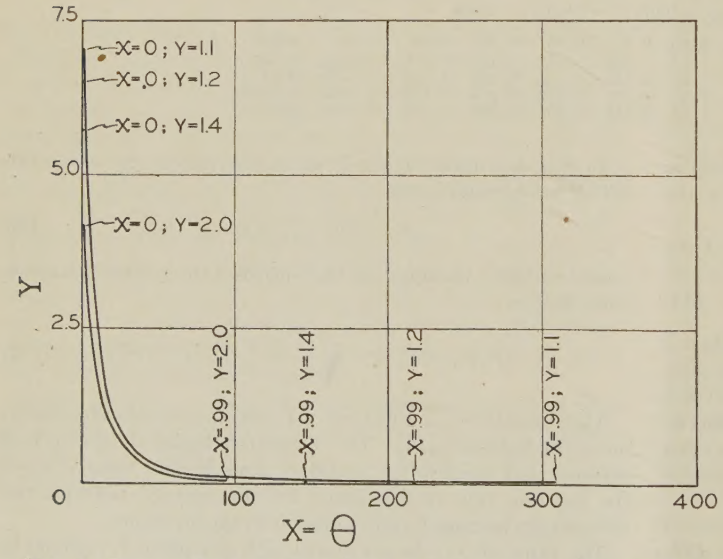

FIG. 5 ENERGY RELEASE RATE FACTOR Y VERSUS Θ. NATURAL GAS
(Variation of Y versus Θ proportional to variation of energy release rate versus real time θ when ψ, P, and T each constant.)

congestion, the only curves shown are those for $y = 1.1$ and $y = 2.0$. The other curves fall between the two shown and their end points are indicated.

In order to relate the preceding extension in Θ to the real time θ and also the Y values to the real energy release rate $dH/d\theta$ for any given case, it is of course necessary to arrive at the values of the preceding scale factors including particularly the value of ψ for that case. A suggested procedure for dealing with existent experimental information on the basis of mean values for this purpose follows.

ABSOLUTE VALUES OF TIME AND ENERGY RELEASE RATE

Consider the case of "constant pressure combustion" and let ψ_m, T_m, and T_{xm} represent mean values of ψ, T, and T_x, respectively, for the total reaction. These will be taken as constants for the process. Then identity Equation [11a] becomes

$$\Theta \equiv 0.21(N_f/n_2)\,\psi_m(T/T_o)\eta\theta \quad \ldots\ldots [18]$$

Noting now that $\Theta = X$ and solving Equation [18] for ψ_m the result may be stated as

$$\psi_m = Y/0.21\,\frac{N_f}{n_2}\,\frac{T}{T_o}\,\eta\theta \quad \ldots\ldots [19]$$

where θ is the time required to burn fraction x of the fuel.

In solving for ψ_m any associated set of experimental values (y, x, θ) may of course be employed for a given fuel and furnace. It is possible for a rough approximation to resort to the available information on the overall or average performance. For example, suppose that furnaces fired with natural gas with $y = 1.2$ may release energy at an average rate of 36,000 Btu per ft^3 × hr with a final loss in undeveloped energy of about 1 per cent, i.e., where $x = 0.99$. The given rate of energy release is

$$\frac{36{,}000}{3600} = \left(10\,\frac{\text{Btu}}{\text{ft}^3 \times \text{sec}}\right)_{\text{avg}} \quad \ldots\ldots [20]$$

In order to relate this figure to time θ let q_m represent the calorific content (Btu/ft^3) of the air-gas mixture under mean furnace conditions but before any combustion has occurred. Then if it requires θ seconds in the furnace to burn to fraction x the relation

$$\frac{xq_m}{\theta} = (dH/d\theta)_m \quad \ldots\ldots [21]$$

exists. But

$$q_m = (P_m/P_o)(T_o/T_m)q_o \quad \ldots\ldots [22]$$

$$q_o = Q_o/\beta_o \quad \ldots\ldots [23]$$

whence by substitution of Equations [22] and [23] in Equation [21]

$$\theta = \frac{xQ_o}{\beta_o(dH/d\theta)_m} \cdot (P_m/P_o)(T_o/T_m) \quad \ldots\ldots [24]$$

For the preceding case of natural-gas firing, the conditions are now as shown in Table 4.

Applying these data first in Equation [24] leads to the result $\theta = 1.33$ seconds. Then applying data in Equation [9a] yields $\eta = 0.136 \times 10^4$. Finally, applying information now available in Equation [19]

$$\psi_m = (\zeta\chi^2\varphi\chi\xi)_m = 16.48 \times 10^{-3} \quad \ldots\ldots [25]$$

TABLE 4 COMBUSTION CONDITIONS

$P_m = P_o = 1$ atm	$y = 1.2$	$Q_o = 1097$	
$T_o = 530$ R	$N = 10.5$	$f = 0.918$	
$T_m = 3180$ R	$N_f = 11.45$	$Q_{of} = 1195$	
$T_\chi = 3250$ R (see Equation [56])	$\beta = 14.74$	$E = 90{,}000$ Btu/lb mole	
	$n_2 \cong 2.00$	$\frac{\gamma+1}{\gamma} \cong 2.75$	

$X = 214$ (Fig. 3, for $x = 0.99$, $y = 1.2$)

Then with $\xi = \varphi_\chi = 1.00$ and $\zeta = l_\chi/l$ assumed as having the same value as $\chi = C_{\chi v D}/C_v = (C_{\chi v}/C_v)\varphi_\chi = 1.00$, for reasons which will become evident later

$$\psi_m = {\chi_m}^3 \text{ and } \chi_m = 0.254 \quad \ldots\ldots\ldots\ldots\ldots\ldots [25a]$$

Refer now to the curve in Fig. 6 which results when conditions of Table 4 (except $T_\chi = 3700$ deg T for curve) are applied in Equation [10] with $\chi = 0.10$. Then, in view of the foregoing relations, the mean ordinate of a similar curve to that

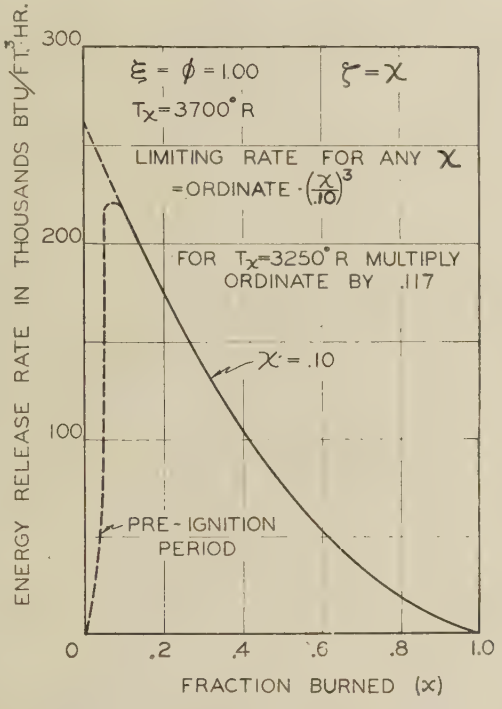

FIG. 6 LIMITING ENERGY RELEASE RATE VERSUS x. NATURAL GAS

(For conditions not noted in legend on chart see Table 4.)

shown in Fig. 6, but applicable to 3250 R and $\chi_m = 0.254$, should be equal to $0.117 \times (0.254/0.10)^3 = 1.64$ that of the curve shown. If ψ itself should be a constant, then the curve in Fig. 6 represents about 60 per cent of the energy release rate of the case just calculated. Thus an increase in value of ψ from 0.10 to 0.254 more than balances the correction required when T_χ drops from 3700 to 3250 R. Variations in both factors are thus seen to be very powerful in their net effects. Such phases of the subject may be somewhat clarified by an application of the interzone equilibrium equation before referred to.

THE EQUILIBRIUM EQUATION

For a steady state of firing, the time mean value of the frequency of effective collisions in the interzone per unit area of interface must have the same value, when expressed in terms of energy release rate as that of the diffusion of either oxygen or fuel molecules per unit area of interface when expressed in the same terms.

The development leading to the diffusion side of this equation is outlined in the Appendix and the result is

$$(dH/d\theta)_{AD} = 0.357 \times 10^{-4} \frac{Q_{of} \cdot N_f \cdot (1-\chi)(y-x)}{n_2 \cdot \beta \cdot l_D} (T/T_0)^{n'} \quad \ldots\ldots [26]$$

where exponent n' is brought in with the coefficient of self-diffusion for oxygen and has a value $n' \cong 0.75$ for average furnace conditions according to Jeans (3).

Equation [9] represents the collision branch of this equation. Equating the right-hand sides of Equations [9] and [26]

$$\frac{\chi^2}{1-\chi} = \frac{1.70 \times 10^{-4} \beta (T/T_0)^{n'}}{(2 \cdot l\chi) \cdot \eta \cdot \varphi_\chi \cdot (1-x) l_D} \quad \ldots\ldots\ldots [27]$$

where η is solved for from Equation [9a].

This condition may be combined with either branch of the equilibrium equation in order to obtain the values of energy release rate which result when all of the factors which have been specified as having an influence on the reaction rate are accounted for.

In the present analysis Equation [27] will be combined with the collision or interzone branch of the equilibrium equation. The effects referred to on the energy release rate include of course the influence of the chemical reaction on the extension, A, of interface. This depends upon the way in which the reaction influences the concentration and depth ratios χ and ζ. In order to investigate the trends of the variation of these factors with combustion progress (x), Equation [27] will be applied to a special set of conditions. These are so chosen as to permit of a numerical solution of χ by means of Equation [27] while, at the same time, being close enough to reality so as to indicate at least the probable trends of variation which may actually exist.

INTERZONE EQUILIBRIUM CONDITIONS FOR SPECIAL CASE

Consider the geometry of a diffusion system in which concentrations C_{1v} and C_{2v} are proportional to the normal distances l_1 and l_2 from the interface. This would be closely approximated when l_χ is small compared to the total distance, l, through the diffusion boundary layer. But when this is true

$$\zeta = \chi = l_\chi/l \quad \ldots\ldots\ldots\ldots\ldots\ldots [27a]$$

Noting now that $l_D = l - l_\chi$ and substituting in Equation [27] and solving

$$l\chi^2 = \frac{0.85 \times 10^{-4} (T/T_o)^{n'} \cdot \beta}{\chi \cdot \varphi_\chi \cdot \eta \cdot (1-x)} \quad \ldots\ldots\ldots [27b]$$

On introduction of the conditions shown in Table 4 which apply

$$l_\chi = 2.89 \times 10^{-3} \sqrt{\frac{1}{\chi(1-x)\varphi_\chi}} \quad \ldots\ldots\ldots [28]$$

Application of this equation with $\varphi_\chi = 1.00$ yields the results shown graphically in Fig. 7. Unfortunately, the coefficient employed in the calculations was 2.28 instead of 2.89; hence the ordinate values for all curves should be multiplied by 1.27 in order to apply strictly to the stated conditions. This shift in values is of no consequence in this discussion since it is only trends which are under consideration.

It is seen that for a given depth ratio $\zeta = \chi$ the total depth, l, of the diffusion layer plus interzone increases as the fraction burned increases. This indicates an increase in average size of concentration zone with combustion progress, which is to be expected since the smaller zones burn out first. As $\zeta = \chi$ is increased the curve becomes flatter but the break at the end is sharper and longer delayed.

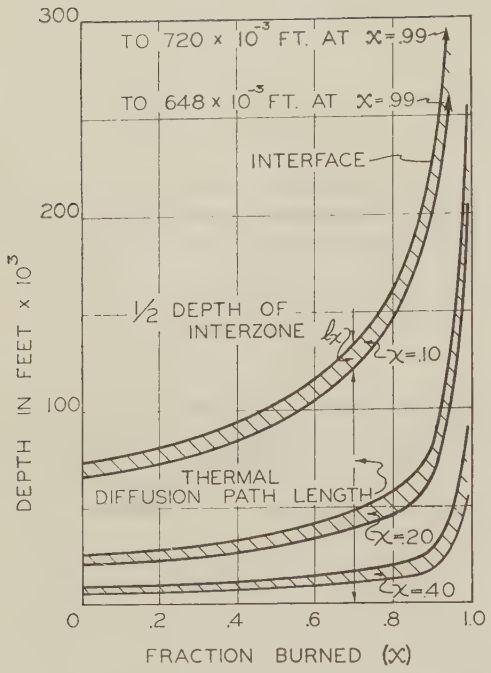

FIG. 7 VARIATION OF INTERZONE RELATIONS WITH COMBUSTION PROGRESS WITH $\varphi_\chi = 1.00$, $\zeta = \chi$ AND ANY VALUE OF ξ. NATURAL GAS
(For other conditions see Table 4.)

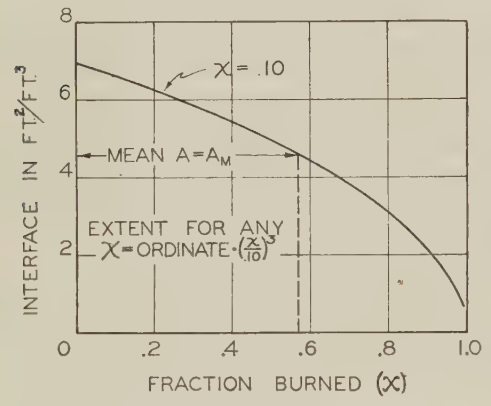

FIG. 8 LIMITING EXTENT OF INTERFACE (A) VERSUS x WITH $\varphi\chi = \xi = 1.00$ AND $\zeta = \chi = 0.10$. NATURAL GAS
(For other conditions see Table 4.)

The limiting extent, A, of interface for the equivalent mixture distribution, defined in arriving at Equation [10e] is shown in Fig. 8 for $\chi = 0.10$ with $\xi = \varphi_\chi = 1.00$. This curve is a plot of the values $A = {}^1/_2.l$ where the values of l are taken from the upper of the two curves which between them define the interzone for $\zeta = \chi = 0.10$ in Fig. 7.

The mean ordinate under the interface curve $\chi = 0.10$ in Fig. 8 falls at $x = 0.57$. The value of l_x for $\chi = 0.10$ at $x = 0.57$ in Fig. 7 is seen to be 10×10^{-3} ft. This locates the point l_x versus χ for $\chi = 0.10$ on the curve in Fig. 9. Repeating this total procedure with respect to the $\chi = 0.20$ and $\chi = 0.40$ interzone curves of Fig. 7 then furnishes data (l_x versus χ) for two additional points, one at $\chi = 0.20$ and the other at $\chi = 0.40$ for the curve shown in Fig. 9.

Referring back now to Equation [25a] where it was found $\chi_m = 0.254$, for the case of natural-gas firing there investigated, and projecting from this value on the abscissa in Fig. 9, the mean ${}^1/_2$ depth of the interzone for that case becomes, as seen, 4.5×10^{-3} ft. Hence $l_m = l_x/\chi_m = 4.5 \times 10^{-3}/0.254 = 17.7 \times 10^{-3}$ ft, and so

$$A_m = {}^1/_2.l_m = 28.2(\text{ft}^2/\text{ft}^3) \text{ for } \xi = \varphi_\chi = 1.00 \ldots\ldots [29]$$

The given value of A_m contains errors on a number of counts. First, correct values of φ_χ would alter the curves shown in Fig. 7.

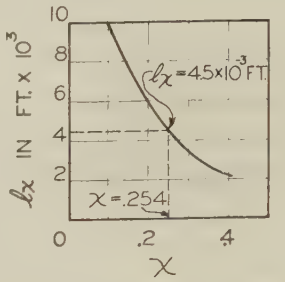

FIG. 9 ONE-HALF INTERZONE THICKNESS VERSUS χ FROM FIG. 8 AS DESCRIBED IN TEXT

But the relation between l_χ and χ in Fig. 9 would not be affected much. However, since both real ξ and φ_χ are less than unity, and A_m varies with ξ and with $\sqrt{\varphi_\chi}$, a closer value is $A_m \cdot \xi \cdot \sqrt{\varphi_\chi}$

MAXIMUM LIMITING VALUES OF ENERGY RELEASE RATES AND EXPLOSION POCKETS

At the maximum limit $\zeta = \chi = \xi = \varphi_\chi = 1.00$. Under these conditions the diffusion boundary layer has shrunk to zero. Then since $\chi_m = 0.254$ for the preceding case of natural-gas firing with a time mean energy release rate of 36,000 (Btu/ft² × hr), it appears that for a uniform mixture, that is, when oxygen and fuel are uniformly distributed, the hypothetical maximum limiting time mean energy release rate for the period in which the combustion is carried from $x = 0$ to $x = 0.99$, with conditions shown in Table 4, is of the order of magnitude

$$({}^1/_{0.254})^3 \times 36{,}000 = 2.18 \times 10^6 \text{ Btu/ft}^3 \times \text{hr} \ldots\ldots [30]$$

Thus it is seen that the mechanism included in the equation has tremendous resources in so far as increasing energy release rates is concerned.

On the way from $\chi << 1.00$ to $\chi = 1.00$ the interface A increases. In the limit, however, where $\chi = 1.00$, interface ceases to have any meaning because both fuel and oxygen molecules are uniformly distributed throughout the mixture. Hence each and every concentration zone has dissolved, as it were, into the total space occupied by the mixture. It is important to note that even though one of the concepts, on the basis of which the equations were developed, has ceased to have any meaning under these maximum limiting conditions, the equations themselves apply even here.

As the mixture distribution progresses toward the state of uniform mixture, some portions of the gas will arrive at this uniform state before others do. Such portions may be called explosion pockets because once the reaction starts from their boundaries it will flash through these pockets with energy release rate of the order of magnitude indicated by Equation [30] if the air-fuel ratios and temperature conditions are favorable. Strictly speaking, the equations cannot apply to such a dual distribution wherein some portions of the mixture have uniform distribution and others contain concentration zones. In such cases the value of χ found from experiment will be greater than its actual value for such portion of the total gases as were in concentration zones rather than in explosion pockets. However, the value of χ found will be that of an equivalent distribution yielding the

same results. Furthermore, the effect of such pockets on the time mean energy release rate should not be large if the pockets are small and well distributed even though they might be numerous, the fraction of the total volume occupied by such pockets being probably quite small under any feasible practical operating conditions. Of course there is the exceptional or accidental case when, after an interval of time without combustion in the cavity, thermal diffusion results in the whole furnace volume becoming an explosion pocket. The results of this afterignition are well known.

Comparison of Form of Combustion Progress Function for Collision Versus Thermal Diffusion Control

If the right-hand side of Equation [26] is multiplied by interface extension A, the product represents the energy release rate $dH/d\theta$ in terms of the diffusion branch of the equilibrium equation. Then noting by reference to Equation [4] that

$$A/l_D = A_o/l_{oD}(P/P_o)^{2/3}(T_o/T)^{2/3} \quad [30a]$$

this product may be stated as

$$(dH/d\theta)_D = 1.7 \times 10^{-4} \cdot \frac{0.21 N_f Q_{of} A_o}{n_2 \beta\, l_{oD}} (y - x)(1 - \chi)(P/P_o)^{2/3}(T/T_o)^{n'-2/3} \quad [30b]$$

where $1 - \chi$ would be solved for from Equation [27] for the general case.

The combustion-progress equation which goes with Equation [30b] is developed from it in the same way as Equation [11] was from Equation [10] with the result

$$X_D = \Theta_D \quad [30c]$$

where

$$X_D = [\varphi_{1D} + \varphi_{2D}] \quad [30d]$$

$$\Theta_D = 0.36 \times 10^{-4}(N_f/n_2) \int_0^\theta \psi_D (P_0/P)^{1/3}(T/T_o)^{n'+1/3} d\theta \quad [30e]$$

$$\psi_D = A_0/l_{oD}(1 - \chi)\xi \quad [30f]$$

and

$$\varphi_{1D} = (\beta_0/\beta_f f) \log_e(y - x)/y \quad [30g]$$

$$\varphi_{2D} = \Delta V/\beta_f [y \log_e(y - x)/y + x] \quad [30h]$$

Here φ_{2D} alone corrects for volume change ΔV in combustion.

Referring now to Fig. 10, the curves χ and D are for the same conditions. The χ curve is the result of Equation [11] and the D curve is the result of Equation [30c]. But in the latter case the abscissa scale has been adjusted so that $X_D = X$ at fraction burned $x = 0.99$.

As χ approaches zero, ψ (Equation [10c]) approaches zero. Hence Θ and θ of Equation [11a] also approach zero. It follows that at the limit $\chi = 0$ the time consumed by the effective collisions in the interzone must be zero. Under the same conditions ψ_D, and hence Θ_D and θ of Equation [30e] have their maximum values. This is the hypothetical limit in which thermal diffusion through the boundary layer takes complete control.

At the other limit, as χ approaches unity, the reverse of the foregoing is true. This limit exists for the ideal case either of a uniform mixture or when turbulence tosses molecules directly into the interzone. Now the diffusion layer has been eliminated.

The diffusion branch of the equilibrium equation as taken by itself indicates, as shown by curve D, Fig. 10, that the curve approaches a finite limit of $X_D = \Theta_D$ for $\gamma > 1.00$. However, investigation with reference to Equation [27] indicates that this can be true only for the hypothetical case in which $\chi = 0$. It

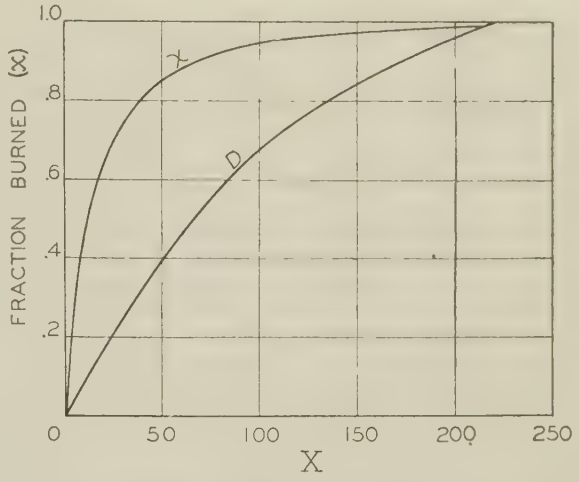

Fig. 10 Comparison of Trend of Combustion Progress for Collisions Versus Diffusion Control. Natural Gas
(For conditions see Table 4.)

follows that for all real cases ($\chi > 0$) the true progress function extends to $X = \Theta = \infty$ when the combustion is completed.

The adjustments which transform the relationships existing for the limiting states, as represented by the χ or D curves of Fig. 10, into the final real relation between x and θ, is in each case accomplished by the time integral. For the collision curve χ this is Θ as evaluated from Equation [11a] with reference to Equations [10g] and [27], and for the thermal diffusion curve D it is Θ_D, as evaluated from Equation [30e] with reference to Equations [30f] and [27].

When these transformations have been accomplished for any given case the development involved will have led to identically the same function, x versus θ, and so will result in exactly the same curve x versus θ regardless of whether the original reference function, from which the transformation started, was based upon the collision or diffusion branches of the equilibrium equations. In the present analysis this starting reference was purposely taken as the collision branch of the equilibrium equation because this affords the means of presenting the subject under discussion, namely, influence of interface extension A, in its most logical order. In some cases, where fairly rough approximations only are in order, it may be found that the diffusion branch of this equation will have advantages. This would be true wherever it is known in advance that by far the greater resistance is in the thermal diffusion layer, under which condition χ may be negligible compared to unity.

Actual evaluation of time integrals Θ or Θ_D for any case involves of course the variation along the path of the ψ or ψ_D. It is not possible at this time to furnish anything very conclusive in this respect. This awaits further development based upon experimental data. A few of the general aspects of this problem are now considered.

Variation of A, χ, and ζ Along Combustion Progress Path

Figs. 7 and 8 indicate the effect of the reaction progress alone on the given variables. As before noted, A increases with turbulence and, in any self-acting process free of chemical reaction, also with time. But as seen now the ever-increasing values of the depth ratio ζ with decreasing concentration along the path tend to decrease A. The following statements may now be added to those before made concerning the behavior of A. These begin by again emphasizing the fact that the curves in Figs. 7 and 8 show the influence of the combustion progress only; therefore:

1 The curve of interface extension shown in Fig. 8 is that which would result if the natural tendency for A to increase did not exist. The true curve of interface extension for conditions of Fig. 8 (except constant $\zeta = \chi$) should therefore start where it does, but subsequent points along the real curve should fall above corresponding points of the curve shown, the difference increasing with increase in x. Since $A = {}^1/_2\, l$, this increase requires a decrease in l which with reference to Fig. 7, indicates that both ζ and χ must increase with x. With respect to the variation of φ_χ along the path, it is first noted that in the limit of a uniform mixture φ_χ = unity. It appears therefore as though φ_χ also will tend to increase with x, since, in general, the mixture distribution is tending toward the state of uniformity. The evidence presented thus indicates that in the absence of turbulence effects, ψ itself probably tends to increase along the path.

2 If initial turbulence is intense and later dies out with increase in x then the change in the thickness l_D of the thermal diffusion boundary layer will be subject to the control of the eddies caused by turbulence rather than to that of the diffusion symmetry resulting from the reaction, as illustrated in Fig. 7. But the boundary layer may be so thin in the initial turbulent zone that both ζ and χ are forced to have higher values in this zone than they will have later after effects of turbulence diminish. Under such conditions ψ may at first decrease with x up to the point in combustion progress where the influences of the diffusion symmetry just balance those of turbulence. Beyond that point ψ increases with x as noted. However, in the early stages, the effects of the decreasing tendency of ζ and χ on ψ are partly compensated for by the increasing tendency of the value of the interior turbulence factor ξ.

3 In view of all of the foregoing it seems probable that the influence of the variation of ψ with x on the form of the combustion progress function is small compared to the very powerful influence, in such respects, of the decrease in value of the concentration product $C_1.C_2$ with increase in x, particularly in the early stages of this progress. But in the later stages of the progress, the factors ξ and φ_χ must be near unity in value. Therefore, during this period the principal variation in ψ must result from whatever variations occur in ζ and χ. But here the forces which disturb the diffusion symmetry shown in Figs. 7 and 8 are at their minimum without special provisions for turbulence augmentation, etc. It seems therefore as though even here the influence of decrease in value of the concentration product $C_1 \cdot C_2$ along the path will be predominant as to the form of the combustion progress function.

4 In any event, whether or not the previous statements are near the real facts in the case, ψ is but one of the members of a group shown by Equation [14] which group is the scale factor connecting X and Θ to real time θ. It contains certain factors the values of which at entrance, e, to the cavity, should be a function of the conditions in the initial turbulent zone for any given case. In this connection it is first noted that ψ contains the factor A, the accumulated value of which at any point along the path consists of its value at entrance after passage through the initial turbulent zone plus the accumulation up to the point under consideration. The entrance condition will henceforth be designated by subscript e and when referred to standard conditions, by subscript oe. This suggests that an attempt be made at correlation between theory and experiment for the factors mentioned by means of the criterion of dimensional consistency.

Correlation Between Theory and Experiment With Reference to Entrance Values of Certain Factors in ψ

For this purpose ψ is stated in the form $A \cdot (2l\chi)\chi^2\varphi_\chi$, as shown by Equation [10c]. If χ^2 from Equation [27] is introduced in this group, the result is an expression from which A/l_D may be separated as containing the factors which on entrance would have their values determined primarily as a result of passing through the initial turbulent zone for a given initial condition of the mixture at entrance to the turbulent zone. But l_{D_e} involves also forces of the reaction whereas l_e by itself does not. Therefore the correlation based on dimensional analysis would be between A/l_e and dimensionless groups such as Reynolds and Prandtl numbers. Then, since $A_e = 1/l_e$ it has dimensions L^{-2}. It appears thus as though the establishment of the function

$$A_o/l_e = 1/d^2\, \varphi_e(Re, Pr) \qquad [31]$$

may be possible for some cases. Here d is a linear dimension defining the initial turbulence-producing system and Re and Pr are Reynolds and Prandtl numbers, respectively. The relation of the left-hand side to the value of this ratio at any pressure and temperature P, T is then as shown by Equation [4] for A/l.

Summary

The analysis does not specifically include the possible influence of two factors. One of these is a shape factor of the concentration zones. The reference geometry employed in arriving at Equation [10e] assumes a thin extended flat slab as the shape of the concentration zone. If the reference geometry had been based on three mutually perpendicular sets of parallel plane surfaces within the unit cube, then the concentration zones would have been cubes. If l in A/l may be considered as a volume hydraulic radius then diffusance A/l has the same value for both cubes and extended slabs when the interface extension is the same in both cases. Furthermore the interzone volume per unit of interface still remains the same as before because this depends only on the kinetics of molecular collisions in the gas volume fronting on the interface. It follows that the shape of the concentration zones should have but a negligible influence on the results provided the total furnace volume is large compared to the average volume of a single concentration zone.

The other omission is the resistance offered to the transfer of molecules across the gap occupied by interior turbulence within the concentration zones. Since the transfer across this gap takes place by eddy diffusion the resistance to such transfer should be very small compared to the space effect of the gap in reducing the mean depth of the thermal diffusion sections of the total transfer path. The latter effect is accounted for. Hence the above omission probably involves a quite negligible error.

In view of the foregoing remarks and the discussion preceding them, it appears as though this analysis provides a reasonably complete outline of the factors involved. It is hoped that this will be of value in pointing the direction of further investigation. The main features of the analysis should, it appears, apply to fuels in the vaporous as well as in the gaseous state.

Acknowledgment

The author expresses his indebtedness to Messrs. Martin A. Mayers and Ray E. Bolz for reviewing an early draft of the paper and for valuable suggestions, but primarily for raising a number of embarrassing questions. After discovering the answers to these, the author found it necessary to rewrite the paper completely, with results here shown.

The author is indebted also to his colleague, Prof. M. L. Wiedmann, for suggesting sources of information concerning certain phases of the subject.

BIBLIOGRAPHY

1 "Combustion Flames and Explosion of Gases," by S. P. Burke and T. E. W. Schuamnn, *Industrial and Engineering Chemistry*, vol. 20, 1928, p. 998.

2 "Der Einfluss der Mischvorganges auf die Verbrunnung von

Gas und Luft Fuerungen," by L. Rummel, *Archiv Für Das Eisenhüttenwesen*, 1936–1937, p. 505; 1937–1938, pp. 19, 67, 113, 163, 215, and 629.

3 "The Dynamical Theory of Gases," by J. H. Jeans, fourth edition, Cambridge University Press, London, England, 1925.

4 "Industrial Furnaces," by W. Trinks, John Wiley & Sons, Inc., New York, N. Y., third edition, vol. 1, 1934, p. 125.

5 "Heat Transmission," by W. H. McAdams, second edition, McGraw-Hill Book Company, Inc., New York, N. Y., 1942, pp. 65–66.

6 "Explosions and Combustion Processes in Gases," by William Jost (Translation by H. O. Croft), McGraw-Hill Book Company, Inc., New York, N. Y., 1946.

7 "Mass Transfer and Friction in Turbulent Flow," by T. K. Sherwood, Trans. A.I.Ch.E., vol. 36, 1940, pp. 817–840.

8 "Modern Developments in Fluid Dynamics," by Oxford Engineering Science Series, edited by S. Goldstein, Clarendon Press, London, England, vol. 1 and 2, 1938.

9 "Applied Hydro and Aero Mechanics," by L. Prandtl and O. G. Tietjens, McGraw-Hill Book Company, Inc., New York, N. Y., 1934.

10 "Combustion, Flames, and Explosions of Gases," by B. Lewis and G. von Elbe, The Macmillan Company, New York, N. Y., 1938.

Appendix

The Collision Frequency F_{12}. From Jeans (3)[3]

$$F_{12}' = 2\nu_1\nu_2\bar{S}_{12}\sqrt{\frac{\pi}{h}\left(\frac{1}{m_1'}+\frac{1}{m_2'}\right)} \quad [32]$$

where

F_{12}' = frequency of collisions/cm³
ν = number of molecules/cm³
$\bar{S}_{12} = {}^1/_2(\sigma_1 + \sigma_2)$
σ = diameter of molecules
$h = {}^1/_2R'T_{xk}$ T_{xk} = temperature, deg K

In the cgs system

$R' = 1.372 \times 10^{-16}$ = molecular gas constant
$m_2' = 52.8 \times 10^{-24}$ = g per molecule for oxygen
$S_{12} = 4.00 \times 10^{-8}$ cm average

Now let $m_1' = \gamma m_2'$. Then with the foregoing information introduced, Equation [32] becomes

$$F_{12}' = 12.94 \times 10^{-12}\,\nu_1\nu_2\sqrt{T_{xk}(\gamma + 1/\gamma)} \quad [33]$$

Note that

$$\nu = C_{xv}N_o(P/P_o)(T_o/T) \quad [34]$$

$N_0 = 2.705 \times 10^{19}$ molecules/cm³ at P_o, T_o

cm³/ft³ $= 2.83 \times 10^4$

$T_{xk} = (T_x/1.8)$ where T_x = deg Rankine

Introducing preceding conditions in Equation [33] results in Equation [6] for the collision frequency F_{12} per cubic foot.

Relative Concentrations C_v. Parameters to be employed are defined in the nomenclature but ΔV also defined there, needs further clarification. Thus suppose a fuel as supplied contains f fraction of combustible composed of combustible constituents 1, 2 . . . of fractions f_1, f_2 . . . where

$$f_1 + f_2 + \ldots = f \quad [35]$$

Then if ΔV_1, ΔV_2 . . . represent the values of ΔV per unit volume for each of the constituents

$$\Delta V = \frac{f_1\Delta V_1 + f_2\Delta V_2 + \ldots}{} \quad [36]$$

Examples of ΔV_1, ΔV_2 . . . etc., are given in the following. Thus for a gas containing f_1 of CO, f_2 of CH_4, etc.

$$2CO + O_2 = 2CO_2 \qquad \Delta V_1 = \frac{2-3}{2} = (-{}^1/_2)$$

$$CH_4 + 2O_2 = CO_2 + 2H_2O \qquad \Delta V_2 = \frac{3-3}{1} = 0$$

Then the ratio of total gas volume to volume of original combustible in fuel gas at any point x in the combustion progress is

$$\beta = yN_f + 1 + \left(\frac{1}{f} - 1\right) + x\Delta V \quad [37]$$

where $[(1/f - 1)]$ represents the volume of inert gas associated with 1 cu ft of combustible constituents in the fuel gas, or

$$\beta = yN_f + 1/f + x\Delta V = 1/f(yN_f{\cdot}f + 1 + x{\cdot}f{\cdot}\Delta V)$$

Let

$$\beta_o = yN_f{\cdot}f + 1 = yN + 1 \quad [38]$$

This is the ratio of initial air plus gas to fuel gas itself as supplied since $N_f f$ is the theoretical air-gas ratio based on the fuel gas as supplied. Then

$$\beta = 1/f[\beta_o + x{\cdot}f{\cdot}\Delta V] \quad [39]$$

At fraction burned x the volume of 1 cu ft of original combustible has been reduced $1 - x$ and is contained in β cu ft of mixture Hence

$$C_{1v} = (1 - x)/\beta \quad [40]$$

The volume of oxygen contained in N_f cu ft of air is $0.21N_f$. Hence at fraction burned x the volume consumed is $0.21xN_f$. The volume in yN_f cu ft of air is $0.21yN_f$. Hence at fraction burned x the volume of oxygen left in the mixture is

$$0.21yN_f - 0.21N_f{\cdot}x = 0.21N_f(y - x) \quad [41]$$

This also is contained in β cu ft of mixture. It follows

$$C_{2v} = \frac{0.21N_f(y-x)}{\beta} \quad [42]$$

For perfect gases the right-hand sides of Equations [40] and [42] have the same value for any given fraction burned x regardless of pressure and temperature.

Combustion Progress Equation. Let q_{iz} represent the initial calorific content (before combustion) per unit volume of the air-gas mixture. This may be stated in terms of its value for standard conditions as

$$q_{iz} = q_o(P/P_o)(T_o/T) \quad [43]$$

where q_o is the initial q when $P = P_o$ and $T = T_o$.

During the interval $d\theta$ when x increases from x to $x + dx$, the energy dH released within a unit of volume of the gas at station x is

$$dH = -dq_{iz} = -q_{iz}\,dx \quad [44]$$

Substituting, Equation [43] in Equation [44]

$$dH = -(P/P_o)(T_o/T)q_o dx \quad [45]$$

where

$$q_o = Q_{of}/\beta_f \quad [46]$$

Transposing $d\theta$ to the right-hand side of Equation [10], inserting Equation [46] in Equation [45], and then equating the right-hand sides of Equations [10] and [45] results in the equation

[3] Reference (3), p. 251

$$-\frac{1}{\beta_f}\int_0^x \frac{\beta^2 dx}{(1-x)(y-x)} = 0.21(N_f/n_2)\int_0^\theta \psi(P_o/P)(T/T_o)\eta\, d\theta \quad [47]$$

After integration of the left-hand side the results may be arranged as shown by Equations [11] to [11e].

Diffusion Branch of Equilibrium Equation. The volume of oxygen (cu ft) diffusing through a unit of interface in 1 sec is

$$(dV_2/d\theta)_A = \left[\frac{C_{2v} - C_{2\chi_v D}}{l_D}\right] D \quad [48]$$

where

$$C_{2\chi_v D} = \chi \cdot C_{2v}$$

Hence

$$C_{2v} - C_{2\chi_v D} = C_{2v}[1-\chi]$$

and

$$(dV_2/d\theta)_A = \frac{C_{2v}[1-\chi]}{l_D} D \quad [48a]$$

Also

$$D = \mu/\rho = D_o(P_o/P)(T/T_o)^{n'+1} \quad [49]$$

where

$$D_o = 1.7 \times 10^{-4}\ \text{ft}^2/\text{sec} \quad [50]$$

for conditions of this problem. Inserting Equation [42] for C_{2v} in Equations [49] and [50], and multiplying by

$$(Q_{of}/n_2)\cdot(P/P_o)\cdot(T_o/T) \quad [51]$$

in order to convert to Btu/sec, the result is that shown by Equation [26]. In expression [51], (Q_{of}/n_2) is the energy released (Btu/ft^3) of oxygen entering in the reaction at standard pressure and temperature P_o, T_o. The whole expression thus represents the energy released per cubic foot of diffusing oxygen when at the pressure and temperature under consideration. In the expression, n_2 represents the cubic feet of oxygen required per cubic foot of combustible in the fuel gas.

Difference in Temperature $(T_\chi - T)$. The difference $T_\chi - T$ at any point x in the path for a steady state of firing is caused by net transfer rate of energy as heat between the concentration zones and the colder surroundings. Temperature T of the concentration zone itself thus assumes such a value that the rate of transfer to it from hotter surroundings is equal to the transfer rate from it to colder surroundings. The transfer from the zone is mainly by radiation and that to it is a combination of radiation from all parts of the cavity hotter than itself plus thermal conduction into it from the reaction interface which bounds it.

In order to estimate the thermal conduction, consider the total interface A in a unit cube as distributed in parallel plane sheets all normal to a cube edge. Then the normal distance l_r between two layers of interface is $\approx 1/A$ since A is now equal to the number of parallel sheets of interface. A given concentration zone then receives thermal conduction from both interface sheets bounding it, or, conversely, thermal conduction passes normally in both directions from an interface into the concentration zones bounding it. The total area of interface from which conduction passes into the concentration zones is thus $2A$ and the total thermal conduction per unit volume is

$$(dq/d\theta)_{\text{cond}} = 2Ak(\Delta T/l_r) \quad [52]$$

where ΔT is the total drop in temperature across normal distance l_r between layers. Then the mean of temperatures in depth l_r from one interface to the other is

$$T \cong T_\chi - \Delta T/2 \quad [53]$$

The latter is taken as the radiating mean temperature of the zone. Inserting $l_r = 1/A$ and for ΔT from Equation [53]

$$(dq/d\theta)_{\text{cond}} = 4A^2k(T_\chi - T) \quad [54]$$

Then, assuming that the net radiant reception in the concentration zones is chiefly from the reaction zones, the equilibrium equation may be stated as

$$4A^2k(T_\chi - T) + \sigma_b(\alpha_\chi T_\chi^4 - \alpha T^4) = \bar{\mu}(dH/d\theta) \quad [55]$$

where $\bar{\mu}$ represents the fraction of released energy which is transferred by radiation from the concentration zones to surroundings from volume under observation. Coefficients α_χ and α are respectively, absorptivities of the concentration zones per cubic foot of mixture, and σ_b is the coefficient of black radiation. The equation assumes zero direct net radiant transfer between reaction zones and walls of the cavity. It will be assumed also that the thickness concentration value PL of the sum of all reaction zones in the furnace cavity (interface zones) which radiate to a given concentration zone is sufficiently large so that for the wave lengths in which the concentration zones absorb, the radiation is nearly black radiation. The errors contained in the two foregoing assumptions tend to cancel each other.

The transfer fraction $\bar{\mu}$ depending as it does chiefly upon concentration and temperature of radiating molecules in the concentration zones (for a given set of conditions as to furnace, fuel, air, etc.) must be relatively small at the beginning of combustion but increases with combustion progress because of resultant increase in concentrations of product molecules. In order to apply Equation [54] to points along combustion progress as burned fraction x increases requires a knowledge of the function $\bar{\mu} = \varphi(x)$. However, a mean value $(T_\chi)_m$ for a given T_m based upon the total reaction in the furnace cavity may be determined. Then $\bar{\mu}_m$ is the furnace-absorption efficiency, i.e., the fraction of released energy which is absorbed at walls of the furnace cavity and $(dH/d\theta)_m$ the mean energy release rate. Equation [55], in terms of mean values, is now applied to the preceding case where the fuel was natural gas. The data may be taken from Table 4 with the following additions

$$(dH/d\theta)_m = 36{,}000\ \text{Btu ft}^3/\text{hr}$$

$$\bar{\mu}_m = 0.215$$

$$A_m = 28.2\ (\text{ft}^2/\text{ft}^3) \text{ from Equation [29]}$$

$$\alpha_\chi \cong \alpha \cong (\epsilon \text{ for } 3180 \text{ deg R}) \cong (\epsilon_{CO_2} + \epsilon_{H_2O}) \cong 0.08$$

$$\sigma_b = 1.72 \times 10^{-9}$$

$$k = 0.07\ \text{Btu/ft}^2 \times \text{deg/ft}$$

Equation [55] now becomes

$$223[T_\chi - 3180] + 0.137[(T_\chi/1000)^4 - 102]\ 10^3 = 7720 \quad [56]$$

Solving $T_\chi - T \cong 30$ deg F. At higher energy release rates this figure will increase.

Discussion

R. E. Bolz.[4] One of the outstanding achievements of the paper is the concept of the reaction interface extension as applied to the combustion of gaseous-fuel constituents, and the clear model that is set up on which is based the subsequent analysis.

As understood by the writer, the model simply presents a picture of a combustion chamber, through which pass air and gaseous fuel in the form of concentration zones, islands rich in oxygen or

[4] Assistant Professor of Aeronautical Engineering, Rensselaer Polytechnic Institute, Troy, N. Y. Jun. ASME.

fuel molecules, respectively. These zones are separated by the reaction interzones into which the fuel and air molecules diffuse from the concentration zones and then react according to the kinetics of molecular collisions. Turbulence then enters the situation in two ways: It causes the original large concentration zones to be broken up and separated into many smaller zones; and it creates jagged eddied interface surfaces along the combustion path. Both of these turbulent effects then result in an increase in interface extension surface or, more precisely, in an increase in reacting surface to volume ratio. In addition, the presence of eddies on the interface surfaces lessens the thickness of the diffusion path through which the reacting molecules must pass on their way to the reaction zone.

An additional concept injected into this condition by the author in the paper is that of interior turbulence. By interior turbulence is meant small-scale turbulence within a concentration zone which influences the molecular distribution within the zone and has no influence upon the shape of the interface surface. This concept of interior turbulence, in agreement with the author, appears to the writer to be of negligible importance in the combustion process. It is necessarily small-scale turbulence, which may possibly arise at the beginning of the combustion zone where air enters the combustion chamber and impinges on the fuel zone, and, subsequently, would be dissipated very quickly because there is nothing to promote its continuance. From this we may conclude that it could exist only during the initial combustion period. During the very early stages of combustion, however, before a concentration gradient has been established in the concentration zones, the diffusion effect on combustion is probably small, and the effect of interior turbulence toward reducing the diffusion path would then be negligible. Later in the combustion progress, when a large concentration gradient in the concentration zones is likely to occur and the effect of interior turbulence could be appreciable, this interior turbulence will, in all probability, have been dissipated.

Now the over-all combustion model that the author has set up first enables an analytical evaluation to be made of the reaction rate based on the three fundamental concepts or primary variables; molecular diffusion, kinetics of molecular collisions, and reaction interface area. These primary variables are then expressed, in so far as possible, as functions of the secondary variables; the temperature, pressure, and velocity of the gases in the combustion chamber, and the fuel to air ratio. The secondary variables are most important because they are the measured physical quantities. It is this second step of the general analysis wherein the complexities and difficulties arise. The temperature and pressure first affect the density, which in turn influences the reaction interface area. The temperature and pressure and fuel-air ratio determine not simply the diffusion processes and the kinetics of molecular collisions and reaction as discussed in the paper. The gas velocity establishes the time factor for any particular combustion chamber and influences (in a relatively obscure relation) the degree and scale of turbulence, or more directly, the value of the reaction interface area. In addition, the turbulence is primarily dependent upon an external factor, i.e., the combustion-chamber design. In the author's analysis, the effect of the gas velocity and the chamber design on turbulence is absorbed conveniently in the reaction interface area, A.

The difficulty of expressing turbulence analytically in terms of velocity, design criteria, and the like, and the complexity of the expressions for diffusion and the kinetics of molecular collisions involving the temperature, pressure, and fuel-air ratio probably resigns us, for the present at least, to the hope of establishing an experimental factor or factors which would relate theory and experiment. Some such factor, ψ, should exist according to the author when the theory is based only upon the kinetics of molecular collisions in the reaction zone, and ψ then includes primarily the reaction interface area, A. An even more realistic link to be used is a factor which relates theory and experiment when the theory is based upon molecular diffusion as well.

It may be realized readily from the subject paper why the development of combustion chambers, such as for compressor-turbine and ramjet engines, is a trial-and-error experimental process, particularly since this type of chamber introduces fuel-vaporization and injection problems associated with liquid-fuel combustion. It is felt that the author very well points the way to additional thinking and analyses on the subject and discloses a need for critical scrutiny into the application to the combustion problem of diffusion and the kinetics of molecular-collision processes. The need also exists for careful experimental work on the combustion of gaseous fuel. In addition, his paper opens up the question of applying similar analytical thinking to the process of liquid-fuel combustion with possible results pointed toward improved high-speed high-altitude aircraft.

R. J. Brun.[5] This paper represents the type of study that more of the combustion work should follow, and these studies should be accepted as a necessary part of the solution of the problems dealing with combustion. The analysis presents hints as to which variables require closer observation and better evaluation than has been the practice in empirical and experimental work. One good reason why data on combustors, involving turbulence in the burning process, are not reproducible is that the mechanism of the energy release in the turbulent region is not well understood, and therefore the important variables actually controlling the release of energy are not the ones considered, as they should be, when two sets of data from different burners are examined. Only by increasing the resolving power of the observations and thoughts can the discrepancies which customarily have been considered in burning processes be eliminated.

A point nicely brought out by the author is that the chance of having furnace turbulence toss molecules directly into the interzone by eliminating completely the thermal-diffusion layer is so small as to be negligible.

J. B. Dwyer.[6] The author deals with the progress of combustion in a system in which air-and-fuel gas streams are introduced into a furnace without premixing. A useful concept is introduced which locates the combustion reaction in an interzone or layer between the fuel-gas mass and the air mass. The rate of that reaction is shown to be dependent upon the concentrations of fuel and oxygen molecules in the interzone, and those concentrations in turn depend upon the concentrations in the fuel-rich zone and the air-rich zone.

In arriving at the concentrations at the interzone, the author goes back to the initial mol fractions of oxygen and fuel in the gases admitted to the furnace, and the fraction of fuel burned, Equation [6*a*] of the paper. Whereas this equation is adequate for premix combustion (in which the interzone concept is of no benefit), it does not in any way fit the case of nonpremix combustion. This is apparent if one takes the initial conditions ($X = 0$), under which the concentration of fuel in the fuel-rich zone may be close to 1.00, no matter what the air/fuel ratio, yet Equation [6*d*] yields a low value for the fuel concentration. The error persists of course in the consequent value of fuel concentration in the interzone. Depending upon the fuel characteristics (and independently of the air/fuel ratio), the initial concentration of fuel gas in the interzone may be 0.5 and not of the order of 0.05 for a

[5] National Advisory Committee for Aeronautics, Cleveland Airport, Cleveland, Ohio.

[6] The W. M. Kellogg Company, Jersey City, N. J.

fuel gas having a molecular weight of 30 and a heating value of 20,000 Btu per lb.

There is also some objection to the assumption that each effective molecular collision will liberate a fixed quantity of heat. Considering that the initial concentration of fuel in the interzone is high, partially oxidized products of combustion will diffuse both to air- and fuel-concentration zones. Those products taking the latter course will be further oxidized at a later time, hence the over-all picture of heat released is not adequate to describe the specific process which takes place.

Author's Closure

The author is indebted to Messrs. Bolz, Brun, and Dwyer for their discussions. The clear presentation by Bolz adds emphasis to important aspects of the problem as does that of Brun.

Dwyer raises some points which need further discussion. He points out the inadequacy of concentration Equations [6*d*] for the case of nonpremix combustion. As a matter of fact, the equations as stated apply, strictly speaking, only to a uniform mixture and that, as will be shown presently, is not attainable even in premix combustion. However, an approximation by means of these equations is still possible to both premix and nonpremix combustion if the left-hand sides of Equations [6*d*] are designated, respectively, as $\chi_1 C_{1v}$ and $\chi_2 C_{2v}$. This assumes that the interzone equilibrium Equation [27] is satisfied when the value of χ is such that it yields within the interzone the concentrations of a uniform mixture for any burned fraction x. As a matter of fact this is substantially what the numerical results, including curves and tables in the paper, are based on even though this was unwittingly accomplished by the author. Hence, they approximate the true solutions to within the error of the foregoing assumption.

The procedure is of course exact for the case of maximum energy-release rates because in that case the concentration Equations [6*d*] apply throughout the mixture, under which condition $\psi = 1.00$, and the result for natural gas is that shown by Equation [30] for the conditions of Table 4. It is of interest to note in passing that such maximum time mean energy-release rates, of which Equation [30] is an example, may be obtained directly on the basis of the mean ordinate under the curve in Fig. 5, which represents the combustion progress of the case under consideration.

The foregoing approximation, that concentrations in the interzone be those of a uniform mixture even in the general case of the nonuniform condition for the mixture as a whole, may take far too much for granted. In principle this may be avoided simply by replacing concentration Equations [6*d*] with others which are correct in form for any case to be considered. In this procedure the general mathematical development, together with definitions and procedure, remains exactly as outlined in the paper, but certain details will be altered. In some cases, these altered details will be restricted entirely to changed values of certain constants appearing in a few of the equations. Such a development follows after considering Dwyer's assertion that the interzone concept has no benefits for the case of premix combustion.

The latter would be true if the premixing resulted in a perfect mixture, that is, a mixture in which the concentration zones have been so reduced in size as to be molecular in scale. The author can see no possible way of accomplishing this in the practically feasible dimensions of a mixing tube or furnace. For example, this cannot be accomplished by passing the mixture through shock fronts or fine-mesh screens. In both cases the fine-scale turbulence produced as the mixture passes through dies out very soon after leaving the front or screen, and the turbulence produced in this region is of such small amplitude that it cannot reach across the diameters of the approaching concentration zones. Therefore, it would seem that the concentration remain large compared to molecular dimensions even with considerable premix and turbulence. Hence, they are fundamental geometrical properties also in premix combustion and must be considered. It follows that the essential characteristics of the interzone must apply for both the premix and nonpremix combustion. The problem is thus to determine the proper concentration equations which replace set [6*d*] and which should thus apply to both the cases of premix and that of nonpremix combustion.

As an approach to this, consider now a system of fuel and air zones, each of which class of zones maintains its integrity with respect to its initial inert contents. This is a limiting case. While this integrity may be maintained in the early stages of the combustion progress, it is probable that in the later stages the inerts have been transferred by turbulence and diffusion between the two classes of zones. Hence, concentration Equations [6*d*] of the paper, which equations specify uniform distribution of inerts throughout the mixture, represent the opposite limiting condition. The true combustion-progress curve should lie between two such curves, one based upon concentration Equations [6*d*], and the other upon the concentration equations to be developed. In the latter stages of the combustion, Equations [6*d*] may represent the true facts in the case more closely than do those to follow. This of course depends upon the particular arrangements of the fuel gas and air flow of the case. Certainly the combustion equations contained in the following section are not applicable when arriving at the maximum possible energy release rates for the uniform mixture. These must be based upon concentration Equations [6*d*].

Concentrations in Fuel and Air Zones at Any Fraction Burned x, Based Upon Maintenance of Integrity as to Inerts

The inert molecules originally in air and fuel zones remain with their original class of zones throughout, the only interchange between zones being by molecules entering the reaction in the interzone. It is further assumed that the product molecules will pass into the fuel and air zones in proportion to the initial concentration of fuel and oxygen molecules in the respective zones. The symbols employed are defined as in the nomenclature at the beginning of the paper.

The initial concentration of fuel molecules in fuel zones is f, and that of oxygen molecules in air zones is 0.21.

When the fraction burned is x then $f \cdot x$ of the fuel molecules have been consumed, and the volume of fuel plus oxygen molecules taking part in the reaction has changed by the amount $x\,\Delta V$ in forming the product molecules. Then, on the basis of the foregoing assumption as to transfer of product molecules, the fraction $f/(f + 0.21)$ of this volume change is to be associated with the fuel zones, and the fraction $1 - f/(f + 0.21) = 0.21/(f + 0.21)$ with the air zones.

Hence, volume of fuel zones at fraction burned x is

$$1 + \frac{f \cdot x \cdot \Delta V}{(f + 0.21)} \text{ (cu ft/cu ft fuel gas)} \quad [57]$$

and that of air zones to be associated with these fuel zones is

$$yN + \frac{0.21x \cdot \Delta V}{(f + 0.21)} \text{ (cu ft/cu ft fuel gas)} \quad [58]$$

The volume of fuel constituents left when fraction burned is x is

$$(1 - x)f \text{ (cu ft/cu ft fuel gas)} \quad [59]$$

and volume of oxygen left is

$$0.21\ yN - 0.21\ Nx \text{ (cu ft/cu ft fuel gas)} \quad [60]$$

The concentration of fuel constituents in the fuel zones at burned fraction x now becomes

$$C_{1v} = \frac{\text{Equation [59]}}{\text{Equation [57]}} = \frac{(1-x)f}{1 + \dfrac{x \cdot f \cdot \Delta V}{f + 0.21}} \quad [61]$$

The concentration of oxygen in the air zones becomes

$$C_{2v} = \frac{\text{Equation [60]}}{\text{Equation [58]}} = \frac{0.21\ N(y-x)}{yN + \dfrac{0.21x \cdot \Delta V}{f + 0.21}} \quad [62]$$

Equations [61] and [62] would thus replace Equations [6*d*] in the development leading to the several equations in the paper which involve the concentrations C_{1v} and C_{2v}. It becomes obvious at once that this procedure will not alter the form of the resulting equations since the only variable is burned fraction x, and this enters both sets of equations, i.e., Equations [6*d*], [61], and [62] in exactly the same way.

It requires merely a redefining of the quantities β, but caution must be exercised in observing the origin of the β to be replaced, i.e., whether originally associated with C_{1v} or with C_{2v}.

Comparison of C_{1v} from Equations [6*d*] and C_{1v} from Equation [61] shows that with [61] included for C_{1v}

$$\beta = \beta_1 = 1/f\left((1 + \frac{x \cdot f \cdot \Delta V}{f + 0.21}\right) \quad [63]$$

and with Equation [62] included for C_{2v}

$$\beta = \beta_2 = 1/f\left(yN + \frac{0.21 \cdot x \cdot \Delta V}{f + 0.21}\right) \quad [64]$$

and

$$\beta^2 = \beta_1 . \beta_2 \quad [65]$$

The changes required to have the equations in the paper applicable are now outlined as follows:

Relations [1] through [6*c*] unchanged.
Relations [6*d*] replaced by [61] and [62].
Relations [7] and [8] unchanged.
Relation [9], $\beta^2 = \beta_1 . \beta_2$ from [65].
Relation [10] unchanged.
Relation [10*a*] $\beta^2 = \beta_1 . \beta_2$ from [65].
Relations [10*b*] through [11*a*] unchanged.
Relation [11*b*] replace β_0 by yN.
Relation [11*c*] replace $(2\beta_0 f)$ by $\left(\dfrac{0.21\ fyN}{f + 0.21}\right)$
Relation [11*d*] replace $(f . \Delta V)^2$ by $\dfrac{0.21\ f\Delta V^2}{(f + 0.21)^2}$

Relations [11*e*] through [24] unchanged, noting however in argument of second paragraph following Equation [15] that $Tx - T \cong 250\ F$ instead of 30 F.

Relation [25] value changes to 1.12×10^{-3}.
Relation [25*a*] value changes to 0.104.
Relation [26] $\beta = \beta_2$ from [64].
Relation [27] $\beta = \beta_2$ from [64].
Relation [27*a*] unchanged.
Relation [27*b*] $\beta = \beta_2$ from [64].

Relation [28] numerical coefficient changes from 2.89 to 2.79. Otherwise unchanged. This follows because in both cases total air and fuel are introduced in the same way with respect to each other, i.e., at entrance to furnace cavity.

Relation [29] $A_m \cong 5.0\ \text{ft}^2/\text{ft}^3$.

Relation [30] unchanged since Equations [6*d*] apply to maximum conditions.

Relation [30*a*] unchanged.
Relation [30*b*] $\beta = \beta_2$ from [64].
Relations [30*c*] through [30*f*] unchanged.
Relation [30*g*] replace β_0 by $y \cdot N$.
Relation [30*h*] replace ΔV by $1/f\left(\dfrac{0.21 \cdot \Delta V}{f + 0.21}\right)$

Relations [31] through [55] unchanged, noting that in arriving at [26] from [48*a*], C_{2v} is taken from [62], i.e., β in [26] is defined by [64].

Relation [56], coefficient 223, first term on left, is now 7, since A in [55] is now 5 instead of 28.2. This results in $Tx - T \cong 250$ deg F instead of 30 deg F.

Table 2. Values of $X = \Theta$ equal tabular values $x(yN/\beta^2)$ since effect of ΔV is negligible.

Figs. 3 and 5. Multiply abscissa $X = \Theta$ by value of (yN/β_0^2) for given y-curve.

Figs. 4 and 6. Multiply ordinate by $\beta^2/\beta_1 \cdot \beta_2 = 14.9$. It should be noted however that for Fig. 6, multiplying factor $(\chi/0.10)^3$ will not apply for arriving at maximum energy release rate as concentration Equations [61] and [62] do not apply. Equations [6*d*] only are applicable to the uniform mixture.

Thus, it is seen how the mathematical development contained in the paper may be adapted to apply to any given definable variation of concentrations of fuel and air along the combustion-progress path. If the modified equations and those contained in the paper are applied to a given fuel fired in a given furnace with given initial air-fuel ratio, with total air and fuel entering the front end in both cases, the two sets of results bound the field within which the real results should fall, provided all involved assumptions are within reasonable approximations of the true facts. One such assumption (constant energy-release rate, ΔH, per effective molecular collision) is objected to by Dwyer. To include the effect of a variable (ΔH) would require expressing it as a function of burned fraction x. It is recognized that, as the subject develops, such refinements may be introduced. Eventually, it may become possible to include also the effects of differences in the surface-volume ratios of air and fuel zones. The interface extension A is expressible in terms of either. Thus, it may be shown that

$$A = A_1/\beta_0 = A_2 yN/\beta_0 \quad [66]$$

where

A_1 = (surface/volume) of mean fuel zone
A_2 = (surface/volume) of mean air zone

Actually these values also will vary along the path. By means of them the following relation may be introduced in the analysis

$$n_2 = \left(\frac{A_2}{A_1}\right)^2 \left(\frac{1-\chi_2}{1-\chi_1}\right)\left(\frac{1-\zeta_1}{1-\zeta_2}\right)\frac{C_{2v}}{C_{1v}} \cdot \frac{D_{12}}{D_{21}} \quad [67]$$

thus furnishing an additional condition equation applicable to the equilibrium in the interzone. Introduction of these refinements into the analysis may be of advantage later.

Finally, the author wishes to take this opportunity to correct several misleading statements contained in the paper concerning information disclosed relative to Fig. 7. What this chart really shows is the relations which must necessarily exist between the co-ordinates there shown for any combustion progress path which might be assigned, provided of course that Equation [27*a*] and other involved assumptions hold.

The combustion-progress curves pass from left to right across the chart. One possible assumption is that the concentration

ratio χ and interzone depth ratios remain constant during combustion progress. In that case the curves on the chart are also combustion-progress curves. If this state of affairs actually existed, it would result in a decrease of interface extension with combustion progress. If this occurs, it is more likely the result of increasing temperature rather than because of a constant concentration ratio χ. Unfortunately, in discussing this the author mentioned early burning-out of small concentration zones in this connection. Although this effect exists, it had nothing to do with the analysis which led to the result, i.e., to Fig. 8. It appears highly probable that both concentration and interzone depth ratios change in the direction of combustion progress. Under such conditions, the true combustion-progress curve cuts across the curves shown on the chart from left to right. Of course, disclosure of the true state of affairs in such respects requires further investigation. For the present, it is important to note that charts of this type may be useful in the further study of the subject.

High-Output Combustion of Ethyl Alcohol and Air

By A. H. SHAPIRO,[1] D. RUSH,[2] W. A. REED,[3] D. G. JORDAN,[2] and G. FARNELL[4]

Test results, obtained under sponsorship of the Bureau of Ordnance, are reported for the combustion at 475 psia of air with a mixture of 92.5 per cent ethyl alcohol and 7.5 per cent water by mass. The exit-gas temperature was varied between 1350 F and 2050 F and was controlled through the introduction of excess fuel. A combustor design which gave combustion intensities up to 11 × 10^6 Btu/hr ft^3 atm was employed. The experimental relations between gas temperature, fuel-air ratio, isentropic enthalpy drop obtainable from the combustion gas, gas composition, and thermodynamic properties of the combustion gas are given in detail. Theoretical results based upon the assumption of chemical equilibrium at the temperature of adiabatic combustion are in moderately good agreement with the measured results. It is inferred from the data that a condition approximating "frozen" equilibrium sets in at about 2500 F. Two methods of evaluating isentropic enthalpy drop were used and compared, one based principally upon the measurement of thrust, and the other based principally upon gas analyses. Small variations in combustor size and design were investigated. A discussion of the principles underlying the thrust method is given in an Appendix.

Introduction

THE work reported herein was initiated by the Navy Department, Bureau of Ordnance, and was carried out during 1944 and 1945 at the Massachusetts Institute of Technology under the sponsorship first of the Office of Scientific Research and Development and later of the Bureau of Ordnance.

Thermodynamic System. The particular system under investigation employs air as an oxidant, and for fuel, a mixture of 92.5 per cent ethyl alcohol and 7.5 per cent water (by mass). For convenience, this mixture will henceforth be called fuel. The stoichiometric fuel-air ratio for this mixture is 0.120.

Unlike most combustion systems, the requirements in this case were such that the exit temperature was controlled through the supply of excess fuel, rather than through the more common practice of supplying excess air.

In these experiments the total rate at which gas was generated was about 0.7 lb per sec, the combustor pressure was about 475 psia, and the exit-gas temperature was varied between 1350 F and 2050 F.

Object. The general objectives were as follows:

1 To develop and compare test procedures.

2 To determine the thermodynamic characteristics of the fuel-air system, and to compare the measured results with theoretical results based upon the assumption of chemical equilibrium at the temperature of adiabatic combustion.

3 To determine the effects of combustor design on item 2.

Evaluation of Performance. From a thermodynamic viewpoint, the fuel-air system and the combustor design are here judged on the basis of the maximum amount of work which could be extracted in an engine from the generated gases. The measure of effectiveness is taken to be the isentropic enthalpy drop of the generated gas for an isentropic expansion from the measured temperature and a pressure of 475 psia to a pressure of 14.7 psia. Two methods of estimating the isentropic enthalpy drop are employed, as follows:

1 Through measurements of the total flow rate of reactants and of the reaction thrust from a nozzle through which the gases are discharged (reaction-stand method).

2 Through measurements of gas composition, exit-gas temperature, and flow rates of the individual reactants, together with the use of published data on the specific heats of the constituent gases (gas-analysis method).

Apparatus

Combustor. Fig. 1 shows the design of the combustor, while Fig. 2 shows the details of the fuel atomizer.

It will be noticed that the regenerative principle is used, with the fuel flowing in a jacket countercurrently to the combustion gas. This scheme permits a thin inner shell of high-temperature alloy to be used with an outer shell whose function is merely to withstand pressure differences. Temperature measurements made after the combustors had been fabricated indicated that the outer shell could well have been made of a low-temperature material, e.g., aluminum.

After passing through a metering orifice, the fuel is distributed from a manifold into the annular cooling jacket via eight ports in the shell. After collection in a manifold at the upstream end of the combustor, the fuel is delivered through an external tube to the atomizer. Two thirds of the fuel passes through eight injection tubes arranged around the circumference of the atomizer, while one third passes through a relatively large central tube. The fuel streams are atomized by streams of high-velocity primary air which flow parallel to the liquid streams. This type of dispersion and mixing is called air atomization and is effected through the shearing action of a high-velocity air stream on a low-velocity liquid stream.

About two thirds of the air supply is used for atomization (primary air). The remaining one third (secondary air) passes through four metering orifices and thence at low velocity through a double distributing baffle into the combustion space. The function of the secondary air is to provide a region of low-velocity air which produces a pilot flame to stabilize burning in the core of the combustion space. Without secondary air it is difficult to obtain stable combustion.

The important ratios and velocities for average conditions of operation are given in Table 1.

[1] Associate Professor of Mechanical Engineering, Massachusetts Institute of Technology, Cambridge, Mass. Mem. ASME.

[2] Formerly Division of Industrial Cooperation, Massachusetts Institute of Teconology.

[3] Research Associate, Department of Chemical Engineering, Massachusetts Institute of Technology.

[4] Formerly, Division of Industrial Cooperation, Massachusetts Institute of Technology, now with Ingersoll-Rand Company, Phillipsburg, N. J. Jun. ASME.

Contributed by the Fuels Division and presented at the Annual Meeting, Atlantic City, N. J., December 1–5, 1947, of The American Society of Mechanical Engineers.

 Paper No. 47—A-25.

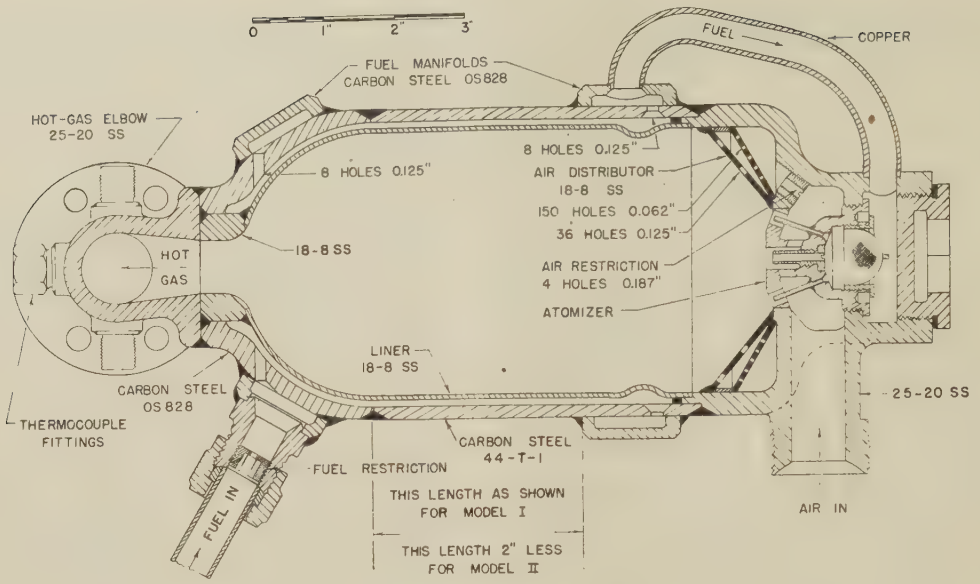

FIG. 1 SCALE DRAWING OF MODEL I COMBUSTOR

(Model II combustor is identical except that cylindrical mid-section is 2 in. shorter.)

TABLE 1 RATIOS AND VELOCITIES FOR AVERAGE OPERATING CONDITIONS

Fuel jets:	
Flow to central jet, per cent	33
Flow to side jets, per cent	67
Velocity leaving atomizer, fps	34
Primary-air jets:	
Flow to central jet, per cent	25
Flow to side jets, per cent	75
Velocity leaving atomizer, fps	77
Secondary-air jets:	
Velocity entering combustor, fps	19
Total air:	
Flow to primary jets, per cent	66
Flow to secondary jets, per cent	34

It may be noted that the fuel-air ratio for the side jets is about 50 per cent smaller than for the central jet. Therefore the side jets tend to atomize more rapidly, and, since fuel is in excess, to produce a relatively short high-temperature flame. The central jet, on the other hand, tends to atomize more slowly and in coarser fashion, and probably furnishes the major fraction of diluent fuel.

Two sizes of combustor were used having internal volumes of 76 and 56 cu in., respectively. The larger, called Model I, is shown to scale in Fig. 1. The smaller, called Model II, is similar except that the cylindrical portion is 2 in. shorter than in the Model I combustor.

An additional volume for combustion of about 8 cu in. was supplied by the hot-gas pipe connecting the combustor and thrust nozzle. This pipe was 1 in. ID, 10 in. long, and had one 45-deg bend.

Flow Systems. Because of the large flow rate, continuous operation was not practicable. Therefore air was stored in a bottle of 6 cu ft capacity at 3000 psi and was supplied to the combustor through a regulating valve. Fuel was stored in a tank and pumped to the combustor by means of high-pressure air acting on top of the fuel in the tank. The flow rate of fuel was controlled by the pressure of the displacing air and also by a metering orifice in the combustor. With this system, runs of 3 min duration were possible.

The gas generated by the combustor passed directly to the thrust nozzle by way of the hot-gas pipe, and thence to the atmosphere.

Thrust System. The combustor and hot-gas pipe were fastened inside a cubical steel tank (*E*, Fig. 3) while the thrust nozzle (*A*, Fig. 3; *A*, Fig. 4) was fastened to the outside of the tank.

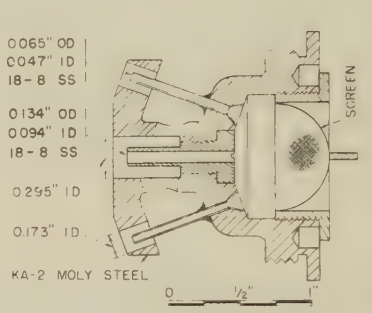

FIG. 2 SCALE DRAWING OF FUEL ATOMIZER

Three flexible-wire cables (*D*, Fig. 3), each 72 in. long, were used for suspending the tank from the ceiling.

To counterbalance moments on the tank caused by slight misalignments of the jet, the front and back ends of the tank were fastened to constraining wires (*H*, Fig. 3) which were aligned in tension in a direction normal to the axis of the jet.

The air and fuel pipes (*C*, Fig. 3) were rigidly fastened to the side of the tank, with their axes perpendicular to that of the thrust nozzle, so that no momentum effects were associated with the incoming streams. Furthermore, these pipes were made as flexible as possible.

A lever system (*J*, Fig. 3) with instrument-type ball bearings, transmitted the nozzle thrust to a Toledo scale (*K*, Fig. 3). A captive free-rolling ball (*L*, Fig. 3) at the end of the lever system permitted free motion of the scale platform.

A calibration system using known weights was employed for determining directly the ratio between thrust force and scale reading.

Differences between the lever-arm ratio and the actual ratio by calibration of thrust force to scale reading might be accounted for by the following:

1 Bearing friction.
2 Resistance of constraining wires to motion of tank.
3 Resistance of piping to motion of tank.
4 Horizontal components in suspension cables of gravity force on tank.

Frictional effects were not detectable, using the customary as-

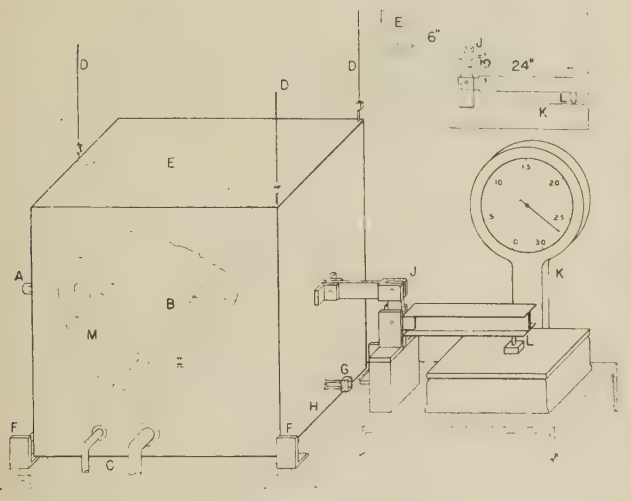

FIG. 3 REACTION STAND

(*A*, thrust nozzle; *B*, combustor; *C*, inlet-air and fuel pipes: *D*, suspension cables; *E*, tank; *F*, fixed terminals for constraining wires; *G*, fastening between tank and constraining wire; *H*, constraining wires, on both sides of tank; *J*, lever system; *K*, Toledo scale; *L*, free-rolling captive ball; *M*, hot-gas pipe.)

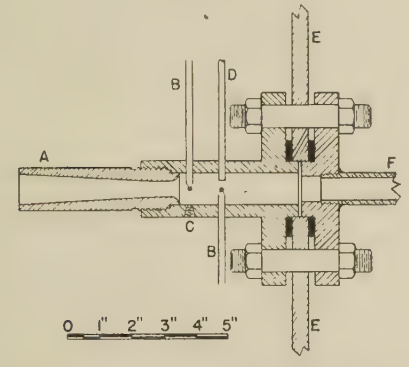

FIG. 4 THRUST NOZZLE AND INSTRUMENTATION

(*A*, thrust nozzle, 0.445-in-diam throat, 0.890-in-diam exit, 6-deg included angle in diverging cone; *B*, thermocouple probes, three in all; *C*, static pressure tap; *D*, gas-sampling tube; *E*, tank wall; *F*, hot-gas pipe.)

cending and descending calibrations. Items 2 to 4 are proportional to the motion of the tank. Through careful design, this motion was kept to about 0.030 in. In any event, the direct calibration under operating conditions eliminated errors due to items 2, 3, and 4. With a lever-arm ratio of 8.003, the calibration ratio was found to be 8.08, and was reproducible to about 0.1 per cent.

The thrust nozzle, Fig. 4, had an area ratio of 4 and a total included angle of 6 deg in the divergent portion. In the Appendix is a discussion of the reasoning underlying the choice of area ratio for this nozzle.

Gas Analysis. A gas sample was drawn continuously through a stainless-steel tube from a location just upstream of the thrust nozzle (*D*, Fig. 4). Since the temperature was found to be uniform at this section, it seems fair to assume that the gas composition was also uniform and that a representative sample was drawn. The rate of sampling was of the order of 0.01 per cent of the total flow rate.

After having condensables removed at —70 C, the dry sample was analyzed over mercury in a precision Orsat apparatus. Facilities were present for measuring directly carbon dioxide, unsaturated hydrocarbons, oxygen, carbon monoxide, hydrogen, methane, ethane, and, by the remainder method, nitrogen.

In order to estimate the amounts of water, ethyl alcohol, and free carbon in the exit gas, it was first assumed that (*a*) aldehydes were absent (confirmed by absence of characteristic odors) and (*b*) unsaturated hydrocarbons were in the form of ethylene. A nitrogen balance on the incoming and outgoing materials was then employed for relating the amounts of incoming air and fuel to the amount of each component in the dry-gas analysis. The introduction of three equations representing carbon, hydrogen, and oxygen balances, respectively, then permitted a solution for the proportions of three unknown components, namely, water, ethyl alcohol, and free carbon.

Instrumentation. The rate of air flow was found to about 0.5 per cent accuracy from simultaneous photographs, at intervals of 5 sec, of a clock and of a Toledo scale on which the air-storage bottle was flexibly mounted.

The thrust force was obtained to about 0.75 per cent accuracy, using the measuring system described previously.

The combustor pressure was measured to about 0.5 per cent accuracy directly upstream of the thrust nozzle (*C*, Fig. 4) with a calibrated Bourdon gage.

The temperature of the exit gas leaving the combustor was measured just upstream of the thrust nozzle (*B*, Fig. 4) by means of three chromel-alumel thermocouples connected to Brown automatically balancing electronic potentiometers. Special precautions were necessary to avoid radiation errors. Fortunately, the flow near the thermocouple beads was at high pressure and high velocity. Because of space limitations, radiation shields were impracticable and the problem of radiation was solved by using bare thermocouples of small size. By comparing the readings of thermocouples of different wire size but at symmetrical locations in the same cross section it was found that, under the test conditions, the use of wires as small as 14 gage would make radiation errors negligible. For the most part the thermocouples were made either of 14 or 20-gage wire. Comparisons of the readings of thermocouples of identical construction and located at different radii of the same cross section showed that variations in temperature across the stream were less than the errors of measurement. Variations between the temperature indications of the three thermocouples were of the order of 10 to 20 F. It is estimated that the reported temperatures, based upon an average of the three probes, have a probable error of about 10 F and a maximum error of 20 F.

The temperature of the air entering the combustor was found with a copper-constantan thermocouple.

The temperature of the fuel leaving the cooling jacket and entering the atomizer was found with a chromel-alumel thermocouple placed directly in the stream of fuel entering the head of the combustor.

All instruments were frequently calibrated. Readings were taken at 5-sec intervals and were carefully averaged. The data for the initial "warm-up" portion of the run were excluded from the results.

DEFINITIONS AND REDUCTION OF DATA

Fuel-Air Ratio. The ratio of mass rate of flow of fuel to that of air, where fuel is defined as a mixture of 92.5 per cent ethyl alcohol and 7.5 per cent water, by mass.

Exit-Gas Temperature. The average temperature recorded by three thermocouples located downstream of the combustor and just upstream of the thrust nozzle (Fig. 4).

Jet Kinetic Energy, Based on Thrust. The value of $V^2/2g_0$, where g_0 is the standard acceleration of gravity, and V is the exit velocity from the nozzle when the latter is supplied with gas at 475 psia, and the nozzle area ratio is such that the nozzle exit-plane pressure is 14.7 psia.

To find the velocity V for the measured nozzle pressure, we write

$$F = wV/g_0 \quad [1]$$

where F denotes the nozzle thrust force and w the mass rate of flow of reactants (fuel and air). In the Appendix is a justification for the use of this equation when the exit-plane pressure is not atmospheric. With this expression we obtain for the uncorrected jet kinetic energy

$$V^2/2g_0 = \frac{g_0}{2}\left(\frac{F}{w}\right)^2 \quad [2]$$

All reported values of jet kinetic energy were corrected to a pressure of 475 psia by assuming that $V^2/2g_0$ is very nearly the isentropic enthalpy drop, and that the latter is affected by pressure (for a fixed gas temperature) in proportion to the quantity (1)[5]

$$1 - \left(\frac{14.7}{p_o}\right)^{\frac{k-1}{k}}$$

This correction factor, which produced not more than a 1 per cent change, was applied to the previously computed values of jet kinetic energy to obtain the values reported here. The ratio of specific heats k, was for this purpose assumed to be 1.275.

Gas Composition. This is described in terms of the number of mols of each constituent of the generated gas in a sample which contains 100 mols of components in the gas phase, i.e., it is the molal percentage in a carbon-free sample.

Molecular Weight. This is the average molecular weight of the generated gas, not including free carbon or unevaporated liquid. It is computed with the expression (2)

$$M_g = \Sigma n_i M_i / \Sigma n_i \quad [3]$$

where M_g is the average molecular weight, M_i the molecular weight of a gaseous component, and n_i the number of mols of that component.

Average Specific Heat for Isentropic Expansion. This is the average specific heat at constant pressure of the combustion gas over the temperature range given by isentropic expansion from 475 psia and the measured gas temperature to a pressure of 14.7 psia. It is found from the expression (3)

$$\bar{c}_p = \Sigma n_i M_i \bar{c}_{pi} / \Sigma n_i M_i \quad [4]$$

where $\bar{c}_p$ is the average specific heat per unit mass of generated gas, and $\bar{c}_{pi}$ is the average specific heat per unit mass of a gaseous constituent over the temperature range described.

To simplify the computations without appreciable sacrifice of accuracy, the values of $\bar{c}_{pi}$ were selected at the arithmetic mean of the temperatures before and after isentropic expansion.

The values of $\bar{c}_{pi}$ were taken from references (4) through (11).

Isentropic Enthalpy Drop, Based on Gas Analysis. The change in enthalpy per unit mass of reactants for an isentropic expansion from 475 psia and the measured gas temperature to a pressure of 14.7 psia. It is found from the expression (1)

$$(\Delta h)_s = \frac{c'_{pg} T_0 \left[1 - (14.7/475)^{R^0/M_g c''_{pg}}\right]}{1 + \frac{n_c}{n_g}\frac{M_c}{M_g}} \quad [5]$$

where $(\Delta h)_s$ is the isentropic enthalpy drop per unit mass of reactants; n and M denote number of mols and molecular weight, respectively; the subscripts c and g denote free carbon and gas, respectively, in the exhaust stream; R^0 is the universal gas constant; and T_0 is the measured gas temperature. Furthermore

$$c_{pg}' = \frac{\int_{T_0}^{T_1} c_{pg}\, dT}{T_1 - T_0} \quad [6a]$$

$$c''_{pg} = \frac{\int_{T_0}^{T_1} c_{pg}\, d(\ln T)}{\ln T_1/T_0} \quad [6b]$$

where T_0 and T_1 are the upper and lower temperature limits, respectively, of the isentropic expansion, and c_{pg} is the average specific heat of the gas phase at the local temperature, T. We compute c_{pg} from the relation

$$c_{pg} = \Sigma n_i M_i c_{pi} / \Sigma n_i M_i \quad [7]$$

where c_{pi} is the local specific heat at temperature T of each constituent.

References (4) through (11) were used for obtaining the values of c_{pi}.

Exit Temperature From Energy Balance. Using the first law of thermodynamics, we may compute the exit-gas temperature from measurements of the incoming reactants and the outgoing products, as in Equation [8]

$$t_g - t^* = \frac{[n_A h^*_A + n_B h_B{}^* + \ldots] + [n_A \bar{c}_{pA}(t_A - t^*) + n_B \bar{c}_{pB}(t_B - t^*) + \ldots] - [n_R h^*_R + n_S h^*_S + \ldots] - [n_R + n_S + \ldots]Q}{[n_R \bar{c}_{pR} + n_S \bar{c}_{pS} \ldots]} \quad [8]$$

where t_g denotes the computed gas temperature, t^* an arbitrary base temperature, n the number of mols, h^* the heat of formation per mol at temperature t^*, $\bar{c}_p$ the average specific heat with respect to temperature over the range from t^* to t_g, Q the heat loss from the combustor per mol of generated gas, and A, B, etc., denote species entering the combustor while R, S, etc., denote species leaving the combustor.

Heats of formation were taken from reference (12), specific heats from references (4) through (11) and Q, which was relatively small, was estimated from simple heat-transfer considerations.

Results

Jet Kinetic Energy and Isentropic Enthalpy Drop. Referring to Fig. 5, we see that the curves of jet kinetic energy and of isentropic enthalpy drop versus temperature lie very close to each other, the isentropic enthalpy drop being about 4.5 per cent greater than the jet kinetic energy. This difference is the consequence principally of friction in the thrust nozzle, together with other effects to be discussed later.

Both curves vary approximately linearly with the absolute gas temperature, indicating that the gas may as a first approximation be treated with the perfect-gas laws. For temperatures below 1800 F, the increase in $(\Delta h)_s$ with temperature is more rapid than would be indicated by the perfect-gas laws, while for greater temperatures the rate of increase is less than that corresponding to the perfect-gas laws. It is evident that operation with high gas temperatures is of advantage from a thermodynamic standpoint.

Gas Composition. Fig. 6(*a*) indicates that the constituent gases may be divided into two groups; (*a*) those whose molal percentages are virtually independent of gas temperature, and (*b*) a group comprising only ethyl alcohol and nitrogen, whose molal percentages depend seriously upon temperature. The proportion of alcohol decreases from 10 per cent to 0 per cent as the

[5] Numbers in parentheses refer to the Bibliography at the end of the paper.

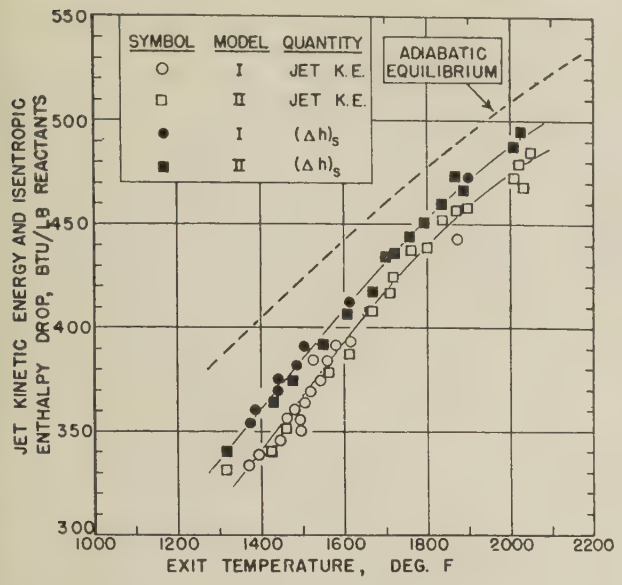

FIG. 5 JET KINETIC ENERGY VERSUS EXIT-GAS TEMPERATURE. ISENTROPIC ENTHALPY DROP $(\Delta h)_s$ VERSUS EXIT-GAS TEMPERATURE

(The jet kinetic energy is based upon the measured thrust and flow rate The isentropic enthalpy drop is based upon the measured gas composition, measured exit-gas temperature, measured flow rates of reactants, and on published specific-heat data. Dashed curve represents theoretical results corresponding to chemical equilibrium at temperature of adiabatic combustion.)

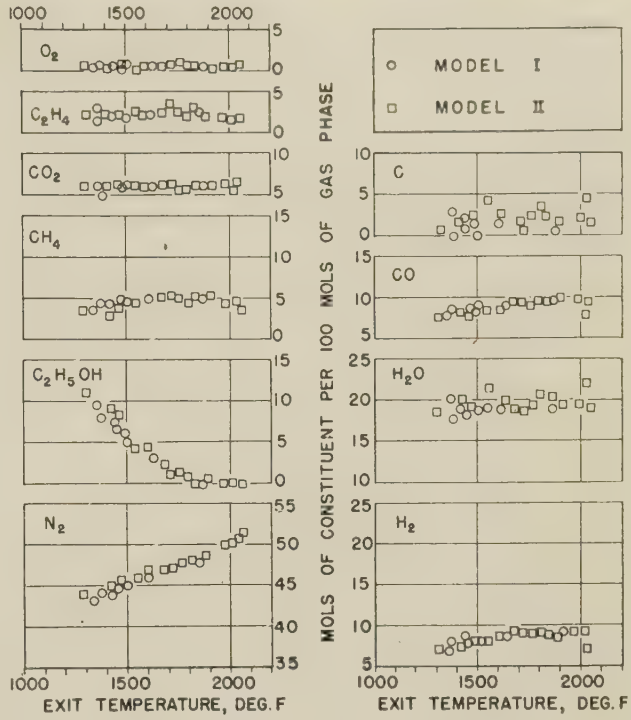

FIG. 6(*a*) MEASURED GAS COMPOSITION VERSUS EXIT-GAS TEMPERATURE

temperature is changed from 1350 F to 2050 F, while for the same temperature variation, nitrogen increases from 44 per cent to 51 per cent. Surprisingly, the amount of water vapor is nearly constant.

These results are in qualitative accord with the theory that at high temperatures chemical equilibrium subsists among the various components, but that at lower temperatures, say, below 2500 F, the reaction rate is so small that the reaction is virtually "frozen," i.e., no further chemical reactions occur. If this description truly represented the state of affairs, we would expect that all alcohol injected at high temperatures would either burn with oxygen or would be decomposed into simpler compounds. After enough alcohol had been introduced to reduce the temperature to the "freezing" condition, additional alcohol injected would merely evaporate without decomposition and without causing a change in the relative proportions of the other constituents.

Several of the constituents, namely, ethane, ethylene, methane, oxygen, and free carbon, are present in amounts less than 5 per cent. The principal components are therefore nitrogen, water, hydrogen, carbon monoxide, ethyl alcohol, and carbon dioxide, named in the order of decreasing magnitude.

The amount of oxygen in the generated gas is so small as to indicate the combustor to be satisfactory in the utilization of the scarcest ingredient of the reaction.

Nitrogen comprises nearly one half of the entire amount of generated gas. It is about as effective as the excess fuel with respect to the dilution and reduction in temperature of the gas.

Fuel-Air Ratio. Fig. 7(*a*) shows that in the range of these tests the curve of fuel-air ratio versus temperature is almost a straight line, with the fuel-air ratio changing from 0.65 to 0.32 for an increase in gas temperature from 1350 F to 2050 F.

These figures may be compared with the temperature of adiabatic combustion of about 3500 F for chemical equilibrium at the stoichiometric fuel-air ratio of 0.12.

Fig. 7(*b*) shows a comparison between the curve representing

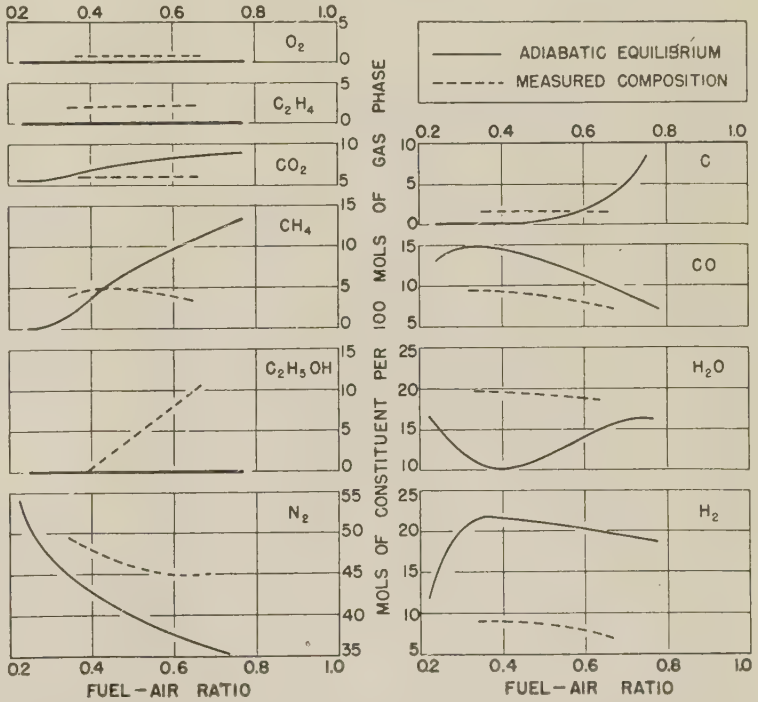

FIG. 6(*b*) GAS COMPOSITION VERSUS FUEL-AIR RATIO

(Comparison between measured results and theoretical results corresponding to chemical equilibrium at temperature of adiabatic combustion. Dashed curve represents average measured results found by combining data in Fig. 6(*a*) with "average curve" in Fig. 7(*a*).)

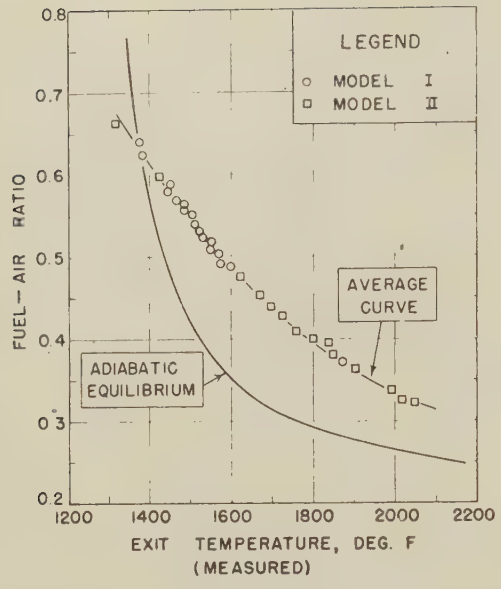

FIG. 7(*a*) FUEL-AIR RATIO VERSUS EXIT-GAS TEMPERATURE

[Comparison between measured results (plotted points, together with average curve) and theoretical results corresponding to chemical equilibrium at temperature of adiabatic combustion.]

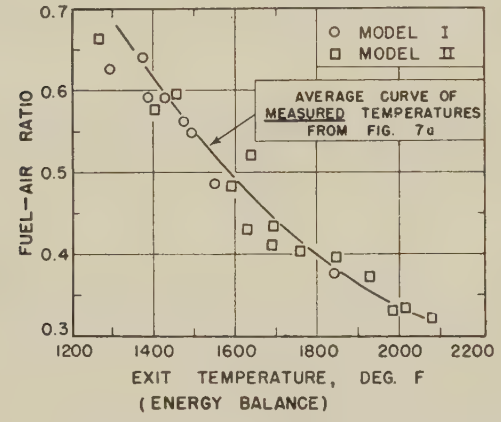

FIG. 7(*b*) FUEL-AIR RATIO VERSUS EXIT-GAS TEMPERATURE

[Comparison between measured exit-gas temperature (curve) and temperature computed from energy balance (plotted points).]

the measured results of Fig. 7(*a*), and the gas temperature computed from the gas composition and the first law of thermodynamics. This comparison provides a severe check on the reliability of the gas analyses, since, because the computed gas temperature involves the taking of small differences between large numbers, slight errors in gas composition may be reflected as very large errors in the calculated gas temperature. Taking this into consideration, the results seem very satisfactory, as Fig. 7(*b*) shows the maximum deviation in the calculated temperature to be less than 100 deg F, while the average deviation is only 40 deg F in the absolute sense and —20 deg F in the algebraic sense.

Thermodynamic Properties of Combustion Gas. From Fig. 8 we see that the molecular weight is diminished from about 27 to 24 as the gas temperature is increased from 1300 F to 1900 F. Further increases in temperature appear to produce a slight but noticeable increase in molecular weight.

The large change in molecular weight in the range of moderate temperatures is the consequence principally of a large reduction in the proportion of alcohol vapor, since the latter is the constituent with the greatest molecular weight.

The average specific heat for isentropic expansion, according to Fig. 9, is reduced as the gas temperature is increased. This change may be thought of as the algebraic sum of two opposing effects. On the one hand we have a decrease in the percentage of alcohol, the constituent with the greatest specific heat. On the other hand, we observe that all the constituent gases have specific heats which increase with temperature, so that, the composition remaining unchanged, the average specific heat would change in the same direction as the temperature. It appears from Fig. 9 that the first of these effects is the stronger.

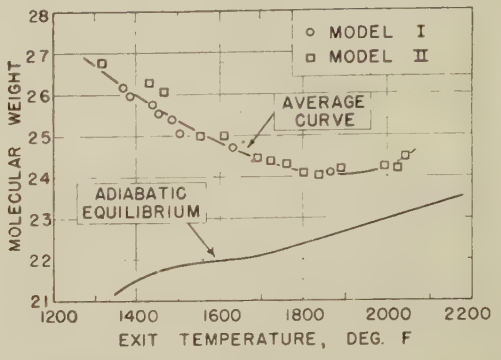

FIG. 8 AVERAGE MOLECULAR WEIGHT OF GAS PHASE VERSUS EXIT-GAS TEMPERATURE

[Comparison between measured results (plotted points and average curve) and results corresponding to chemical equilibrium at temperature of adiabatic combustion.]

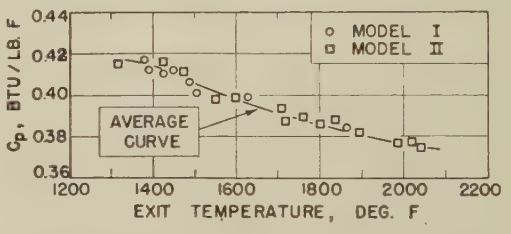

FIG. 9 AVERAGE SPECIFIC HEAT AT CONSTANT PRESSURE FOR ISENTROPIC EXPANSION VERSUS EXIT-GAS TEMPERATURE

In Table 2 the molecular weight and average specific heat for isentropic expansion are summarized for three temperatures, together with the corresponding ratio of specific heats, $\bar{k}$, where

TABLE 2 ISENTROPIC EXPANSION DATA

Temperature, deg F.....	1350	1700	2050
Molecular weight.....	26.8	24.9	24.7
$\bar{c}_p$, Btu/lb F.....	0.416	0.391	0.374
$\bar{k}$.....	1.22	1.26	1.27

$$\frac{1}{\bar{k}} = 1 - \frac{R^0}{M\bar{c}_p} \quad \ldots\ldots [9]$$

Equation [5] may be rewritten approximately as

$$(\Delta h)_s \cong \bar{c}_p T[1 - (14.7/475)^{(k-1)/k}] \quad \ldots\ldots [10]$$

Therefore the slope of the curve of $(\Delta h)_s$ versus T is increased by an increase in either $\bar{c}_p$ or $\bar{k}$. With this in mind it is easy to see how the data in Table 2 are reflected in the results of Fig. 5.

Comparison Between Results Based on Nozzle Thrust and Results Based on Gas Analysis. Systematic differences between the jet kinetic energy and the isentropic enthalpy drop, assuming the measurements are reliable, may be attributed to (*a*) nozzle friction, (*b*) errors in data on specific heats, and (*c*) unevaporated

liquid in the gas stream. Of these, nozzle friction is probably the most influential.

In the Appendix it is shown through a comparison of the measured thrust with the thrust for a frictionless nozzle that the effect of nozzle friction in these tests was to reduce the jet kinetic energy by 4.8 per cent. If no other effects were present this figure would represent the difference between the isentropic enthalpy drop and the jet kinetic energy. Since the average difference between these quantities, from Fig. 5, is about 4.5 per cent, it seems fair to conclude that in the present tests the net effects of errors in specific heats and of unevaporated liquid are negligible.

From a more general viewpoint we may enumerate the advantages and disadvantages of the thrust method as follows:

(*a*) Operation is virtually trouble-free when once the equipment has been set up and calibrated.

(*b*) Interpretation of results is dependent upon nozzle design and nozzle friction.

(*c*) Despite (*b*), good accuracy is usually obtainable.

The gas-analysis method, on the other hand, may be appraised as follows:

(*a*) Operation has many pitfalls and requires considerable skill.

(*b*) Unevaporated liquid in gas stream cannot easily be discovered or taken account of.

(*c*) Representative sampling sometimes may be difficult.

(*d*) Chemical reactions may proceed in sampling line.

(*e*) Results are subject to errors in specific-heat data.

(*f*) Results provide an insight into the mechanism of the process.

In the tests reported here it is felt that the two methods were equally reliable. In general, the methods may be regarded as complementary to each other.

Comparison Between Measured Results and Results Based on Assumption of Chemical Equilibrium at Temperature of Adiabatic Combustion. The theoretical computations of Goff (13) for the fuel-air system of these tests were made for entering air and fuel conditions which approximate closely those of this report. In Figs. 5, 6(*b*), 7(*a*), and 8, the curves representing these theoretical results are compared with average curves representing the experimental results.

We see from Fig. 6(*b*) that the agreement as to gas composition is fairly good in the case of ethylene, nitrogen, oxygen, carbon dioxide, and free carbon, particularly at low fuel-air ratios (or high temperatures). Deviations of about twofold exist, however, in the proportions of methane, ethyl alcohol, hydrogen, carbon monoxide, and water. The agreement is better at high than at low temperatures. Extrapolation of the curves seems to indicate that the agreement would be quite good in all respects at a fuel-air ratio corresponding to a gas temperature of 2500 F. These considerations are in accord with the concept of frozen equilibrium and seem to indicate that in these tests the freezing temperature was in the neighborhood of 2500 F.

Fig. 8 shows that the deviation in the theoretical molecular weight is about 10 per cent in the range of these tests. Here again, the agreement is relatively better at high temperatures, with an indication that near 2500 F the difference would be very small.

From Fig. 7(*a*) we see that the assumption of chemical equilibrium leads to poor results with respect to a prediction of the gas temperature corresponding to a given fuel-air ratio. The large discrepancy in temperature is accounted for by the fact that even small errors in the estimated gas composition can, by virtue of the large heats of formation of most of the components, act to alter the theoretical temperature by relatively large amounts. A curious consequence of this is illustrated in Fig. 7(*a*), where we find that the agreement in fuel-air ratio is best at low temperatures, contrary to the fact that the agreement in gas composition is best at high temperatures.

According to Fig. 5, the assumption of chemical equilibrium leads to an error in the isentropic enthalpy drop of 13 per cent at a gas temperature of 1350 F, while for a temperature of 2050 F the error is only 4 per cent. It seems reasonable to suppose that at higher temperatures the error would be further reduced and might in fact be negligible.

Temperature of Fuel at Atomizer. It is interesting to note from Fig. 10 that the fuel leaving the cooling jacket remained

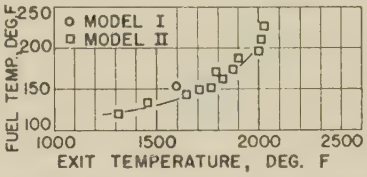

Fig. 10 Fuel Temperature at Entrance to Atomizer Versus Exit-Gas Temperature

below 250 F even for exit-gas temperature greater than 2000 F. It appears that with this design there is little danger of boiling and vapor-binding in the jacket,[6] and, moreover, that a low-temperature metal would be adequate for the outside shell.

Effect of Combustor Size. By comparing the results for the Model I and Model II combustors, as shown in Figs. 5, 6(*a*), 7(*a*), 8, and 9, it is evident that for the flow rates of these tests the two sizes of combustor produce equivalent results. Except for heat-loss effects, therefore, an increase in combustor size, it seems reasonable to suppose, would not have an appreciable effect on performance. Decreases in size would necessarily lead ultimately to adverse effects on thermodynamic performance.

Based upon the total amount of ethyl alcohol used in these tests, the Model II combustor had a combustion intensity at 1500 F of the order of 11×10^6 Btu/hr ft^3 atm. On the basis of the amount of ethyl alcohol which could be oxidized by the oxygen present, the combustion intensity was about 2.4×10^6 Btu/hr ft^3 atm. Because of the necessity for vaporization and decomposition of most of the excess fuel, the first figure is perhaps more nearly representative of the performance. Table 3 compares these figures with representative results for other types of combustors (14).

Effect of Combustor Design. A number of variations in combustor design were tested, the combustion volume in all cases being about the same as for the Model I combustor of the tests reported herein.

The effects investigated included the following:

1 The use of air atomization with the fuel injected at right angles rather than parallel to the air stream.

TABLE 3 COMPARISON BETWEEN VARIOUS COMBUSTOR TYPES

Combustor	Combustion intensity, Btu/hr ft^3 atm
Model II of present tests, at 1500 F (total alcohol)	11×10^6
Model II of present test, at 1500 F (stoichiometric alcohol)	2.4×10^6
Bunsen flame	1.3×10^6
Oil-fired boilers	$0.036 - 0.18 \times 10^6$
Four-stroke aircraft engine	4×10^6
German V-1 engine	1.8×10^6
Cordite rocket	8.3×10^6
German V-2 rocket	11×10^6
Aircraft turbojet engines	$1.5 - 4 \times 10^6$
Elliott marine gas-turbine (reference 18)	0.4×10^6

[6] At 475 psia the boiling temperature of ethyl alcohol is about 400 F.

2 The use of pressure atomization with a whirl-type spray.

3 The introduction of the fuel in two streams, one stream near the entrance to the combustor and the other stream, comprising diluent fuel, near the middle of the combustor.

4 The introduction of a baffle near the middle of the combustion volume.

5 The introduction of all the air through the atomizer.

The effects of items 1 through 4 were either imperceptible or of minor significance with respect to thermodynamic performance. As to item 5, it was not possible to maintain stable combustion without the introduction of secondary air at low velocity around the main stream of air and atomized fuel.

Acknowledgment

The authors gratefully acknowledge the assistance and cooperation provided them by the Bureau of Ordnance, Navy Department, by the OSRD, and by Dr. H. S. Mickley and Mr. C. S. Hofmann of the Massachusetts Institute of Technology.

BIBLIOGRAPHY

1 "Thermodynamics," by J. H. Keenan, John Wiley & Sons, Inc., New York, N. Y., 1941, p. 102.

2 Ibid., p. 204.

3 Ibid., p. 206.

4 H. L. Johnston and C. O. Davis, *Journal of the American Chemical Society*, vol. 56, 1934, p. 271 (data on CO and N_2).

5 L. S. Kassel, *Journal of the American Chemical Society*, vol. 56, 1934, p. 1838 (data on CO_2).

6 C. O. Davis and H. L. Johnston, *Journal of the American Chemical Society*, vol. 56, 1934, p. 1045 (data on H_2).

7 A. R. Gordon, *Journal of Chemical Physics*, vol. 2, 1934, pp. 65 and 549, (data on H_2O).

8 G. von Elbe and B. Lewis, *Journal of the American Chemical Society*, vol. 55, 1933, p. 507 (data on O_2).

9 D. R. Stull and F. D. Mayfield, *Industrial and Engineering Chemistry*, vol. 35, 1943, p. 639 (data on CH_4,C_2H_4 and C_2H_6).

10 "Handbook of Chemistry and Physics," twenty-third edition, Chemical Rubber Company, Cleveland, Ohio, 1939, p. 1358 (data on C).

11 "Empirical Heat Capacity Equations of Gases," by H. M. Spencer and G. M. Flannagan, *Journal of the American Chemical Society*, vol. 64, 1942, p. 2511 (data on C_2H_5OH).

12 "Thermochemistry of Chemical Substances," by F. R. Bichowsky and F. D. Rossini, Reinhold Publishing Corporation, New York, N. Y., 1936.

13 "Thermodynamic Analysis of the Combustion of Ethyl Alcohol," by J. H. Goff, OSRD Report No. 6.1-sr 1131–1847, Sept. 18, 1944.

14 "Combustion in the Gas Turbine," by Peter Lloyd, from *Lectures on the Development of the Internal Combustion Turbine*, Proceedings of The Institution of Mechanical Engineers, 1945, vol. 153 (War Emergency Issue No. 12), p. 463.

15 "Principles of Engineering Thermodynamics," by P. J. Kiefer and M. C. Stuart, John Wiley & Sons, Inc., New York, N. Y., 1930, chapt. 11.

16 "Comparative Results of Tests on Several Different Types of Nozzles," by M. S. Kisenko, N.A.C.A. Tech. Memo, No. 1066, June, 1944.

17 "Mechanical Engineers' Handbook," edited by L. S. Marks, McGraw-Hill Book Company, Inc., New York, N. Y., fourth edition, 1941, pp. 355 and 358.

18 "The Elbow Combustion Chamber," by M. A. Mayers and W. W. Carter, Trans. ASME, vol. 68, 1946, p. 391.

Appendix

Design of Thrust Nozzle

Fundamental Equations. Considering the one-dimensional flow of a perfect gas through a frictionless, adiabatic nozzle, we may write the following well-known expressions (15)

$$V_e = \sqrt{2g_0 R \frac{k}{k-1}} \sqrt{T_0} \sqrt{1 - \left(\frac{p_e}{p_o}\right)^{\frac{k-1}{k}}} \quad \ldots [11]$$

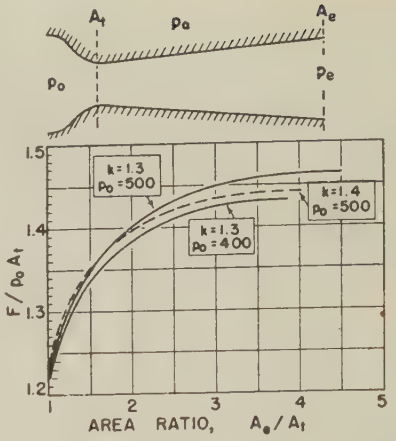

Fig. 11 Characteristics of Frictionless Thrust Nozzle

$$\frac{A_e}{A_t} = \frac{\sqrt{\left(\frac{2}{k+1}\right)^{\frac{2}{k-1}} - \left(\frac{2}{k+1}\right)^{\frac{k+1}{k-1}}}}{\sqrt{\left(\frac{p_e}{p_o}\right)^{\frac{2}{k}} - \left(\frac{p_e}{p_o}\right)^{\frac{k+1}{k}}}} \quad \ldots [12]$$

$$\frac{w}{A_t} = \sqrt{\frac{2g_0}{R}\frac{k}{k-1}} \frac{p_o}{\sqrt{T_o}} \sqrt{\left(\frac{2}{k+1}\right)^{\frac{2}{k-1}} - \left(\frac{2}{k+1}\right)^{\frac{k+1}{k-1}}} \quad \ldots [13]$$

where R is the gas constant, A the cross-sectional area, the subscripts o, e, and t the corresponding cross sections in Fig. 11, and the remaining symbols are as defined previously.

Assuming zero momentum flux in the jet direction of the streams entering the tank, Fig. 3, and that atmospheric pressure is exerted on all external surfaces of the nozzle and of the tank to which it is attached, we may write for the thrust delivered to the lever system

$$F = wV_e/g_0 + (p_e - p_a)\,A_e \quad \ldots [14]$$

Dividing through by p_oA_t, and introducing Equations [11], [12], and [13], we may re-form Equation [14] as follows

$$\frac{F}{p_oA_t} = \frac{2k}{k-1}\sqrt{\left(\frac{2}{k+1}\right)^{\frac{2}{k-1}} - \left(\frac{2}{k+1}\right)^{\frac{k+1}{k-1}}}\sqrt{1 - \left(\frac{p_e}{p_o}\right)^{\frac{k-1}{k}}} + \left(\frac{p_e}{p_o} - \frac{p_a}{p_o}\right)\frac{A_e}{A_t} \quad \ldots [15]$$

Design. Using Equations [12] and [15], Fig. 11 shows how F/p_oA_t varies with A_e/A_t for $p_a = 14.7$ psia, and for several combinations of p_o and k.

As the area ratio is increased from unity, the thrust increases to a maximum. At the same time, the first term (representing momentum flux) on the right-hand side of Equation [15] increases, while the second term (representing a pressure-area force) decreases. At the maximum value of F/p_oA_t, the pressure in the exit plane is atmospheric, the second term vanishes, and the thrust is then equivalent to the leaving momentum flux.

Fig. 11 shows that the curve of F/p_oA_t is extremely flat in the neighborhood of its maximum value. For area ratios not too greatly different from that corresponding to the total thrust, therefore, the total thrust may be taken as virtually equivalent to the momentum component of thrust if the nozzle were to expand the stream to atmospheric pressure. Under these conditions we may write Equation [1] with good accuracy.

Taking into consideration the value of p_o which was to be used

(475 psia), the anticipated value of k (about 1.3), and the results of Fig. 11, a nozzle area ratio of 4 was chosen for these tests.

Results. The analytical conclusions illustrated in Fig. 11 are in substantial agreement with the experimental results reported by Kisenko (16).

Using Equation [13] and the measured values of p_o, T_o, k, w, A_t, and R, the discharge coefficient of the nozzle was found to be 0.980.

By comparing the measured value of F/p_oA_t with the frictionless value from a curve similar to those in Fig. 11, but corresponding to the average p_o and k values of the tests, the jet velocity computed from Equation [1] was found to be 2.4 per cent less than the value corresponding to frictionless expansion. From this it follows that the isentropic enthalpy drop should be about 4.8 per cent greater than the jet kinetic energy, which compares favorably with the data in Fig. 5.

These results for the discharge and velocity coefficients of the nozzle are in accord with published data, in so far as the latter are available (17).

Economies in Power-Plant Design

By EDWIN HOLMES KRIEG,[1] NEW YORK, N. Y.

The primary objective of power-plant design is to secure the highest over-all return on the investment in the plant. This means that the design attempts to attain the best combination or balance between: (*a*) lowest fixed charges through low first cost and high availability, and (*b*) lowest operating charges through low fuel, labor, and maintenance costs. True, this is not the whole story, for it presumes adequate system planning which analyzes the "need" for the station. In other words, when is the plant needed; where is the plant needed; and how large a plant is needed? An outline of these elements is covered by long strokes with a wide brush in the Appendix, as plant design is the main point of discussion. Furthermore, the cost of fuel, the lifetime load factor of the plant, and other considerations such as cost cycles (1)[2] influence the selection of the plant heat cycle and equipment (2). This paper outlines a few examples of economies in the design of public-utility power plants mostly along the lines of first cost and availability.

Plant Design for Lowest Long-Term Cost

Design for Low Investment Cost and Availability. In designing a plant for optimum financial return, there may be some temptation to hold first cost and operating expense the sole criteria. But for a system having a high load factor of 70 per cent, first cost and availability go hand in hand, for the longer that a plant is out of service for repairs and overhaul, the more investment is required in reserve capacity. A system needing 10 boilers to insure carrying the average yearly load can save the cost of one by improving annual availability by 10 per cent. *Neither low first cost nor fuel economy means anything to a plant that is shut down.*

It may be argued that high availability is important only for a system having the high annual load factor of 70 per cent. But this is not necessarily the case, for in one industrial plant on a one-shift basis with a 26 per cent load factor, it was most difficult to secure the needed three consecutive weeks for a turbine or boiler overhaul. The low load factor prevailed almost every day, so that high-availability equipment was most essential since major repairs cannot be made during the offshifts.

High availability does not mean keeping equipment in service come what may and regardless of loss in efficiency; it is noteworthy that those units having high availability often maintain their efficiency better than low-availability units. This recalls to mind the fact that an efficient plant is often characterized by good housekeeping. The operating attitude which values good housekeeping, values efficiency; the design and operating attitude which values availability, also values the maintenance of efficiency.

Because it is somewhat difficult to classify separately the economies stemming from first cost and availability, the discussion will center around economies possible in major plant equipment, whether such economies derive either from lower first cost or improved availability.

Boilers. One of the really major economies in first cost is adoption of the single-boiler single-turbine combination, provided that special attention is given to availability and reserve capacity. It is true that a few boiler availabilities on the author's and other systems have been brought up to about 95 per cent, but naturally this cannot be done year after year unless the design in even its earliest stages is pointed toward that objective. Designing for high availability costs more; the lower heat-transfer rates in the boiler require more surface and more liberal proportioning of the equipment. However, such extra costs for single-boiler-turbine units are, in most cases, well justified by such savings as the following:

1 Improved availability permits a decrease in reserve capacity.

2 The unit cost of equipment generally decreases with size.

3 Building and foundation costs decrease materially with the single boiler.

4 Operating labor costs decrease; usually no more labor is involved to run a 600,000-lb per hr boiler than one of 300,000 lb per hr.

5 Maintenance costs are usually less as the size increases.

When the 1,000,000-lb per hr Logan boiler (3) was purchased, it was a step in the right direction. However, unforeseen circulation difficulties, resulting in oxygen formation and corrosion at Logan, together with some early difficulties with large boilers at Windsor and Twin Branch No. 3, made it advisable to return to two boilers per turbine at Philo and several subsequent stations, to insure availability. However, the difficulties at Logan, Windsor, and Twin Branch were finally understood and solved, bringing yearly boiler availability to over 90 per cent and making it desirable to return to the one-boiler one-turbine combination.

For the three most recent extensions authorized, single boilers will serve single turbines as listed in Table 1.

TABLE 1 PLANTS WITH SINGLE-BOILER, SINGLE-TURBINE COMBINATION

Plant name and unit no.	Turbine, gross kw	Boiler, lb per hr	Pressure, psi	Temp deg F boiler/reheater	Approximate starting date
Tidd No. 2.....	115000	950000	1300	925	Fall, 1948
Twin Branch No. 5	145000	945000	2000	1050/1000	Spring, 1949
Philip Sporn No. 1	145000	945000	2000	1050/1000	Summer, 1949
Philip Sporn No. 2	145000	945000	2000	1050/1000	Summer, 1950

Turbine Generators. One means of economizing on turbine-generator cost in sizes from 11,500 kw, up to and including 60,000 kw, is to use the preferred sizes listed in the ASME-AIEE Preferred Standards for Large 3600-Rpm, 3-Phase, 60-Cycle Condensing-Steam-Turbine Generators. The preferred sizes built to the standard characteristics listed will run as high as 7 per cent lower in cost than nonstandard turbines.

To obtain the lowest over-all cost of turbines, particularly in sizes above 60,000 kw, a more thorough study of the various types available is warranted, e.g., a generalization cannot be made that the improved efficiency of a cross-compound turbine is worth the higher cost over a single-casing type. Sometimes it may be worth more, but not for all fuel costs and load factors.

---

[1] Consulting Mechanical Engineer, American Gas and Electric Service Corporation. Mem. ASME.

[2] Numbers in parentheses refer to the Bibliography at the end of the paper.

Contributed by the Power Division and presented at the Semi-Annual Meeting, Chicago, Ill., June 16–19, 1947, of The American Society of Mechanical Engineers.

One means of reducing the cost of turbine generators is by improving their availability. In 1930 the service-demand availability for all turbines of 1000 psi or higher pressure in the United States was only 82.68 per cent, which advanced to 89.75 per cent (5) by 1935. The average for 55 such turbines throughout the country during 1943 was 93.45 per cent (6), and 95 per cent or higher is the present objective.

Various features were developed to improve the reliability and safety of turbines on the American Gas and Electric System, some of which are described in the Appendix.

Circulating-Water System. The novel circulating-water system at Philo was developed to obtain the economies, both in first cost and fuel cost, derived from being able to use a plant site that apparently had been completely developed. A study in 1939–1940, showed that the Philo plant offered unusual advantages for adding some 190,000 kw of capacity. It was near the load center, coal costs were lower than at many other sites, no new transmission lines were needed, and first cost would be a minimum, since many existing facilities were already installed, e.g., coal storage and handling, railroad tracks, intake canal, etc. However, insufficient river water, even for the existing 245,000-kw capacity, actually had caused curtailment of load in previous "dry" years, although the entire Muskingum River was being passed through the four plant condensers, Nos. 1, 2, 3-1, and 3-3. It would be costly to build spray ponds or cooling towers for 190,000 kw because of the extremely low use factor of such equipment, periods of insufficient water lasting only from 1 to 30 days per year. Although there was no known precedent for placing large condensers (of 95,000-kw units) in series, there seemed no simpler nor more economical means of practically doubling the capacity of the river for condensing purposes at low river flows.

Fig. 1 shows in light lines the basic equipment needed for units Nos. 3-3 (installed 1930) and 95,000-kw unit No. 4 (installed 1942). The heavy line indicates the simple and relatively inexpensive additional piping which made it possible to add two 95,000-kw units at just the location on the system where they were needed. Similar piping not shown is installed for old condenser No. 3-1 and new condenser No. 5 Condensers Nos. 3-1 and 3-3 serve the two low-pressure turbines of a 165,000-kw triple-cross-compound turbine. This has a 600-psi, 53,000-kw noncondensing turbine whose reheated exhaust goes to two condensing, 125-psi, 56,000-kw, low-pressure turbines, (4). Ordinarily a 9-ft dam provides circulating water without using pumps, but for flood conditions when the dam offers no head, pumps are required.

The heavy line shows the small amount of additional piping needed to almost double the condensing capacity of the Muskingum River, and Figs. 2 to 6, inclusive, show how the system operates. Ancillary advantages make the scheme still more attractive, e.g., the ability to de-ice the intake canal for all 5 units, shown by Fig. 6.

The obvious alternative of recirculating water from the condenser-discharge tunnels back to the intake canal, Fig. 7, would not suffice at this particular site, having the following serious disadvantages:

1 A limited and insufficient amount of water would reach the suctions of the recirculating pumps since:

(*a*) The river bed between condenser discharges and recirculation pumps slopes too much when the lower pool level drops during extremely low water.

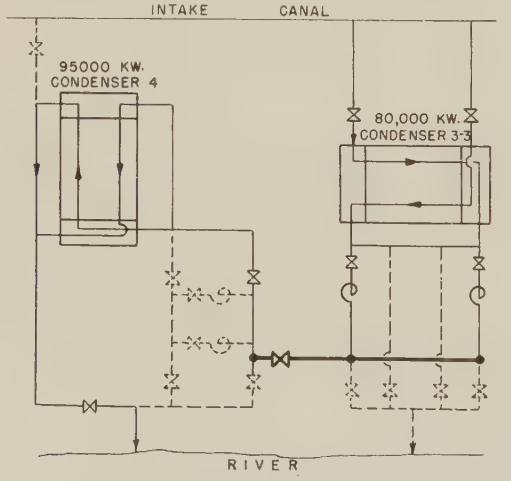

Fig. 1 Heavy Line Shows Simple and Relatively Inexpensive Piping for Placing Old Condenser No. 3–3 in Series With New No. 4. Condensers Nos. 3–1 and 3–3 Serve Two Low-Pressure Condensing Elements of a 165,000-Kw Triple-Cross-Compound Turbine

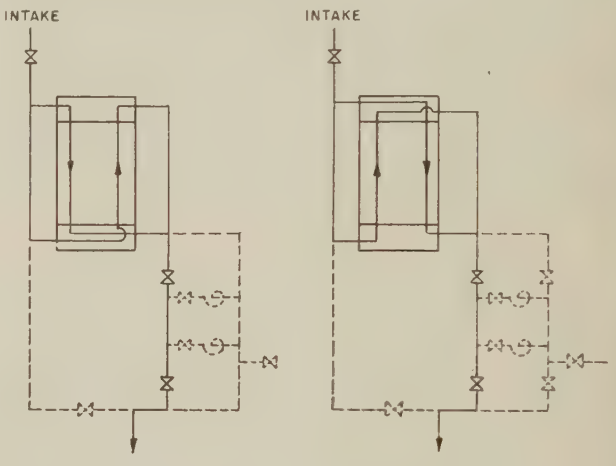

FIG 2 FIG 4

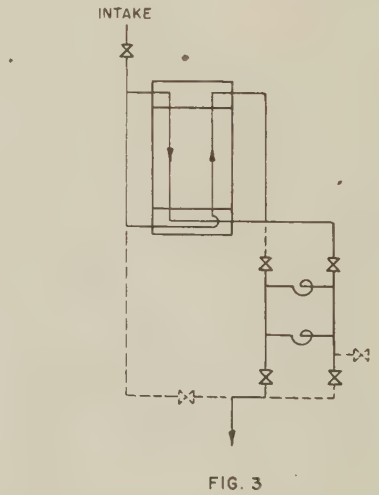

FIG. 3

Fig. 2 Normally, Circulating Water Flows Through the Condensers by Gravity, a 9-Ft Dam Being in the River as Shown in Fig. 7

Fig. 3 Annual Flood Conditions Often Reduce Drop Across Dam to 1 Ft or Less, Thus Requiring Pumps During Such Periods

Fig. 4 Reversing Water Boxes Permit Full Reversal of Circulating-Water Flow During Operation, Insuring Complete Removal of Trash Accumulations From Tube Sheets; Especially the Feltlike Blanket That Is Most Difficult to Remove Except by Flow Reversal

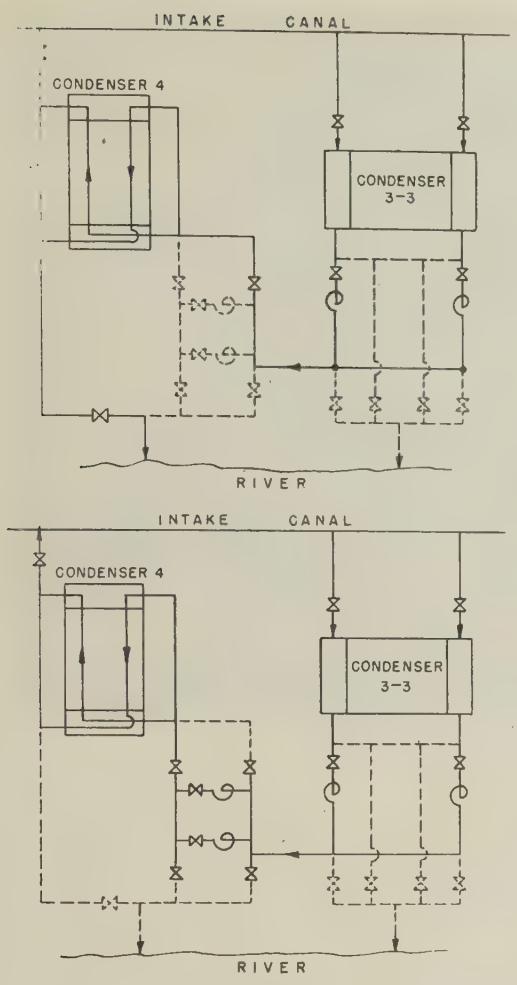

Fig. 5 (*Top*) During Extremely Low River Flows or Low Pool Level When Recirculation System for Fig. 7 Cannot Function Adequately, Series Circulation Together With Recirculation Permits Full-Load Operation

(This doubles the amount of plant capacity possible on the Muskingum River.)

Fig. 6 (*Bottom*) Slush or Frazil Ice on Grizzlies and Screens Make Deicing a "Must" on Certain Rivers to Preclude a Shutdown

(Such past difficulties are eliminated by pumping some warmed water from units Nos. 3–1 and 4 condensers back into intake that serves five units totaling 435,000 kw.)

(*b*) The flashboards may be damaged or removed from the downstream dam, lowering the pool level.

2 The installation cost for positive recirculation would be much more than the piping layout shown in Fig. 1. A deep enough channel from the condenser discharges back to the recirculating-pump house to insure water at all times would be very costly because of the rock river bed. However, a partial recirculation system was installed for the following reasons:

(*a*) An emergency circulating water supply is needed to back-up series circulation during the occasional insufficiency of river flow for full load, perhaps twice in a decade.

(*b*) Cool water leaking through the dam and locks is recirculated during hot summer weather. This is preferred to drawing water upstream from condenser-discharge tunnels.

(*c*) Acts as reserve for the unit No. 3 circulating-water pumps during low water, and gives opportunity for rebuilding the flood pumps of units Nos. 4 and 5, Fig. 3, which was done in late 1946 and 1947.

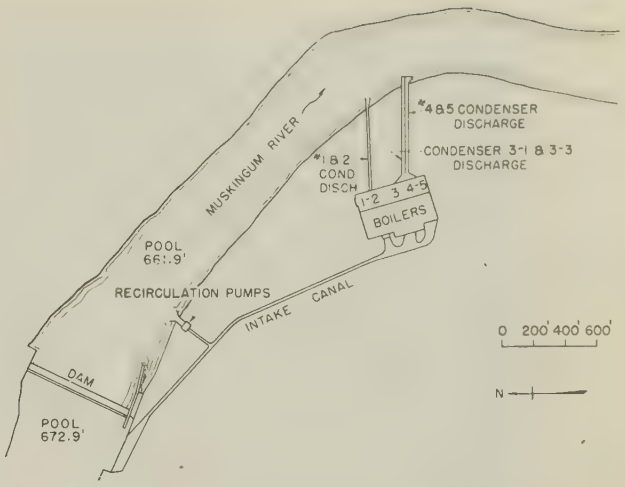

Fig. 7 The Muskingum River Flow Is Not Always Sufficient, for Full Plant Capacity, Even With Series Circulation Shown by Fig. 5

This recirculation scheme pumps the lock leakage and dam leakage back into the intake canal, together with such flow that may go upstream to the pump suctions. These pumps can handle three of the five units.)

(*d*) Can be used to help keep the river channel for coal barges free from ice in winter by drawing some water upstream from the condenser-discharge tunnels.

Logan (3) was another example where additional capacity was badly needed but where river flow was hardly sufficient at times to supply spray-pond make-up. Situated in the heart of an excellent coal district and enjoying a 13-cent per ton freight rate, it was a natural location for a plant. However, the stream flow often barely met spray-pond make-up needs, and a larger spray pond would only require still more make-up water. In addition, there was little ground area, the site being hemmed in by a mountain, the river ravine, railroad, and county road.

By superposing, the capacity was raised from 36,000 to 90,000 kw, without enlarging the original spray pond nor requiring more spray-pond make-up, Fig. 8. The spray pond was built right over the river bed as space was so limited. An unusual feature is downward spraying to induce air flow into the sprayed water as the nozzles are some 25 ft above low-water level.

Condensers. At Atlantic City and Scranton, it was possible to hang the condensers directly to the exhaust of 25,000-kw turbines, saving the cost of springs or expansion joints, and condenser foundation. Tie-rods take the twist caused by changes in circulating-water flow so that load is not transmitted to the turbine.

In large units, an expansion joint between the turbine and condenser is favored to afford more certain relief from strains on the turbine. At least one case of turbine vibration has been cured on the Central System by breaking the turbine-to-condenser joint and correcting unequal loading on springs that loaded the turbine eccentrically. During hydrostatic testing, much of the weight of a spring-supported condenser and the testing water within the steam space may be thrown on the turbine:

(*a*) If blocks are not placed to take the load off the springs.

(*b*) Cool water for a hydrostatic test will contract a warm condenser shell and neck and may lift it off the blocks.

(*c*) The foregoing may or may not result in serious damage to the turbine if the top exhaust hood is bolted on, and quite certainly if not bolted.

Condenser costs are reduced by using long condenser tubes; 24 ft 11 in. is a good length at which to stop, as tube prices increase not only at 25 ft, but also for longer lengths. It is usually

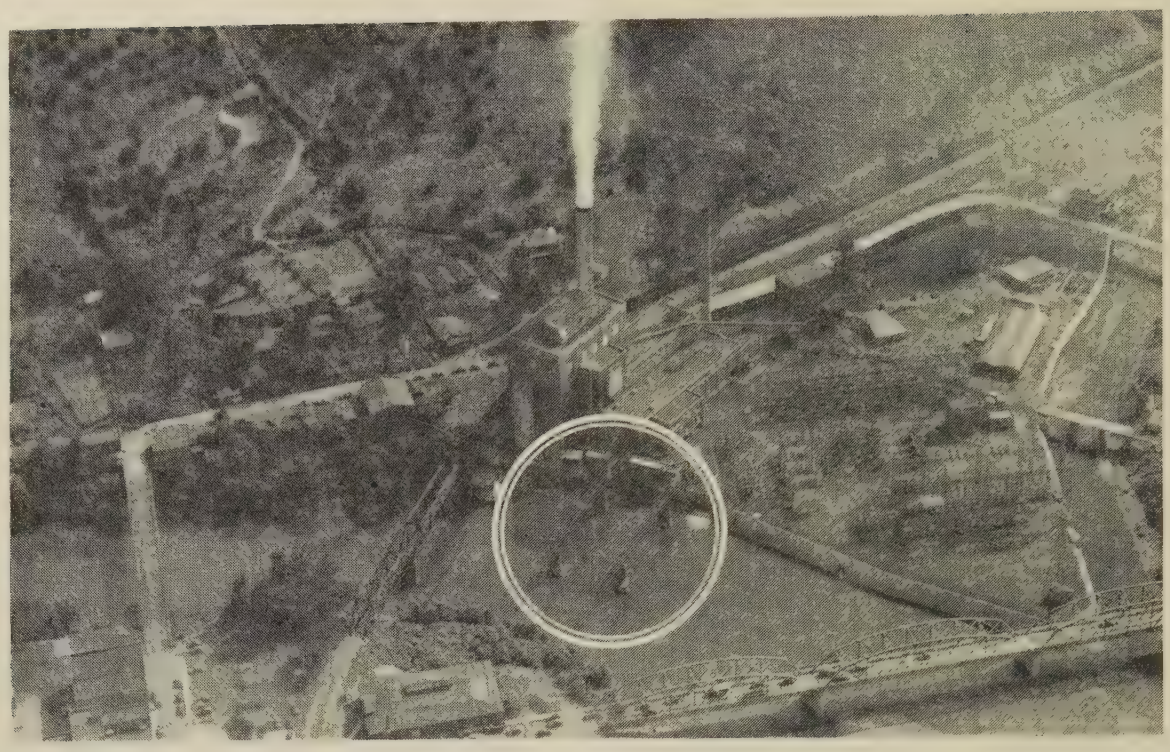

FIG. 8 LOGAN SPRAY POND, 25 FEET ABOVE RIVER BED

cheaper to manufacture the longer shell with decreased diameter. Tube length is limited by the withdrawal space needed for retubing; also more vertical height is needed for a transition piece to insure proper distribution of exhaust steam to the longer tubes.

Deaerator. General experience has shown that the deaerator can be placed anywhere in the cycle and still do a good job; therefore there is no advantage in making other than a minimum-cost installation.

A subatmospheric-pressure deaerator costs more because of the large steam volume to be handled by the deaerator head. At lower temperatures increased water surface tension and lower water viscosity require more trays to obtain longer contact time between the water and steam. Thus a larger shell and more air-relieving surface are needed. Steam-jet air pumps are needed involving extra operating cost for steam.

There is a middle ground from about 15 to 70 psig, which is usually the most economical. With such pressures it is possible to place the deaerator at a reasonable height above the boiler feed pumps (about 40 to 60 ft) to preclude flashing therein.

Evaporator. Unlike a deaerator, the choice of an economical evaporator shell pressure covers a wider range:

(*a*) A subatmospheric-pressure evaporator costs more than an atmospheric evaporator because the physical size is much larger to handle the larger steam volumes; larger shells, piping, and separator are required. A blowdown pump is also needed to remove the concentrated liquor, either periodically or continuously, which may call for some automatic control.

(*b*) However, high shell pressures increase the cost of shell, piping, valves, and accessories such as feed pumps.

As in the case of the deaerator, it probably is most economical to place the evaporator within the same pressure range, i.e., shell pressures from 15 to 70 psig, supplying it with steam from the same source used for the deaerator.

Heater Drip Pumps. Since the 1936 Logan design, duplicate heater drip pumps have not been used. Instead of a duplicate pump, a loop seal back to the condenser is less expensive, having the advantage of operating automatically and without attention in case of drip-pump failure. In giving excellent turbine protection in case of high water level in the heater, it has unique safety as well as low-cost advantages. The few hours per year that a duplicate would operate during the overhaul of the other pump, cannot justify the extra cost of pump, motor, and motor control.

Piping and Valves. The design of 2300-psi Twin Branch unit No. 3 was highlighted by the desire to economize in piping and valves. Although there was no precedent, the boiler stop valve was omitted between the boiler and the turbine emergency stop valve, although the need for such a stop valve in a single-boiler single-turbine installation had apparently not been previously challenged. To eliminate the usual gate valve between boiler and turbine, it was necessary to consider whether the turbine emergency stop valve would permit a satisfactory hydrostatic test on the boiler. Practical operating experience has confirmed that conclusion.

The cost of main steam piping may often be reduced by placing it in torsion as well as in bending. For a given pipe size, piping shaped as a coiled spring gives a low end reaction with less fiber stress for a given deflection than most other shapes, the reason being that the modulus of elasticity in torsion is much lower than in bending. Thus to use less pipe material to suit given conditions, the entire system can often be designed to place the major portion of it in torsion, somewhat like a huge spring coil.

To facilitate both design and erection, anchored emergency stop valves were first used on a 60,000-kw topping turbine for Windsor in 1938, and on all subsequent turbines. By so doing, the piping design can be started earlier without waiting for turbine outline prints to give the location, expansion movements, and allowable thrust on the emergency stop valve. There is more freedom in locating the valve, and the turbine manufacturer

has the sole responsibility for the loads placed on the turbine by the piping. This is advantageous.

At Logan (3) in 1936, and at subsequent stations, a large saving was made by providing only one boiler feed line from the boiler feed pumps to boilers, although it had been previous standard practice on the central system to install an "auxiliary" boiler feed line, often with a "raw" feed supply in addition to condensate.

Maintenance of valves also involves outages of the equipment served, i.e., boilers, turbines, pumps, and the like. Few contributions to valve design did so much to reduce maintenance as welded-in seats and disks which are stellite-faced. These improvements have been standard in all company plants since 1936, although the development[3] was started in 1927–1928.

Valve costs are materially lowered by using one size smaller than the pipe, e.g., a 6-in. valve in an 8-in. line, having 8-in. ends, Table 2.

TABLE 2 APPROXIMATE VALVE COSTS—1250 PSI, 950 F

Pipe size	Valve of pipe size	Valve of 1 pipe size smaller	Saving per valve
12.....	$5100	$3900	$1200
10.....	3900	2700	1200
8.....	2700	2120	580
6.....	2120	900[a]	1220
5.....	900[a]	560[a]	340

[a] No motor operator for 5 in. and under.

It is not thrifty to purchase valves merely to meet a given pipe size. Valves cost so very much more than does pipe that a higher pressure drop through the more expensive equipment can well be tolerated, using less pressure drop through the larger and cheaper piping.

The bottom outlet on the condenser-discharge water box that was developed for Twin Branch 3, Fig. 9, saves expensive out-

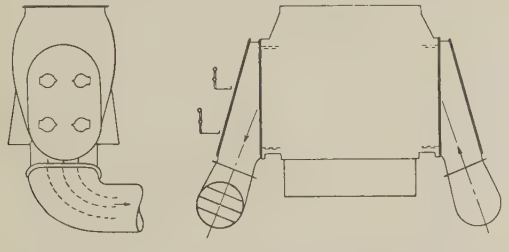

FIG. 9 RECENT SINGLE-PASS CONDENSERS HAVE A BOTTOM OUTLET ON THE DISCHARGE WATER BOX TO SAVE CIRCULATING-WATER PIPING AND HYDRAULIC HEAD LOSS

let circulating-water piping. The outlet water box with an elbow is identical with the inlet; this departs from the usual practice of having the outlet on the top of the discharge water box. When the flow of circulating water is established, experience shows that there is no lack of water in the uppermost condenser tubes because of the bottom outlet, and the performance of the hydraulic circuit in its entirety has come up fully to expectations. There is also less friction loss. Eight condensers having bottom outlets have been installed during the last decade on American Gas and Electric Company turbines totaling 750,000 kw, and four more have been purchased to serve an additional 550,000 kw of turbine capacity.

Piping cross-connections between one-boiler one-turbine units were found uneconomical, besides introducing operating complications.

Building and Plant Layout. One means of lowering building costs is the outdoor plant which has been well described in the technical press. In smaller-sized plants having units around 25,000 kw, the savings may be appreciable, but the saving is proportionately less for 100,000-kw units.

The condenser pits for plants on rivers having wide variations in level between high and low water are often made deeper than need be. The level duration curve for the Ohio River near one of the company's central system plants, shows that for 4 to 7 days a year, the pool level maintained by a dam may be lowered some 9 ft when the locks and flashboards are opened to permit ice or trash to run out. Normally the depth of the condenser pit is set by placing the highest portion of the condenser-discharge water box about 27 ft above the minimum tail water, so the siphon would not be broken. However, in this case, the "high spot" of the condenser was placed 36 ft above minimum tail water, and two-speed motors obtained for the circulating-water pumps. For the few days a year that the pool level may be 9 ft low, the higher speed will be used at which the pumps will have enough capacity to maintain full load at the higher head. A condenser-discharge valve (as well as stop logs) are available if needed to prevent loss of the 36-ft siphon leg if it tends to "break." The extra cost of the two-speed motors and higher pumping cost for a few days is far cheaper than investing in a pit 9 ft deeper.

For plants where circulating-water temperatures do not exceed 85 F, building costs may sometimes be lowered by using a little more than the usual 25 ft between the condenser high spot and tail water; for example, adding the friction drop between the condenser outlet and the river which may be 2 ft would make 27 ft.

Design for Low Fuel Cost

Fuel or thermal economy is worthy of patient search, but only within the limits of financial economy. It should not be mere Btu chasing.

The efforts made by the author's company to minimize the fuel costs of electricity through pressures up to 2300 psi and temperatures of 1000 F, as well as improved cycles (such as reheat) are well known, having been reported elsewhere (3, 4, 7–11).

A most important element of fuel cost is incremental scheduling of loads, not only between the units in a particular plant, but also between all the individual units on the system (not merely one plant as against another plant). But this subject is too extensive and complex other than to mention its great significance (12).

Proper incremental loading of units is also a factor influencing the type of equipment, e.g., low loads cannot ordinarily be carried on "wet-bottom" boilers. The type of furnace bottom of pulverized-coal-fired boilers must be selected to suit the range of coals that is available to the plant, as well as the range of load. A wet bottom is ideal for low-fusion-ash coals and a high load factor that will keep the furnace hot. But if the coal changes to a high-fusion-ash type and loads of less than half-rating must be carried for long intervals, the ash will not melt and run out, and may possibly build up to several feet in depth, until it is necessary to shut down and drill or dig it out.

Low fuel cost also requires an awareness of the trend of future fuel costs. It is not enough, in a depression year when fuel costs are low, to select an inefficient, 250-psi, 750 F plant cycle to save the small extra cost of a more efficient plant cycle. For when fuel costs again swing back, that plant may be saddled with a high fuel cost which makes it obsolete.

For units of 85,000 kw and over with throttle conditions of 1300 psi, 925 F, cross-compound turbines are more efficient than single-casing units. Eight cross-compound units have been selected since 1938. However, two 100,000-kw units were made single-casing only at request of the War Production Board (9).

[3] By E. T. Davis of Indiana & Michigan Electric Company.

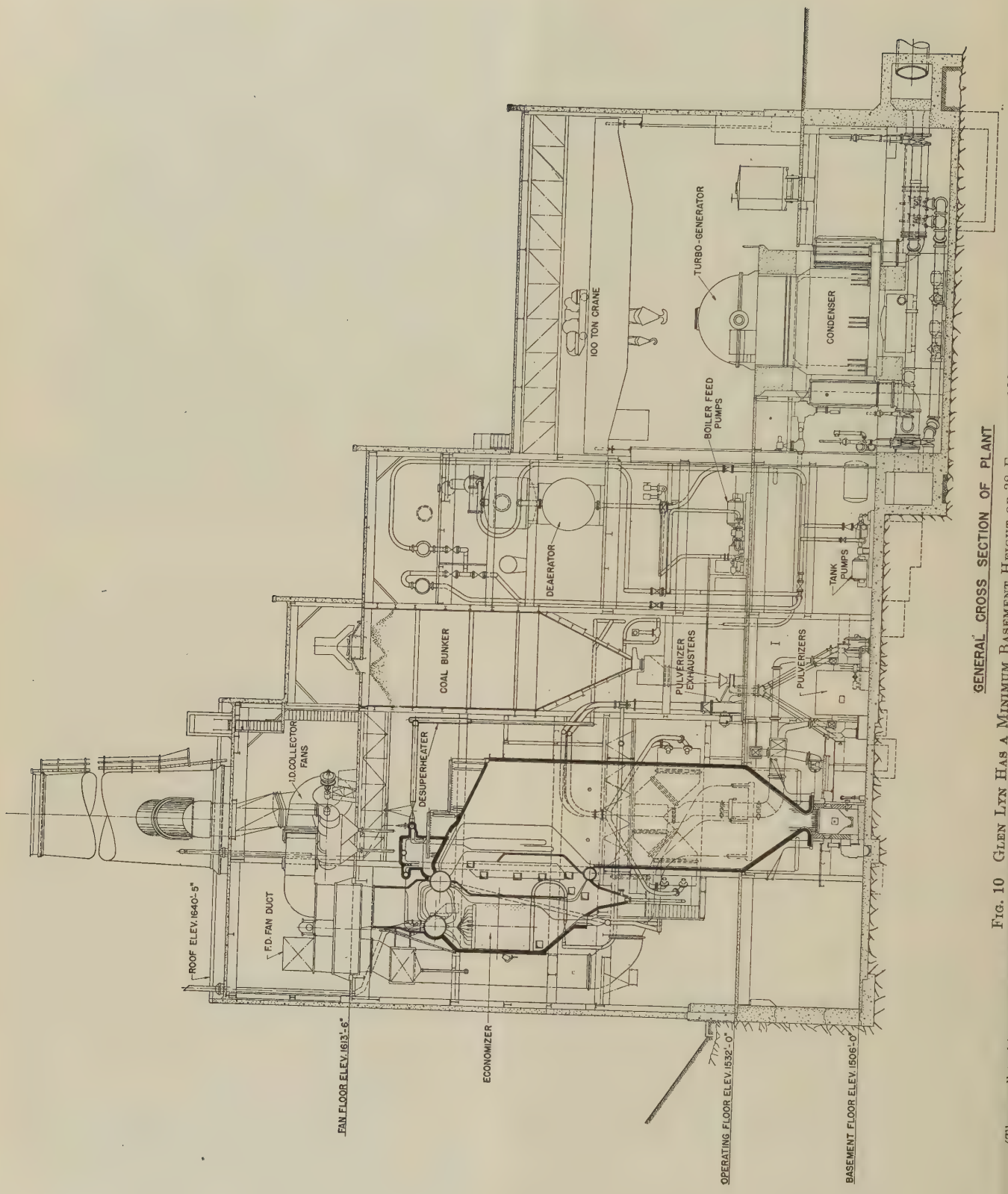

FIG. 10 GLEN LYN HAS A MINIMUM BASEMENT HEIGHT OF 38 FT FOR A 100,000-KW UNIT

(The small turbine room, [illegible])

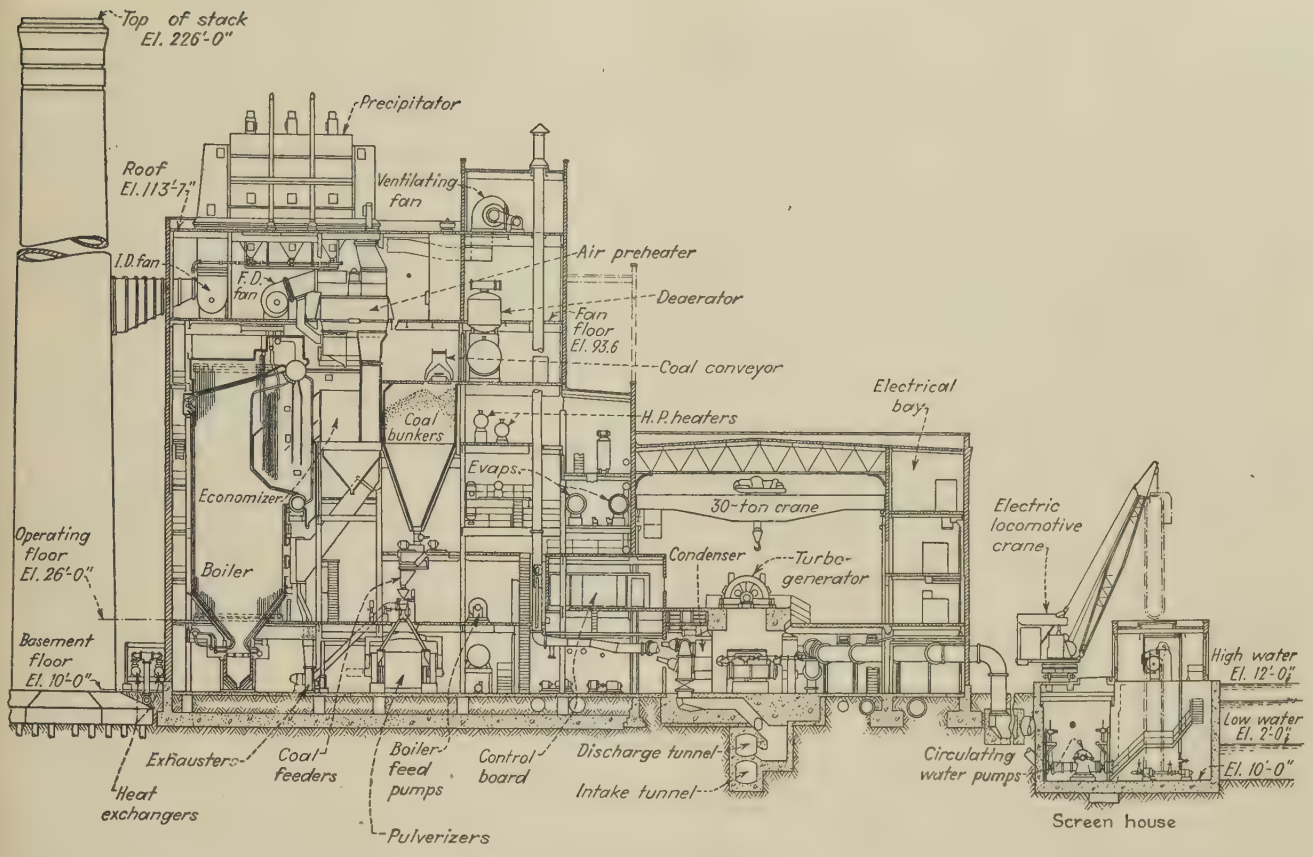

FIG. 11 ATLANTIC CITY NO. 7, A 25,000-KW TURBINE, WITH 30,000-KW CAPABILITY, WAS INSTALLED IN EXISTING PLANT WITH ONLY 16-FT-HIGH BASEMENT

(The compact arrangement gives high kilowatts per square foot of building area. The condenser is hung from turbine with no spring supports.)

Evaporators. Single-unit plants need two evaporators, in case one is out of service. At Atlantic City and at Tidd, the two evaporators were arranged for either (*a*) parallel operation as single-effect for high make-up capacity, or (*b*) when thermal efficiency is the objective, they are operated double-effect. This is better than other expedients of increasing evaporator capacity, e.g., cutting back on the next lower bleed heater to increase terminal temperature difference on the vapor condenser

Fuel Cost and Availability. Just as investment cost and availability go hand in hand, there is likewise a close relationship between fuel cost and availability. To a plant that is shut down, Btu efficiency means little. It is only by keeping running that the efficient plant has the advantage over an inefficient plant.

Naturally the unavailability that increases fuel costs also increases maintenance costs, but the fuel costs are usually much the larger.

DESIGN FOR LOW MAINTENANCE COST

In designing for low maintenance and high availability, the needs of the plant maintenance men are analyzed. It is a foregone conclusion that certain equipment will be dismantled relatively frequently, i.e., induced-draft fans on pulverized-coal boilers, and pulverizer mills. Over each piece of such equipment, motor-operated hoists on monorails are available to facilitate quick week-end jobs. Other equipment comes apart less often, boiler feed pumps, evaporator heads, etc. For these, only an I-beam with perhaps a trolley and hook is sufficient, facilitating transferring a motor-operated hoist from another location.

No hot drains are flashed in the heaters or deaerator; separate flash tanks are provided so only flashed steam goes to the steam space of the heater, drips going to the hot well. Among reasons for doing this are the following:

1 Save heater maintenance caused by erosive action of flashing mixture on shells, tube sheets, and tubes.

2 Better control of drainage system through more area at water line.

3 Good level control precludes steam by-passing to next lower heater, also prevents dangerous flooding.

Bends in piping such as boiler-feed-pump labyrinth and emergency leak-off lines where flashing frequently occurs, were found to wear rapidly. These bends were replaced by tees with one run connection blanked; this gives a water cushion, as the water outlet uses the side connection.

The coal bunker at Tidd is completely sealed by the concrete floor over it; the slots through which the coal tripper discharges are covered by belting which is raised automatically by the tripper to discharge coal. This reduces maintenance cost as the plant stays much cleaner.

Boiler Feed Pumps. In 1935, when designing the Logan plant, the need for maintaining the close clearances in boiler feed pumps became evident, so single-type strainers were permanently installed in each feed-pump suction line to catch small welding beads, bits of welding rod, and other metallic objects. The monel-metal baskets have $^1/_{32}$-in-diam perforations whose area equals 2.5 times the pipe area. These were most successful in catching foreign material, and similar strainers have been used before all boiler feed pumps installed since 1936.

To check the condition of boiler feed pumps, test orifices are installed in the balancing drum and labyrinth leak-off lines to

check when pumps require overhaul. These, together with a flowmeter in the pump suction, and measurement of the motor input, are most valuable indications of pump condition.

Likewise, test orifices are placed in the main-turbine gland-seal leak-off to check whether glands may require renewal.

Maintenance and Availability

As was previously mentioned, poor availability increases investment costs to protect against outage; also poor availability increases fuel costs because less efficient units are used to carry the load. Likewise, poor availability increases maintenance costs, because the equipment causing the outage must be repaired, costing both material and labor.

Epilogue

In deciding to prepare this paper around some specific cases of plant economies, it was known that the comment could be made: "Well, you solved your problems, but how about ours?" There are many books which cover the generalizations of power-plant design and the few cases cited herein are naturally limited in scope and cover less ground. But how the other engineer worked out his problems often has the human interest of "well, I certainly could have done better than that." And that is stimulating.

BIBLIOGRAPHY

1 "Cycles as an Aid to Postwar Planning," by E. R. Dewey, *General Electric Review*, vol. 46, 1943, pp. 264–268.

2 "Power Supply Economics," by J. D. Justin and W. G. Mervine, John Wiley & Sons, Inc., New York, N. Y., 1934.

3 "Logan Steam Station," by Philip Sporn, *Southern Power Journal*, vol. 56, June, 1938, pp. 26–34; also Trans. ASME, vol. 60, 1938, pp. 421–422, and vol. 62, 1940, pp. 253–256.

4 "New 165,000-Kw Unit No. 3 at Philo in Service," *Power Plant Engineering*, vol. 33, 1929, pp. 965–967.

5 "Superposition," by E. H. Krieg, *Mechanical Engineering*, vol. 58, 1936, pp. 562–572 and 584.

6 "Turbines, Condensers and Feedwater Heaters, 1943–1944," Edison Electric Institute, Publication L3, 1945.

7 "Windsor Steam Plant Modernization," by Philip Sporn, *Combustion*, vol. 8, March, 1937, pp. 20–24.

8 "Twin Branch Extends High-Pressure Economies," by Philip Sporn, *Electrical World*, Oct. 18, 1941, pp. 80–82.

9 "Glen Lyn 100,000 Kw Unit," by Philip Sporn and E. H. Krieg, *Southern Power and Industry*, vol. 63, December, 1945, pp. 50–55, 84, 86, 88, 92, and 94.

10 "One Thousand F—a New High in Steam Temperature—the Missouri Avenue Plant," by Philip Sporn, *Electrical World*, August 17, 1946, pp. 60–67.

11 "The Tidd Plant," by S. N. Fiala and E. H. Krieg, *Power Plant Engineering*, vol. 51, March, 1947, pp. 68–73.

"Steam Generation at New Tidd Plant," by S. N. Fiala and L. B. Schueler, *Combustion*, vol. 18, October, 1946, pp. 30–35.

12 "Economy Loading of Power Plants and Electric Systems," by M. J. Steinberg and T. H. Smith, John Wiley & Sons, Inc., New York, N. Y., 1943.

Appendix

The complete picture of power-plant economies includes the vital function of system planning. The following is a partial outline of the factors involved:

When Is the Plant Needed. Need for capacity; forecast system peaks and load factor by various types of curves, e.g., growth of yearly peak loads, monthly peaks, load duration, etc. (2). Especially important, as it now takes 3.5 years to build a plant.

Need for savings; sometimes a plant can pay for itself by reducing system operating costs by more than the amount of fixed charges (3):

Effect of cost and business cycles (1).

Comparisons with national averages.

Fitting in with extension plans of interconnected utilities.

Canvass of industrial and large commercial customers as to their future plans.

System-load flow diagrams.

Where Is the Plant Needed. Plant location relative to future load center.

Plant location relative to transmission system and interconnections:

Water supply.

Range of water level of condensing water.

Cost of flood protection.

Cost of fuel at various possible sites.

Transportation costs of coal or electricity.

Foundation conditions.

Cost of site improvements: railroad, roads, etc.

Operators' housing facilities.

Alternate sources of fuel supply over 40 to 60 year period.

Extension of existing plant versus new site.

Cost of purchasing power from others.

Life of fuel field to be used; early exhaustion may prematurely antiquate a plant.

How Large a Plant Is Needed. Among the elements entering into sizing a unit are the following:

Ratio of size of system to size of unit may be 10:1 for a large system, or 3:1 for a small system having interconnections.

Load forecasts on rate or growth—how many years of growth should be handled by the proposed unit.

Relation between unit size, firm capacity during outage, spinning reserve.

Large units give economies in investment, better turbine efficiency, lower maintenance, and lower operating labor.

Availability: To enjoy the benefits of large-sized units, high availability is needed. Availability is a function of engineering attitude and skill in the design and selection of equipment. A meticulous attitude toward details is often developed if the designer is also responsible for working out operating problems. Whether equipment is purchased on a "first-cost" basis, or "quality is cheapest in the long run" basis greatly affects availability.

Turbine Availability

Some means of improving turbine availability are described herewith.

Initial-Pressure Regulator. Protection against sudden temperature changes is afforded by an initial-pressure regulator which closes the turbine control valves in case of a drop in steam pressure and maintains throttle pressure. The boiler is protected against sudden loss of pressure and resulting carry-over from "swell," the thermal shock to superheater, and thick drum from sudden temperature change. High-pressure boilers have small storage capacity, hence drum pressure drops rapidly on sudden load demand or change in firing rate.

Benefits to turbine: preclude water slugs from boiler on account of "swell," thermal shock.

Underspeed Release. First developed for Atlantic City turbine 7 as a result of loss of the station load in the preceding year during a system disturbance. When an efficient turbine is connected to a large system, it often is economical to carry a fixed load on it by positioning the control valves by handwheel so they will not respond to the normal minor changes in frequency. However, in a system disturbance, the turbine cannot maintain its speed, and frequency may decrease to an extent that the station load is dropped. The underspeed release permits the governor automatically to revert to speed-governor control in case of abnormal frequency swings.

Protection Against Excessive Starting Speeds. Main operating governors have a motor-operated handwheel for starting con-

trol. A recent innovation, first used in Tidd in 1945, is a two-speed motor for normal speed opening of the control valves but which permits fast closing.

The amount of steam "to break the turbine free" when starting up, is more than needed to keep it rolling at low speed. After "breaking loose," the turbine accelerates too rapidly, and somewhat excessive speeds are often reached as the usual motor on the starting handwheel is too slow in the "to close" position. The new two-speed motor permits closing the starting handwheel rapidly to prevent excessive speeds during the starting operation. The $^1/_8$-hp motor has a solenoid brake to minimize coasting and to position the handwheel accurately from the remote-control board when starting and bringing the turbine to speed.

Availability and Turbine Deposits. Most recent high-pressure high-temperature turbines have had more or less difficulty with turbine deposits, usually during the first year of operation before treatment of feedwater has become a stabilized and routine matter. To minimize the amount of outage during the washing period, several different methods have been devised. At Twin Branch, turbine-washing while under full load was developed, using an attemperator between two portions of the superheater to drop throttle temperature about 150 F which was sufficient to get saturated steam at the location of the deposits and effect cleaning.

For Atlantic City turbine No. 6, facilities were provided to wash it as quickly and conveniently as possible, using 200-psi steam from the old boilers, especially since washing was dictated by deposits.

Lubricating and Control Oil System Reliability. In the past, turbines which have an oil tank on the basement floor about 25 ft below, had their availability somewhat impaired. Trouble sometimes occurred with misalignment of the long shaft from which the gear-type oil pumps in the oil tank were driven from the driving gears on the main turbine shaft. This and other difficulties prompted the development of independently driven oil pumps with no shaft-driven pump. The Glen Lyn turbine was probably the first to have its bearing and control oil pumps entirely separated.

Automatic Steam-Seal Regulator and Unloading Valve. The new steam seal and unloading valve, developed for Tidd, are designed to maintain 1 psig in the high-pressure seal before the water seal has become effective. As the turbine begins to pick up load, steam is dumped from the leak-off line to the gland steam condenser until the leak-off pressure has dropped back to 1 psig, which is maintained during normal operation.

The foregoing equipment protects against the following:

(*a*) Loss of water in water seal during sudden load changes which would result in steam and water being blown along shaft into adjacent bearing causing oil contamination.

(*b*) Precluding vacuum in steam seal especially while at low speed before water seal is effective, which would pull in cold air and distort the first-stage wheel.

Water Sealing System. An operating convenience to facilitate a quick restart after a shutdown, is remote indication and control of the water seals on the high- and low-pressure shaft packings. Sealing water can be turned on and off from the control room from where its pressure and temperature may be adjusted.

Bearings. Each bearing is protected by a remote-indicating thermometer, and all thermometers are equipped with temperature alarms connected to an annunciator. The operator in the control room has an oil-temperature indicator and control of water to the coolers by a motorized valve to assure proper oil temperature to the bearings.

Nonreturn Valves. A new type of positive-closing extraction-line nonreturn valve was developed to prevent overspeeding of unloaded turbines. Sufficient leakage of steam into an unloaded turbine (such as one whose load has just tripped off) may cause dangerous overspeeding. If turbine extraction check valves should stick open or fail to close when a turbine is tripped, the stored hot water in bleed heaters and particularly deaerators would flash into steam and could run the turbine at dangerously high speeds. Sufficient potential danger exists in bleed lines where sufficient heat energy may be stored to warrant positive closing of the check valves.

Increasing Availability of Cross-Compound Units. When starting the design for the 95,000-kw units, Philo 4 and 5, the war suddenly made the system peak increase rapidly. Needing capacity badly, No. 4 was scheduled to start March, 1942, and No. 5 August, 1942; it was early seen that good delivery was possible on the low-pressure turbines, but it was not so early on the high-pressure turbines and boilers. An arrangement was provided to operate the 125-psi low-presssure turbine from surplus capacity in the existing 600-psi boiler room. With no pressure-reducing system except a system of orifices, the first low-pressure turbine ran $4^1/_2$ months, and the second 2 months at around half load. The 600-psi boilers were fixed up beforehand so the low-pressure turbines could be used to the best advantage. The value of capacity was then very high and the several months of emergency operation fully justified the extra cost of the cross-compound turbines, even without the much higher thermal efficiency.

Another noteworthy feature of the five 95,000-kw cross-compound units at Philo, Cabin Creek, and Twin Branch, is the ability to run the low-pressure elements from the high-pressure boilers when the high-pressure-turbine element is out of service.

Discussion

SABIN CROCKER.[4] The subject of this paper is timely and in keeping with the need for balancing first cost against availability particularly during the present period of high prices. The author's comment in the "Epilogue" about citing a few cases as a stimulant for other engineers to tell how they could have done better is a friendly challenge. At the risk of disappointing the author, however, the opposite course is being taken of mentioning the following instances wherein Detroit Edison, working independently, has adopted similar measures for reducing costs or increasing availability.

Choice of Large Turbine Generators. Detroit Edison experience with the over-all cost of turbine generators of 50,000 kw and larger confirms the author's observation that the economic choice of unit size, steam conditions, number of cylinders, etc., varies from time to time, depending upon system peak, load factor, first cost, and fuel price. Availability also is a factor in that both unit size and reliability affect reserve requirements. Table 3 of this discussion, giving the choice of new units for the Detroit Edison system over a period of some 20 years, shows the trend to larger and more efficient units as dictated by system load growth and changing fuel prices.

An interesting break in the trend is the drop to 14-stage turbines installed during the depression years of the 1930's when fuel was cheap. This choice still seems economically sound because these units will soon be relegated to peaking service when a 100-mw unit now on order is installed and takes over the base load at that plant.

Another interesting point brought out by the table is the number of identical units installed (ten 50's, three 60's, and five 75's) on the system, thus making it possible to increase availability at relatively small cost by keeping a spare turbine rotor on hand.

Initial-Pressure-Regulator Switch on Steam Load to Turbine Which Activates the Governor to Reduce Load on Turbine in Case

[4] Senior Engineer, Design Engineering Staff, Ebasco Services, Inc., New York, N. Y. Mem. ASME.

Steam Pressure Falls Off. This device, which serves to prevent excessive flashing in the boiler with attendant carry-over to the turbine, is considered to afford worth-while protection and has been installed on both Detroit Edison turbines delivered since 1942.

Piping and Valves. Detroit Edison experience with valves and piping corroborates that reported by the author. The use of welded-in seat rings with stellite facing has been found to give valves a degree of reliability that has permitted using welded-bonnet construction with entire satisfaction. The use of valves one size smaller than the pipe also has been tried and adopted as a worth-while economy measure.

Evaporators and Heater Drains. Here again Detroit Edison practice verifies, in general, that recommended by the author. Single heater-drain pumps with loop seals to function in case of high water level have been found adequate and economical. A further step has been the substitution of orifice control of heater drains in lieu of float-operated drainers.[5] The orifices are less expensive, more trouble-free, and can be placed near the low-pressure end of the line so as to protect it from erosion due to flashing. The need for an impingement fitting or flash chamber for receiving discharge from the orifice is recognized, and several different arrangements have been tried.

So much for the instances where experience in the writer's company verifies the author's recommendations.

Another important factor in increasing turbine availability, in the Great Lakes region at least, which seems to have escaped mention is the chlorination of circulating water. Several specific examples that the author has cited are associated with special conditions obtaining with central control rooms or in plants located on small rivers or in coal-mining regions. With these the writer has no firsthand knowledge and is not in a position to comment. At least one instance remains, however, where advantage can be taken of the invitation to argue for an alternate solution.

Deaeration of Condensate. In discussing the location of deaerators, the author ignored the attractive possibility of omitting them entirely and accomplishing deaeration in the main condenser. This not only eliminates an entire piece of equipment, but it also obviates the pumpage complications and hydraulic losses associated with any open heater. Ever since the regenerative feed-heating cycle was adopted for Trenton Channel over 20 years ago, Detroit Edison has made a practice of deaerating condensate and make-up water in the main condenser.

To accomplish deaeration in the main condenser, make-up water is introduced through a header extending the length of the steam space and equipped at definite intervals with spray nozzles. Atmospheric-pressure head has been found adequate for good dispersion of water through the nozzles with sufficient spray action to insure effective deaeration. Spray falls back onto a baffle over the air cooler, down which it flows in a thin sheet which facilitates further release of entrained air and gases for removal through the cooler. Where deaeration is accomplished in the main condenser, reciprocating or rotary dry-vacuum pumps have proved superior to steam-jet air ejectors through better elimination of ammonia, carbon dioxide, and oxygen, at less over-all cost and with less outage for maintenance. Average values for dissolved oxygen can be kept below $^1/_{100}$ ppm, while any remaining trace of ammonia or carbon dioxide is too small to measure.

[5] See (*a*) "The Flow of Saturated Water Through Throttling Orifices," by M. W. Benjamin and J. G. Miller, Trans. ASME, vol. 63, 1941, pp. 419–429.

(*b*) "The Flow of a Flashing Mixture of Water and Steam Through Pipes," by M. W. Benjamin and J. G. Miller, Trans. ASME, vol. 64, 1942, pp. 657–664.

Questions on Boiler-Turbine-Unit System

Without intending to be in any way critical of this excellent paper, the writer would like to take advantage of this opportunity to ask questions about points where supporting data would be particularly useful to others working on such problems. Any existing factual data would be of great help in reducing the possibilities of the boiler-turbine-unit system to a dollars and cents basis. Interest in the unit system is bound to increase because of its application in the reheat cycle that is becoming more attractive, owing to increasing fuel prices, coupled with diminishing returns from further pressure-temperature increases in the straight regenerative cycle. Hence the author's ideas are sought concerning the following questions associated with unit-system design and operation:

1 Means for increasing turbine availability are discussed at some length in the paper. What equivalent measures would the author suggest for increasing boiler availability?

2 To what extent was two- and three-shift maintenance work used in bringing boiler availabilities up to 95 per cent and at what percentage increase in cost?

3 What is the combined availability of such a boiler-turbine unit and how does this compare with the availability of (*a*) the two-boiler one-turbine unit system; and (*b*) the boiler-battery system with crossovers?

4 What are the bases for the statement that "Piping cross-connections for one-boiler one-turbine units were found uneconomical besides introducing operating complications"?

5 How does the unit system behave when relegated to peak-load service?

Further Measures for Reducing Plant Costs

The author has mentioned several measures for reducing over-all costs, to which the following possibilities might be added for consideration:

Stack Support. The choice between using self-supporting stacks as against supporting them on the building steel involves several considerations which seem worth studying. With self-supporting stacks, the boiler fans can be placed at grade level where they can be tended by operators who look after other rotary equipment. This arrangement also shortens the piping required for cooling water and drains for the induced-draft-fan bearings and speed-reducing couplings, if used. Should it ultimately become necessary to wash the stack gases to eliminate sulphur as well as dirt, this could be done to much better advantage at grade level instead of at the top of the building. Where desirable, either the fans or washing equipment, or both, can be placed outside the building proper.

These considerations are in addition to the basic one of whether it costs more to support a stack on top of the building structure or to build it independently from the ground up. The illustrations accompanying the paper show that the author's company has experience with constructing stacks both ways. Hence he may be in a position to contribute helpful data on the economic merits of these alternate methods.

Simplifications in Building Structure. As an alternative to the "outdoor" (or "semi-outdoor") plants mentioned by the author, less drastic simplifications in building structure are possible. Economies can sometimes be made in items of a more or less optional nature such as omitting an auxiliary bay or the wall separating the boiler room from the turbine room. The outlay on certain other items can be reduced at some sacrifice in appearance and maintenance expense. Glazed tile brick, for instance, will save on cleaning and painting, but at increased first cost.

As a war-emergency measure, at least one Pacific Coast plant was built without windows, the primary purpose in this case being

TABLE 3 DESCRIPTION OF MAIN TURBINE GENERATORS INSTALLED ON DETROIT EDISON SYSTEM SINCE 1924

Period	Number and size of units	Rpm	Throttle steam conditions	Number of turbine stages	Number and arrangement of turbine cylinders	Annual heat rate, Btu per net kwhr
1924–1930	Ten— 50 mw	1200	375 psig 700 F[e]	21	Single	14000
1936–1939	Three—60 mw[a]	1800	600 psig 825 F	14	Single	12200
1938–1947	Five— 75 mw	1800	850 psig 900 F	17	Single	11300[b]
1949	Two—100 mw	1800	1300 psig 950 F	23	Tandem compound, double-flow exhaust	10400[c]
1950	One—100 mw	1800	1300 psig 950 F	56[d]	Tandem compound, double-flow exhaust	10500[c]

[a] Omitting from consideration three 30-mw units at Connors Creek where the size was selected to utilize existing generators and condensers.
[b] Estimated figure only owing to mixed operation of plants.
[c] Estimated from manufacturers' proposals.
[d] Impulse-reaction type, whereas all others are straight impulse.
[e] Includes one similar unit actually operated at 300 psig.

to facilitate blackout and to eliminate hazard from shattered glass. There are certain other advantages, however, which tend to offset the loss of daylight, among which are reduced first cost and the elimination of window washing.

Extension of Existing Plant Versus New Site. In the Appendix this topic is listed under the heading "Where is the Plant Needed?" Assuming that added capacity can be used to advantage at an existing plant site, there are several reasons why it may be more economical to extend an existing plant than to start a new one, among which are the following:

(*a*) In any one plant a certain amount of new and highly efficient equipment usually is desirable for base-load purposes in conjunction with older equipment that can be used for peaking service.

(*b*) The coal-handling facilities, canals, etc., of the old plant can often be made to serve the new equipment for less cost than wholly new facilities could be provided. Likewise, the existing offices, repair shops, and warehouses may be adequate for the extended plant.

(*c*) The increase in pay roll for a given increase in system capacity in plant extensions may be only one third to one half what it would be in a new plant.

(*d*) It is reasonable to expect that the transmission facilities for a plant extension would cost considerably less than for equivalent generating capacity at a new site.

G. A. Orrok, Jr.[6] One of the most important matters which the author mentions is the great increase in cost of building and in the cost of switching facilities which has occurred during the past 20 years. Although, by and large, stations are built today at the same over-all costs per kilowatt that they were 50 years ago, the proportionate cost of these two items is much greater. For this reason the writer is inclined to differ with the author, who does not believe the outdoor-type construction can be used for large-size units. It has always seemed to the writer that the waste space, particularly in the turbine room, and the cost of the turbine-room crane are increasing with modern design. Surely some better and cheaper means of constructing turbine rooms will be developed.

Although the cost of the switch house and electrical equipment is largely an electrical problem, the mounting costs of these items indicate that something must be done about them. The structural costs of the building and of the cell work in the switch house call for radical revision in design.

In this regard the costs of foundation and other site limitations are often controlling. To minimize this difficulty, the power-plant designer should be consulted early in the power-plant study so that the most advantageous site may be selected.

The paper throughout stresses the importance of the availability of the units, and maintenance considerations. Much more can be done by our operating departments to develop maintenance figures properly segregated so that they can be used in the design studies in selecting the different types of equipment. However, many of these maintenance costs will remain unmeasured and can be evaluated only by judgment, particularly in studying new types of equipment. It is therefore necessary in making selections or comparing bids not to let financial pressure force the selection of the low bid blindly. A substantial margin—10 per cent is not too great—should be reserved to reflect the combined judgment of the operators and the designer as to the merits of the alternate in regard to unevaluated availability and maintenance costs.

J. A. Powell.[7] At a time when the index of construction cost and the index of electric-plant cost are making new all-time highs, this paper, pointing out many ways to reduce the capital cost of steam-power stations, is particularly timely. Many of the designs here described are boldly original, and the multiple use of condenser circulating water at Philo is a stroke of genius. Like most manifestations of genius it is so simple and even obvious, one wonders why it had not been developed years ago on many sites when the water supply is deficient.

It would have been interesting if the author had given some operating data regarding the vacuums obtained with the series-condenser operation, and the effects on fuel consumption. It would no doubt amaze us to find how small an annual expenditure for fuel was required to effect the enormous savings in plant cost which this plan made possible.

Although there is no compromise with capacity or reliability, the economies that the author reports are all obtained at some sacrifice of operating convenience, flexibility, or thermal efficiency. For 30 years we have been able to combat rising costs of material, equipment, and labor by use of larger units, and by improved design of plant and equipment, but the designers are approaching the end of their resources. Further efforts to hold plant costs within reason will involve sacrifices of this sort, and the author appears to have had the complete co-operation of his operating organization in the acceptance of these features of design. These economies will be particularly gratifying to the stockholders and customers of his company if we ever again experience the conditions prevailing in 1932, when the over-all load factor on the steam stations of the United States dropped to less than 25 per cent. We are deeply indebted to the author for this stimulating report on the achievements of his organization in its efforts to solve today's number one problem of the electrical industry—cost of plant.

Author's Closure

Mr. Sabin Crocker's comment on the value of chlorinating circulating water to increase turbine availability is well taken.

[6] Assistant Superintendent of Engineering, Boston Edison Company, Boston, Mass. Mem. ASME.

[7] Chief Mechanical Engineer, Stone & Webster Engineering Corporation, Boston, Mass. Mem. ASME.

In 1934, studies made on several plants led to the conclusion that chlorination would easily pay for itself as a fuel-economy measure, since cleaner condensers mean better vacuum. However, a concomitant advantage was the elimination of a great deal of manual condenser cleaning, particularly at the Deepwater Station where trouble with algae formation required frequent shooting with plugs. Since then all new and most old condensers have been equipped with chlorinating equipment

As regards omitting deaerators, many studies were made on what savings might be possible. The conclusion reached was that the safety factor that a deaerator affords in precluding oxygen corrosion in the boilers and consequent loss of availability was well worth the incremental cost, particularly since mechanical deaeration is believed to be inherently safer than chemical deaeration. But there are many engineers who take the opposite view.

Mr. Crocker raises several points on the single-boiler single-turbine combination:

1 Measures for increasing boiler availability are largely a function of close co-operation between purchaser and user in discussing the details of boiler design, particularly such factors as:

(*a*) Insuring continuous flow of coal from bunkers to mills by using flared drop pipes from coal bunker to mill feeders.

(*b*) Minimizing sharp turns and corners in the gas passages which tend to concentrate fly ash and cause cutting of boiler tubes; boiler availability apparently is helped by low draft loss in boilers which means less erosion and less fan trouble.

(*c*) Protecting pressure-part surfaces from soot-blower impingement.

(*d*) Using conservative heat-transfer and furnace factors so that boiler is not pushed too hard.

(*e*) Providing for adequate circulation of boiler water, especially to waterwall tubes.

(*f*) Precluding plugging of boiler gas passages by analyzing proper relation between ash-fusion temperature, gas temperature, and gas velocity, especially of gas entering the first-row boiler tubes and the superheater tubes.

(*g*) Checking the relation between ash-fusion temperature, required minimum rating on the boiler, and whether furnace should have a wet or dry bottom.

In other words, increasing boiler availability involves studying in detail the types of boiler outages that have occurred under similar fuel and operating conditions and designing to eliminate them, or, at least, designing so that the outages can be scheduled rather than tolerate emergency outages that compel a sudden shutdown.

2 It is difficult to summarize the extent of multishift maintenance work as it is frequently necessary to use overtime on one or possibly two shifts, as normally not enough maintenance men are available to staff three shifts. One plant even organized a round-the-clock maintenance job when economics warranted taking on temporary employees. On large units whose operating costs are considerably lower than for small inefficient units, there is no question but that multishift maintenance work as well as overtime are easier to justify from an economic standpoint. Shortage of capacity during an outage has frequently required overtime or multishift work regardless of economics.

3 The combined availability of one single-boiler-turbine unit has averaged 92 per cent over six years, but of the 8 per cent outage time, only 1.38 per cent was emergency outage. The objective of the design is to avoid emergency outages and endeavor to schedule outages at such times when the capacity can be spared. It was shown in an EEI Prime Movers' Committee Study (October, 1947, not published), that 39 boilers had 93 per cent availability for 1946. Of the 7 per cent outage time, 5.66 per cent was due to all other causes. This means that by having several boilers, a turbine could gain only 1.34 per cent availability and no more. With only such a small improvement in availability possible, it is indeed difficult to prove out the economics of installing more than one boiler per turbine.

4 The reason, it is believed, that pipe cross-connections between single-boiler single-turbine units are found uneconomical is for the same reason given in paragraph 3 viz.: (1) Emergency outages are such a small per cent (1 to 2 per cent) of the total operating time and both turbine and boiler are overhauled during the longer scheduled outages; (2) this 1 to 2 per cent of outage time would ordinarily not occur simultaneously with full load on the system, which may not be more than 10 per cent of the time; (3) the number of hours per year that necessitate such a cross-connection do not justify the cost.

Isolating valves in cross-connections between units were found to make for unavailability rather than improved availability. Time and again in multiboiler installations, the valve at the interconnection has been found to leak which necessitated taking two boilers out of service instead of one, and involved a valve repair as well. This happened many times with Philo unit No. 3 which is a 165,000-kw unit served by eight boilers, truly a multiboiler installation.

5 It is true that the unit system may possibly give trouble when relegated to peak-load service if an attempt is made to carry low loads of less than 40 to 45 per cent capacity on the boiler instead of shutting it down. But few units are regulated to solely peak-load service. Most plants are interconnected with others and since it is usually more economical to shut down a unit completely rather than run it much below half load, it is only occasionally that inability to operate satisfactorily at less than half load becomes a serious factor. Low-load operation of wet-bottom furnaces can give just as much trouble when there are several boilers per unit as when there is a single boiler.

Mr. Crocker has contributed several worth-while suggestions in making savings in plant design and these emphasize the need for making an economic evaluation of each detail of design, it being almost impossible to make broad generalizations when costs are varying so rapidly.

Mr. Orrok does have a point that space is frequently wasted, particularly in the turbine room. However, compactness of design is just as possible in an enclosed station as in an outdoor station. It does seem that the matter of compactness would be advanced by modeling a new station after one that has managed to operate successfully with a compact arrangement. A plant design that wastes space is sometimes the result of requests by the operating organization for such space, particularly an organization that has operated a plant which has been too cramped in working space around equipment requiring occasional overhaul. Waste space is not so often the result of seeking architectural effects that are not necessarily functional as it is lack of generating an economy-minded attitude throughout the designing organization.

Mr. J. A. Powell is correct in appreciating that the 10-deg F higher water temperature to condensers 4 and 5 at Philo, when operating in series and taking water discharged from the unit-3 condensers, has relatively little effect on plant operating costs when compared to the savings in investment.

For a 95,000-kw unit the extra annual fuel cost is estimated at only around $3000 at current fuel prices, whereas the savings in first cost alone were something over $800,000 per unit. Among the reasons why the extra fuel cost is smaller than might be expected at first glance, are: (1) The river flow is low enough to require recirculation only about 30 days per year; (2) 10-deg F higher circulating-water temperature worsens the vacuum by 0.3 to 0.5 in. Hg (corresponding to 60 F and 75 F water temp); (3).

The average load is 75 per cent of capacity or about 71,000 kw, and has less effect than at full load.

The expected condenser performance with clean tubes is shown in Fig. 12. When operating in series with the unit-3 condensers,

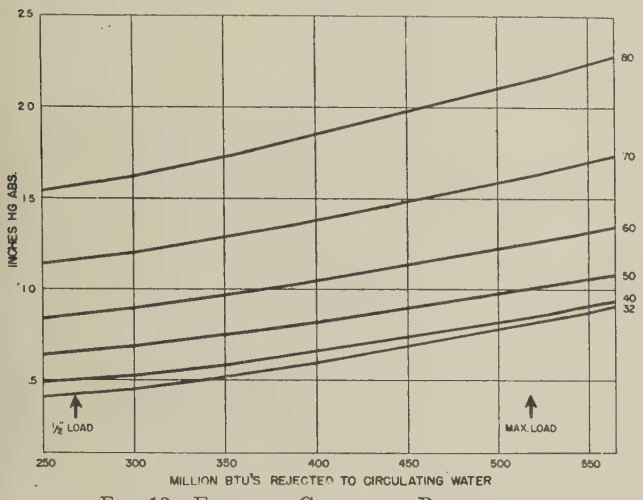

FIG. 12 EXPECTED CONDENSER PERFORMANCE

the circulating water reaches condensers 4 and 5 some 10 deg F warmer. These curves show clearly the loss of vacuum with the warm water.

As Mr. Powell states, designers of plants have explored most trails that may lead to further economies in over-all generating costs: larger units, stripped plants with little spare equipment, single-boiler-turbine combinations, higher pressures and temperatures and reheat. More intensive efforts than ever are called for in the attempt to balance increased labor costs by technological improvements, not to reduce first cost, but to obtain the lowest sum of first cost and operating costs. The examples given herein are only the first blazes on new trails; others will surely cut new blazes to advance those trails or start new and better trails.

That the power industry is aware of its responsibility in holding the cost of generating power to a minimum is evidenced by the efforts being made by so many plant engineers who are making every effort to reduce such costs by technological developments. The work that has been done and is being done by designers must be implemented by careful attention to operation, keeping in mind that, on a system having an output of 10 billion kwhr per yr.

$\frac{1}{4}$ in. Hg low vacuum may cost	$200,000 per year
25 F low superheat may cost	$150,000 per year
1 cent per ton of coal extra for mill maintenance	$50,000 per year
25 F higher temperature of flue gases leaving the stack	$125,000 per year

The author is deeply grateful for the stimulating comments of the discussers, feeling the paper worth while for having called forth such useful observations.

An Investigation of Boiler-Drum Steel After Forty Years of Service

By H. S. BLUMBERG[1] and G. V. SMITH[2]

Examination of materials from seven riveted boiler drums removed from service after forty years' operation at a temperature and pressure of 388 F and 200 psi has revealed no evidence of deterioration in the properties of the steel from which they were made.

Introduction

FROM time to time in recent years there have been proposals that boiler-inspection codes be modified to require an arbitrary derating of drums after some thirty years' service. In each case it was proposed that the derating be made, even though careful inspection might have failed to disclose any significant loss in thickness of the metal or any observable deterioration of joints. Therefore it is implied in such proposals that the metal itself undergoes a deterioration in properties.

There are numerous different kinds of changes which may occur in metals during service. The extent to which these changes take place in any specific instance depends upon the service conditions of temperature, time, stress, and medium to which they are subjected. Consideration of the possible changes which might occur in boiler-drum steel, such as that investigated here, during service at the comparatively low maximum temperature of 400 F indicate that only so-called strain-aging embrittlement and caustic embrittlement appear to be of any concern. Caustic embrittlement results from localized corrosive attack, while strain-aging embrittlement occurs in certain steels during "aging" after being plastically deformed. The latter type of embrittlement occurs during service at temperatures ranging from slightly below atmospheric up to some 500 F to 600 F. The embrittlement, which, in terms of mechanical-property changes, involves an increase in yield and tensile strengths, and a decrease in ductility, and particularly in notch impact strength, results from a precipitation phenomenon, and develops more rapidly with increasing temperature. However, at the higher temperatures the embrittlement attains a maximum degree and then "overages" toward the initial unaged condition.

An extensive search of related technical literature[3] failed to uncover any reports of a comprehensive investigation of this problem. Records of operating experience with boilers provided some measure of support of the theory that deterioration was not great, but the evidence was not conclusive. There was also a wealth of material based on experience with bridges and similar structures, but the applicability of such data, although not without logic, might be questioned, owing to differences in temperature and other conditions. Accordingly, when it was found that a considerable amount of suitable material would be available from a group of boiler drums which had been in service since 1902, the present investigation was undertaken in an effort to determine the extent of metal deterioration.

The materials were examined visually before and after shot-blasting. Representative sections were tested to destruction to determine chemical analyses and the mechanical properties, strength, ductility, and notch toughness. Additional tests were made, including macroscopic and microscopic examinations, magnaflux and hardness tests. Finally, "strain-aging" tests were made on plate materials to determine the susceptibility of the steels to strain-aging embrittlement. From these data it was possible to determine whether there was any evidence of metal deterioration. A comparison was also made between properties of the materials in these forty-year-old drums and those of present-day manufacture and processing.

Description of Materials Investigated

The materials investigated consisted of one complete boiler drum (No. 3) and six separate specimen plates from a group of drums (Nos. 5, 6, 8, 9, 10, and 19) that were being removed from Waterside No. 1 Station of the Consolidated Edison Company of New York, Inc., in order to provide space for new boilers of higher pressure and larger capacity.

The boiler drums were part of a group of fifty-six that were placed in service during 1901 and 1902. They were of the "Cahall" type, manufactured by Aultman and Taylor Machinery Company, Mansfield, Ohio, and were rated 650 hp, at a working pressure of 200 psi. Fig. 1 shows the arrangement of the boilers after they had been modified by the installation of superheaters (in 1904), and by underfeed stokers instead of hand-fired grates (in 1910–1911).

Each drum had a nominal outside diameter of 42 in. and a length (straight portion) of 22 ft. The straight portion was made in three sections from $^{9}/_{16}$-in. plate with longitudinal seams butt-strapped with $^{1}/_{2}$-in. plate and triple-riveted. Girth seams were double-riveted. All rivets were 1 in. in diam. The drum heads were formed from $^{11}/_{16}$-in. plate. Fig. 2, which has been redrawn from the manufacturer's original blueprint, shows the general constructional details.

A search of records of the manufacturer (now the property of the Babcock and Wilcox Company) disclosed evidence that test coupons were removed from the plate materials and that the tests met specification requirements. However, the test records could not be found and there is some doubt as to the exact specification requirements.

Until 1904 the boilers supplied saturated steam to reciprocating engines at 175 psi. The condensate was too contaminated by oil to permit use as boiler feedwater and consequently, during this period, the feed consisted entirely of raw water from the New York City water supply. Chemical analyses of the water are not available, but on the basis of analyses made on present supplies from the same source, it is probable that the "hardness" was about 45 ppm, and the total solids about 90 ppm. During the life of the boilers the oxygen content of the water ranged from $1^{1}/_{2}$ to 3 ppm.

As turbines began to replace the reciprocating engines in 1904,

---

[1] Chief Metallurgist, The M. W. Kellogg Company, Jersey City, N. J.

[2] Research Metallurgist, United States Steel Corporation Research Laboratory, Kearny, N. J.

[3] C. A. Zapffe (Trans. ASME, vol. 66, 1944, pp. 81 to 126) has made a very complete review of the literature of boiler embrittlement.

Contributed by the Power Division and presented at the Semi-Annual Meeting, Chicago, Ill., June 16–19, 1947, of The American Society of Mechanical Engineers.

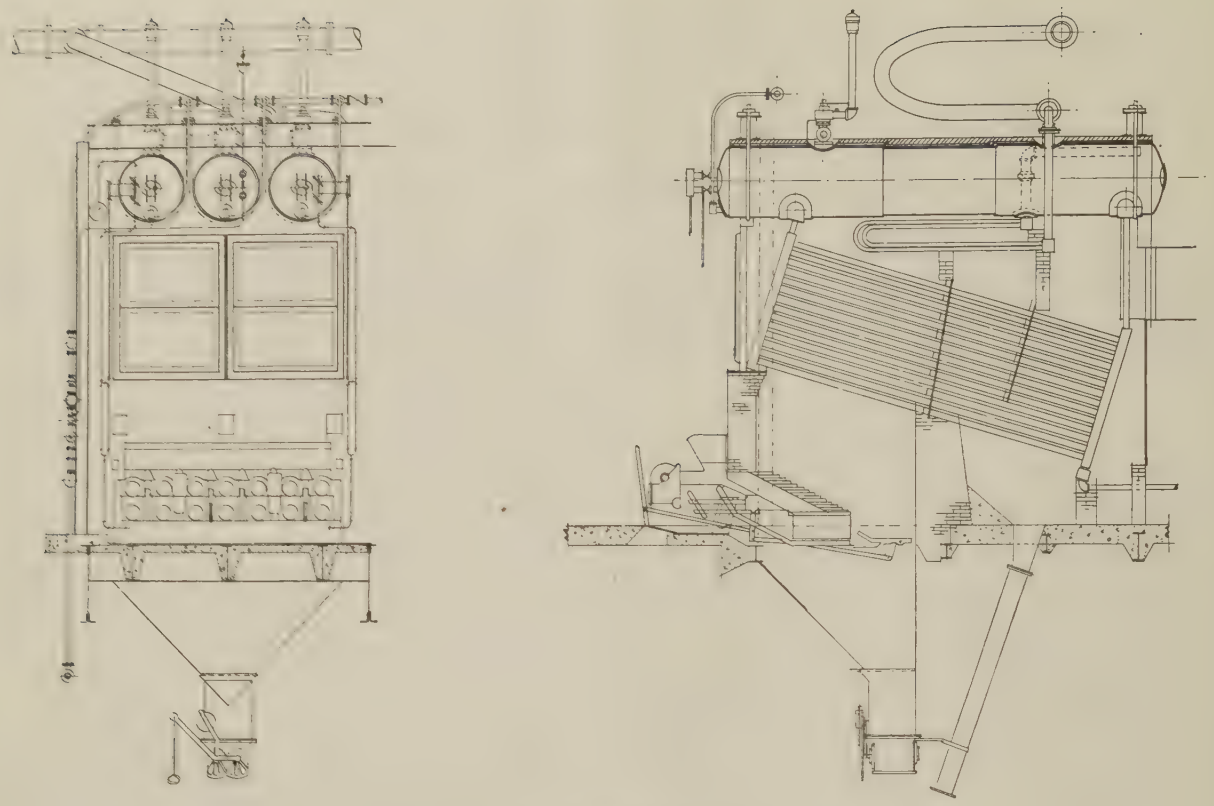

FIG. 1 ARRANGEMENT OF BOILERS

the amount of usable condensate increased and raw water make-up decreased. The last of the engines was removed in 1918.

The hand-fired grates were replaced by underfeed stokers in 1910 and 1911, and after that the boilers were often operated for long periods of time at 200 per cent or more of rating, at 200 psi pressure.

Until 1924 the feedwater was treated with sal soda (Na_2CO_3). In 1924 the plant began furnishing steam to the district heating system of the New York Steam Corporation. As no condensate was returned, the quantity of make-up increased correspondingly. This emphasized the problems of chemical water treatment, and advantage was taken of advances in the art to change to a combination of caustic soda (NaOH) and trisodium phosphate (Na_3PO_4), which was continued with slight modification during the further service of the boilers. The principal change, which was a result of the installation of high-pressure topping units at Waterside Station No. 2, was made in 1937, when a zeolite system was installed and water thus treated became available for much of the make-up.

From the time of their initial installation until the last few years of their life, these boilers were taken out of service once every year for an annual overhaul. During these overhauls the boiler drums were carefully scraped and wire-brushed until they were metal clean. The inner walls of the drums were then painted with a gray lead-oxide paint and, in addition, the surface below the water line was painted with a mixture of graphite and fish oil. The tubes were all carefully turbined, all caps and cap seats cleaned, all tube headers and mud drums carefully cleaned and washed down. This careful maintenance program resulted in the very good operating condition of these boilers up to the time when they were retired from service.

PROCEDURE

Visual Examination As-Received: Drum No. 3. The outer surface of drum No. 3 as-received for study was covered on the upper half with a loosely adhering gray-colored powder which resulted from insulation adherence. The lower half of the drum surface was discolored with a thin red-brown oxide. No defects were observed on the outer surface. Fig. 3 shows the drum as received.

Six plates were removed from each of boilers Nos. 5, 6, 8, 9, 10, and 19. These six plates removed from six separate drums consisted entirely of base metal with no rivets or riveted joints present. Each plate was 24 in. × 24 in. × $^9/_{16}$ in. thick. The outer and inner surfaces were covered with a light-gray deposit which was easily brushed away from the material. No defects in any of the metal surfaces were observed. Table 1 gives pertinent details.

TABLE 1 SAMPLE-PLATE DATA

Plate mark	MWK mark	Boiler no.	Location with respect to water line	Drum description	From front or back section of drum
5-WEF	A	5	Below	End drum	Front
6-WCB	B	6	Below	Center drum	Back
9-WCF	D	9	Below	Center drum	Front
8-SCB	C	8	Above	Center drum	Back
10-SEB	E	10	Above	End drum	Back
19-SCF	F	19	Above	Center drum	Front

Visual Examination of Drum No. 3 After Shotblast. Both heads of drum No. 3 were separated from the unit by acetylene-torch-cutting at a location in the shell several inches beyond the circular riveted seam joining the heads to the shells.

A thorough visual inspection of the inner drum surfaces was made. A thin light-gray deposit which was probably the paint coating was observed adhering uniformly to the entire inner shell and head surfaces. No visual defects were observed.

The entire inner surfaces of the head and shell sections were lightly shot-blasted so as to expose bare metal. In addition,

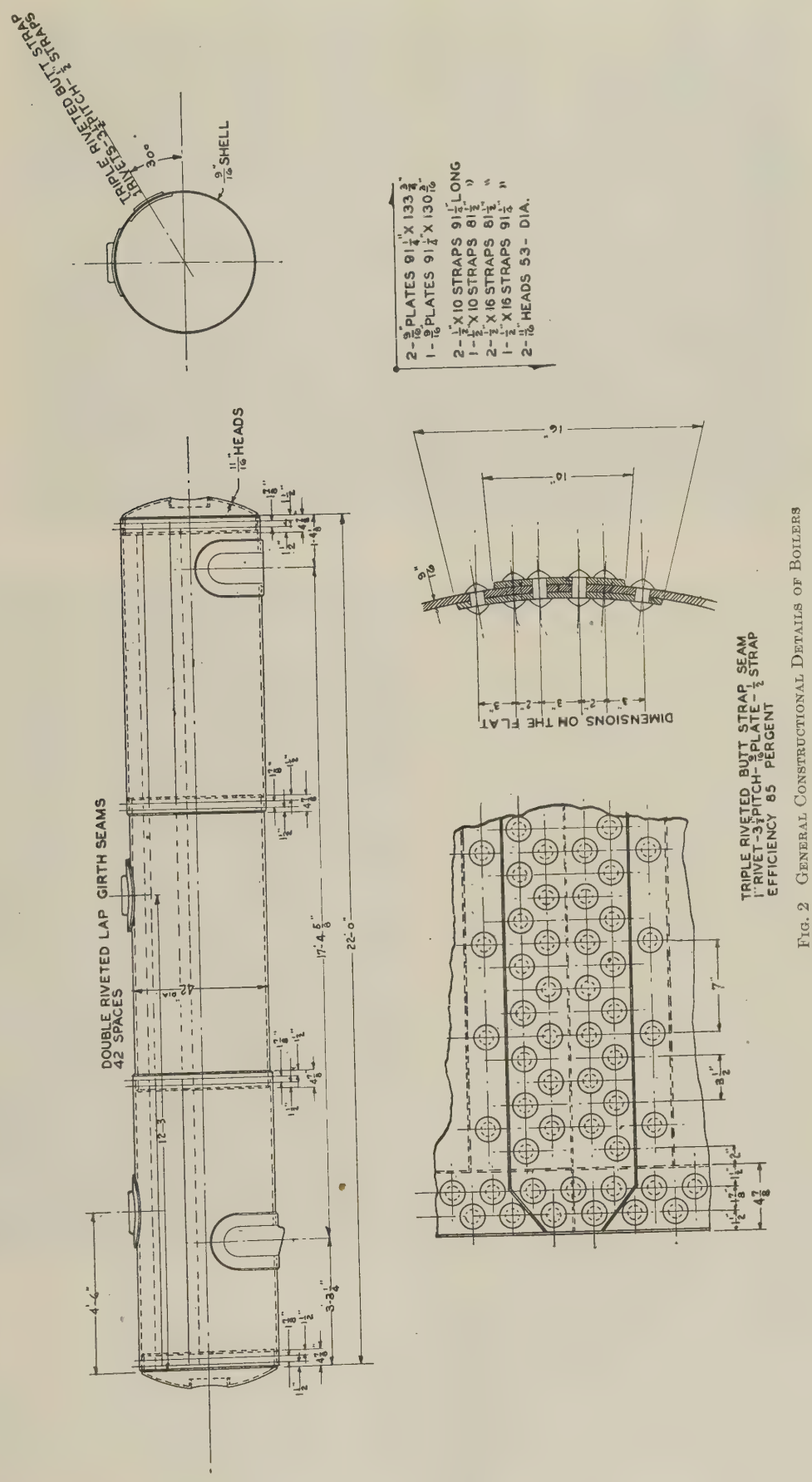

FIG. 2 GENERAL CONSTRUCTIONAL DETAILS OF BOILERS

FIG. 3 DRUM NO. 3 AS RECEIVED, VIEWED FROM FRONT END

outer metal surfaces were shotblasted in the vicinity of all rivets. Photographs were taken to show the typical surface condition at various locations, as well as to illustrate freedom from visual defects. A typical view of rivets in longitudinal and circumferential seams after shotblasting, from drum No. 3, is given in Fig. 4.

Inspection of Drum No. 3 by The M. W. Kellogg Company Shop-Inspection Division. In addition to the visual examinations made as part of the metallurgical investigation, several inspections of the riveted drum were carried out by two senior shop inspectors, each of whom has had over fifteen years of experience in the inspection and fabrication of drums and vessels for power-plant and oil-refinery services.

The plate surfaces had no indication of pitting or wasting away of metal at any location. Rivets and rivet-joint surfaces appeared to be in the same condition as must have existed when the drum was fabricated and no defects were reported. The very good operating condition of the riveted drum is evidently attributable to the careful maintenance program followed as described previously.

Metallurgical Study. In planning the metallurgical study, drum No. 3 was considered in terms of three essential components, namely, plate material, rivets, and riveted joints. The six separate plates consisted wholly of plate material.

The term "plate" material refers to those parts of the drums formed from rolled steel plates. Five such units were present in the complete drum submitted for study (drum No. 3), consisting of the three straight sections and the two heads; six separate plates from as many boilers were also received. Therefore there was available for this study a total of eleven plate materials from seven separate drums. In testing, consideration was given to mechanical properties of each of the plate sections in the "longitudinal" and "circumferential" directions and also to location above or below the water line during service operation.

Longitudinal direction refers to the long axis of the drum, while circumferential denotes the direction of the circular periphery of the drum. These terms do not have any significance as to the direction of rolling of the plate in the steel mill. In selecting specimens from the two heads of the complete drum, two directions were chosen, horizontal and vertical.

Drum No. 3 contained seven riveted seams, three of these

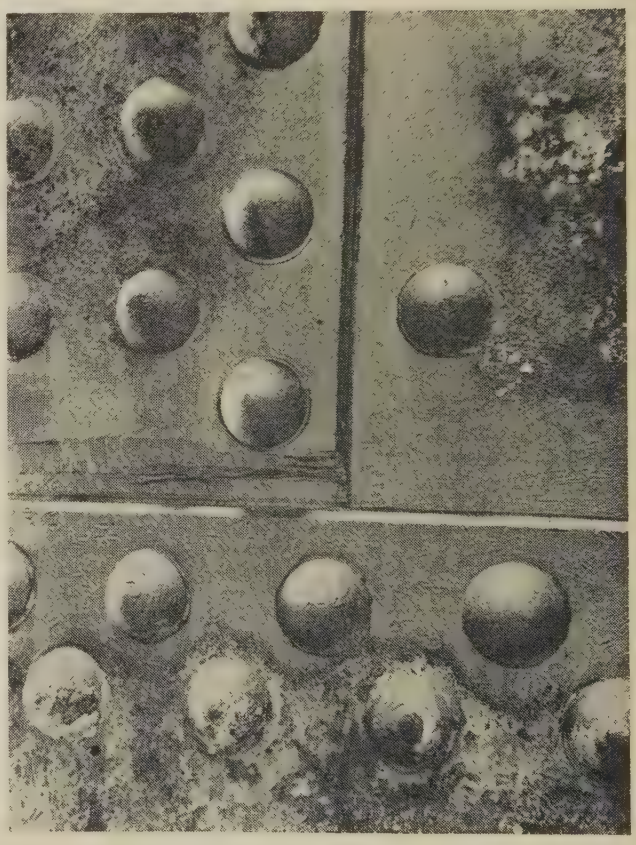

FIG. 4 RIVETS IN LONGITUDINAL AND CIRCUMFERENTIAL SEAMS AFTER SHOTBLASTING; DRUM NO. 3

longitudinal and four circumferential. The former occurred only in straight sections and were located entirely above the water line, whereas the circumferential seams joined straight as well as head sections and were partly above and partly below the water line in service. Representative selections of material were

made in testing rivets and riveted joints; these selections are shown in detail in Table 2. Locations of specimens are given in Fig. 5.

The chemical composition and mechanical properties of each of the plate sections were determined so that a comparison could be made with the requirements of present-day materials as standardized in current ASTM specifications. In addition, other data not required by standard specifications were obtained, so that a more complete evaluation of the condition of these materials after forty years of service could be developed.

Analyses on Tests

Chemical Analyses. Drillings from each of the shell and head plates and from one rivet of drum No. 3, as well as from each of the six separate plates were analyzed as indicated in Table 2, for the five common elements, carbon, manganese, phosphorus, sulphur, and silicon. The results are reported in Tables 3 and 4.

Tension Tests. Two types of tension tests were made, conventional full-thickness specimens from each of the eleven plate materials, and specially prepared riveted-joint specimens from drum No. 3.

The test bars, consisting wholly of plate material, were obtained from each of the straight and head sections composing drum No. 3 and also from each of the six separate plate sections available for this investigation. Standard rectangular tension test specimens with 8-in. gage length were prepared in accordance with

TABLE 2 RÉSUMÉ OF TESTS MADE AND LOCATIONS FROM DRUM NO. 3

MATERIALS and LOCATIONS			PLATE MATERIALS								RIVETS			RIVETED JOINTS		
			SHELL SECTIONS				HEADS									
			Three circular sections, each composed of one plate.				Two head sections, each composed of one plate				Longitudinal Seams*	Circumferential Seams		Longitudinal Seams*	Circumferential Seams	
			Above water line.		Below water line		Above water line		Below water line							
			Longitudinal direction	Circumferential direction	Longitudinal direction	Circumferential direction	In direction Horizontal	In direction Vertical	In direction Horizontal	In direction Vertical	Above water line.	Above water line.	Below water line.	Above water line.	Above water line.	Below water line.
CHEMISTRY			From each section.		From each section		From each head		From each head		From one Rivet			NONE		
PHYSICAL PROPERTIES	TENSION TESTS		From each section	From each section	From each section	From each section	From each head	From each head	From each head	From each head	NONE					
	BEND TESTS		From each section	From each section	From each section	From each section	From each head	From each head	From each head	From each head				NONE		
	IMPACT TESTS	CHARPY (KEYHOLE NOTCH) As Received	From each section	From each section	NONE		NONE									
		CHARPY (KEYHOLE NOTCH) After 1200° F Stress Relief	From each section	From each section												
		IZOD (VEE NOTCH) As Received	From each section	From each section												
		IZOD (VEE NOTCH) After 1200° F Stress Relief	From each section	From each section												
	HARDNESS TESTS		From each section	From each section	From each section	From each section	From each head	From each head	From each head	From each head						
MACROSCOPIC EXAMINATION			From each section		From each section		From each head		From each head		FROM REPRESENTATIVE SECTIONS			FROM REPRESENTATIVE SECTIONS		
MICROSCOPIC EXAMINATION			From each section		From each section		From each head		From each head							
MAGNAFLUX EXAMINATION			NONE		NONE		NONE									
STRAIN AGING TESTS			FROM SELECTED SECTIONS								NONE					
REMARKS											* Longitudinal Seams all above water line.					

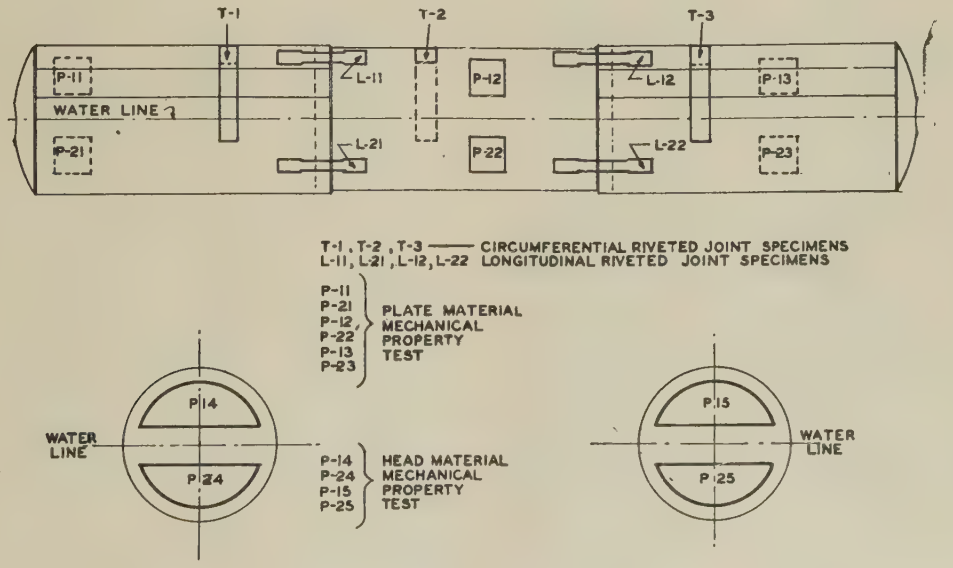

FIG. 5 LOCATION OF TEST SPECIMENS

TABLE 3 RESULTS OF CHEMICAL AND MECHANICAL TESTS FROM DRUM NO. 3

APPENDIX PAGE 23

MATERIALS and LOCATIONS.		THREE CIRCULAR SHELL SECTIONS EACH COMPOSED OF ONE PLATE												TWO HEAD SECTIONS EACH COMPOSED OF ONE PLATE							
		ABOVE WATER LINE						BELOW WATER LINE						ABOVE WATER LINE				BELOW WATER LINE			
		LONGITUDINAL DIRECTION			CIRCUMFERENTIAL DIRECTION			LONGITUDINAL DIRECTION			CIRCUMFERENTIAL DIRECTION			HORIZONTAL DIRECTION		VERTICAL DIRECTION		HORIZONTAL DIRECTION		VERTICAL DIRECTION	
M. W. K. MARK		11L	12L	13L	11C	12C	13C	21L	22L	23L	21C	22C	23C	14A	15A	14B	15B	24A	25A	24B	25B
CHEMICAL ANALYSES	C.	.19	.23	.24	SEE			.24	.22	.23	SEE			.26	.25	SEE					
	Mn.	.33	.35	.32				.34	.37	.30				.36	.36						
	P.	.009	.010	.009				.010	.009	.009				.008	.009						
	S.	.037	.031	.032				.033	.038	.032				.039	.039						
	Si	nil	nil	nil				nil	nil	nil				nil	nil						
TENSION TESTS	T.S. (p.s.i.)	57,500	59,600	60,500	59,000	62,000	60,000	60,000	62,000	62,200	59,600	61,900	61,500	60,000	60,800	60,600	61,800	60,400	59,950	61,000	61,800
	Y.P. (p.s.i.)	31,600	34,400	33,800	33,900	37,000	34,000	33,000	35,400	35,900	34,700	36,500	33,700	29,200	28,100	33,000	32,100	31,900	31,700	33,000	36,000
	% Elongation 8"	28.0	28.3	25.5	29.6	25.6	27.6	25.5	30.5	25.6	28.0	24.4	26.8	26.9	26.0	47.5(2")	44.0(2")	25.7	25.2	47.5(2")	47.5(2")
	% Reduction Area	55.7	53.2	51.7	54.2	52.0	55.0	40.0	41.0	39.0	51.7	48.8	47.5	47.7	48.2	50.2	52.7	53.0	51.2	53.6	50.8
BEND TESTS	Bent to	180°	180°	180°	180°	180°	180°	180°	180°	180°	180°	180°	180°	180°	180°	180°	180°	180°	180°	180°	180°
	% Elongation	36.0	39.0	40.0	39.0	39.0	40.0	40.0	41.0	39.0	40.0	38.0	39.0	47.0	44.0	46.0	45.0	36.0	43.0	43.0	43.0
	Remarks	No Def.	No Def.	No Def.	No Def.	No Def.	No Def.	No Def.	No Def.	No Def.	No Def.	No Def.	No Def.	No Def.	No Def.	No Def.	No Def.	No Def.	No Def.	No Def.	No Def.
IMPACT TESTS — CHARPY — As Rec'd.	Actual Ft. Lbs. Values	24.5 23.5 22.0	22.0 23.5 23.0	24.5 24.5 23.0	23.0 20.5 23.0	23.0 22.0 23.0	23.5 24.0 24.5	NO TESTS MADE													
	Average	22.4	22.8	24.0	22.7	22.7	24.0														
CHARPY — 1200° F S. R.	Actual Ft. Lbs. Values	22.2 25.0 22.5	22.0 23.0 25.5	26.0 25.5 26.0	23.5 27.5 27.0	22.5 23.0 23.0	25.5 26.5 Lost														
	Average	23.2	23.5	25.8	26.0	23.0	26.0														
IZOD — As Rec'd.	Actual Ft. Lbs. Values	28.3 20.0 27.5	20.0 27.3 20.5	31.0 28.5 15.5	27.5 24.0 13.5	32.0 27.0 13.0	29.5 20.8 17.8														
	Average	25.2	22.6	25.0	21.7	24.0	22.7														
IZOD — 1200° F S. R.	Actual Ft. Lbs. Values	28.0 34.5 28.3	30.3 18.5 17.5	34.0 34.5 34.5	34.3 31.0 35.8	31.5 33.8 38.0	33.5 33.3 32.0														
	Average	30.2	22.1	30.8	33.7	34.4	32.9														
HARDNESS (Brinell)		128	130	131	128	134	134	130	140	132	137	138	131	133	130	140	131	134	143	138	

* "Def" refers to "defects".

TABLE 4 RESULTS OF CHEMICAL AND MECHANICAL TESTS FROM DRUMS NOS. 5, 6, 8, 9, 10, AND 19

CONSOLIDATED EDISON CO.	DRUM NO. / PLATE MARK	5 / 5-WEF		6 / 6-WBC		9 / 9-WCF		8 / 8-SCB		10 / 10-SEB		19 / 19-SCF	
M. W. KELLOGG CO. MARK		A		B		D		C		E		F	
LOCATION OF PLATE WITH RESPECT TO WATER LINE IN DRUM.		BELOW		BELOW		BELOW		ABOVE		ABOVE		ABOVE	
DIRECTION OF TEST SPECIMENS.		LONG.	CIRC.	LONG.	CIRC.	LONG.	CIRC.	LONG.	CIRC.	LONG.	CIRC.	LONG.	CIRC.
CHEMICAL ANALYSES	CARBON	0.23		0.22		0.26		0.20		0.32		0.22	
	MANGANESE	0.41		0.32		0.35		0.36		0.38		0.37	
	PHOSPHORUS	0.011		0.013		0.009		0.010		0.017		0.009	
	SULFUR	0.043		0.038		0.038		0.036		0.031		0.032	
	SILICON	Trace		Trace		Trace		Trace		Trace		Trace	
TENSION TESTS	T. S. (p. s. i.)	60,200	61,100	58,400	59,700	60,000	59,000	56,000	57,500	63,900	68,200	59,000	60,200
	Y. P. (p. s. i.)	35,400	37,600	32,200	34,100	36,700	34,800	32,600	33,000	34,000	41,200	34,800	34,900
	% ELONGATION 8"	26.4	23.0	27.0	25.6	25.0	26.8	26.4	25.2	24.6	26.8	24.0	24.0
	% REDUCTION AREA	50.0	51.3	53.6	53.9	52.0	52.6	56.0	53.3	Not Obtained	54.0	50.2	49.6
BEND TESTS	BENT TO	180°	180°	180°	180°	180°	180°	180°	180°	180°	180°	180°	180°
	% ELONGATION	42.0	45.0	45.0	45.0	49.0	42.0	45.0	48.0	49.0	44.0	33.0	34.0
	REMARKS	No defects	No defects	No defects	No defects	No defects	No defects	No defects	No. defects	No. defects	No. defects	No. defects	No defects
IMPACT TESTS — CHARPY — AS RECEIVED	ACTUAL VALUES FT. LBS.	21.0 19.0 18.0	20.5 21.0 23.0	NONE		NONE		28.0 28.0 25.5	30.0 30.0 24.0	NONE			
	AVERAGE	19.3	21.5					27.2	28.0				
CHARPY — 1200° F. S. R.	ACTUAL VALUES FT. LBS.	21.0 22.5 22.5	23.0 20.5 24.5					31.0 33.0 30.5	29.5 27.0 32.0				
	AVERAGE	22.0	22.7					31.5	29.5				
IZOD — AS RECEIVED	ACTUAL VALUES FT. LBS.	20.5 25.8 26.5	11.0 13.0 9.8					31.3 40.0 31.0	20.5 12.5 25.5				
	AVERAGE	24.1	11.2					34.1	19.5				
IZOD — 1200° F. S. R.	ACTUAL VALUES FT. LBS.	23.0 18.0 15.3	23.3 11.5 30.0					20.5 12.5 25.5	28.3 32.8 32.5				
	AVERAGE	18.7	21.6					19.5	31.2				

ASTM Designation E-8-42, except in the case of specimens taken in the vertical direction from the heads, where the length of specimen was adequate for a gage length of only 2 in. Specimens were prepared in both longitudinal and circumferential directions, above and below the water line. In no case was there any metal removed from the plate surfaces.

Twenty specimens from drum No. 3 and twelve specimens from the plates from the other drums were tested in a 100,000-lb tensile testing machine with an accuracy within $\frac{1}{2}$ per cent as recently calibrated. Tensile strength, yield point (by beam drop) elongation, and reduction of area were determined. Careful visual observation of each test bar was made to ascertain whether any

LONGITUDINAL SPECIMENS

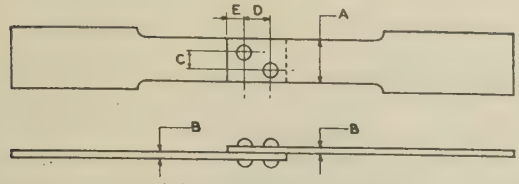

ALL DIMENSIONS IN INCHES

LOCATION	SPECIMEN Nº	A	B	C	D	E
ABOVE WATER LINE	L-11	3.650	.548	2	2	1.5
	L-12	3.780	.560	2	2	1.5
BELOW WATER LINE	L-21	3.630	.548	2	2	1.5
	L-22	3.740	.560	2	2	1.5

CIRCUMFERENTIAL SPECIMENS

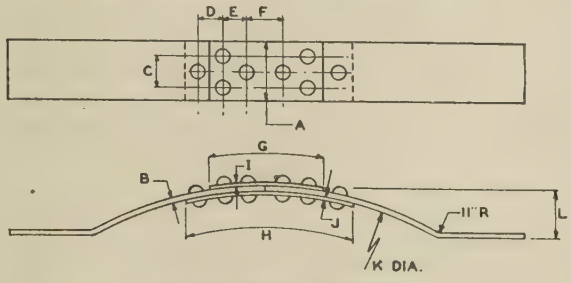

ALL DIMENSIONS IN INCHES

SPECIMEN Nº	A	B	C	D	E	F	G	H	I	J	K	L
T-1	5.55	.594	3.5	3.3	2.1	3.1	10	15	.6	.5	41	4.33
T-2	5.55	.585	3.5	3.3	2.1	3.1	10	15	.6	.5	41	4.33
T-3	5.55	.609	3.5	3.3	2.1	3.1	10	15	.6	.5	41	4.33

ALL ABOVE WATER LINE

FIG. 6 RIVETED-JOINT SPECIMEN DETAILS

evidence of metal deterioration was present which was not disclosed by test data. Results obtained in testing these specimens will be found in Tables 3 and 4.

One full-thickness tension specimen was prepared from each of the three longitudinal and the four circumferential riveted seams of the whole drum (No. 3), after consultation with the Mechanical Testing Division of Columbia University. Each test specimen contained the riveted joint in the center and was prepared in accordance with sketch shown in Fig. 6. Because the longitudinal specimens from the girth seams were approximately flat no shaping other than machining of the sides was necessary. The circumferential specimens from the longitudinal seams, however, were purposely hot-shaped at their end portions so that they could be properly gripped in the jaws of the 600,000-lb-capacity machine at Columbia University. Typical longitudinal specimens after testing are shown in Fig. 7, and typical circumferential test specimens in Fig. 8. In testing, the specimens were gripped and slowly loaded until maximum load was reached and failure produced. The maximum load at failure was recorded and each broken bar was studied for mode of failure. Results are given in Table 5.

Bend Tests. Specimens were prepared from plate materials of drum No. 3 and the six other plates at locations adjacent to the tension specimens previously described (see Tables 2, 3, and 4, respectively). Full-thickness specimens were machined to a width of 1 in. with no metal removed from either surface of the steel. Two lines 1 in. apart were scribed at the center of each specimen on the surface of the test bar corresponding to the inner drum surface which was tested as the outer fiber of the bend specimen. Bending was carried out in accordance with the Stand-

FIG. 7 LONGITUDINAL RIVETED-JOINT SPECIMENS AFTER TESTING

FIG. 8 CIRCUMFERENTIAL RIVETED-JOINT SPECIMENS AFTER TESTING

TABLE 5 RESULTS OF RIVETED-JOINT TENSION TESTS

SPECIMEN No.	SPECIMEN LOCATION IN BOILER	MAXIMUM LOAD POUNDS	TYPE OF FAILURE	REF. PHOTO No.	REMARKS
L-11	ACROSS CIRC. SEAM [1]	73100	NET TENSION	FIG. 11 APP. P. 13	FAILED ALONG DIAGONAL THRU BOTH RIVET HOLES
L-12	ACROSS CIRC. SEAM [1]	74500	RIVET SHEAR	FIG. 11 APP. P. 13	SHEARED CLEANLY THRU TWO RIVETS
L-21	ACROSS CIRC. SEAM [2]	73900	NET TENSION	FIG. 11 APP. P. 13	FAILED THRU ONE RIVET HOLE IN EACH PLATE
L-22	ACROSS CIRC. SEAM [2]	70000	RIVET SHEAR	FIG. 11 APP. P. 13	SHEARED CLEANLY THRU TWO RIVETS
T-1	ACROSS LONG. SEAM [1]	127000	NET TENSION	FIG. 12 APP. P. 14	NON-DUCTILE FRACTURE THRU HALF MAIN SHELL PLATE AT FIRST SINGLE RIVET DUCTILE FAILURE ON BALANCE
T-2	ACROSS LONG. SEAM [1]	135000	NET TENSION	FIG. 12 APP. P. 14	NON-DUCTILE FRACTURE THRU MAIN SHELL PLATE AT FIRST SINGLE RIVET
T-3	ACROSS LONG SEAM [1]	82500	NET TENSION	FIG. 12 APP. P. 14	NON-DUCTILE FRACTURE THRU MAIN SHELL PLATE AT FIRST SINGLE RIVET HALF OF SHELL PLATE FAILED AT 57100 LBS. REMAINING HALF SUSTAINED 82500 LBS.

1 ABOVE WATER LINE
2 BELOW WATER LINE

ard Method of Bend Testing for Ductility of Metals, ASTM Designation E-16-39. Testing was continued until 180 deg was reached. Results will be found in Tables 3 and 4.

Notch-Impact Tests. A considerable amount of notch-impact testing was done (see Tables 2, 3, and 4, respectively). Specimens were prepared from the center of the plate thickness of the three straight sections of drum No. 3 and from two of the six separate plates, with the long axes of the test bars, respectively, longitudinal and circumferential. No notch-impact specimens were obtained from head material.

Two types of standard notch-impact specimens were made, Charpy keyhole notch and Izod vee notch, in accordance with ASTM Designation E-23-41T, with the notch perpendicular to the plate surface. Test bars were made from plate material as-received for study and also after stress relief at 1200 F for 1 hr, followed by furnace-cooling. Three test specimens of each type were prepared for each condition described. The Charpy specimens were tested in an Amsler machine with a 75-ft-lb blow and simple beam loading, and the Izod bars in a Sonntag Universal testing machine with a 60-ft-lb blow and cantilever loading. All tests were made at room temperature. The results of tests upon seventy-two bars are reported in foot-pounds (absorbed) at room temperature in Tables 3 and 4.

Hardness Tests. Hardness was measured by means of a Brinell hardness machine, using the standard 3000-kg load. One reading was obtained upon one end of each tension specimen from plate material.

Macroscopic Examinations. Specimens were sectioned from each of the plate materials and from representative rivets and longitudinal and circumferential riveted joints. Samples were selected from above and below the water line and these were deep-etched in 1-1 HCl for 20 min at 140 F to 160 F.

Microscopic Examinations. Specimens were prepared from each of the plate materials from drum No. 3 and the six separate plates. These were carefully mounted in thermoplastic medium to insure that microscopic study could be made of the full cross sections, especially at the plate surfaces. Examinations were made before and after etching and representative photomicrographs were taken.

Cross sections through several riveted joints were also prepared for microscopic study. These were taken from both longitudinal and circumferential joints. Careful examination was made for evidence of metal deterioration and representative photomicrographs were taken.

Magnaflux Examinations. This type of testing was done on each riveted-joint specimen selected for both the macroscopic and microscopic studies, before the latter tests were made. The samples represented the cross sections through riveted joints at the long centers of rivets and were taken from longitudinal and circumferential joints, at locations above and below the water line. Cross sections through six separate rivets and contiguous plate from one nozzle of the riveted drum were also prepared. Magnafluxing was done by the "wet" method, with 300-amp current applied continuously for 30 sec. No indication of defects was found in any of these specimens.

Strain-Aging Tests. In addition to the quality tests of the material in drum No. 3, the strain-aging characteristics of the material were investigated, and a comparison was made with material currently supplied under ASTM A-70 Specification for Carbon-Steel Plates for Stationary Boilers and Other Pressure Vessels.

This test was made in accordance with a procedure first proposed by Graham and Work.[4] Essentially it consists of cold-working a tapered round specimen by drawing it through a cold-draw die and then notching at convenient intervals of known reduction of area along the cold-drawn bar. The material is then aged at a suitable temperature (in this case 2 hr at 450 F) and broken at room temperature as an impact test at each notch as in the Izod test.

Test Results and Discussion

Chemical Analyses; Plate Material. Results are summarized in Tables 3 and 4. A number of ASTM plate-steel specifications are used today as a basis for choosing materials for boiler drums. ASTM Designation A-70 has been selected as typifying such plate material. Table 6 offers a basis for judging the chemistry of the plate material in the seven riveted drums, in comparison with specification requirements, and with a summary of 100 random heats from recent records of A-70 steel.

The chemical analyses of the eleven plate materials from the seven drums compare very favorably with those of present-day steels. All eleven plates easily conform to the composition required for "flange" steel requirements of Specification A-70. Ten of the plates would be acceptable for "firebox" quality. The other plate (10-SEB) would not be acceptable as firebox, but only because the carbon content (0.32 per cent) exceeded the permissible limit.

Rivets. The chemical analysis of the one rivet so examined follows: C—0.12; Mn—0.33; P—0.011; S—0.032; Si—none.

Tension Tests; Plate Material. The results of the thirty-two tests are given in Tables 3 and 4. For comparison, these data are summarized in Table 6, together with the mechanical-property requirements of ASTM A-70 and the results of tests recently made on one hundred rolled plates of A-70 steel of similar thickness.

The data charted in Tables 3 and 4 have been made the basis of the graphic presentation in Fig. 8, in which comparison is made with chemical analyses and with specification requirements. The chemical analyses are recorded in terms of an index number which is the sum of the manganese content and five times the carbon content. This is logical since it represents the approximate quantitative effect of each element on strength properties. Tensile strength is given in 1000 psi, yield point as percentage of tensile strength (elastic ratio), and percentage elongation as a ratio to the minimum requirement in A-70 flange-quality steel.

It is apparent that except for the one plate containing higher

[4] "A Work Brittleness Test for Steel," by H. W. Graham and H. K. Work, Proceedings of the ASTM, vol. 39, 1939, pp. 571–582.

TABLE 6 COMPARISON OF CHEMICAL AND MECHANICAL PROPERTIES OF BOILER-DRUM STEELS, 100 RECENTLY MADE A-70 STEELS, AND CURRENT A-70 REQUIREMENTS

CHEMICAL COMPOSITION

	ASTM A-70 REQUIREMENTS		PLATE MATERIALS FROM SEVEN (7) DRUMS			CHEMISTRY OF 100 RANDOMLY SELECTED RECENTLY MADE ROLLED STEEL PLATES (A-70)		
	FLANGE QUALITY	FIREBOX QUALITY	AVERAGE	MAX.	MIN.	AVERAGE	MAX.	MIN.
C (%)	NOT REQUIRED	.25 MAX.	.235	.32 *	.19	.206	.26	.12
Mn (%)	80 MAX.	80 MAX.	.355	.41	.30	.331	.55	.32
P (%)	.04 MAX.	.035 MAX.	.011	.017	.008	.017	.040	.010
S (%)	.05 MAX.	.04 MAX.	.036	.043	.031	.032	.040	.025

* PLATE FROM DRUM # 10; FOR ALL OTHERS 0.26 % CARBON MAX.

MECHANICAL PROPERTIES

	ASTM A-70 REQUIREMENTS		PLATE MATERIALS FROM SEVEN (7) DRUMS			MECHANICAL PROPERTIES OF 100 RANDOMLY SELECTED RECENTLY MADE ROLLED STEEL PLATES (A-70)		
	FLANGE QUALITY	FIREBOX QUALITY	AVERAGE	MAX.	MIN.	AVERAGE	MAX.	MIN.
T.S. P.S.I.	55000 – 65000		60500	68200 **	56000	59000	65000	55000
Y.P. P.S.I. MIN.	0.5 TENSILE STRENGTH		31300	41200	29200	37200	40000	35000
% ELONG. 2" MIN.	$\frac{1.5 \times 10^6}{T.S.}$	$\frac{1.55 \times 10^6}{T.S.}$	———	———	———	———	———	———
% ELONG. 8" MIN	$\frac{1.7 \times 10^6}{T.S.}$	$\frac{1.75 \times 10^6}{T.S.}$	26.6	30 5	23.0	31.8	36.0	28.0
R.A (%)	NOT REQUIRED		50.0	56.0	39.0	———	———	———

** PLATE FROM DRUM # 10; FOR ALL OTHERS 62,200

carbon content (10-SEB, 0.32 per cent), the tensile strengths all fall within the range required in A-70, that is, 55,000 psi to 65,000 psi. Elastic ratio is below 0.5 in two out of the eleven plates (head plates marked 14 and 15 from drum No. 3), but this deficiency is not great and is true only for specimens prepared in the longitudinal direction from these plates. Elongation requirements are satisfactorily met in all plate materials from drum No. 3, but are slightly below formula minimum in three plate materials from the six separate drums.

Reduction of area, which is not required in ordinary plate steel specifications, was measured in each specimen. The results which vary from 39 to 55.7 per cent indicate excellent ductility.

The plate materials in the seven drums therefore compare favorably in tensile properties with present-day steels used for boiler-drum service.

Riveted Joints. The results of tests are given in Table 5 for the four longitudinal and the three circumferential riveted-joint specimens.

Fig. 7 shows the four longitudinal specimens after testing. It will be observed in specimens L-12 and L-22 that the rivets failed, whereas in specimens L-11 and L-21 the plates fractured. Table 7 gives stresses which are calculated as having existed at the time of failure at the various critical sections of the riveted joint.

Fig. 8 shows the three circumferential specimens after testing.

TABLE 7 CALCULATION DATA FOR LONGITUDINAL RIVETED JOINTS

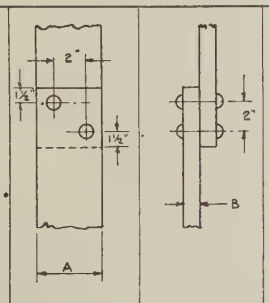

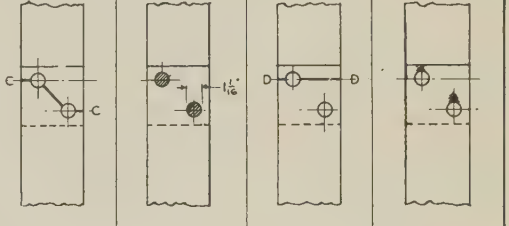

SPECIMEN NUMBER	SPECIMEN WIDTH A Inches	SPECIMEN THICKNESS B Inches	ULTIMATE LOAD ON TEST SPECIMEN W Pounds	ULTIMATE LOAD PER INCH OF RIVETED JOINT W / A Pounds per inch	NOMINAL OUTSIDE DIAMETER OF SHELL, D = 42" CALCULATED INTERNAL PRESSURE TO PRODUCE ULTIMATE LOAD PER INCH $P = \frac{4W}{DA}$ psi	DIAGONAL THROUGH RIVET HOLES – STRESS ON SECTION CC $\frac{W}{B(A-4297)}$ psi	RIVET SHEAR – STRESS ON CROSS SECTION OF RIVETS $\frac{W}{1.773}$ psi	NET SECTION – STRESS ON SECTION DD $\frac{W}{B(A-1.063)}$ psi	CRUSHING OF PLATE – BEARING PRESSURE ON PLATE BEHIND RIVETS $\frac{W}{B \times 2 \times 1.063}$ psi
L11	3.650	0.548	73,100	20,000	1905	56,700	41,200	51,500	62,700
L12	3.780	0.560	74,500	19,700	1875	53,700	42,100	49,000	62,700
L21	3.630	0.548	73,900	20,400	1940	57,800	41,700	52,700	63,600
L22	3.740	0.560	70,000	18,700	1780	51,200	39,500	46,700	58,800
						L11 FAILED IN THIS MANNER	L12 AND L22 FAILED IN THIS MANNER	L21 FAILED IN THIS MANNER	

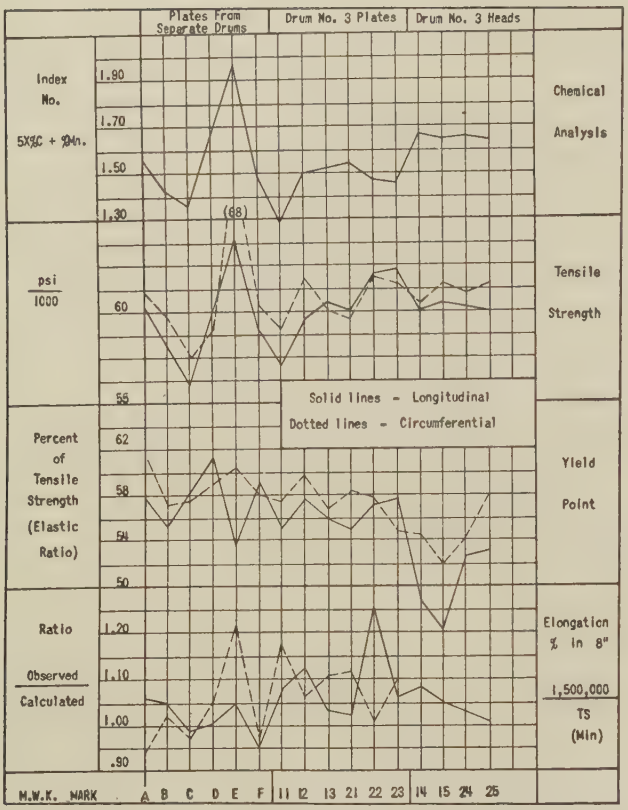

FIG. 9 COMPARISON OF CHEMICAL AND MECHANICAL PROPERTIES OF PLATE MATERIALS AND PRESENT-DAY A-70 REQUIREMENTS

In each case fracture took place through the plate at the line of the first single rivet. Due to the curvature of these specimens, they were subjected both to tensile stress and to a bending moment in testing. The failure occurred at the point of minimum section modulus. An inspection of these specimens after failure indicated that the plate, which was not reinforced by the butt straps, straightened out almost entirely, but that the section reinforced by the butt straps retained its original curvature. It is highly probable that at the instant of failure even more straightening occurred than that which was observed after failure, and correspondingly reduced the bending moment which existed on the section when it failed. It was not considered practical to make a calculation of the stress existing at the time of failure in these circumferential specimens owing to the uncertainties of the actual bending moment. The variable nature of the bending moment is reflected in the variance of the loads recorded at the time of failure of these specimens. The nonductile type of failure observed is not surprising in view of the complex state of stress.

These riveted-joint test results indicate the suitability of the joints for continued service. Although the strength of the joints as originally made is unknown, it seems quite improbable, in view of the calculation listed in Table 7, that they could have been significantly greater than now observed.

Bend Tests. Results of bend tests are given in Tables 3 and 4. In each case the inside fibers of the drums were bent in tension to 180 deg without any signs of defects on any of the surfaces. Elongations in 1 in. ranged from 36 to 46 per cent, indicative of satisfactory ductility on the inner surfaces, after forty years' service.

Notch-Impact Tests. The results obtained for test specimens in both plate directions at room temperature are given in Tables 3 and 4. Both Charpy and Izod testing was carried out in order to explore fully any data which might reveal change of properties resulting from service. Tests were made in plates "as-received" to obtain results of these materials after forty years of service. Tests were also made in the laboratory stress-relieved condition after such service to determine whether strain-aging embrittlement had occurred, since heating to 1200 F may be expected to return the metal to its original condition as regards this embrittlement. A basis of reference is thus provided for these materials, which is not otherwise available, since none of the original material is at hand.

The notched-bar impact values of the plate materials after forty years are typical of results to be expected of present-day materials of this quality even before entering service. Thus eighteen Charpy specimens taken in two directions from the three straight sections from drum No. 3 varied from 21.5 to 24.5 ft-lb. As would be expected, Izod values were less consistent,[5] but averages varied from 21.7 to 25.2 ft-lb for both directions, which is quite consistent with the Charpy values. Generally, similar data were obtained for the two plates selected for notch-impact testing from drums Nos. 5 and 8, except that greater inconsistencies were found.

Stress-relieving at 1200 F had but slight effect upon the Charpy values of the plate materials tested since they are quite similar to results after removal from service. However, stress relief has resulted in variable effect of notch-impact Izod values, some sets of values being improved and some being made worse, in an apparently random manner.

The Charpy tests indicate that either strain-aging has been inappreciable or that "overaging" has occurred during the forty years of service of the plates examined. The variability of the

[5] It is not unlikely that the transition-temperature range between "ductile" and "brittle" behavior is near room temperature for the vee-notch specimens and that this explains the variability of these results and sensitivity to test conditions.

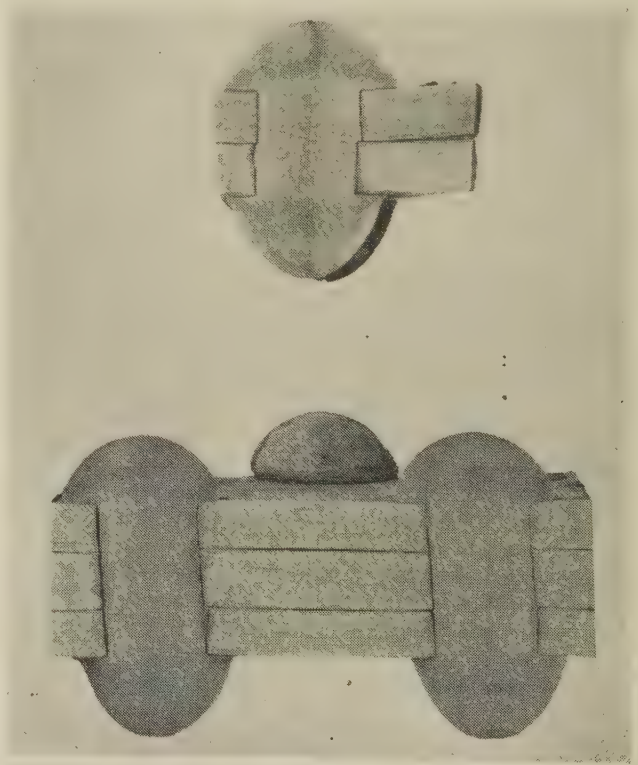

FIG. 10 TYPICAL DEEP-ETCHED CROSS SECTIONS THROUGH LONGITUDINAL AND CIRCUMFERENTIAL RIVETED JOINTS

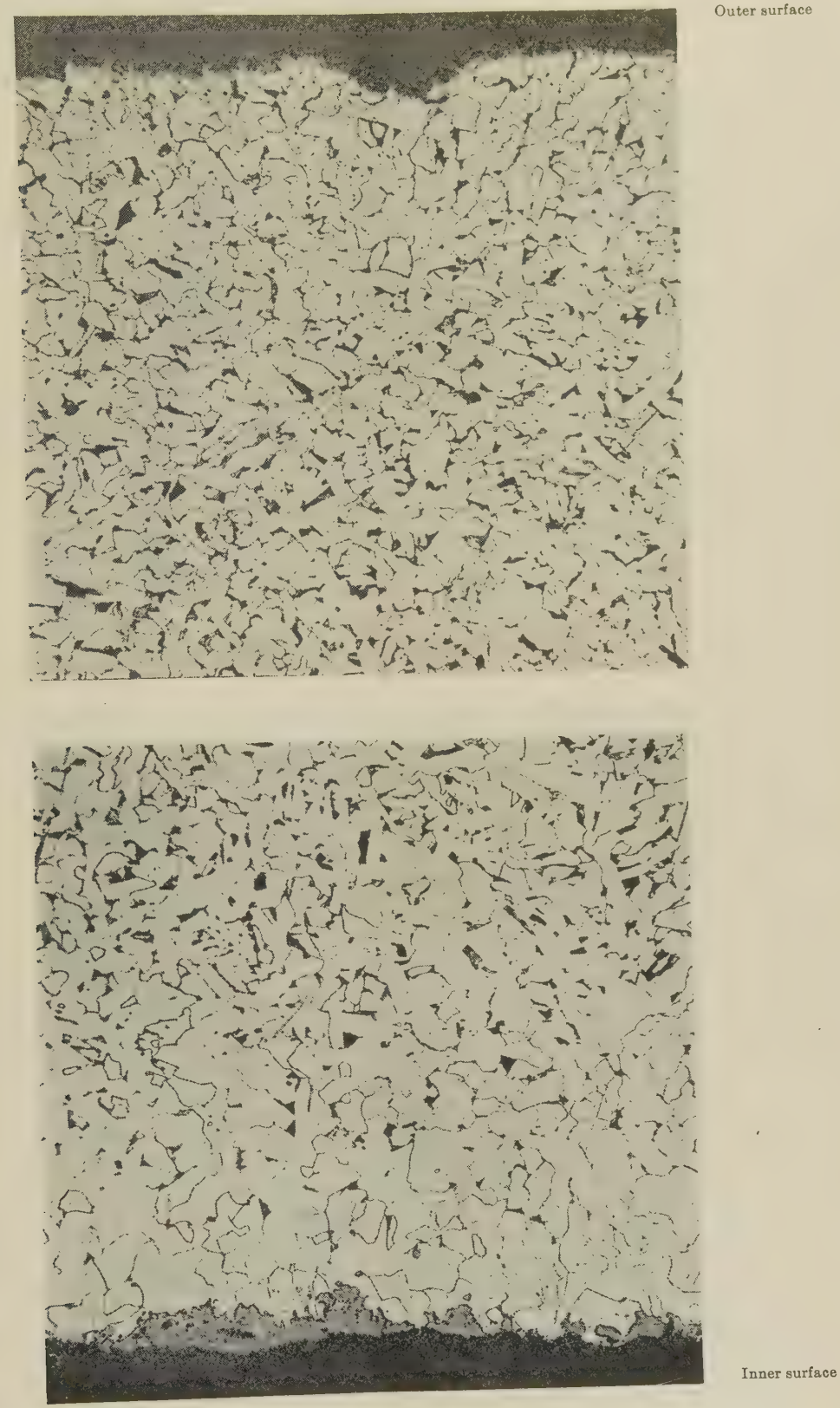

FIG. 11 PHOTOMICROGRAPHS OF CROSS SECTIONS AT OUTER AND INNER SURFACES BOILER-DRUM PLATE; 2 PER CENT NITAL ETCH; ×100

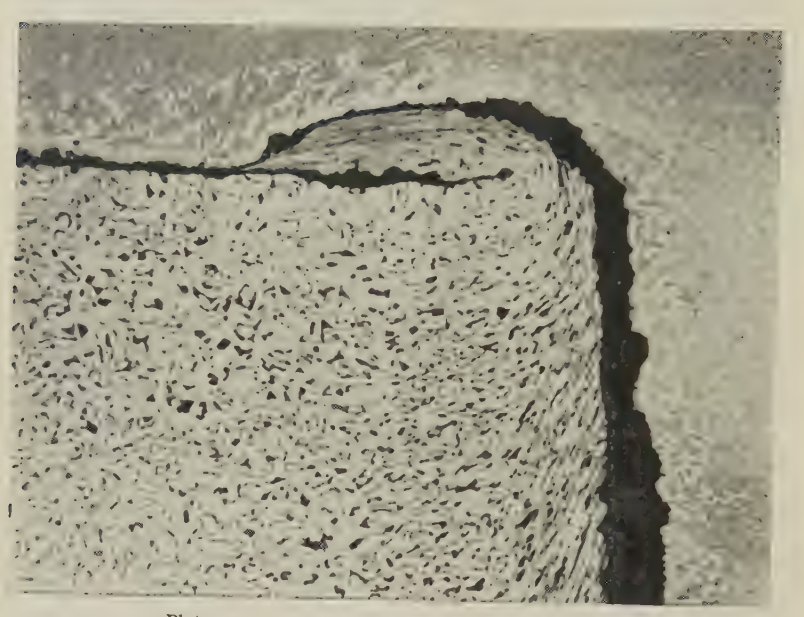

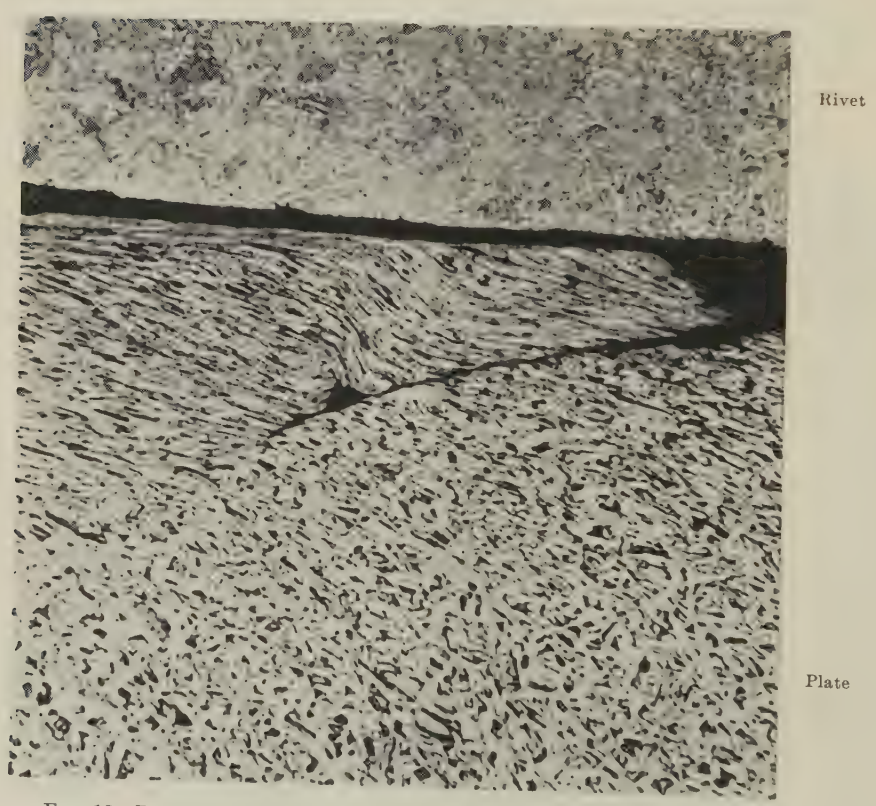

FIG. 12 PHOTOMICROGRAPHS OF RIVETED JOINTS; PICRAL ETCH, ×100

Izod values is not believed to be evidence of strain-aging embrittlement in view of their random character, but this appears to be rather inherent in the test, owing particularly to the type of notch and to the relatively high transition temperature of material then and now employed in the manufacture of boiler drums.

Hardness Tests. The Brinell values, listed in Table 3, are typical of the steels under consideration.

Macroscopic Examinations. All plate materials showed etch patterns consistent with present-day rolled open-hearth steels of low carbon content. There was only very slight difference between the etch patterns of longitudinal and circumferential directions. Some few stringers were found in the etched cross sections but these were comparable to present-day steel practice.

Deep-etched cross sections were prepared through the riveted joints, representing the longitudinal seams, present only above the water line. In addition, several cross sections were prepared through rivets from a nozzle opening. No defects were disclosed by careful examination of the sections under a low-power microscope. No difference was noted between specimens taken from above and below the water line. Fig. 10 shows the deep-etched pattern of a typical cross section through the circumferential riveted lap joint, and also of a typical longitudinal joint. No defects were noted in these rivets or in adjacent plate material.

All macrospecimens disclosed that rivet holes had been punched without subsequent reaming or drilling of such holes; this differs from best practice of today. The lack of true plate alignment and the severe local distortion of rivets near their centers are apparent in the illustration.

Microscopic Examinations. Specimens were examined from all plate materials from drum No. 3, with particular observation of the microstructure at the outer and inner surfaces. Typical photomicrographs are shown in Fig. 11. The plate materials were quite clean and reasonably free of nonmetallic inclusions; microstructures consisted of medium-size grains of pearlite and ferrite, indicative of air-cooling from a temperature somewhat above the upper critical temperature. The slight differences between the microstructures are due to slight variations in finishing temperatures in hot-rolling and to small differences in carbon content. These are of minor significance. Slight decarburization and scaling at the inner surface undoubtedly resulted during heating and rolling of the plate.

Specimens were also examined from locations in riveted joints adjacent to samples prepared for macroscopic etching. Cross sections were prepared perpendicular as well as parallel to the plate surfaces. Microscopic examinations were made at $\times 100$ and $\times 1000$ in both etched and unetched conditions, with particular reference to the rivet-plate interfaces.

The rivet joints represent the location in the drums where possible cracking or deterioration is most likely to occur. The only type of defect found was traceable to folds in the plate materials caused in the original riveting operation. It is interesting to note that the lap in Fig. 12 has not progressed during service. The absence of any cracks at the rivet-plate interfaces during service indicates an absence of so-called caustic embrittlement, as well as an absence of detrimental strain-aging embrittlement.

Magnaflux Examinations. All specimens prepared for macroscopic and microscopic examination were magnafluxed. In addition, one circumferential riveted joint was cut into four parts for further magnafluxing. No signs of defects were observed in any case.

Strain-Aging Tests. The results of these tests, comparing a sample of present-day A-70 steel, one plate from drum No. 3, and one plate from drum No. 6, are shown in Fig. 13 in which the resistance to notch impact is given for various percentages of cold reduction with subsequent aging at 450 F for 2 hr. It is apparent that the boiler-drum materials exhibit a slightly greater but probably insignificant degree of strain-aging than A-70 steels.

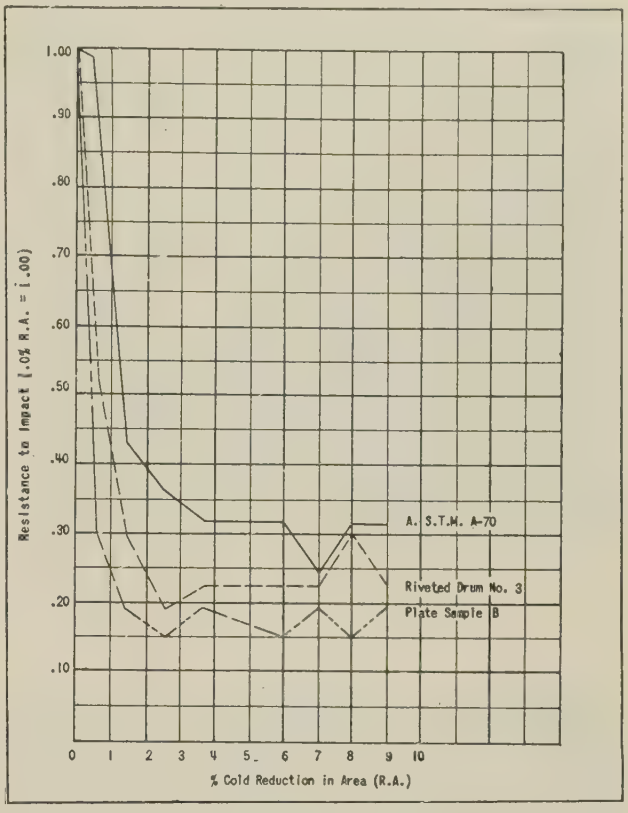

FIG. 13 STRAIN-AGING CHARACTERISTICS OF DRUM STEELS COMPARED WITH PRESENT-DAY A-70 STEEL

SUMMARY AND CONCLUSIONS

An investigation has been made of boiler-drum material removed by the Consolidated Edison Company to be replaced by modern boilers after forty years of service at 400 F and 200 psi.

No evidence of deterioration was found. No signs of any general corrosion were observed. Caustic embrittlement was clearly absent. The mechanical properties of these materials after service are similar to those of present-day steels of similar composition. There is no indication that strain-aging has occurred as a result of service.

It is to be noted that inspections of these drums were very thorough, since examinations were made annually upon scraped and brushed surfaces. The maintenance program was also of a very high order, consisting of painting the inner drum surfaces with selected coatings each year.

The absence of over-all corrosion and caustic embrittlement may be attributed largely, if not entirely, to the careful maintenance program carried out annually. This is particularly true since feedwater was originally untreated, and the rivet holes in these drums were not formed by best practice of today, i.e., they were punched without subsequent reaming or drilling to remove severely cold-worked metal.

The mechanical properties of these materials compare favorably with steels which would be applied today for similar service, indicating no deterioration of the properties examined. This is consistent with the results of macroscopic and microscopic studies, since there was no indication of structural change such as spheroidization or graphitization.

Strain-aging embrittlement is apparently the only structural change or deterioration of the metal proper which requires any consideration in the study of these materials. The tests performed in this investigation show that the subject material is

susceptible to strain-aging embrittlement, but probably not significantly more so than steel which would today be applied to the same service. Therefore it seems evident that boilers manufactured in the past need not necessarily be classed separately as regards their need of derating because of strain-aging embrittlement.

It seems clearly evident that these boiler drums were still suitable for continued service under the temperature and pressure for which they were originally designed.

It is concluded, in view of the facts, that neither corrosion, caustic embrittlement, loss of mechanical properties, nor strain-aging embrittlement was found, derating of boiler drums operating under these particular conditions with careful inspection and maintenance program is not warranted.

Acknowledgments

The authors wish to express their appreciation of the assistance rendered by members of the technical staffs of Consolidated Edison Company, U. S. Steel Corporation Research Laboratory, and The M. W. Kellogg Company, especially that of R. H. Caughey, metallurgist, and H. G. Oliver, mechanical engineer, of the latter organization.

Discussion

W. F. Davidson.[6] There are two slight additions the writer wishes to make to the authors' clear and lucid treatment of a complex subject. Both of the additions deal with decisions that were made at an early stage of the investigations before they had become the full responsibility of the authors.

First should be emphasized the random selection of the samples. The samples were not preselected to insure favorable test results but were as nearly representative of the 168 drums in the 56 boilers as could be made. An arbitrary decision had to be made as to the number of drums to be cut up. When this had been set at seven, seven boilers were designated at random from those then being dismantled. Then we considered the number of variables—above or below the water line; front end, center section, rear end; right, center or left drum, etc., and made up a schedule of locations from which the specimens should be removed. Next, and still without first looking at the drums, we matched the drum designations with the specimen schedules and sent the necessary instructions to the field to deliver the samples to the laboratory. Our belief that the samples are as truly representative as it is possible to make them is strengthened by an examination of the detailed data as reported in the paper.

Then, a brief explanation is in order why hydrostatic tests were not used. These were considered and discarded in place of the tests that have been reported only after an analysis had indicated the results might be of doubtful value. It was known that the drums would withstand the routine hydrostatic test, but that was largely negative information. To get positive information it would be necessary to make very elaborate and costly provisions for strain measurements at many points of the drum, and even were this done the test might become more one of checking the design rather than the material. Our chief interest was not in checking the design or fabrication methods, which were out of date in many details, but in checking the steel as such. The comprehensive study reported by the authors suggests that the decision not to make the hydrostatic test was sound.

I. A. Rohrig.[7] The authors present considerable evidence to show that the metal of seven different boiler drums was unaffected by 40 years of service at 400 F and conclude that derating or retirement of boiler drums might more logically be determined by the condition of the metal rather than by the length of service to which it has been subjected. The following statements from the paper are significant: "There are numerous different kinds of changes which may occur in metals during service. The extent to which these changes take place in any specific instance

[6] Research Engineer, Consolidated Edison Company of New York, Inc. Fellow ASME.

[7] Research Department, The Detroit Edison Company, Detroit, Mich.

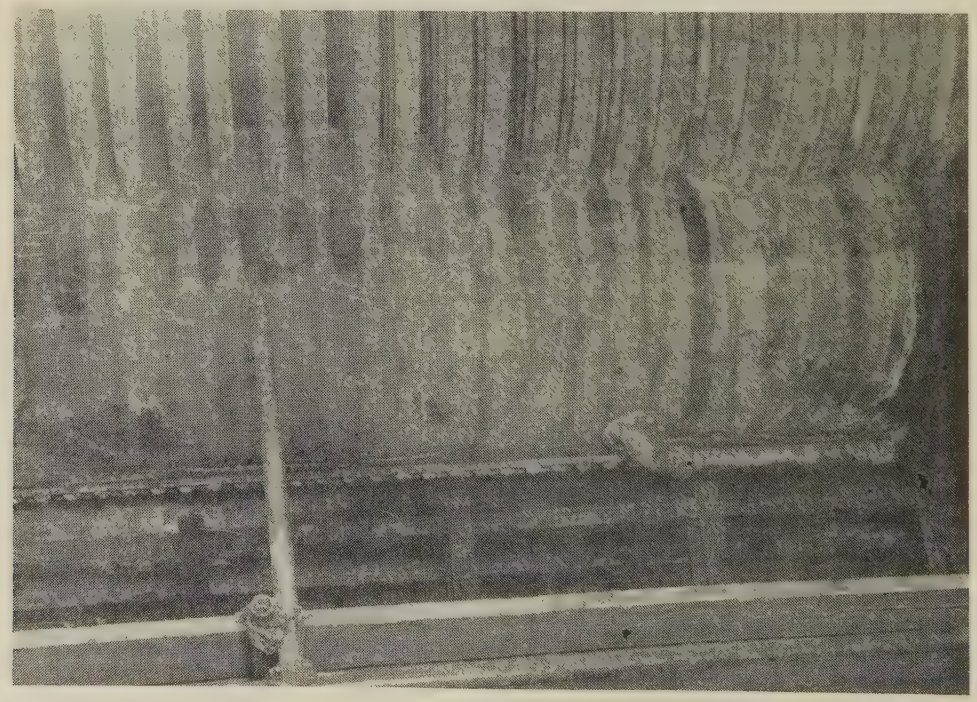

Fig. 14 Marysville Power Plant, No. 3 Boiler; General View of Location of Fire Cracks on South Mud Drum

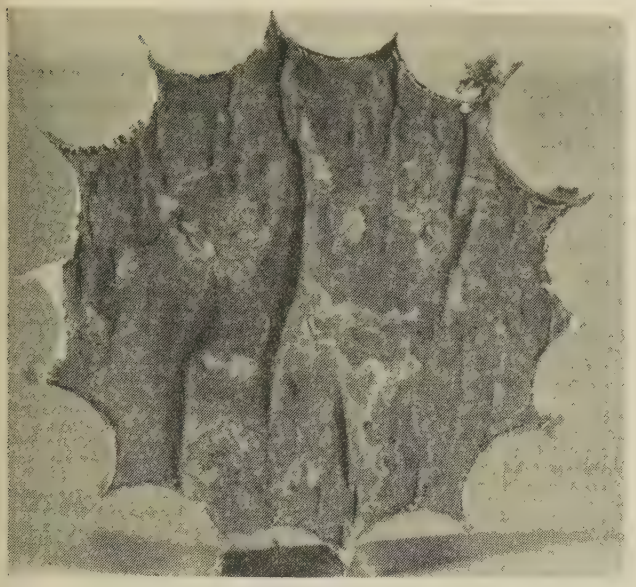

FIG. 15 END VIEW OF THE SAMPLE; ×3.5

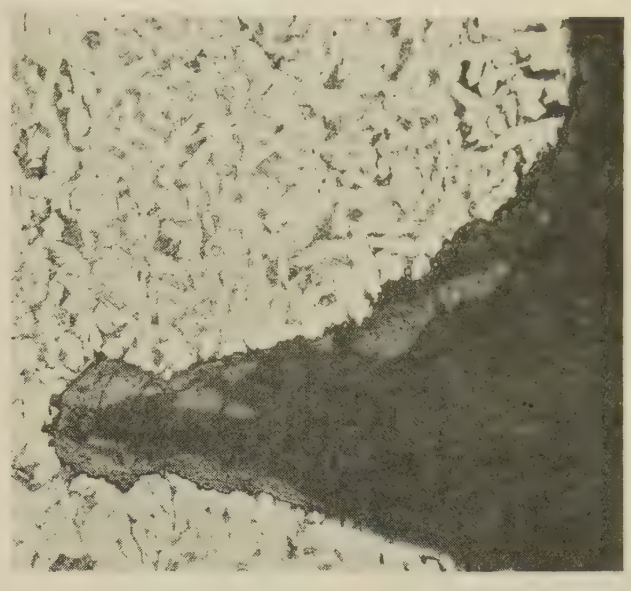

FIG. 16 STRUCTURAL CONDITION AT OUTER SURFACE OF BOILER DRUM SHOWING TYPICAL BLUNT CONDITION OF CRACKS AND SPHEROIDIZATION OF CARBIDE; ×100

depends on the service conditions of temperature, time, stress, and medium to which they are subjected."

In 1946 an examination was made of a sample removed from the mud drum of a boiler that had been in use for 24 years in the Marysville power plant of The Detroit Edison Company. Transverse cracking had occurred on the outer surface of the drum. The cracking was restricted to a band approximately 1 ft wide extending across the outer surface of the drum below the first row of tubes on the fire side as shown in Fig. 14 of this discussion. The drum is of riveted construction and is made of steel plate $1^{15}/_{32}$ in. thick, and is 27 ft long × 47 in. diam. The boiler is of a Stirling "W" type with drums operating at 300 psig and 422 F, which has been in use since 1922.

Because of the cracks on the surface of the drum, the inspector for the insurance company requested that a sample be removed and an examination made to determine the depth and character of the observed cracks. Accordingly, a sample approximately 1 in. diam was removed from the drum so that the structure of the metal could be examined from the outer surface to the inner surface. A tapered plug was welded into the hole cut through the drum.

Examination of the sample showed that, although the cracks were $^{5}/_{32}$ in. deep, maximum (see Fig. 15 and 16, herewith), and extended 10 to 11 per cent through the wall of the drum ($1^{15}/_{32}$ in. thick), the metallographic structure of the remaining thickness of the metal was satisfactory (see Fig. 17), and had the general appearance of hot-rolled boiler plate even though it had been in use for 24 years at approximately 422 F (saturation temperature at 300 psig). The cracks had been caused by temperature-differential stresses resulting from flame impingement on the surface of the drum below the first row of tubes. The height of the fire wall was increased to prevent further flame impingement and the boiler was returned to service. The suitability of the boiler drum for continued use was determined by its fundamental condition rather than by the length of time that it had been in use.

FIG. 17 STRUCTURAL CONDITION AT INNER SURFACE OF BOILER DRUM; REPRESENTATIVE STRUCTURE OF THE DRUM WALL; ×100

E. H. KRIEG.[8] This valuable paper will do much to build up a rational basis of understanding between boiler inspectors and boiler operators. There have been cases in the past where boiler inspectors were inclined to derate boilers on account of age only, regardless of their condition, and there is real need to arrive at a more factual and logical basis for derating of allowable pressures.

It is probable that, originally, there was so little common knowledge of metallurgy a "factor of ignorance" had to be applied by the boiler inspectors to keep claims for losses within reasonable limits. In the light of the large amount of metallurgical data and knowledge that are available to every boiler inspector today, or at least to the heads of inspection bureaus, there is no basis for continuing a reactionary and backward method of derating boilers solely as a function of age. It may be that a boiler should be retired and eliminated because of

[8] Consulting Mechanical Engineer, American Gas and Electric Service Corporation, New York, N. Y. Mem. ASME.

economic obsolescence, but such a condition is beyond the scope of the boiler inspector's authority, which is limited to matters of safety and avoidance of insurance claims.

This paper is the first attempt, at least for some time, to call attention to the problem of derating boilers, and it is hoped that more factual data may be forthcoming on which to arrive at a rational decision as to whether it is necessary to derate a boiler.

F. X. Gilg.[9] The results of these careful and thorough tests on the old drums from Waterside is a welcome confirmation of the fact that boiler drums, made from good-quality steel, good workmanship, and properly taken care of over the years, do not deteriorate with age. During the war there were many instances of 30-, 40-, and even 50-year-old boilers being reset and certified for further use.

The Waterside drums were fabricated in 1900. The drum heads, formed from $^{11}/_{16}$-in. plate, had the old-style short-radius bend where the cylindrical portion merges with the spherical portions of the head. The code no longer permits the short-radius transition, because it is known that high stresses occur in these areas. However, a careful examination of these heads showed absolutely no signs of deterioration or stress in these areas.

The feed, steam, and safety-valve nozzles were made from "flowed steel," a semisteel casting. They were riveted to the drums. The steam outlet pads on each drum were designed for a nominal 5-in. connection but the hole in the drum shell was $15^1/_2$-in. diam being reinforced by the pad flange which was 21-in. diam. The code no longer permits such large unreinforced openings because of the concentrated stresses around the edges of the holes. Here, too, a careful examination showed no evidences of deterioration or stress.

The general good condition of these boiler drums after 40 years of service is due primarily to the excellent care which they received from the plant personnel by proper feedwater treatment, and the avoidance of external and internal corrosion. There are other cases on record from other plants where drums had to be replaced in considerably less time due to neglect.

From the results of the careful examinations of these drums, it is believed we can safely conclude that it is not necessary arbitrarily to reduce the safe operating pressure of an existing boiler because of age. The safe operating pressure of any boiler should be determined on the basis of a complete and careful inspection of the pressure parts.

[9] Application Engineer, The Babcock & Wilcox Company, New York, N. Y. Mem. ASME.

Authors' Closure

The authors thank Messrs. Davidson, Rohrig, Krieg, and Gilg for their discussions of our paper.

They are especially grateful to W. F. Davidson of the Consolidated Edison Company, who followed the work closely from its inception, and assisted greatly with advice during the formulation of the test program and the interpretation of test results. His detailed description of the random nature of the selection of samples, and also the discussion as to the reasons for the omission of hydrostatic tests are a helpful addition.

Mr. Rohrig's discussion is valuable as representing additional data in this field. His conclusion that "the suitability of boiler-drum material should be determined by its actual condition, rather than by length of time that it has been in use" is welcome reinforcement to the viewpoint of our paper.

The discussions by Mr. Krieg and Mr. Gilg are pertinent in view of their experience in the power-plant field.

Quick Starting of High-Pressure Steam-Turbine Units

By J. C. FALKNER,[1] R. S. WILLIAMS,[2] AND R. H. HARE,[3] NEW YORK, N. Y.

This paper describes a new method of "quick starting" high-pressure steam-turbine units at locations where, because of their light night loads, in comparison with heavy day loads, some of the high-pressure units must be shut down and started up each night. The method described reduces the thermal start-up stresses in the turbines and boilers, reduces the "rolling-on" fuel losses, reduces the crew personnel required, and increases the available reserve factor, as compared to the conventional start-up methods.

FOR many years the turbines of the Consolidated Edison Company have been started in the conventional manner as prescribed by the manufacturer, which calls for approximately 90–120 min to put the turbine on the line. As the load grew and the number of turbines increased, it became necessary, due to the load characteristic, to shut down approximately thirty-five turbines each night, some of which are topping turbines, and start them up again the next morning. At present there are six topping turbines and forty-four condensing turbines, with three additional topping turbines and four condensing turbines to be installed by 1951. System load and capacity data for minimum load conditions are given in the Appendix.

Typical load curves and the projected curve for 1950 are shown in Fig. 1. Note the rapid rise between 5:00 a.m. and 9:00 a.m.

The quick-starting idea was discussed with the General Electric and Westinghouse turbine engineers approximately 2 years ago, and consists simply of admitting steam to the turbine at a temperature corresponding to that of the main parts of the turbine, such as the valve chest, heavy flanged joints, top and bottom of casing, etc., after a "shutdown" period up to 10 hr.

We well appreciate that starting and stopping high-pressure and temperature boilers and turbines 200 or more times per year introduces problems not heretofore encountered. With this in mind, investigations were made to see what could be accomplished in a way that would reduce the heat stresses in both turbine and boilers to a minimum and to reduce the starting cost, which in itself is a considerable item. As our greatest number of high-pressure units is at Waterside, the investigation was made at that location.

Waterside High-Pressure Installation

The present high-pressure installation at this station consists of four units, each made up of two boilers and one high-pressure turbine, the turbines exhausting into a common 200-psig header, which supplies steam to seven low-pressure condensing turbines and to two steam mains of the New York Steam Corporation. The capacities of the boilers and the turbines are given in Table 1.

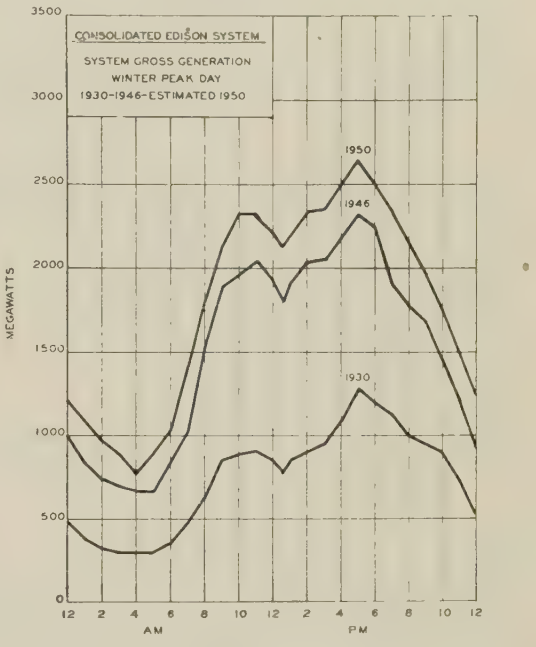

FIG. 1

Conventional Start-Ups. The manufacturers have given operating instructions stressing the fact that temperatures should not be changed rapidly in either the turbines or in the boiler drums, but there has been no attempt to synchronize the temperatures, although both must work as a team.

As a first step in our investigation, thermocouples were installed in the main leads to the turbine throttle, on the turbine steam chest, and at different locations on the turbine cylinder and flanges on all four of the Waterside high-pressure turbines. The location of these thermocouples is shown diagrammatically in Figs. 2, 3, 4, and 5, for the four units. In Table 2 the normal operating temperatures at these locations are given.

The temperatures found for normal start-up for two of the units are shown in Figs. 6 and 7, for each of the test locations, and

TABLE 1 WATERSIDE STATION; DESCRIPTION OF BOILERS AND TURBINES

High-Pressure Boilers
Two boilers per unit

Unit no.	Manufacturer	Rating each, lb per hr	Steam conditions— Pressure, psig	Steam conditions— Temp, deg F
4	Combustion Engrg.	500000	1200	900
5	Combustion Engrg.	500000	1200	900
6	Combustion Engrg.	615000	1250	925
7	B & W	615000	1250	925

High-Pressure Turbines
One turbine per unit

Unit no.	Manufacturer	Rating, each, kw
4	Westinghouse	53000
5	General Electric	53000
6	Westinghouse	65000
7	General Electric	65000

[1] Manager, Electric Production Department, The Consolidated Edison Company of New York. Mem. ASME.

[2] Superintendent, Waterside Station, The Consolidated Edison Company of New York.

[3] Assistant Engineer, Waterside Station, The Consolidated Edison Company of New York.

Contributed by the Power Division and presented at the Semi-Annual Meeting, Chicago, Ill., June 16–19, 1947, of The American Society of Mechanical Engineers.

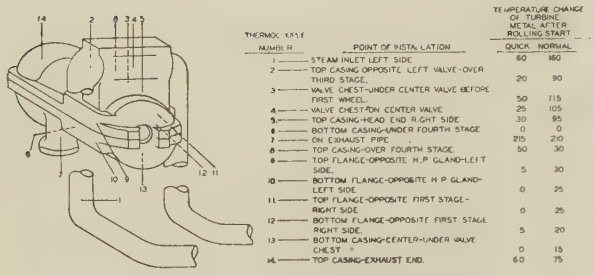

FIG. 2 WATERSIDE STATION, HIGH-PRESSURE UNIT NO. 4, SHOWING THERMOCOUPLES PEENED ON TURBINE CASING

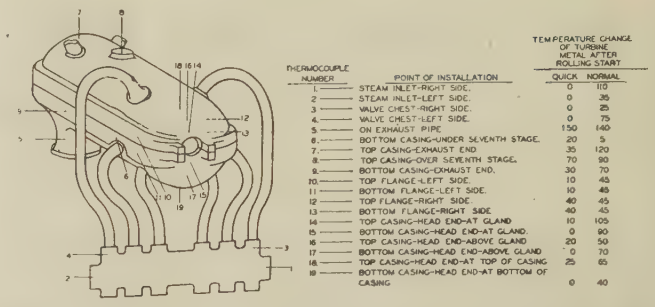

FIG. 3 WATERSIDE STATION, HIGH-PRESSURE UNIT NO. 5, SHOWING THERMOCOUPLES PEENED ON TURBINE CASING

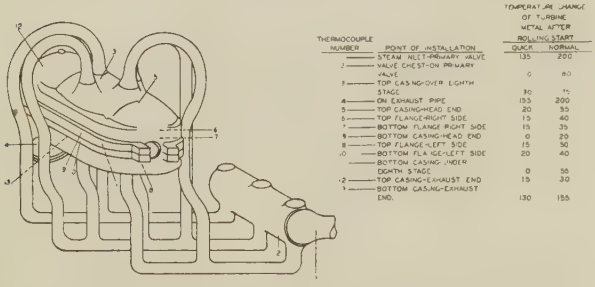

FIG. 4 WATERSIDE STATION, HIGH-PRESSURE UNIT NO. 6, SHOWING THERMOCOUPLES PEENED ON TURBINE CASING

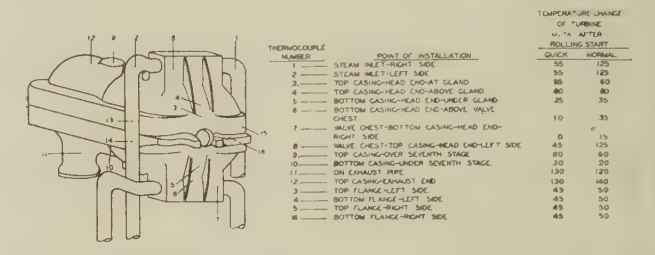

FIG. 5 WATERSIDE STATION, HIGH-PRESSURE UNIT NO. 7, SHOWING THERMOCOUPLES PEENED ON TURBINE CASING

on the bottom of these curves is given the turbine speed and the boiler output plotted at 30 min intervals.

A study of these data revealed that the superheater and line drains were normally left open, so that the boiler pressure was reduced to 200 to 400 psig at the beginning of the rolling period, and was then gradually increased to approximately 800 psig at the time the turbine was up to speed. It was noted that the steam chests with temperatures of 650 to 700 F at the start were actually cooled 50 F to 120 F during the first hour of the rolling period, due to the low initial steam temperature and the length of the rolling period. At the time the generator was synchronized, the steam-chest temperatures had been brought back to approximately the same as at the beginning of the rolling period.

Quick Start-Ups. Following the idea of maintaining minimum temperature differences between the turbine and the entering steam, the quick-start-up procedure was developed. It was determined that the boiler could be "bottled up" by closing the induced-draft-fan vanes, boiler stop valves, superheater and line drains, so that, after an outage of 6 or 7 hr, the boiler pressure was approximately 850 psig. It was also found that at low steam flows from the boiler, the steam temperature could be controlled

TABLE 2 TURBINE-CASING TEMPERATURES FOR NORMAL OPERATION, DEG F[a]

Location	On turbine no. 4	5	6	7
1	900	900	925	925
2	900	900	910	925
3	875	900	710	830
4	900	900	520	840
5	900	530	855	850
6	720	740	790	860
7	530	520	755	920
8	685	820	835	920
9	725	525	810	765
10	715	785	775	765
11	800	790	750	525
12	790	820	530	520
13	830	820	530	745
14	530	820	...	745
15	...	820	...	745
16	...	845	...	745
17	...	830	...	...
18	...	850	...	...
19	...	825	...	...

[a] For temperature locations see Figs. 2, 3, 4, and 5.

readily by varying the excess air. Test start-up procedures were then formulated for the boilers and turbines in an attempt to hold heat in the boiler and to eliminate the cooling effect on the turbine by rolling it with steam at a temperature approximately the same as that of the metal temperature of the turbine casing.

QUICK START-UP PROCEDURE

Shutdown. The procedure at shutdown is as follows:

1 When the turbine is to be shut down, maintain normal drum pressure on both boilers, and take one off the line in a normal manner.

2 When rating is zero on the boiler taken off, open superheater drain until pressure falls to 1000 psig. Then close the superheater drain, the fan vanes, the boiler stop, or nonreturn valves.

3 Drop rating on second boiler in normal manner to 300,000 lb per hr, maintaining normal drum pressure.

4 Boiler operator shall notify the high board that boiler is at 300,000 lb per hr rating.

5 Both coal feeders are then tripped on this boiler.

6 High board shall signal "load off" at 5000 kw and 1000 psig boiler pressure.

7 Turbine throttle shall be tripped (turbine to be kept on turning gear).

8 "Bottle up" second boiler as prescribed in item 2.

9 If during the outage period the drum pressure falls below 700 psig on either boiler, bring pressure back to 850 psig by intermittent coal firing.

Starting Up. Procedure for starting-up is as follows:

10 When the turbine is to be started the turbine-room engineer shall note the temperature of the selected turbine-casing thermocouple and give this temperature to boiler-control operator.

11 The boiler operator shall purge one boiler furnace, crack open superheater drain, light ignition gas, open superheater drain wide, put one coal feeder in service.

12 Boiler operator shall maintain steam temperature at superheater outlet as nearly as possible to that of the turbine-cas-

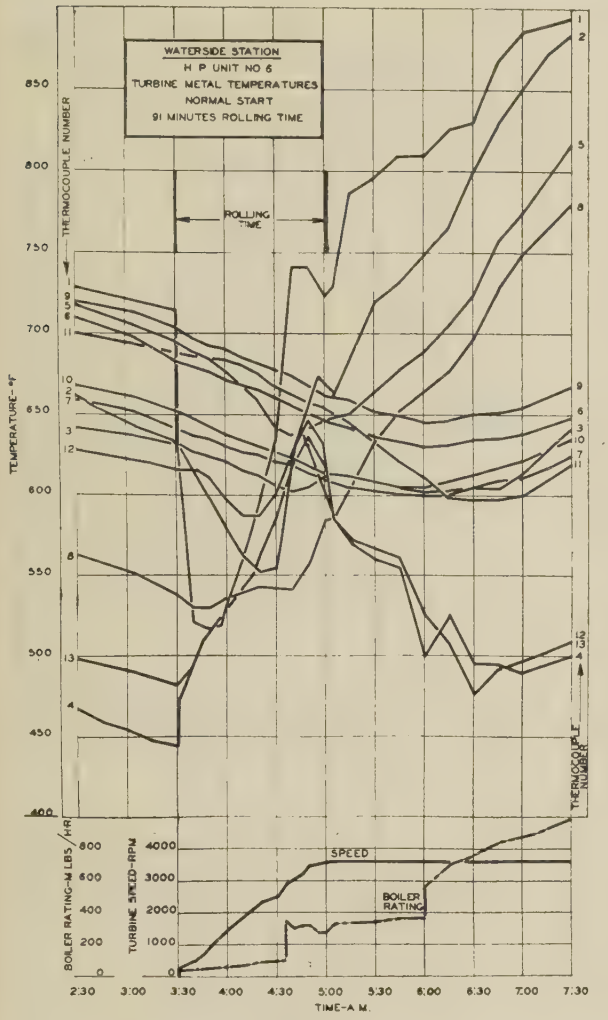

FIG. 6

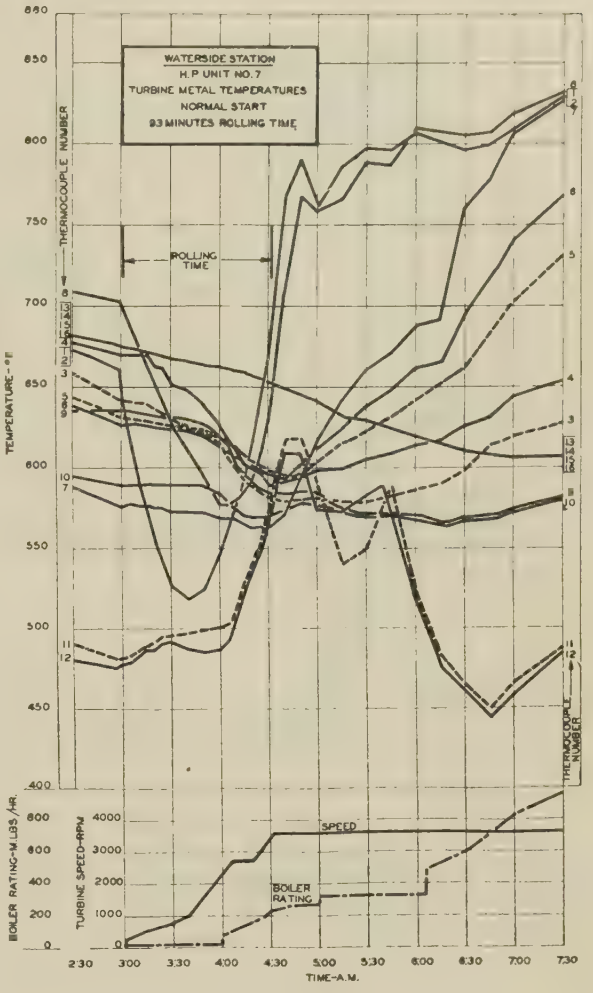

FIG. 7

ing temperature, as given in item 10. (This regulation is obtained by adjusting the excess air.)

13 The superheater by-pass damper shall be kept open.

14 When boiler pressure has been stabilized at 800 to 850 psig, open the turbine throttle and roll the turbine, increasing speed at rate of approximately 300 rpm per min.

15 Both coal feeders shall be placed in service within 7 min after turbine rolls.

16 Generator shall be synchronized within 15 min after start of the roll.

17 During the entire rolling period the turbine metal and inlet steam temperatures shall be checked at frequent intervals.

18 Both coal feeders shall be maintained at approximately minimum speed and superheater drain shall be closed.

19 During the rolling time, the second boiler shall be lighted off and its pressure brought up to within 200 psig of line pressure.

20 As soon as turbine is on the line, the second boiler shall be put on the line with superheater drain and by-pass damper wide open. The excess air shall be regulated in order to hold the steam temperature of the second boiler at the same temperature as the first.

21 Both boilers shall be at line pressure within 20 min.

22 Superheater by-pass damper shall be regulated to increase steam-inlet temperature at the rate of 100 deg F per hr.

23 The turbine shall be loaded in normal manner.

A complete set of start-up data, using the quick-start-up procedure was taken for each unit after a 5- to 7-hr shutdown. Figs. 8 and 9 show the metal temperature changes during this method of starting for two of the units. It may be noted that the cooling of the steam chest and heavy metal of the turbine casing was reduced considerably as compared with that of the normal start-up, and that the temperature stresses were not increased. For comparison between the conventional and the quick start-ups refer to Figs. 10, 11, 12, 13, and 14.

Exhaust Temperature. The 200-psig turbine-exhaust temperature charts for both types of start-up are shown in Fig. 15. Note the length of time the exhaust temperature remains high for the normal start-up, as compared with the quick start-up.

Turbine Vibrations. Vibrations at various points on the turbine are better, or the same, during the quick start-up, as compared with the normal. With the quick method, the difficulty of bringing the unit through the critical-speed period is completely eliminated.

Turbine Casing Movement. The relative movement between the top casing and the stationary pedestal showed no change with one manufacturer's machine and a decided change on another. Turbines No. 5 and 7 have double casings so it is impossible to know the movement of the inner one, but with less chilling there should be less movement and strains.

Generator Maintenance. We do not expect any increase in stator or field maintenance due to quick starts of the units.

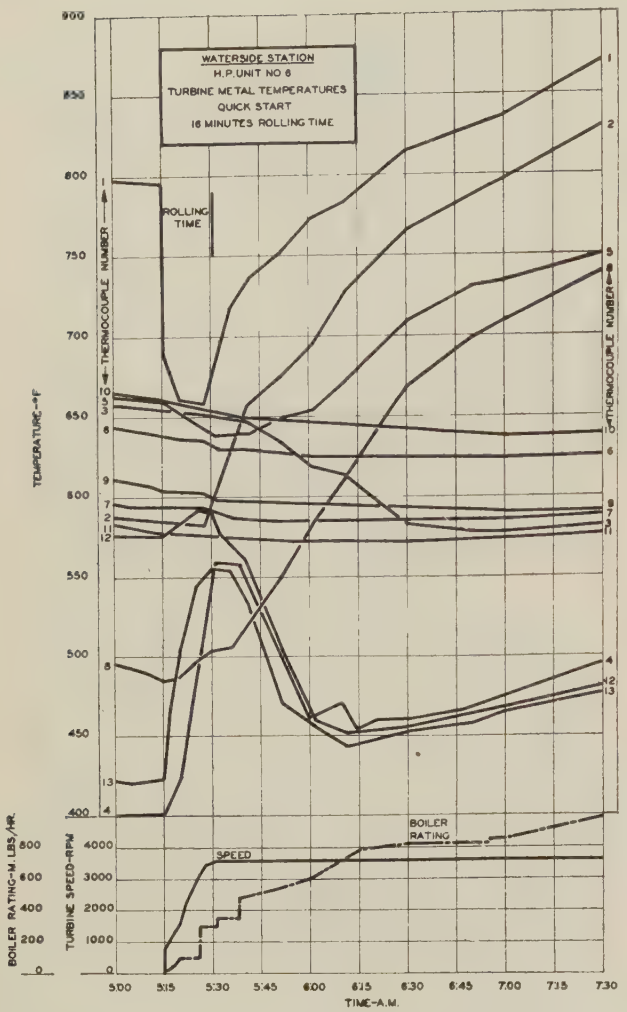

FIG. 8

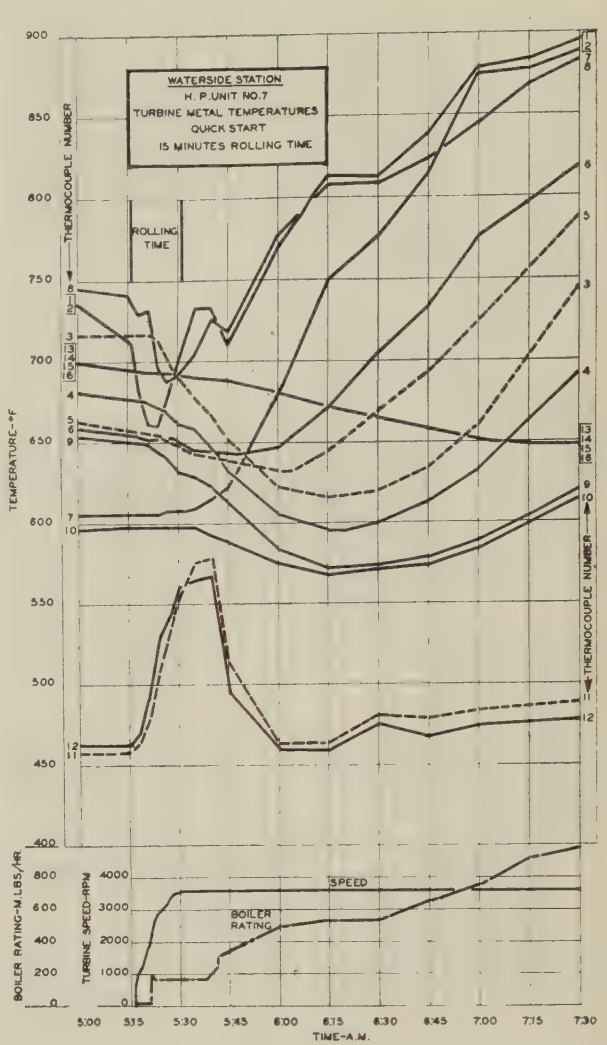

FIG. 9

CONCLUSIONS

High-Pressure Turbines (based on 24 quick starts). With the reduction of starting time, the existing personnel will be sufficient to take care of all necessary starts By not increasing the personnel, and with the reduction in starting costs, there will be an appreciable saving. In addition, this method will also be used at such times as either boilers or turbines must be taken off the line for minor maintenance.

Advantages attributed to the quick start-up are as follows:

1 Reduces the thermal stresses in the turbine and boiler.
2 Reduces fuel costs for idle rolling.
3 Reduces additional personnel costs.
4 Gives a better available reserve factor.

Low-Pressure Turbines. Quick starting may be used on turbines taking steam from a main steam header, fed from any number of boilers and with other turbines running from the header, as long as desuperheating water is injected into the steam used for starting the turbine, and the temperature of the inlet steam is held equal to the temperature of the turbine-inlet valve, heavy flanged parts, and turbine casing.

With the conventional start, high-temperature steam is used to start a unit which may be several hundred degrees cooler, with a resultant quick expansion toward the generator of the turbine spindle, which heats up more rapidly than the casing. This reduces the clearances between stationary and rotating parts and may cause serious damage.

Appendix

SYSTEM LOAD AND CAPACITY

The load of the Consolidated Edison Company of New York has almost doubled in the last 16 years, as Table 3 indicates.

TABLE 3 COMPARISON OF CONSOLIDATED EDISON COMPANY LOAD IN 1930 AND IN 1946

Year	Net generator output for the year, kwhr	Peak, gross generated, hr-kw
1930	4,983,512,182	1,282,000
1946	9,706,321,290	2,326,000

There have been no new stations added to the system to take care of this load increase, but it has been accomplished by modernizing the existing stations by the introduction of topping units exhausting into the low-pressure mains.

In Fig. 1 is given the typical hourly loads for a winter day in 1930 in comparison with 1946, and on this same curve has been added an estimated peak day in 1950. These curves bring out very well the type of system load throughout the 24 hr. There is no marked morning peak; the load increases rapidly at a fairly uniform rate from 7:00 a.m. to 10:00 a.m., levels, with a noon drop

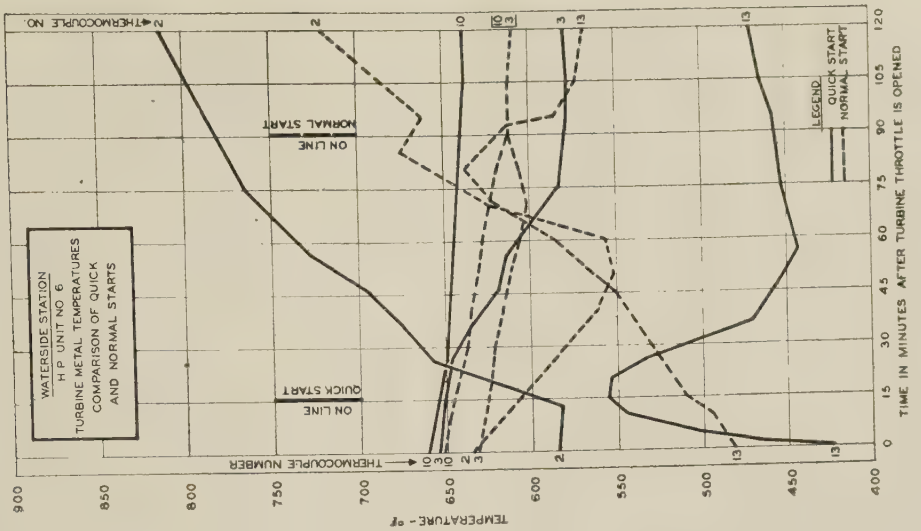

Fig. 12

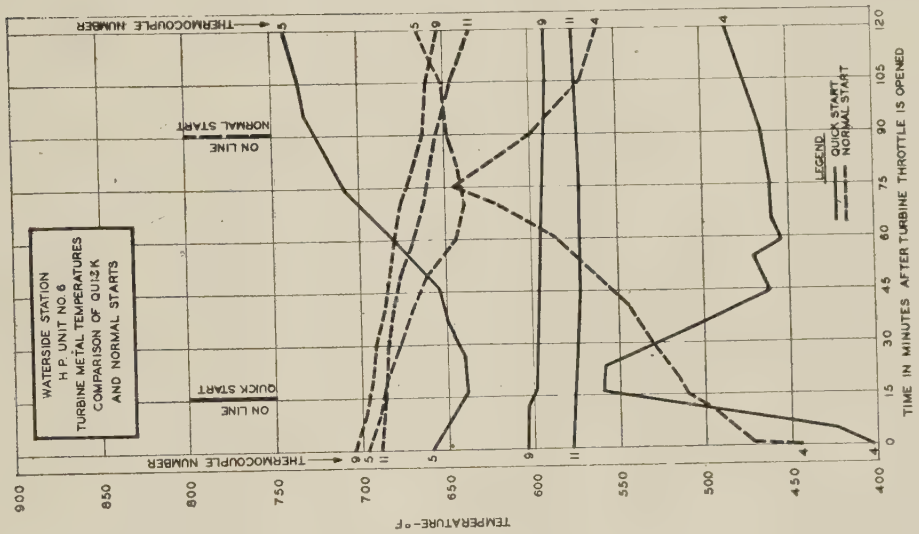

Fig. 11

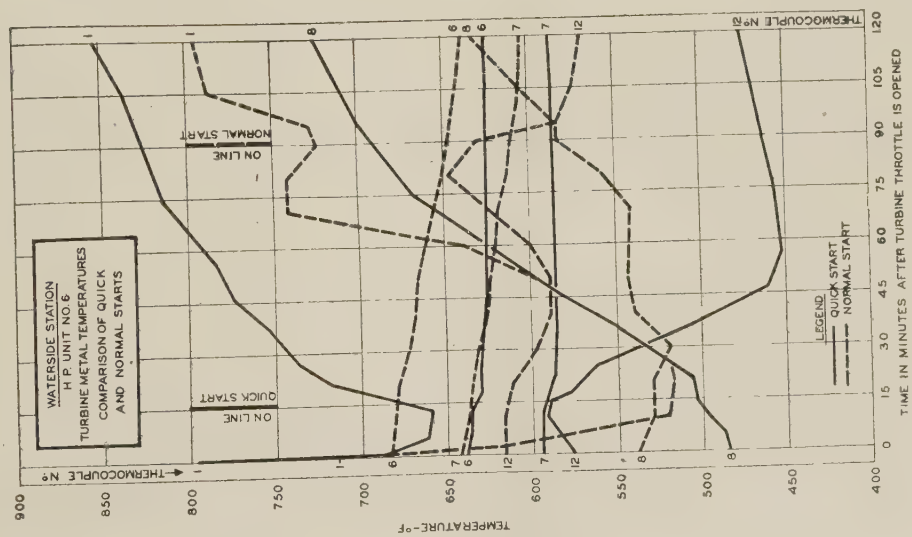

Fig. 10

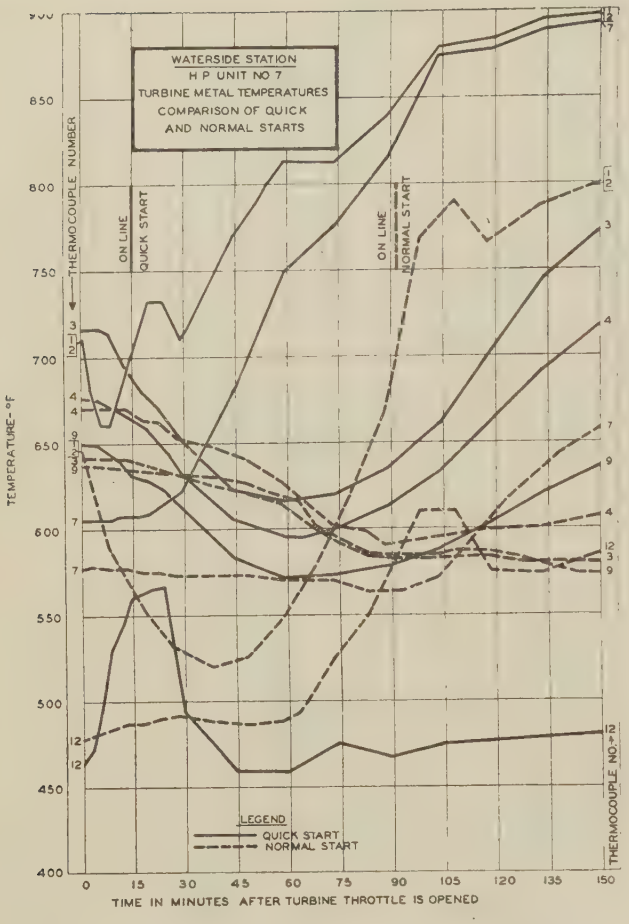

FIG. 13

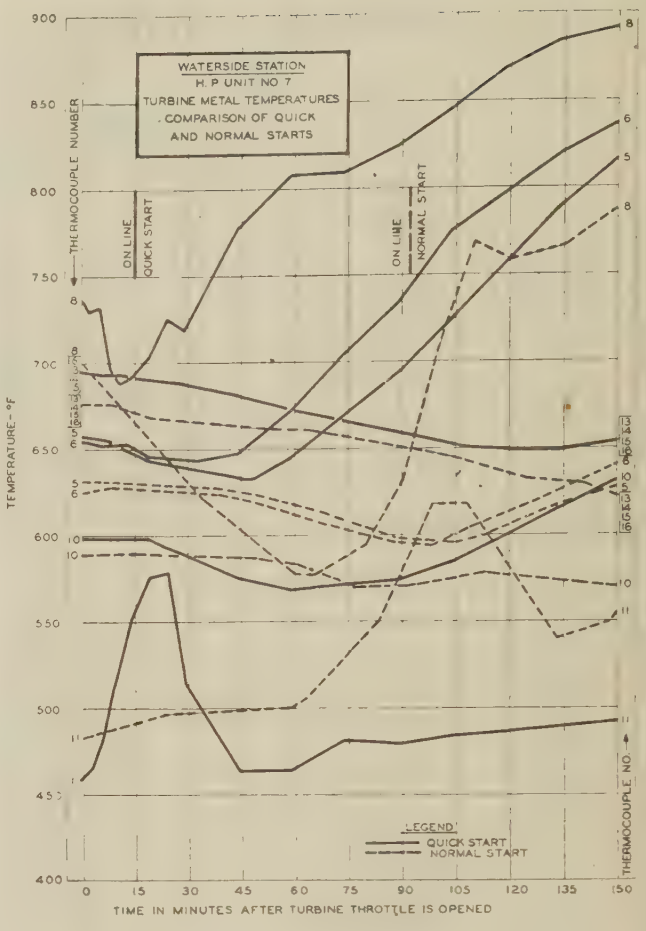

FIG. 14

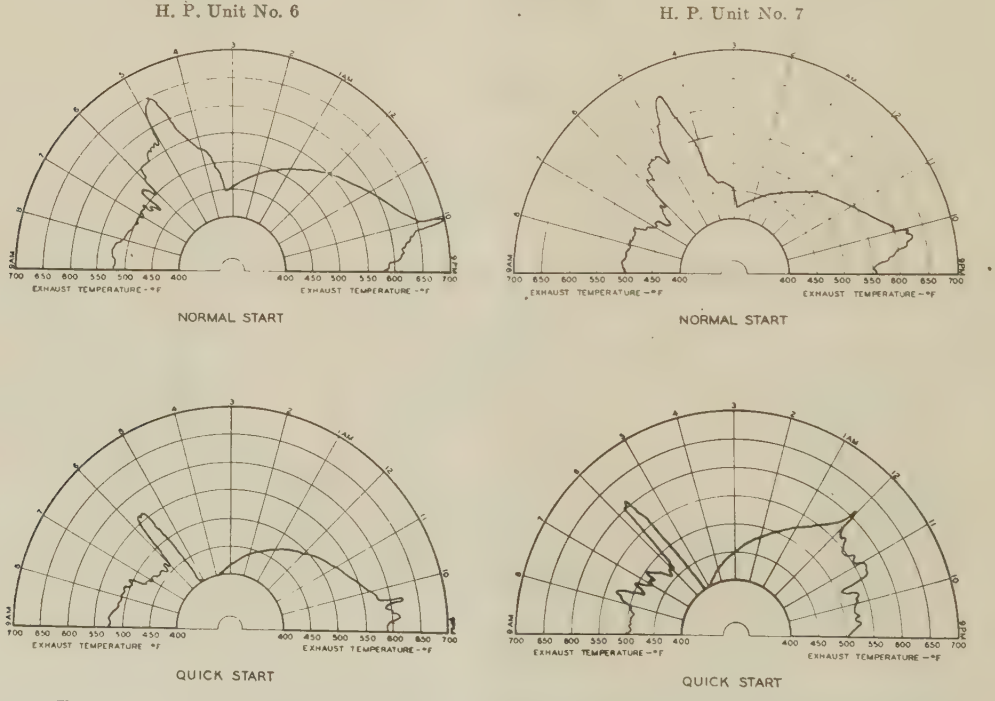

FIG. 15 TYPICAL TURBINE-EXHAUST TEMPERATURE CHARTS FOR BOTH TYPES OF START-UP

of about 15 per cent and then climbs from 3:00 p.m. to a peak at 5:00 p.m. It then falls at a fairly rapid uniform rate to a low at 4:00 a.m.

The system is tied in with the Niagara-Hudson Corporation for power interchange. During periods of high run-off, we may be receiving hydropower up to 150,000 kw per hr which still further reduces the night load. When this situation arises the system load generation is as given in Table 4.

TABLE 4 STATION LOADING NIGHT WATCH

Station	Night load, kw	Present capacity, kw
Hudson Ave.	80000	770000
Sherman Creek	50000	221000
Hell Gate	160000	630000
Waterside	160000	438000
Gold Street	Shut down	111000
East River	Shut down	280000
Long Island	Shut down	89000
Port Morris	Shut down	60000
All stations	450000	2599000

The 80,000-kw load at the Hudson Avenue Station is the minimum load carried by two 160,000-kw turbines with most of the 32 stoker-fired boilers in a banked condition, ready to carry 770,000-kw load by 9:00 a.m.

The 50,000-kw load at the Sherman Creek Station is the minimum load on one high-pressure topping turbine, with one high-pressure boiler, plus the necessary low-pressure condensing turbines.

The 160,000-kw load at the Hell Gate Station is the minimum load on one high-pressure topping turbine with two high-pressure boilers, plus the necessary low-pressure condensing turbines to carry the minimum exhaust from the high-pressure turbine and 600,000 lb of steam per hr from the low-pressure boilers. This low-pressure-boiler evaporation is necessary to supply make-up to the high-pressure boilers and to furnish generated load for regulation on the system.

The 160,000-kw load at the Waterside Station is the minimum load on four high-pressure topping turbines, with seven high-pressure boilers, plus the necessary low-pressure condensing turbines. Two topping turbines, plus the necessary low-pressure condensing turbines are sufficient to carry this load and therefore one, or possibly two, may be shut down.

Discussion

H. P. Dahlstrand.[4] With the adoption of high steam pressure and temperature in power plants, the reliable and efficient operation of the steam-turbine equipment has become a problem of great interest to operating and designing engineers. For these reasons this paper is of vital importance, as it covers a detailed report of an investigation to determine how to control the steam pressures and temperatures during short shutdowns and starting periods of large topping units. The result is a minimum variation in temperatures and with it a reduction of both distortions and thermal stresses in the turbine structure.

Operating experience has shown that there is less chance of dangerous distortions during the heating than during the cooling period. Therefore the rate of heating can be greater than the rate of cooling. If the cooling rate is too great, the inside of a cylinder will shrink and open the horizontal joint from the inside, causing the joint to leak; whereas, if heating at the same rate, the inside of the cylinder will expand and merely increase the loading on the joint. The heating rate, nevertheless, must be limited to prevent excessive distortions and stresses. From the foregoing it can be seen that the method described in the authors' paper is entirely sound.

[4] Consulting Engineer, Steam Turbine Department, Allis-Chalmers Manufacturing Company, Milwaukee, Wis. Mem. ASME.

The steam temperature at the superheat outlet is specified to be as nearly as possible to that of the turbine casing. If the control of this temperature will permit, there does not seem to be any objection to allowing this temperature to be from 50 to 100 deg higher than the casing temperature. With this higher temperature, the starting time may be shortened and with it the rise in exhaust temperature decreased. The rapid increase in exhaust temperature is due to the fact that, during the starting period, only a limited amount of available energy in the steam is absorbed in the work of bringing the turbine up to speed, but as the unit is loaded the temperature will decrease.

Valuable information for the industry could be obtained if a similar investigation were made on large 3600-rpm condensing steam turbines. These units, built during the past 10 to 15 years, will soon be required to be shut down and started every day as new large turbines for higher temperatures are being added to the power systems. The problem is somewhat more complicated than on topping units because of the condenser. Control of the vacuum may be the deciding factor in determining the time required. It is safe to assume that an effort should be made to obtain full vacuum in the shortest possible time in order to prevent too high a temperature in the exhaust.

Up to this time, all our large topping units are operating for long periods without shutdowns. For this reason the required time for starting has not been of vital importance. In all our instructions for starting and shutting down, both topping and condensing turbines, the importance of gradual temperature changes has been emphasized. Starting after a short shutdown, it is specified that the steam temperature should be high enough so that the turbine structure will not be shortened but will start to expand as soon as steam is admitted. The expansion is measured by micrometers installed at the thrust end. The rate of expansion during the starting period, both after a long or short shutdown, is determined at the initial operation of the turbine unit and is included in the operating instructions.

With the use of a turning gear, the rotating parts are kept straight during short shutdowns and in condition to be started without any delay. The speed at which the turning gear operates the turbine spindle will have some influence in maintaining the cylinder straight. For small turbine structures, this speed may not be of any special importance, but for large units, the speed should be high enough to circulate the vapors evenly around the circumference.

C. J. Lamb.[5] There is ample precedent for such work as that of the authors in another field. While marine and naval turbines are generally smaller in size and weigh less per horsepower than do central-station turbines, for over 30 years prominent turbine builders and the large private and naval shipyards have been designing and building turbines, supplied with steam by marine water-tube boilers, to be lighted off and brought up to speed and load from cold in 1 hr normally, and in 15 min in an emergency.

The worst condition, from the viewpoint of rapid temperature change, is that of quick reversal from full ahead to full astern speed, and the many rapid changes when maneuvering. Merchant and naval vessels, ranging from 450 psig 750 F to 800 psig 850 F, reverse from full ahead to full astern in 15 to 30 sec time. The astern turbines are generally simple impulse wheels, located in the exhaust ends of the low-pressure turbines, rotating backward at a temperature corresponding to the vacuum being carried. When reversing, ahead steam is shut off instantly and steam at designed pressure and temperature is admitted to the astern element, whose nozzles, blades, and wheels are at temperatures in the neighborhood of 100 F. At the same time, all of the

[5] Staff Engineer, Douglas M. McBean, Inc., Consulting Engineers, Rochester, N. Y.

ahead blading, rotors, nozzles, and cylinders instantly are subjected to full vacuum temperature. The same changes occur when going ahead again.

With respect to boilers, the latest cruisers generate steam for 130,000 bhp in four oil-fired boilers, which have a heat release in the neighborhood of 500,000 Btu per cu ft of furnace volume. Such boilers are normally lighted off and put on the line in 1 hr, although in emergency this may be reduced to 15 min.

Such practice is not new, but has prevailed practically since the adoption of geared turbines to propel ships, and does not affect turbines or boilers adversely, due mostly to the fact that the turbine and boiler builders have willingly designed equipment to meet the needs of such service.

There should be no good reason why they cannot accomplish comparable results for the central-station industry. Beyond any question they have both the experience and the ability.

G. B. Warren.[6] It is to be hoped that numerous other operators of large steam turbines will make a similar survey and study of the combined boiler-turbine plant shutting-down and starting conditions inasmuch as such information is badly needed by the industry. It would be desirable of course if some of these additional studies would include the action of condensing units as well as that of topping units, as covered in the present paper. Although the question of starting and stopping turbine-generator units has been with the designers of these machines from the beginning, there is a feeling on the part of many that the conditions of operation imposed by present utility loads may be increasing the necessity of and frequency of such short-time periods of shutdown.

The designing of turbine generators to meet such conditions has been a progressive one, and through the years we have been ever conscious of the necessity of taking greater precautions to see that we can meet the requirements imposed by changes in temperature, expansion, loadings, and so forth, imposed by such operation. The continuing increases in pressure, temperature, and size of units have imposed added problems, which we believe have been met at a rate such that, despite these conditions, our modern units are more capable today of meeting such conditions than at any time in the past.

Where a unit is to be started and stopped frequently, it is highly important that a careful study and analysis of conditions be made and a well-developed procedure established and rigorously followed. If this is done, we believe adverse effects from this type of operation can be reduced greatly. During the period the unit is shut down, it is important that the valving be tight so that there is no steam leakage into the turbine. We believe the discovery mentioned by the authors that a quick start will reduce the temperature stresses during starting may be correct and fundamental. It needs to be investigated by others on their installations. Where this is true we have no objections to quicker starts from the turbine standpoint.

We are inclined to the belief that frequent light-load operation and shutdowns of modern turbine units may involve increased corrosion problems which are largely the responsibility of the operators, and on which much study should be expended in the future. Existing evidence would indicate that in the efforts which have rightly been made to reduce turbine-blade deposits, steam purity may have advanced so far that the low pH value of the resulting condensing steam may cause severe corrosion in the turbine. This has been noted in boiler feed pumps. Low-load operation, by increasing the moisture zone in the turbine, together with making conditions more favorable for entry of oxygen, which is particularly apt to happen on shutdown, may aggravate this condition. This situation is under active study by the writer's company, and turbines in current production are being much more completely protected against these conditions than in the past. Probably this problem is one of mutual concern between manufacturers and operators of power-plant equipment.

With regard to the generators, we feel that operating practice involving frequent shutdowns—of perhaps 200 times per year—is very strenuous, on account of expansion and contraction effects, particularly in the rotor, where there will be a tendency for considerable wear and tear on the insulation, and also for gradual distortion of the coils. Present materials, for both insulation and coils, have been developed as the best now known for these operating conditions, and we are confident that our newer generators will stand up well, giving service which will compare favorably with any machines available to the industry.

Recognizing the physical behavior of the materials, however, we feel that the bad effects of frequent stops and starts can be offset to a considerable extent by giving the generators the same kind of warm-up treatment accorded to boilers, steam lines, and turbines. Therefore, on large units (say, 40,000 kw and larger), we recommend the practice of preheating the generator fields at low speed, as a means of obtaining maximum service. Observations on the coils of generators which have had such preheating indicate that it is beneficial. We recommend this, however, as a desirable practice, and do not consider it strictly necessary on recent machines with improved rotor materials. We are also making a study of the method of handling the generator coolers during frequent shutdowns and starts which we believe may have an appreciable effect upon this situation.

We would like to point out that our turbines are designed to operate with high economy at light loads. If, in this connection, means can be provided to keep the temperature high and to obtain the higher vacuum possible with light-load operation on the condenser, the actual economy of the machines at light load, particularly hydrogen-cooled generator machines, might not be so bad as to warrant shutdown. We assume the operating groups are making such studies and would be glad to give such data as they may not now have upon which such studies can best be based.

We presume of course the operating companies are also doing everything possible to permit their customers to make use of the extremely low incremental cost at which power can be produced during these low-load periods. If, in connection with the normal low costs of such periods of operation, the fact that depreciation on boilers, turbines, generators, and so forth, is apt to be greater if operated under these conditions of shutdown or extremely light loads is taken into consideration, it might make the cost of power very low at these periods and stimulate its further use during such time.

C. C. Franck.[7] Mr. Falkner and his associates are to be commended for the excellent paper which they have prepared in connection with "Quick Starting of High-Pressure Steam-Turbine Units." The careful planning of the experimental layouts and the painstaking efforts put forth in both the assembling and the analysis of the test information is evidenced by the data presented in the paper.

Mr. Falkner is faced with a problem of operation which will gain more widespread concern as time goes on. With the installation of new and more efficient power-generating equipment, the present "preferred" system units will be relegated to the peak-power generation class. When other operators of high-pressure plants are confronted with the same situation, they will find the paper of great assistance in planning their operating schedule.

[6] Turbine-Generator Engineering Division, General Electric Company, Schenectady, N. Y. Mem. ASME.

[7] Manager, Land Turbine Engineering, Steam Division, Westinghouse Electric Corporation, Philadelphia, Pa. Mem. ASME.

Mr. Falkner's operating problem is associated with the shutting down of superposed units following the evening-night peak and then starting the units again in the morning in time to be in a position to take the morning load. In terms of the steam turbine, the shutdown would be classified as a "short shutdown."

In normal operation, the throttle valve, steam chest, and nozzle chamber operate at full throttle temperature. The cylinder walls, flanges, and bolting of the horizontal joint actually operate at temperatures less than the inlet as a result of the gradients through the machine. In general, it might be concluded that at any given section of the turbine, the maximum temperature would be at the center of the turbine and a temperature gradient will exist from the center to the outermost portion of the casing. As a result of this condition, a shutdown is followed by a gradual readjustment of temperature resulting from the outward flow of the heat emanating from the center of the machine. The authors' curves demonstrate this point and indicate that the stored-up heat is gradually being dissipated through the outer portions of the turbine.

After a shutdown period of approximately six to eight hours, there is still a considerable amount of heat stored in the unit and any starting process which admits steam at less temperature than that of the turbine parts, only prolongs the start-up period, since the turbine must be first cooled down and then heated up again. The authors' solution to this problem is to bring steam of sufficiently high temperature into the turbine and eliminate this period of unnecessary cooling and heating.

Even if the steam admitted to the turbine was at a temperature somewhat higher than the temperature of the turbine parts, no difficulty would be anticipated. In fact, it would be desirable to have the incoming steam at a slightly higher temperature in order to eliminate the contraction of the walls, etc., which would result from a drop in temperature.

There is one very essential point which must be kept in mind when applying Mr. Falkner's methods in the starting of high-pressure-temperature steam turbine units. This qualification is that the shutdown is of short duration. This is very important since, if the period of shutdown is sufficiently extended, the turbine parts will cool to a greater degree and any subsequent starting must be carried out in accordance with the established rules for starting the turbine. This word of caution is probably superfluous for the experienced turbine operator but it is better to have mentioned the point rather than to have an impression created that any high-pressure-temperature turbine, regardless of period of shutdown, can be started in a manner similar to that described in the paper.

Continuous Determination of Oxygen Concentration Based on the Magnetic Properties of Gases

By ROBERT D. RICHARDSON,[1] MICHIGAN CITY, IND.

A new instrument for the continuous analysis of industrial gases for oxygen concentration has been developed. This instrument is based on the magnetic properties of oxygen and therefore the readings are not disturbed by any extraneous gases except some of the oxides of nitrogen. Actual tests show that the effect of gases other than oxygen are less than predicted by an examination of published values of the magnetism of gases. The electrical impulse is picked up directly and measured on a recording bridge. A response of about 3 mv for one per cent oxygen is obtained. This instrument should prove to be a universal oxygen recorder for industrial gases.

A RECORDER for the measurement of oxygen based on the magnetic properties of gases has been developed as a result of a study of the best methods of continuously analyzing the gas. The measurement of oxygen in industrial gases has become increasingly important with the expansion of the chemical industry and the increased interest in the control of combustion processes. Almost every process dealing with heat and gas reaction can be improved by the knowledge or detection of oxygen at some point in the cycle.

This instrument has been named "Magno-therm" because it operates by the change in paramagnetism of oxygen with temperature. This paper describes the theoretical basis for this analyzer and then discusses the detailed description of the final instrument. This is followed by a description of the operating characteristics and further by a discussion of the range of usefulness of this instrument.

A gas-analyzing instrument presents unusual problems to the instrument designers. Most instruments measure a physical quality such as temperature or pressure by its effect on physical substance, for instance, temperature is measured by the expansion of liquids. Often an industrial instrument uses a principle of operation that is close to the fundamental standard of measurement.

However, a gas-analyzing recorder is called upon to measure chemical composition where no simple fundamental standard of measurement is available. Precise chemical analyses are complicated and involve chemical reactions unsuitable for adaptation to continuous analysis.

Most oxygen recorders depend upon a chemical reaction for the primary determination which introduces problems in maintenance because of replacement of chemicals or precise mixing of gases. A more ideal method of analysis would use a physical quantity as the measurement. This type of analyzer would be adapted to continuous measurement because the chemical maintenance could be eliminated and the physical quantity perhaps measured without metering, mixing, or otherwise changing the gas sample and thereby increasing the maintenance problems. However, the physical quantity used should be specific for the gas being determined.

Another desirable feature in industrial instruments is the absence of moving parts that may wear and otherwise vibrate and give erroneous readings. For the greatest reliability and freedom from unusual service, the measurement should be quickly transferred to an electrical quantity that can be measured by the highly reliable electrical null balance recorders used in industry.

Principles of Operation

Oxygen is unique among all other common gases in its paramagnetic properties. As shown in Fig. 1,[2] none of the more common industrial gases show paramagnetism but exhibit a slight diamagnetism. A paramagnetic gas is defined as a gas that will pass magnetic flux more easily than a vacuum, and a diamagnetic gas is one that passes a magnetic flux less easily than a vacuum. This property is caused by an uncompensated electron spin within the oxygen atoms and occurs because of the arrangement in the O^2 molecule (1).[3] As shown in Fig. 1, the only gases beside oxygen exhibiting this property are some of the oxides of nitrogen. The common gases containing the oxygen atoms such as carbon dioxide and carbon monoxide do not exhibit a paramagnetism because of the molecular arrangement.

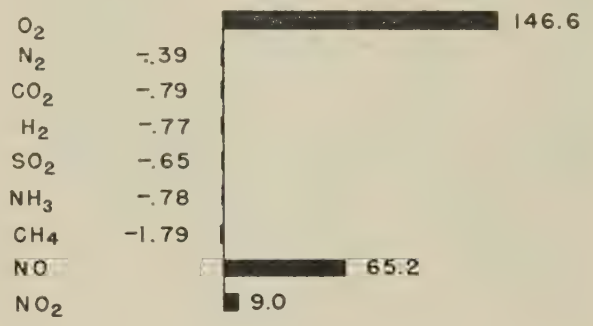

Fig. 1 Magnetic Properties of Common Gases

The magnetic susceptibility of gases cannot be measured easily by direct electrical means because it is a property having a very small magnitude. Researchers in the field of magneto-

[1] Research Engineer, The Hays Corporation.

Contributed by the Industrial Instruments and Regulators Division and presented at the Annual Meeting, Atlantic City, N. J., December 1–5, 1947, of The American Society of Mechanical Engineers.

Note: Statements and opinions advanced in papers are to be understood as individual expressions of their authors and not those of the Society. Paper No. 47—A-38.

[2] Values given are volume susceptibility of gases connected to 20 C from various sources. These figures should be used for comparison only.

[3] Numbers in parentheses refer to the Bibliography at the end of the paper.

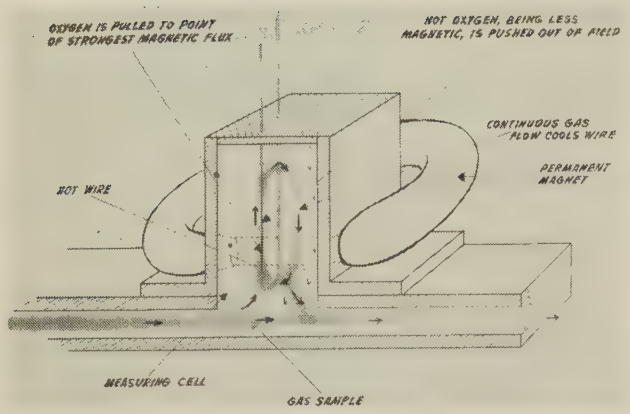

FIG. 2 PRINCIPLES OF OPERATION

chemistry have developed elaborate and very accurate apparatus for measuring the magnetic properties of gases. These devices usually consist of large electromagnets and laboratory balances to measure the forces involved. These methods are generally exclusively for the laboratory and cannot be adapted to industrial measurements where continuous records under severe operating conditions are required. Smaller instruments using spring torsion have been developed (2) but they involve a mechanical movement and are therefore subject to errors because of the magnification of the small forces involved.

The Magno-therm oxygen recorder uses a principle that was noticed by a colleague of Senftleben while studying the thermal conductivity of gases in a magnetic field (3). This effect is illustrated in Fig. 2. If a hot wire is suspended in a closed chamber containing a paramagnetic gas and a strong magnetic field is placed at the bottom of the wire, a magnetic convection is generated. This convection current cools the heated wire in proportion to the paramagnetism of the sample and therefore can be used as a measurement of oxygen concentration. This phenomenon can be explained easily by the Curie law and the temperature effect on the volume susceptibility of oxygen.

The Curie law states that the mass susceptibility of a gas is inversely proportional to the absolute temperature

$$Xm = \frac{K}{T}$$

If the expansion of the gas because of the temperature is considered in converting to a volume basis, the volume susceptibility then becomes inversely proportional to the square of the absolute temperature. What happens in the apparatus shown in Fig. 2 is explained by this relationship. The oxygen in the magnetic field is heated by the hot wire. It then loses its magnetism in proportion to the square of the temperature and becomes practically nonmagnetic. Since the heated oxygen is no longer magnetic, it is therefore forced out of the magnetic field by the cooler and more magnetic oxygen. The oxygen that is forced out of the field is eventually cooled on the sides of the chamber and then is recirculated into the magnetic field. A continuous stream of the sample gas is thereby set up whose strength and therefore cooling effect is proportional to the magnetism of the gas in the measuring cell. This cooling effect on the wire changes its resistance and this change in resistance is measured by an automatic Wheatstone bridge calibrated in per cent oxygen.

The operation of this convection current depends upon the inhomogeneous magnetic field appearing at the edge of the heated wire. This has been proved by placing the magnetic pole pieces at the top of the heated wire. In this case the deflection is in the opposite direction, indicating that the magnetic forces are bucking the normal thermal convection around the hot wire. However, when the oxygen content is increased sufficiently, the readings then reverse themselves and are in the same direction as when the pole pieces are at the bottom of the hot wire. For a good design of oxygen-measuring cell this reversal occurs below one per cent oxygen, indicating that the convection currents caused by the heating of the spiral are a small part of the convection because of the magnetic effect.

DESCRIPTION OF INSTRUMENT

A practical instrument built on this principle was developed as shown in Fig. 3. This arrangement contains two electrically heated elements in cylindrical chambers mounted vertically in a brass block. The brass gives thermal stability between the two chambers but the interior of the cell is lead-lined for corrosion resistance. One of these chambers has magnetic steel wedges through the brass block. At this point a powerful permanent magnet surrounds the measuring cell and develops about 13,000 gausses across the measuring chamber. The magnetic convection takes place in the chamber having the magnetic wedges; the second chamber is built physically identical except for the absence of the magnetic flux. The heated resistor in the comparison cell is so placed in a Wheatstone bridge circuit that it opposes the resistor in the measuring cell. Since both cells contain the same gas sample, the effects of thermal convection, thermal conductivity of the gas, or radiation are canceled out, and only the magnetic effect appears as a net reading.

The permanent magnet is so constructed that it may be swung out of place and the bridge circuit set to electrical zero. This allows for a zero check while an oxygen sample is in the instrument. This is a great practical convenience because oxygen-free gases are difficult to obtain in normal industrial plants.

The heater element is of unique design. It balances out the magnetic forces caused by the passage of current in a strong magnetic field. This heating element is composed of a platinum conductor which carries the current down the center of the element, a 0.001-in-diam platinum coil bringing the current back. The net effect of the magnetic forces on this element is zero. The entire coil is encased in glass for electrical insulation and to prevent corrosion.

To complete the Wheatstone bridge the balance arms are

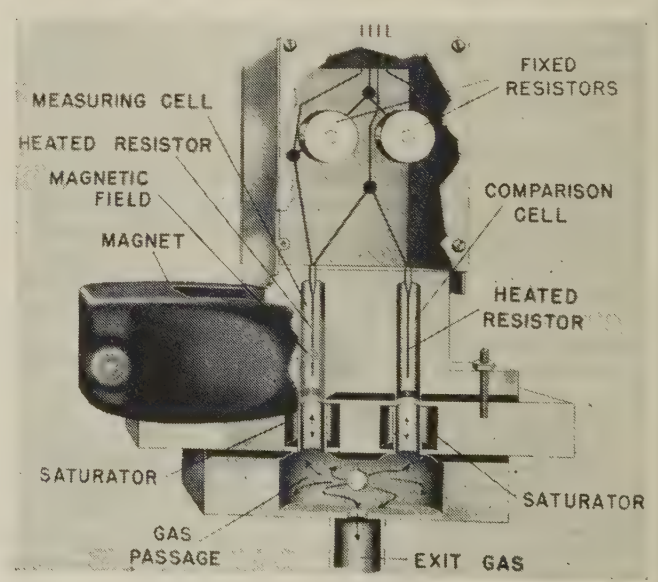

FIG. 3 ANALYZER CELL DESIGN

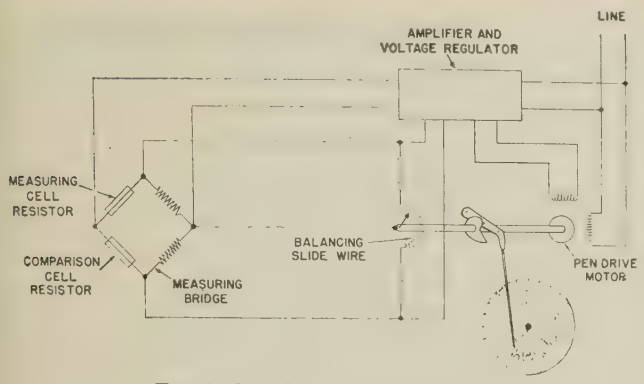

FIG. 4 SELF-BALANCING RECORDER

placed in the upper section of the cell. This is then connected to a self-balancing Wheatstone bridge recorder shown in Fig. 4. The unbalance across the analyzer is picked up by a high gain amplifier and increased sufficiently to run a reversing motor. This motor finds a balance on the measuring slide-wire and this position is taken as a measure of the resistance change in the spiral element. The information is transferred mechanically to the recorder pen through a cam to take out any nonlinearity in calibration and obtain a linear reading in per cent oxygen.

Referring again to Fig. 3, it will be seen that the sample gas passes into the measuring cell by diffusion. This system effects the transfer of the sample into the measuring cell without the sample flow disturbing the magnetic convection. This method of construction is commonly used in gas-analyzing cells of the thermal-conductivity type. When the gas composition is changed in the chamber marked, "Gas Passage," at the bottom of the assembly, this change in composition is transferred to the measuring cell by the molecular movement of the gas molecules. Since all gas molecules are in a state of constant motion at comparatively high velocity, a few molecules will get to the upper chambers almost instantly. These molecules are followed by those with a shorter free path that have more molecular collisions before reaching this point. This interchange of molecules works in both directions and will gradually slow down as the compositions in the gas passage and measuring cells equalize. This process takes about 15 sec for a 90 per cent change in composition for the particular design under consideration.

The time lag up to the bottom of the cell depends upon the sampling system used. For the most rapid response, the sample must be moved to the analyzer as fast as possible in a large volume. However, there is a diminishing return because of the difficulties of conditioning the gas and the more frequent service and larger apparatus required for filtering systems. The sampling systems must be studied individually for each process under consideration for the minimum time lag.

The reading is independent of rate of sample flow until the velocity becomes high enough to cause forced convection around the heated elements. In order to adapt the instrument to various sampling systems the bottom gas-passage block is made in two designs to eliminate large time delays when small sample rates are used, and forced convection when large flow rates are used. A gas-passage block with a maximum flow of one liter per minute uses $^1/_4$-in. gas passages. The design shown in Fig. 3 accomodates a maximum flow of about 500 liters per min.

Between the gas-passage block and the cell block are two porcelain sleeves, one for the measuring cell and one for the comparison cell. These porcelain sleeves are kept moist by a water reservoir behind them. The nature of this porcelain allows the water to seep through but the surface tension does not allow the sample to be forced into the water reservoir. The gas, in diffusing through these moist porcelain sleeves, is saturated with water vapor at the temperature of the block. Therefore the gas is measured at a constant water-vapor dilution. If this were not controlled, the variable amounts of water vapor would dilute the sample to a varying degree and thereby change the percentage composition of oxygen in the analyzed gas. The advantages of this saturator are the unlimited reservoir that may be used and the absence of any necessity to open the sampling line to replenish the supply. Also, only that amount of water that is needed to saturate the gases reaching the measuring cell is required, thus reducing the maintenance considerably, especially for the very high rates of sample flow.

To maintain stable operation of the measuring bridge and calibration of the cell, the entire analyzer is placed in an insulated temperature regulated case, as shown in Fig. 5. This, besides

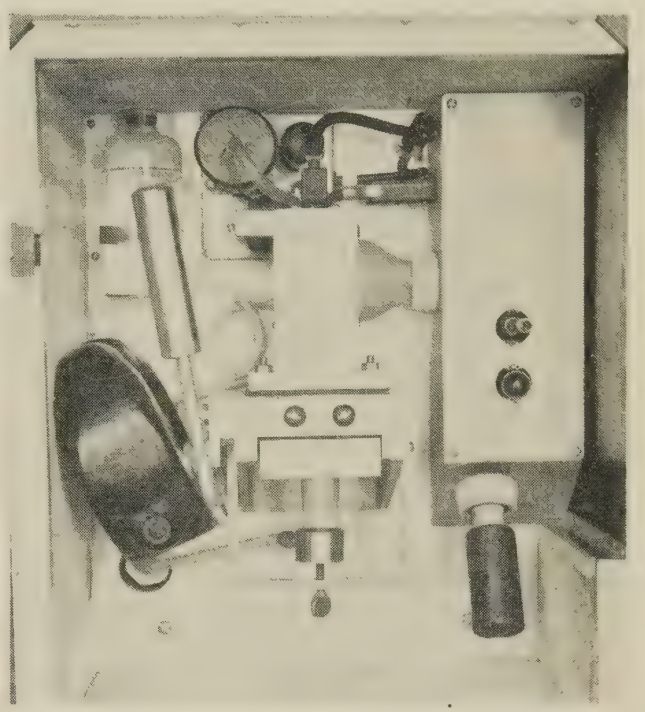

FIG. 5 EXPERIMENTAL MODEL ANALYZER CASE WITH MAGNET SWUNG BACK FOR ZERO CHECK

maintaining a constant calibration, maintains a constant saturation and therefore water-vapor dilution. Since the reading depends on the change in magnetism with temperature, it can be expected that the calibration will be reduced by an increase in temperature. The temperature of the case is maintained at 130 F ± 2 F which keeps the error, because of this variation, below $^1/_2$ per cent of the measure value. Of course at zero oxygen measurement there is no change in reading because the temperature error is a change in calibration.

A pressure compensator is placed in the upper center of the analyzing case which works into the recorder circuit to correct the calibration for changes in pressure. Fundamentally, this oxygen recorder measures the actual partial pressure of oxygen and not the per cent by volume as is required for general gas-analysis work. This change of reading with pressure is caused by the change in density of the oxygen. For instance, an increase in pressure does not change the percentage composition of an oxygen sample but the amount of oxygen per unit volume has increased. The instrument therefore would have a proportionately stronger magnetic force and give a proportionately higher reading.

In order to make the instrument read per cent by volume, regardless of changes by barometric pressure or changes in process pressure, an electrical pressure compensator has been devised. This compensator contains a constant mass of gas in a closed metallic chamber under a pressure, at room temperatures, lower than that expected for the lowest operation of the instrument. One end of this enclosed space has a metallic diaphragm and electrical contacts. The metallic container is wound with heater wire. The contacts are so connected into the grid of a thyratron tube that when the pressure on the outside of the diaphragm is higher than the pressure within the metal container, the thyratron passes current through the heater coils. This heats up the gas in the chamber until the internal pressure equalizes the external pressure and thereby opens the contacts and controls heat in the chamber to maintain a zero pressure differential. The temperature of the gas in this chamber therefore becomes a measure of the absolute external pressure on the diaphragm. A temperature-sensitive resistor is placed in the heated chamber and is so connected into the recorder circuit as to continuously correct the calibration for pressure variations.

Operating Characteristics

The resistance change for oxygen-nitrogen mixtures on a 65-ohm heater element is shown in Fig. 6. Since a 1.46-ohm change

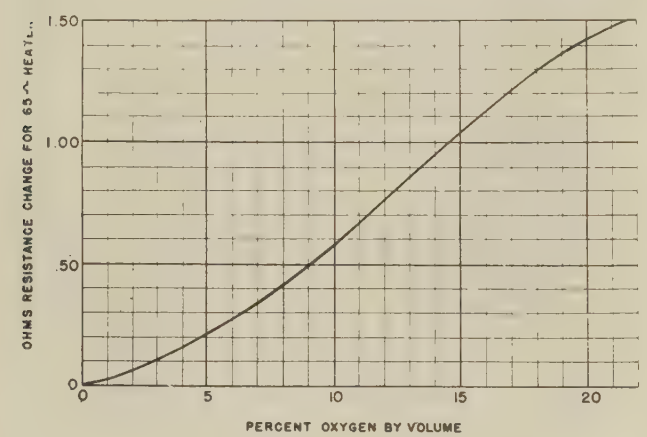

Fig. 6 Electrical Response to Oxygen Changes

in resistance is obtained with air the bridge unbalance developed by this gas is approximately 67 mv. The calibration is almost a straight line but all of this curvature is removed by the cam shown in Fig. 4 and therefore the graduations on the chart are linear. The instrument can be used for measuring up to 100 per cent oxygen.

The actual deflections for 100 per cent of some of the common industrial gases are shown in Fig. 7. These deflections are so small as to be insignificant for normal industrial measurements. It will be noted that for both diamagnetic and paramagnetic gases the deflection is less than is predicted by the theory in Fig. 1. The deflection for water vapor is not given because 100 per cent of this vapor cannot be obtained in an analyzer operating at 130 F and at atmospheric pressure. However, an experiment was run by measuring both the deflection because of nitrogen when it was saturated with 15 per cent water vapor and when it was dry. No change in deflection could be noted on an analyzer sensitive to 0.01 per cent oxygen.

The oxides of nitrogen present an interesting case. The deflections are less than predicted by the table in Fig. 1. However, the interchange in molecular arrangements of oxides of nitrogen from the paramagnetic to diamagnetic form makes exact data difficult. The readings for NO are much smaller than expected

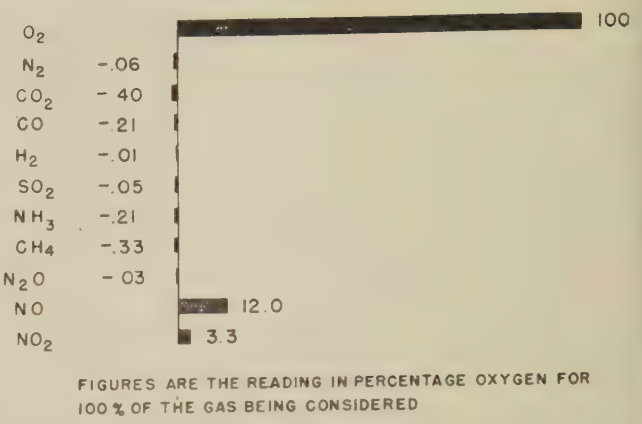

Fig. 7 Relative Deflection of Various Gases on the Magnotherm Oxygen Recorder

because this gas does not follow the Curie law (4). The readings for N_2O and NO_2 were taken with commercial gases in a dry condition. Since NO was not available commercially, it was generated both by adding nitric acid to ferrous sulphate in dilute sulphuric acid and by the action of dilute nitric acid on copper. Both methods gave the same results. All readings for the cell are to be considered empirical and can be changed by physical design of the analyzer.

For all practical purposes, the calibration of the analyzer is independent of the interfering gases. However, a decrease in calibration value is noted as the gases increase in thermal conductivity. Hydrogen, being the most conductive gas thermally, has the greatest effect. This necessitates the use of a special cell design for the measurement of oxygen in the presence of high concentrations of hydrogen.

Discussion

The over-all design of the Magno-Therm oxygen recorder has produced an instrument with a very high electrical response capable of good zero stability. The deflection of 3 mv for each one per cent oxygen gives as much electromotive force for 5 per cent oxygen as standard platinum thermocouples over most of their working range. The absence of any moving parts or chemical replenishing minimizes the difficulties because of servicing.

The interference of the zero point by commercial gases other than oxygen is less than predicted. This can be explained by the fact that this instrument depends not on the susceptibility of the oxygen but on the change of susceptibility with temperature. Apparently, diamagnetic gases have no susceptibility changes with temperature (5). Therefore the only effect because of the heating would be the expansion of the gases making the change in diamagnetism the first power of the temperature change. This would therefore reduce the reading accordingly.

The readings of this instrument should be taken as an empirical value since the actual response depends on many parameters that cannot be evaluated. For instance, it was found that the variation of calibration with pressure could be altered by cell design. The responses shown are for the analyzer as described but this may be altered to cover unusual gas-analyzing problems.

The instrument itself measures substantially partial pressure which may be useful in some chemical industries where the partial pressure of oxygen and not its percentage composition is required. However, this error when measuring gases under normal atmospheric pressure changes, amounts to about one per cent oxygen for a reading of 20 per cent. The compensator therefore can easily correct this to the desired accuracy in the recording.

The sensitivity of the instrument is dependent upon the electrical recorder to which it is attached which amounts to 0.1 per cent of full scale reading. There is no noticeable or detectable hysteresis in the oxygen measurement.

Summary

The Magno-therm oxygen recorder accomplishes the results set out in its original development. It measures oxygen by measurement of a physical property, in this case magnetic susceptibility, which is exhibited by no other gases except some of the oxides of nitrogen. The instrument contains no chemicals or mixing orifices and is free of moving mechanical parts. The impulse is picked up electrically to utilize the advantages of the present-day electrical recorders and their high precision of null measurement.

This instrument should prove a useful tool as a universal oxygen recorder for industrial gases.

Acknowledgment

Acknowledgment is given to Mr. Paul Copp and Mr. Ginther Wassel, both of The Hays Corporation, for their laboratory assistance in the development of this instrument.

BIBLIOGRAPHY

1 "Magnetochemistry," by P. W. Selwood, Interscience Publishers, Inc., New York, N. Y., 1943, p. 116.

2 "Modern Magnetism," by L. F. Bates, Cambridge University Press, London, England, 1939, p. 122.

3 "Untersuchungen über das Verhalten paramagnetischer Gase im inhomogenen Magnetfeld," by F. Klauer, E. Turowski, and T. v. Wolff, *Zeitschrift für Technische Physik*, no. 9, 1941, pp. 223–228.

4 "Magnetochemistry," by P. W. Selwood, Interscience Publishers, Inc., New York, N. Y., 1943, p. 120.

5 "Modern Magnetism," by L. F. Bates, Cambridge University Press, London, England, 1939, p. 50.

Discussion

J. G. Fleming.[4] The paramagnetic property of oxygen[5] has long been known. However, it was only during the recent war emergency that sufficient drive appeared in the problem of measuring oxygen concentration to stimulate the development of several applications of this principle as industrial oxygen meters. The first instrument of this type to be developed was a contribution of Linus K. Pauling[6] of the California Institute of Technology. This device directly measures the paramagnetic property of the gas sample. Another instrument was developed by the I. G. Farbenindustrie[7] and called a magnetic-type oxygen recorder. This was discovered by a special committee on measurements which studied the industrial-processing-instrument industry in Germany after World War II, and published its finding in a report under the Office of Military Government for Germany (U. S.). This latter-type instrument appears to be similar to that described in the present paper.

Specific comments are included under the following headings:

Calibration. It seems misleading to compare the data indicated in Fig. 7 of the paper with those in Fig. 1. The data for Fig. 1 are given for 20 C, and the instrument described is operated at about 55 C. In addition, the temperature of the gas in the measuring chamber is further increased by the heat of the measuring element and the oxygen molecules cutting the magnetic-flux lines. It is also interesting to note that N_2, H_2, and SO_2 at this elevated temperature approach a paramagnetic characteristic.

In comparing the author's calibration with that indicated by Pauling, there is a 30 per cent discrepancy in the center of the range if both ends of 0–20 per cent oxygen range are adjusted to be equal.

Time Lag and Hysteresis. A figure of 15 sec has been cited as the time lag for 90 per cent deflection. This is believed to apply only to the measuring cell, in view of the statement of difficulties in conditioning the gas as factors which limit the over-all time lag of the complete instrument. This of course brings up the question as to whether or not the filtering is critical:

(*a*) Do dirt or foreign particles interfere with the saturation in the porcelain saturating cylinders?

(*b*) Is there some effect on the magnetic-convection currents?

It is known that hysteresis is not a factor when dealing with single dipoles, but in the case of this measurement, we have a stream of oxygen dipoles, with those close to the platinum heater much warmer than those near the wall of the block. We might draw the analogy here to a "gaseous bar magnet." What is the practical magnitude of hysteresis in this connection?

A further consideration on the time lag concerns that of "starting up." If, when the instrument is put into service, the measuring cell is filled with air (20 per cent oxygen and 80 per cent nitrogen), but the sample contains zero oxygen, then, since the magnetic convection currents are much greater than the diffusion currents, is it not true that considerable time would be necessary for ultimate equilibrium? Would this also apply to any large sudden change in oxygen concentration?

Saturation. Reference is made to porcelain sleeves which are kept moist by a water reservoir behind them. It is further indicated that this porcelain allows the water to seep through, but the surface tension does not allow the sample to be forced into the water reservoir. This is good if the porcelain is actually a perfect semipermeable membrane. The question is not concerned with water, or gas transfer through the water, but rather dilution of the sample in the measuring chamber by dissolved oxygen from the saturation supply. What is the practical effect of this action on the operation?

Interfering Gases. There seems to be some question about a decrease in calibration as the thermal conductivity is increased. This statement seems to be based upon tests with hydrogen, and it would appear that catalytic action at the hot platinum surface may possibly be responsible for such a decrease rather than any thermal conductivity effect.

N. B. Nichols.[8] The instrument described in this paper presents an ingenious use of a physical property which has been industrially neglected. The reader who is interested in a mathematical treatment of the design parameters of a German instrument which uses the same general principles may be interested in reading an English translation of an I. G. Farbenindustrie report.[9]

The pressure compensator which is described also offers some interesting possibilities as an absolute-pressure-measuring element. One might call it a temperature-balance transmitter in contrast to the usual pneumatic transmitter which has been used for this purpose.

P. W. Selwood.[10] There appear at the present time to be four

[4] Research Engineer, The Bristol Company, Waterbury, Conn.

[5] "The Magnetic Susceptibility of Nitrogen Dioxide," by G. G. Havens, *Physical Review*, vol. 41, 1932, pp. 337–344.

[6] "An Instrument for Determining the Partial Pressure of Oxygen in a Gas," by Linus K. Pauling, et al, *Journal of the American Chemical Society*, vol. 68; 1946, pp. 795–798.

[7] Study of the Industrial Processing Instrument Industry in Germany, Report No. PB-4600, Field Information Agency Technical November 17, 1945.

[8] Director of Research, Taylor Instrument Companies, Rochester, N.Y.

[9] "Instrumentation and Control in the German Chemical Industry," Mapleton House, Publishers, Brooklyn, N. Y., 1947.

[10] Department of Chemistry, Northwestern University, Evanston, Ill.

methods, all based upon magnetic properties, for the determination of oxygen in gas mixtures. All these magnetic methods have the great advantage over other physical methods, such as density, of possessing high sensitivity. They possess advantages over chemical methods of analysis because they require no replacement of units or handling of liquids. There is no doubt that the magnetic methods are preferable for most applications.

The four magnetic methods are somewhat different in the exact nature of the property measured, and are quite different in the mechanical and electrical details.

Direct measurement of magnetic susceptibility is achieved in an instrument developed during the war by Prof. Linus Pauling and his associates. This instrument, which has been on the market for several years, is purely mechanical. A small glass test piece is suspended so as to move in a nonhomogeneous field. The motions of this test piece are governed by the magnetic susceptibility of the surrounding atmosphere. The instrument gives considerable satisfaction, but is not very easy to manufacture, and it is not particularly well adapted for rugged service.

The second method, discovered in Germany about 1932 by Sack and his students, is based upon the change of viscosity of oxygen in a magnetic field. This method seems to have received no industrial development and probably could not compete with the other methods.

The third method is the decrease of thermal conductivity of oxygen in a homogeneous magnetic field. This effect was reported about 1930 by Senftleben, also in Germany. The method appears to have been developed into a commercial instrument by Rein for use in German war research.

The fourth method was apparently discovered by Turowski in Germany, and was reported in 1941. This method depends upon an apparent increase in thermal conductivity of paramagnetic gases in a nonhomogeneous magnetic field. The increase is apparent because it depends upon thermal convection currents. This is the method used by the author in the developments described in the paper under discussion.

A comparison of the various methods shows that the two electrical methods have much in their favor. To be sure, they are not self-contained (unless supplied with batteries, which would in any event require recharging or replacement). However, the electrical methods require no delicate moving parts, and they are readily adaptable to continuous recording without undue complication.

We do not have much information on the relative merits of the two electrical methods. The Turowski principle would appear to be more sensitive. There is some doubt as to the stability of calibration of this method, as compared with that based upon the Senftleben principle.

Author's Closure

The comments by Mr. Fleming bring up important considerations in the practical design of this instrument. Fig. 1 in the text was used to indicate that an oxygen determination can be based on the magnetic properties of gases. The data on Fig. 1 and Fig. 7 have greater differences than those mentioned by Mr. Fleming. The data on Fig. 7 are the actual deflections obtained by use of the instrument and no attempt is made to analyze their theoretical significance. The differences are more than a matter of temperature variation. Actually the instrument operates on a change in temperature and therefore the data on Fig. 7 must be theoretically analyzed as a question of the temperature coefficient of magnetism of the various gases listed.

The calibration curve shown on Fig. 6 is also an empirical curve obtained by testing the instrument with various mixtures of gases. It would not necessarily follow a straight line because it comes from the cooling effect of the magnetic convection and therefore theoretical analysis is almost impossible. As was noted in the paper, the curvature of this calibration curve can be changed appreciably by altering the design of the cell.

The 15 sec time lag mentioned is the time required for the instrument to respond to 90 per cent of a sample change occurring in the chamber marked *Gas Passage* in Fig. 3. Taking Mr. Fleming's example, if the instrument initially contained air, and if nitrogen were passed through the instrument fast enough to change the composition in the *Gas Passage* chamber almost instantly, the reading would start to change in three seconds and would read 90 per cent of the change, or 2.1 per cent oxygen in fifteen sec. This is qualified when the sampling line is included because additional time is required to bring the sample to the instrument.

In a practical application dirt does not affect the operation of the porcelain sleeves because of the self-washing action of the water passing through the saturator. These have been found to operate satisfactorily when covered with soot. There is no effect on the magnetic convection due to the sample flow because it is completely isolated by the molecular diffusion passage formed by the porcelain sleeves. There has been no hysteresis noted in the operation of the instrument and it seems illogical that the integral sizes of an oxygen molecule would cause any hysteresis effects.

The porcelain sleeves are made of a type of ceramic common in industry for removing water from compressed air lines. They will withstand 50 lb pressure without allowing sample to pass through the porcelain. The amount of dissolved oxygen carried by this water or carried even by the total reservoirs is very small and can be shown by simple calculation to have a minute effect on the reading. This was proved correct by changing the water behind the saturators and noticing no increase in the oxygen reading.

The decrease in calibration as the thermal conductivity is increased is based on tests not only with hydrogen but also with most common industrial gases. However, the effect is negligible except when hydrogen in large concentrations is present. It would be impossible for any catalytic action to occur on the platinum heaters because they are solidly encased in glass.

The discussion by Mr. Selwood gives a clear picture of the status of various magnetic methods of determining oxygen. The method of measurement referred to by Mr. Selwood as the Turowski principle is used in this instrument. As pointed out by Mr. Selwood, this system is much more sensitive than that based on the change in thermal conductivity. Producing a stable instrument is a matter of designing a measuring cell in which changes in parameters do not critically affect the calibration.

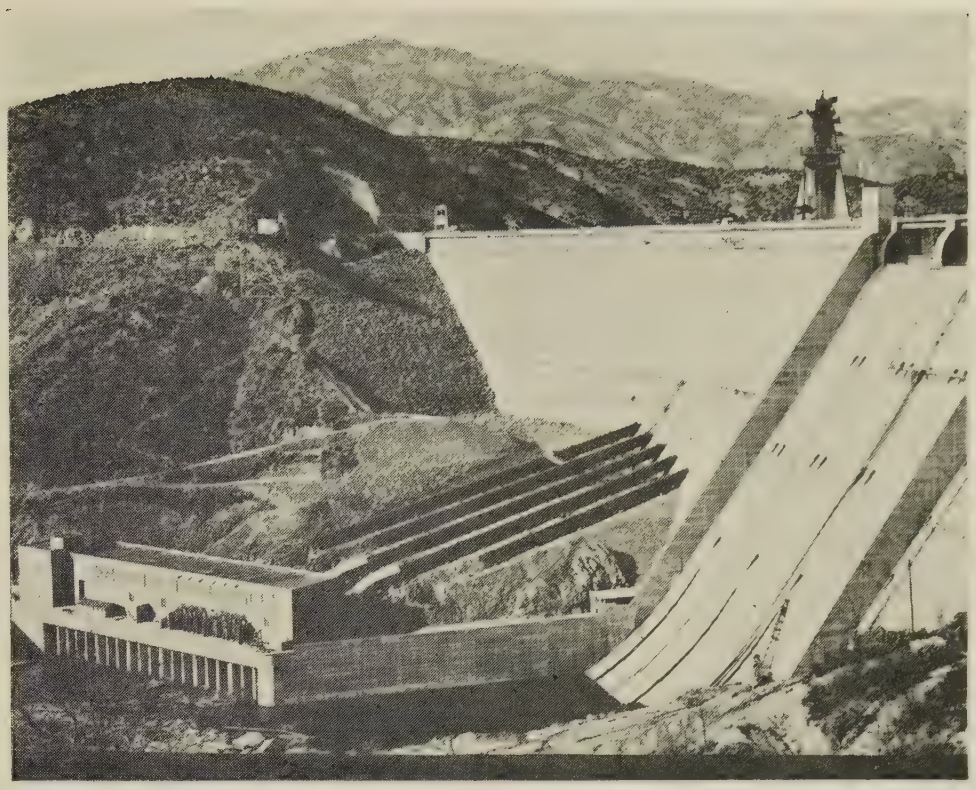

Fig. 1 General View of Shasta Power Plant

The 103,000-Hp Turbines at Shasta Dam

By J. F. ROBERTS,[1] MILWAUKEE, WIS.

Details are given of the special features incorporated in the single-runner vertical-shaft reaction-type hydraulic turbines installed by the Central Valley Project at Shasta Dam. Performance curves are given and a comparison made with model-test results and predicted efficiencies.

IN May, 1939, the Bureau of Reclamation placed an order with the Allis-Chalmers Manufacturing Company for four 103,000-hp turbines for the Shasta Dam plant of the Central Valley Project, this plant being located on the Sacramento River about 20 miles from Redding, Calif. Fig. 1 shows a general view of the plant, the powerhouse being located at a slight angle on the right bank of the river and somewhat downstream from the gravity-type concrete dam. Separate penstocks, each some 750 ft in length and approximately 15 ft diam, conduct the water from the upstream face of the dam to the individual units in the powerhouse.

The turbines are of the single-runner vertical-shaft reaction or Francis type discharging vertically downward through an elbow-type draft tube and delivering power to the generators mounted immediately above the turbines. Fig. 2 shows a cross section through the Shasta turbines. The generators are rated 75,000 kw and were furnished by the General Electric Company.

The turbines are rated 103,000 hp at 330 ft net head. They are also required to deliver 50,000 hp under a minimum head of 238 ft, and are specified to give their best efficiency between 380 and 400 ft net head. The turbines operate under an extreme variation of head from the minimum of 238 ft net head to a maximum of 475 ft net or from 72 per cent to 144 per cent of rated head. The principal variation is due to drawdown of the storage water in the pond upstream from the dam. Some slight variation occurs in the tail water below the dam owing to variations in discharge both through the turbines and to water spilled over the dam.

When these turbines were purchased it was the intention that they would be installed as quickly as possible in the Shasta powerhouse. The deliveries specified at that time were for the first unit in 840 days and additional units 90 days apart. This scheduled delivery of the first unit approximately September, 1941, and completion of the fourth unit May, 1942.

Early in 1942 the War Production Board and the Bureau of Reclamation authorized the installation of two of the Shasta turbines in the vacant stalls in the already completed Grand Coulee power station. The temporary installation of the Shasta turbines at Grand Coulee, together with their subsequent removal and transfer to Shasta Dam, has been treated in a paper[2] by H. H. Sloane, of the Bureau of Reclamation.

---

[1] Manager of Hydraulic Department, Allis-Chalmers Manufacturing Company. Mem. ASME.

Contributed by the Hydraulic Division and presented at the Fall Meeting, Salt Lake City, Utah, September 1–4, 1947, of The American Society of Mechanical Engineers.

[2] "Temporary Installation of Shasta Turbines at Grand Coulee," by H. H. Sloane, Trans. ASME, vol. 70, 1948, pp. 49–56.

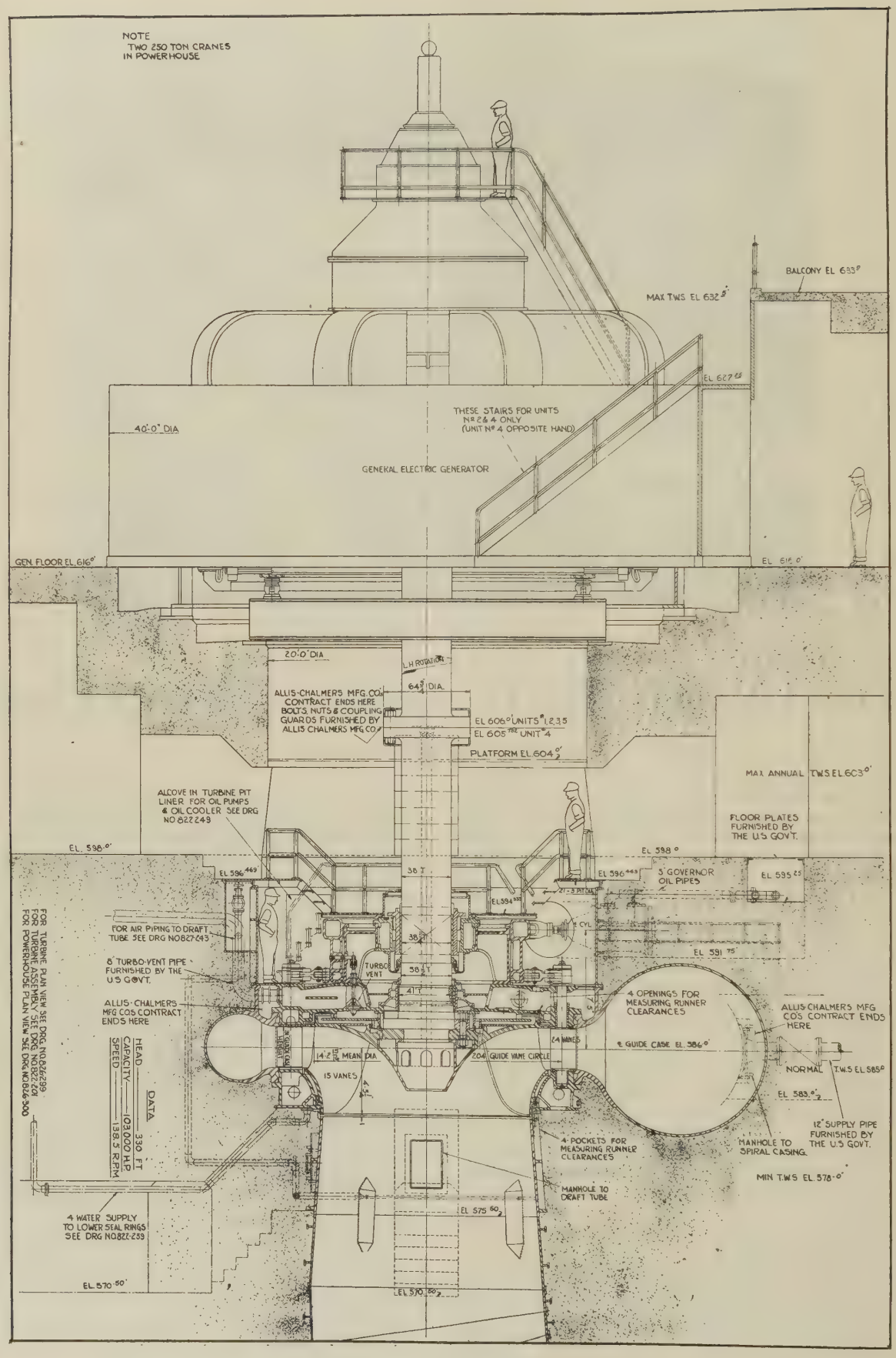

FIG. 2 SECTION THROUGH SHASTA TURBINE SHOWING DETAILS OF 103,000-HP TURBINE

Details of Turbines

The runners in the Shasta turbines are of the Francis type made of cast steel. They have a maximum diameter of 184 in., with an inlet diameter of 171 in. and a discharge diameter of 156 in. The center line of the runner is set 8 ft above low tail water, giving a sigma value of 0.082.

Each finished runner weighs approximately 75,000 lb, although a total of approximately 140,000 lb of steel had to be poured at the steel foundry. This weight included the weight of the runner plus the usual allowance for finish, plus the weight of the risers and feeders required in order to produce a sound casting. Wearing rings of carbon steel SAE-1045, having a Brinell hardness of 150, are shrunk onto the runner at both the crown and band where close clearances are required to reduce leakage and increase efficiency. These renewable wearing rings are held on by fillister-head machine screws.

On the stationary parts adjacent to the runner crown and band, that is, in the top cover and in the bottom cover, similar removable wearing rings are provided, also made of SAE-1045 carbon steel. These stationary wearing rings are also provided with two bronze inserts, these inserts being approximately $^5/_8$ in. thick and $1^1/_8$ in. in width. They are inserted in tapered grooves cut in the steel wearing rings and calked in with a copper-nickel alloy. The purpose of the bronze inserts is to prevent seizing, in case the runner should rub against the stationary parts as the dissimilar metals would act more as a bearing with water lubrication. The usual practice in such wearing rings is to make the stationary wearing rings of a harder metal so that any wear will occur on the removable rings on the rotating parts which are easily removed. The addition of the bronze rings is an added safeguard to prevent scoring.

The 38-in-diam main shaft is provided with a forged flange both top and bottom. The upper flange is for connecting to the generator shaft and the lower flange for bolting to the runner with straight fitted bolts. These bolts are designed for a light press fit, the bolts being between $^1/_4$ and $^1/_2$ thousandth inch larger than the reamed holes. The bolts have a nominal diameter of 5 in. both at the generator coupling and for attaching the runner. The main shaft is also hollow-bored to approximately 8 in. diam for internal inspection of the forging. Radial holes are provided from the outside of the shaft to this hollow bore for the admission of air into the draft tube.

The main turbine bearing is of the babbitted pressure-oil-lubricated type, and no sleeve is provided on the shaft in this bearing, as the polished steel itself makes a good bearing. However, below the guide bearing, where the shaft passes through the stuffing box, the shaft is protected with a removable chrome-steel sleeve. This sleeve is approximately 10 in. high, $1^1/_2$ in. thick, 41 in. OD, with from 12 per cent to 15 per cent chromium, 0.25 per cent carbon, and a Brinell hardness of from 200 to 235. The sleeve is made in two halves and set into a tapered recess in the shaft, the side walls of the recess having an angle of approximately $5^1/_3$ deg. The recess in the shaft is approximately $^1/_4$ in. wider than the sleeve, this surplus space being filled with a composition approximately 80 per cent copper, 20 per cent nickel which is calked in to hold the sleeve solidly into the recess. In addition, 1-in-wide keys prevent the sleeve from turning on the shaft, and dowels threaded into the joints in the sleeve hold the halves rigidly in line. The joints in the sleeve are beveled slightly and welded, using 18-8 welding rod. Experience has shown that this 13 per cent chromium steel with approximately 220 Bhn has excellent properties for resisting wear even with silt and other foreign matter which get into the stuffing boxes when the river is in flood.

Plate-Steel Spiral Casing

The spiral casing on the Shasta turbines is of the welded-steel type with riveted field joints held by double butt straps. Fig. 3 shows a plan of the casing. The casing is made with seven sections, these sections being designed for the maximum shipping space allowable. The casing inlet is 12 ft 8 in. ID, the plates in that section being $1^7/_8$ in. thick. This section is a true circle. The next section downstream, which also includes the first opening where the water is fed through the speed ring and guide vanes into the turbine runner, is made up of four different pieces. The outer half of the casing is of $1^7/_8$-in. plate. The inner quarter of the circle is formed by the cast-steel parts of the speed ring which consists of columns and flanges cast integrally. Joining the edges of the speed-ring flanges are welded plates $2^5/_{16}$ in. thick, which form approximately one quarter of the circumference of the 12-ft 8-in-ID circle. Heavier plates are used throughout the casing where the plate section joins the cast-steel speed ring. The greater thickness of plates is required in the smaller radius since this inner width of plate must carry the same total load as the plates on the large radius on the outside of the casing.

This is one of the first and, undoubtedly, the largest welded-plate-steel spiral casing to be built in this country. Fig. 4 shows an assembled view of this casing in the manufacturer's shops. The shop-welded joints between the various plate sections show up clearly, and seven riveted field joints are also clearly visible. Fig. 5 shows a section of the speed ring and casing assembled in the shops, the method of joining the speed-ring sections with fitted bolts, and the double-riveted double-butt-strap field joints. When each of the seven sections was welded in the shops it was placed in a furnace and stress-relieved in order to remove all welding strains. Following this, the speed-ring joints were carefully machined to the proper angle and drilled and fitted together so as to produce a complete circle. The plate sections were carefully rolled to the proper radius and held with the welded pipe stiffeners visible in the illustration. A considerable amount of shop fitting and bending had to be done in order to make the adjacent plates lie flush with each other so as to make a satisfactory riveted joint. Considering the thickness of these plates varying from $2^5/_{16}$ maximum to 1 in. minimum, the magnitude of this fitting work can be appreciated.

The plates used in the casing were ASTM-A-89-33 firebox quality B of flange and firebox quality for forge welding. All welding was done in accord with paragraph U-69 of the ASME specification for unfired pressure vessels and all of the shop-welded joints were x-rayed and carefully examined.

Riveting of the field joints was decided upon because of the impossibility of satisfactorily stress-relieving welded field joints of this magnitude. While field welding of similar joints has been successfully accomplished in more recent turbines, the engineers of the Bureau of Reclamation felt that a riveted joint offered a safer job.

Types of Riveted Joints and Tests

The riveted joints with plates having a maximum thickness of $2^5/_{16}$ in., joined together with 1-in. butt straps on both sides and two rows of $1^1/_4$-in. rivets, offered a major riveting problem. Extensive experiments were conducted to determine whether special high-stress manganese rivets using ASTM A-195-39R with an ultimate strength of 85,000 to 90,000 psi would give better results than mild-steel rivets, ASTM A-141-39, with an ultimate strength of 52,000 to 62,000 psi. In addition, two different types of rivets were tested, i.e., round-headed rivets, and hourglass-type rivets. Fig. 6 shows sample rivet specimens cut open and etched to study the tightness of the rivets in the holes and to observe the firmness with which the three plates are held together by the two different types of rivets. It was found that either type of rivet could be driven satisfactorily by hand to fill the

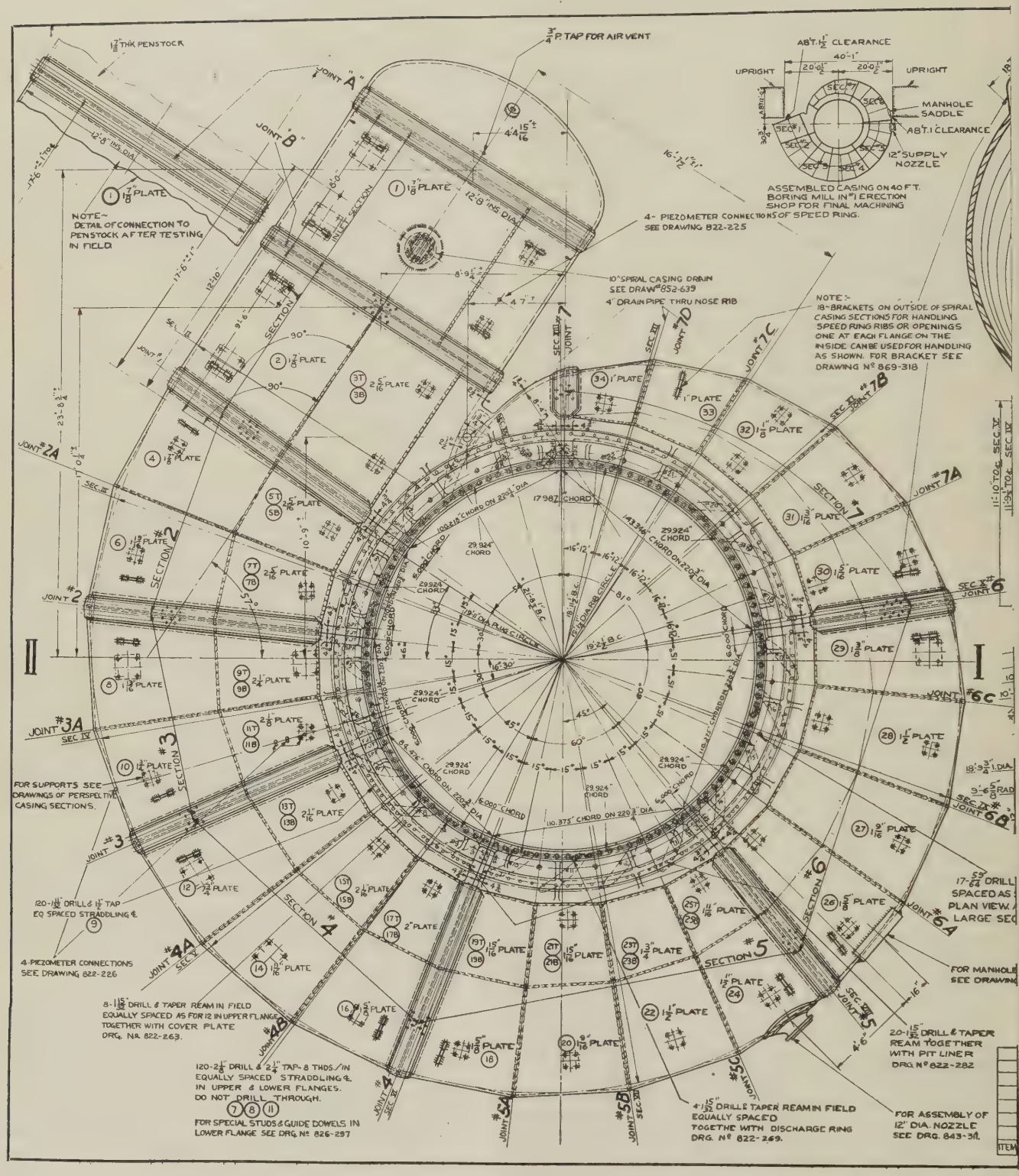

FIG. 3 CONSTRUCTION DETAILS AND ASSEMBLY OF WELDED-

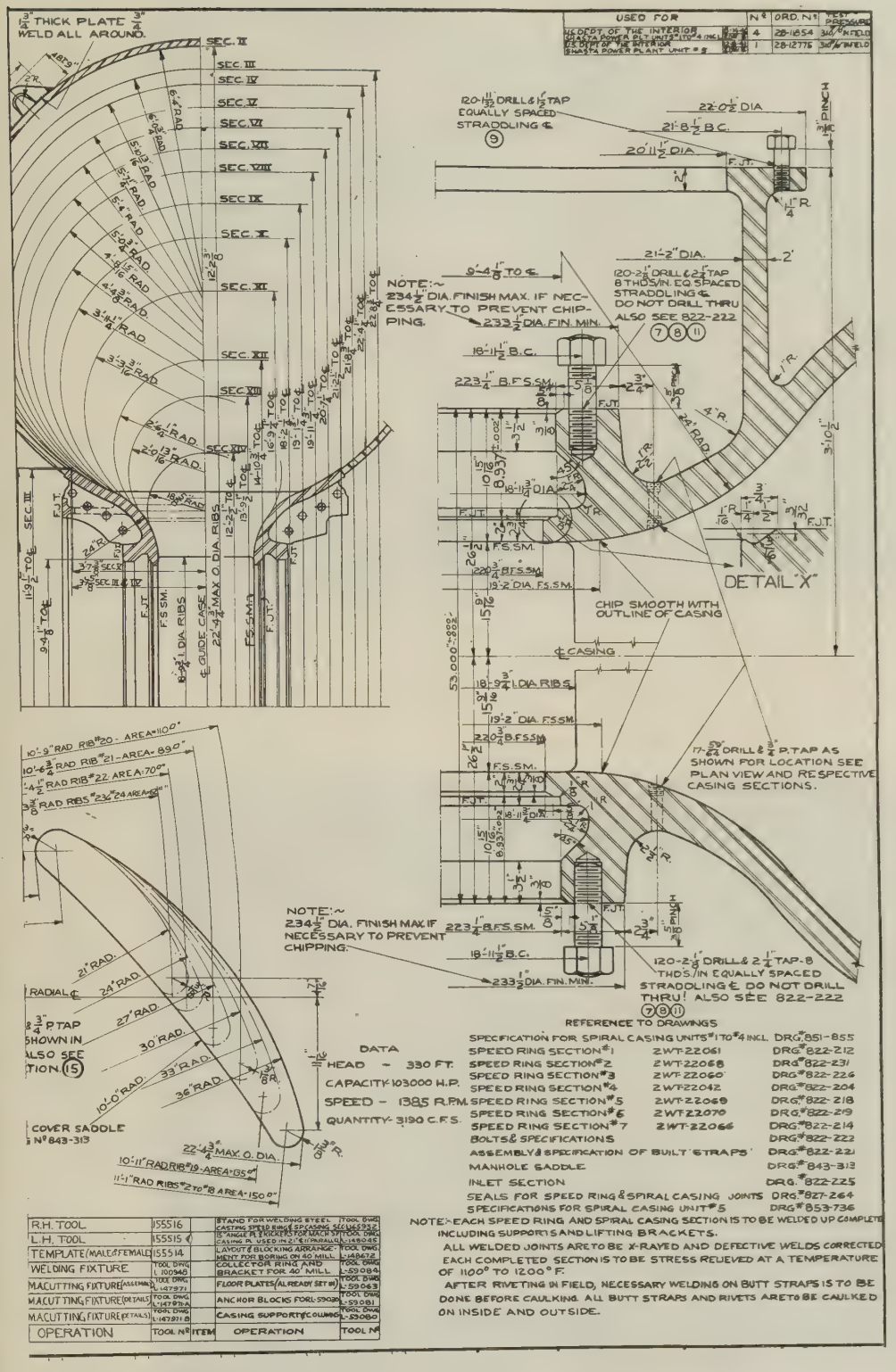

PLATE-STEEL SPIRAL CASING WITH 12-FT 8-IN-DIAM INLET

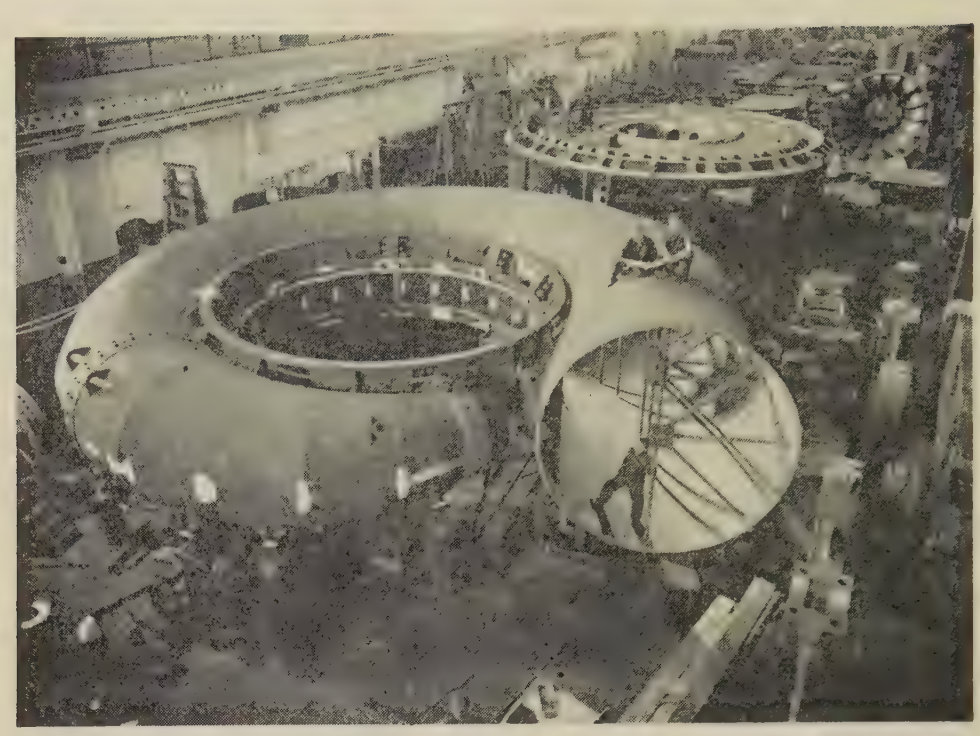

FIG. 4 SHOP VIEW SHOWING ASSEMBLY OF WELDED SPIRAL CASING WITH RIVETED FIELD JOINTS

FIG. 5 SHOP ASSEMBLY OF THREE WELDED SECTIONS OF SPIRAL CASING SHOWING CAST-STEEL SPEED RING

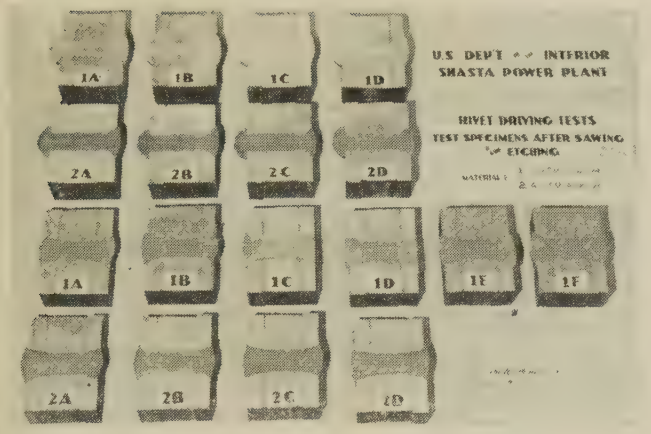

Fig. 6 Sample Rivets $1^{5}/_{16}$ In. Diam of Different Types and Grades Cut Through Center, Showing 1-In. Butt Straps and $2^{5}/_{16}$-In. Plate

holes and force the plates together. Test samples were then prepared and pulled to destruction in a testing machine.

Fig. 7 gives a comparison of all the specimens tested where load in thousands of pounds is plotted against deflection in inches. This shows that the round-headed rivets with the lower tensile strength, namely, ASTM A-141-39, showed the least deflection before the yield point is reached. This combination was able to carry a load of slightly over 30,000 lb on a test specimen 4 in. wide, consisting of two pieces of $2^{5}/_{16}$-in-thick plate with 1-in-thick butt straps on each side and held together with two $1^{1}/_{4}$-in. rivets driven by hand. All the other combinations, including the higher-tensile-strength rivets and the hour-glass rivets, show deflections for a total load of 30,000 lbs of from 3 to 6 times as much as the round-headed softer-steel rivets.

Following the deflection tests, each of the test specimens was pulled to destruction, Fig. 8 showing a comparison of these results with total load in thousands of pounds, plotted against deflections. In this case the higher-strength rivets were able to stand a greater load before destruction. Within the working loads required, however, it was proved conclusively that the mild-steel rivets of the round-head type held the plates more firmly together for watertightness and allowed less distortion. The round-headed rivets of the softer type were selected. It was found that a considerably longer rivet was required than ordinarily used to produce a satisfactory job. The final formula arrived at called for the rivets to have a length 1.1 times the grip length, plus $1^{1}/_{4}$ in., or for rivets having a grip of $4^{5}/_{16}$ in., a length of 6 in. under the head was found necessary.

The turbine casing was not pressure-tested in the shop before shipment, as this would have required complete shop-riveting of all the field joints. In the shop a complete assembly of the seven sections and reaming of all the field-riveted joints to approximately $^{1}/_{16}$ in. under final size was made. The butt-strap plates were bolted onto these field joints to insure that they could be bolted down with fitting bolts so as to make a satisfactory riveting job. After assembly and riveting in the field, the casings were pressure-tested to 310 lb static pressure or approximately 50 per cent above maximum net head of 475 ft. The design of the plate-steel casing was based upon a stress of not exceeding 12,000 psi for a water pressure of 260 lb, which allowed for about 25 per cent water-hammer pressure above normal working pressure.

Estimated and Actual Performance of Turbine

Fig. 9 shows the estimated and actual performance of the tur-

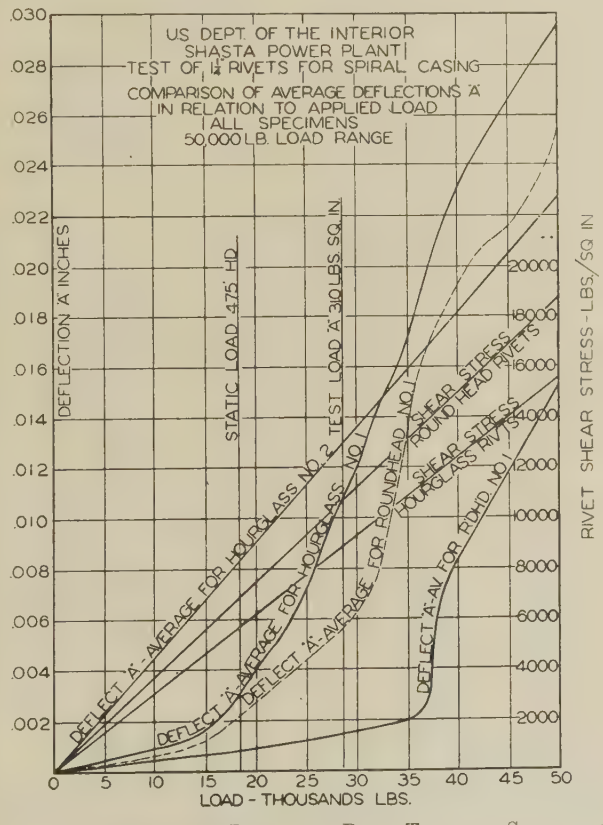

Fig. 7 Curves Showing Results of Rivet Tests and Superiority of Softer Round-Head Rivet for Loads Within Working Range of Casing

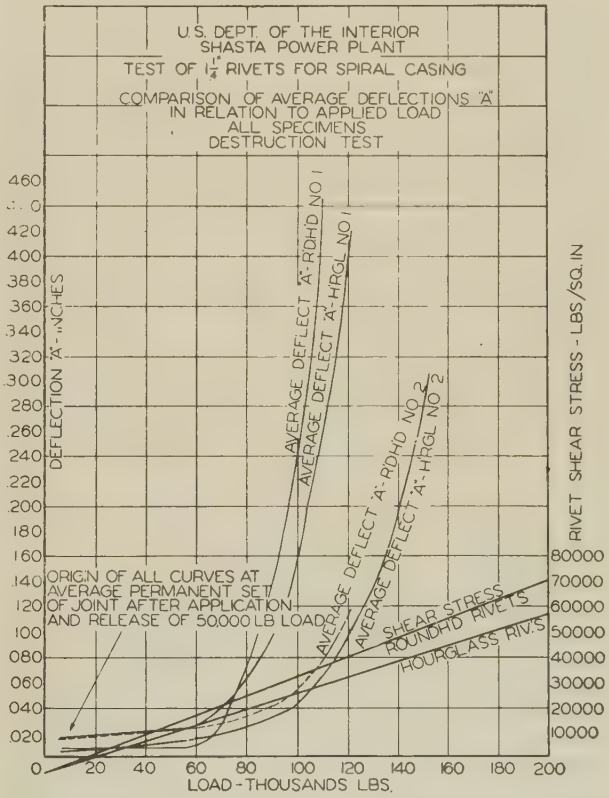

Fig. 8 Curves Showing Results of Riveted-Joint Tensile Tests When Joint Is Pulled to Destruction With Higher-Strength Rivets Carrying Greater Loads After Passing Yield Point

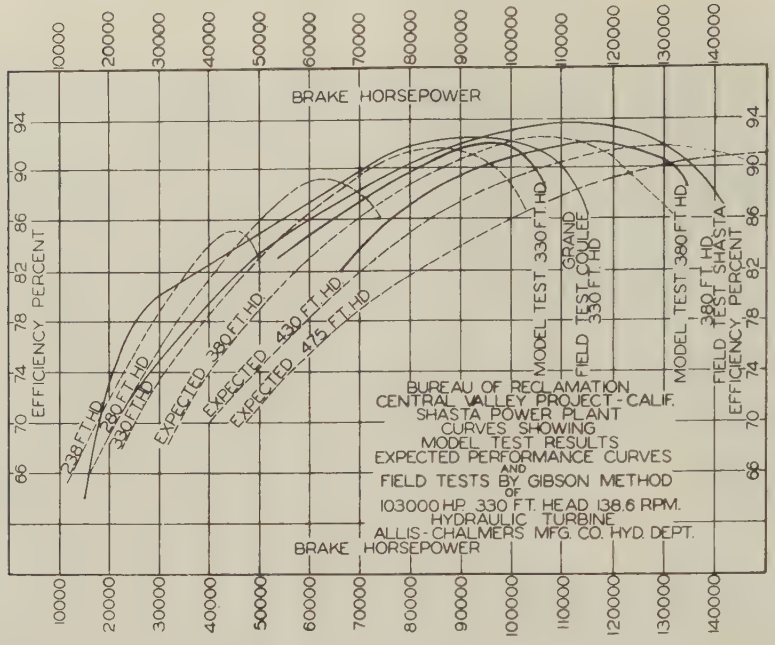

Fig. 9 Curves Showing Comparison Between Model-Test Results, Expected Powerhouse Performance, and Actual Field-Test Results of 103,000-Hp Turbine at Heads From 238 Ft to 475 Ft

bine under various heads from 238 ft minimum to 475 ft maximum. The model tests were run under a head of 125 ft with 20 ft of suction on the draft tube using a model of approximately 17$^3/_4$-in. inlet diam, the model including a complete spiral casing, speed ring, and draft tube homologous with that to be used in the powerhouse. The model tests showed a maximum efficiency of approximately 92 per cent. Field tests conducted on one of the two units installed in the Coulee powerhouse and using the draft tube originally designed for the 150,000-hp Coulee turbines are shown, as well as the field tests conducted on one of the two units installed at Shasta powerhouse in their proper setting. The results are very satisfactory. A maximum efficiency of 93.2 per cent was obtained and a considerable increase in output over the model tests. In the field tests the water measurements were made by the Gibson time-pressure system, and the electrical output was taken by specially calibrated electrical instruments.

Fig. 10 shows the expected power and efficiency of the Shasta turbines at various heads, plotted with gate opening as a horizontal scale, and brake horsepower and efficiency as a vertical scale. Since the 103,000-hp, corresponding to 75,000-kw generator capacity is developed at 330 ft net head, it is obviously impossible to hold the full output of the turbine estimated at 187,000 hp under the maximum head of 475 ft. Under this maximum-head condition, the rated output of the generator is obtained at approximately 43 per cent gate opening. Under these conditions it is necessary to change the rate of governor movement in order to prevent excessive water hammer when full load is thrown off under the high-head operating condition. Assuming that the governor is set to close from full load to zero load in 5 sec under 330-ft-head conditions, then the rate of closing from 43 per cent gate to no-load under the high-head conditions would be approximately 2 sec. While the discharge under the high-head condition is considerably less than under 330 ft head, nevertheless a serious water-hammer condition would result. Provisions were made on the governing mechanism so that the rate of closing and opening of the governor could be adjusted, and these adjustments changed to suit the head conditions under which the plant is operating.

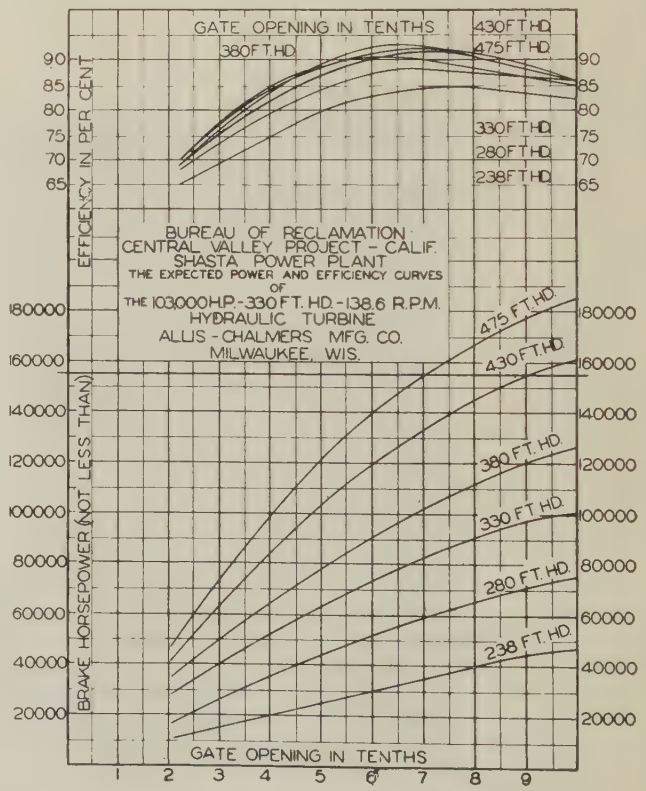

Fig. 10 Curves Showing Expected Performance of 103,000-Hp Turbine at Various Heads Plotted With Horsepower and Efficiency Against Turbine-Gate Opening

Discussion

H. J. Petersen[3] The similarity of the Shasta units and the Fontana units which the Tennessee Valley Authority purchased from the same company is very marked. The Fontana units are rated 91,500 hp at 330 ft head, while the Shasta units are rated 103,000 hp at 330 ft head. However, several points of major difference will bear discussion.

The Shasta-unit scroll cases were field-tested to 150 per cent of the maximum net head, while the Fontana scroll cases were field-tested to 200 per cent of maximum net head. The reason for this was that the Fontana units were completely field-welded while the Shasta scroll cases were shop-welded and field-riveted. As no heat-treatment for stress-relieving of field welds was available, these welds were made with great care and under rigid inspection. They were stress-relieved by peening. Extensometers were placed on the Fontana scroll cases at strategic points to measure movement during welding and testing.

Another feature incorporated in the Fontana design which was not used at Shasta was the protection of several vulnerable places with chromium plating. Under ordinary circumstances these various parts would have been protected by stainless-steel-clad metals; however, due to the war exigencies, stainless steel was not available so chromium plating was used.

Under the Authority's operating schedule, one or both of the Fontana units may be operating as a synchronous condenser part of the time. Under such a condition, with the unit operating at full speed and no load, the high head causes leakage to flow past the closed gates at very high velocity. To prevent scouring, the mating surfaces of the gates are covered with a 4-in-wide strip of chromium plating, 0.004 in. to 0.006 in. thick, from top to bottom. The whole top and bottom faces of the gates are covered in a similar manner. The results have been very good, for although there is considerable leakage with the gates closed, there has been no scouring.

In an effort to control this leakage, another feature was incorporated into the Fontana design. Chromium-plated facing plates were installed above and below the guide vanes. A rubber sealing strip was fitted in each plate in such a manner that in the closed position the guide vanes compressed the strip which extends above and below the facing plates a distance equal to the guide-vane clearance plus 0.003 to 0.005 in. As noted, considerable leakage is present with closed guide vanes, but it is believed to come mostly from the vertical mating faces.

The writer notes that air-admission fins are incorporated in the Shasta draft tubes. Similar provision was made at Fontana, but they have not yet been installed. At Fontana, at rated head and approximately half gate, a rumbling noise occurs in the draft tube. Did the Shasta units have a similar noise under those conditions, and did the fins eliminate this noise?

H. H. Sloane.[4] The many special design features of the 103,000-hp turbines of the Shasta power plant are well presented in this paper.

The welded-steel type of spiral casing with field-riveted joints connecting each of the sections appears to be one of the outstanding developments in this turbine design. The writer is particularly interested in the author's reference to more recent turbines where the field joints have been successfully welded in lieu of being riveted.

Circumferential penstock joints in many power-plant installations are satisfactorily welded in the field. Therefore it would seem logical to continue this type of construction for the remainder of the water passage around the casing, providing the field-erection-procedure problems which result are successfully and economically solved.

The important considerations appear to be the welding procedure to follow, and the location of field welds, with respect to the speed ring, to prevent distortion of the speed ring during erection. The cover-plate seats on the speed ring are usually machined in the shop within close tolerances. If this accurate alignment is not maintained after the turbine parts are finally connected, pressure-tested, and embedded in the concrete of the powerhouse substructure, it will be extremely difficult to make a satisfactory assembly of the complete generating unit.

It is also believed that field welds should be stress-relieved in a pressure vessel as important and complex in design as the spiral casing of a turbine. As the author states, there was no practical method of accomplishing this for the Shasta turbines and this was one of the principal reasons why the field-welded type of construction was not used.

Further data which show the developments made to obtain a dependable welded casing would be of great interest and value.

Author's Closure

The author wishes to thank both Mr. Petersen and Mr. Sloane for their very interesting and pertinent discussions, particularly their emphasis on the possibilities of welding the field joints instead of riveting them as was done on the Shasta turbine casings.

Mr. Petersen brings up the differences in the field assembly of the casings for the tubines at Fontana Dam, which were also built by the Allis-Chalmers Manufacturing Company. These turbines were nearly as large as the Shasta tubines, and had a rating of 91,500 hp at 330 ft head and were pressure-tested to 200 per cent of maximum net head. Careful planning was done prior to the field erection of the Fontana turbines and probably somewhat unnecessary precautions were followed throughout the entire field welding program in order to make doubly sure there would be no slip-ups in the first turbine to be field-welded in this country. Extensometer points were placed at several locations adjacent to all of the important welds. These extensometer points were placed both at right angles and parallel to the heavy welds and located about $^3/_4$ in. away from the weld itself. Following each pass of welding, which added about $^1/_8$ in. in the weld, heavy peening was done before the weld could cool. During the early stage of the welding, the extensometers were held on the plate as the peening progressed and observations made to find out just how much heavy peening was required in order to bring the extensometer back to the original reading. Very heavy peening was required and in some cases where the weld was allowed to cool, it was impossible to bring the metal back to the original reading. The last course of welding was not peened because of the possibility of producing cracks, which might later progress into the other metal.

In order to test the soundness of each weld, a sample of metal approximately 3 in. square was burned out of the plate in the area covering one day's work of each welder. From this 3-in-square metal with the thickness varying from one in. to nearly two in., two test bars were machined, one directly across the weld and one entirely in the weld metal running lengthwise. These test bars were machined to fit a special portable testing machine, which was located directly on the job. This used $^1/_4$-in-diam test bars about 2 in. long and was operated by turning a small handwheel. In this manner the strength and soundness of each day's weld for each welder was tested and it was surprising how much interest the welders themselves showed in these test results. It was felt that the psychology of the test on the welders had as much benefit as the actual results recorded in the engineers' field-data book. No x raying was done on these field

[3] Head Mechanical Engineer, Tennessee Valley Authority, Knoxville, Tenn. Mem. ASME.

[4] Engineer, Bureau of Reclamation, Denver, Colo.

welds, but careful inspection was made to make sure that any minor cracks were chipped out and no porous weld metal was left in.

Many persons have questioned the amount of danger involved if certain initial stresses are set up in the plate-steel structure. Actually, any plate-steel structure must have initial stress, because the ordinary method of rolling steel plate to form a circular chamber starts out on this basis; because the plates must be deformed beyond their elastic limit in order to hold their circular shape after passing through the bending rolls. Furthermore, the quality of the plate used was such that while some deflection and stress beyond the elastic limit caused partial deformation, it did not seem to embrittle the plate itself, but only served to slightly increase the elastic limit of that particular section of plate.

Some tests were run by using samples of this plate and on ten consecutive tests on the same sample plate, the strain was brought up to about 10 per cent above the elastic limit. On this particular test sample, the load was increased in 3000-lb intervals above the initial load of 30,000 lb until actual failure resulted, the load being backed off and a stress-strain diagram made of each consecutive application of the load. The only change found in these diagrams was a slight increase in the elastic limit with each consecutive application of the load until the elastic limit was brought up to the ultimate strength of the plate, around 65,000 psi.

Another interesting case of field welding was the eight 100,000-hp 208-ft-head turbines installed in the Shipshaw plant of the Canadian Aluminum Company, Ltd. In this case there was no shop welding done. The plates were welded to the speed ring and to each other in the field, and after six years of satisfactory operation there has not been the slightest sign of trouble. The same welding precaution was taken, in that, consecutive welds were heavily peened and test-bar samples were cut from each day's weld of each welder and tested right on the job. While it was originally planned to make a field pressure test on the Shipshaw casings, the urgency of getting the units into operation was so great that the field pressure tests were omitted and the units placed directly into service. Another manufacturer who was installing four similar turbines in the same powerhouse used field welding only for the radial joints on his casing, and where the plates joined the cast-steel speed ring he used double-butt-strap-riveted joints. Our feeling is that the smoother section inside of the all-welded spiral casings was partly responsible for the higher efficiency of the all-welded turbines as compared with those which had the riveted joints adjacent to the speed ring.

It is felt that with the experience which has now been gained, future turbines in the class of the Shasta and Fontana turbines can safely be built with field-welded casings.

Rubber Springs—Shear Loading—II

By J. F. DOWNIE SMITH,[1] AMES, IOWA

In a previous paper[2] the author developed theoretical stress-strain relationships for rubber of various shapes loaded in shear. In this paper the author presents additional theory and data.

Case 1 Trapezoidal Pads

THE cross section of an ordinary shear pad is approximately a parallelogram, where the height of the rubber is constant. This is desirable because of uniformity of shear stress. On the other hand, in certain places where space is restricted it is sometimes impossible to have this cross section, and occasionally a pad similar to that shown in Fig. 1 is installed. This trapezoidal shape does not give uniform stress. Should it be desirable to calculate the deflections one would expect with such a shear pad, the following theoretical development will be of interest:

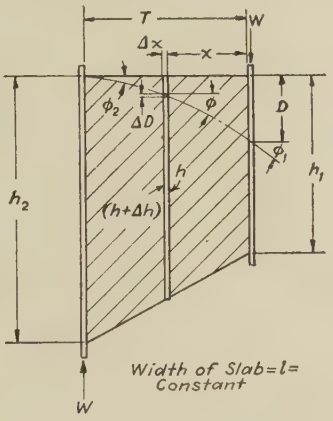

Fig. 1

Shear Slab With Linearly Varying Height. Refer to Fig. 1.

Stress at element of height $h = \dfrac{W}{lh}$

and

$$\frac{h_2 - h_1}{T} = \frac{h - h_1}{x}$$

$$h = h_1 + \frac{x(h_2 - h_1)}{T} = h_1 + bx$$

where

$$b = \frac{h_2 - h_1}{T}$$

and

$$A = A_1 + lbx = A_1 + cx$$

where

$$c = lb$$

Also

$$G = \frac{\text{stress}}{\text{strain}} = \text{modulus of elasticity in shear}$$

Experiment indicates that better results are obtained if strain is defined as the angle of movement rather than the tangent of the angle.

$$\frac{W}{l(h_1 + bx)G} = \phi = \text{strain}$$

and

$$\frac{\Delta D}{\Delta x} = \tan\phi = \tan\left[\frac{W}{lG(h_1 + bx)}\right]$$

Let

$$\frac{W}{lG(h_1 + bx)} = y$$

When

$$x = 0 \qquad y = \frac{W}{lGh_1}$$

$$x = T \qquad y = \frac{W}{lG(h_1 + bT)} = \frac{W}{lGh_2}$$

$$\frac{lG}{W}\,y = \frac{1}{h_1 + bx}$$

$$\frac{lG}{W}\,dy = -\frac{b\,dx}{(h_1 + bx)^2} = -b\left(\frac{lGy}{W}\right)^2 dx$$

$$-\frac{dy}{y^2} = \frac{lGb}{W}\,dx$$

$$\therefore \frac{dD}{dx} = \tan y \qquad \therefore dD = -\frac{W}{lGb}\,\frac{dy}{y^2}\tan y$$

$$\therefore D = -\frac{W}{lGb}\int_{\frac{W}{lGh_1}}^{\frac{W}{lGh_2}} \frac{\tan y}{y^2}\,dy$$

$$\therefore \frac{DlGb}{W} = \int_{\frac{W}{lGh_2}}^{\frac{W}{lGh_1}} \frac{\tan y\,dy}{y^2}$$

$$= \int_{\frac{W}{lGh_2}}^{\frac{W}{lGh_1}} \left[\frac{1}{y} + \frac{y}{3} + \frac{2y^3}{15} + \frac{17y^5}{315} + \frac{62y^7}{2835} + \cdots\right] dy$$

$$= \left[\log_e y + \frac{y^2}{6} + \frac{y^4}{30} + \frac{17y^6}{1890} + \frac{31y^8}{11{,}340} + \cdots\right]_{\frac{W}{lGh_2}}^{\frac{W}{lGh_1}}$$

$$= \log_e\left(\frac{h_2}{h_1}\right) + \frac{1}{6}\left(\frac{W}{lG}\right)^2\left[\frac{1}{h_1^2} - \frac{1}{h_2^2}\right] + \frac{1}{30}\left(\frac{W}{lG}\right)^4\left[\frac{1}{h_1^4} - \frac{1}{h_2^4}\right]$$

---

[1] Dean of Engineering, Iowa State College; Director of the Iowa Engineering Experiment Station, and Director of the Engineering Extension Service. Fellow ASME.

[2] "Rubber Springs—Shear Loading," by J. F. Downie Smith, *Journal of Applied Mechanics*, Trans. ASME, vol. 61, 1939, p. A-159.

Contributed by the Rubber and Plastics Division and presented at the Semi-Annual Meeting, Detroit, Mich., June 17–20, 1946, of The American Society of Mechanical Engineers.

$$+ \ldots\ldots \quad \therefore Db = \frac{W}{lG}\log_e\left(\frac{h_2}{h_1}\right) + \frac{1}{6}\left(\frac{W}{lG}\right)^3\left[\frac{1}{h_1^2} - \frac{1}{h_2^2}\right] + \frac{1}{30}\left(\frac{W}{lG}\right)^5\left[\frac{1}{h_1^4} - \frac{1}{h_2^4}\right] + \ldots\ldots$$

$$\therefore D = \frac{WT}{lG(h_2 - h_1)}\log_e\left(\frac{h_2}{h_1}\right) + \frac{T}{6(h_2 - h_1)}\left(\frac{W}{lG}\right)^3\left[\frac{1}{h_1^2} - \frac{1}{h_2^2}\right] + \frac{T}{30(h_2 - h_1)}\left(\frac{W}{lG}\right)^5 \times \left[\frac{1}{h_1^4} - \frac{1}{h_2^4}\right] + \ldots\ldots [1]$$

Now

$$lh_2 = A_2 \quad \text{and} \quad lh_1 = A_1$$

$$\therefore D = \frac{WT}{G(A_2 - A_1)}\log_e\left(\frac{A_2}{A_1}\right) + \frac{T}{6(A_2 - A_1)}\left(\frac{W}{G}\right)^3\left[\frac{1}{A_1^2} - \frac{1}{A_2^2}\right] + \frac{T}{30(A_2 - A_1)}\left(\frac{W}{G}\right)^5 \times \left[\frac{1}{A_1^4} - \frac{1}{A_2^4}\right] \ldots\ldots [2]$$

or

$$\frac{D(A_2 - A_1)G}{TW} = \log_e\left(\frac{A_2}{A_1}\right) + \frac{1}{6}\left(\frac{W}{G}\right)^2\left[\frac{1}{A_1^2} - \frac{1}{A_2^2}\right] + \frac{1}{30}\left(\frac{W}{G}\right)^4\left[\frac{1}{A_1^4} - \frac{1}{A_2^4}\right] + \ldots\ldots [3]$$

Case 2 Double-Shear Sandwich With Linearly Varying Height

A similar theoretical development would be expected for the case of the double-shear sandwich with linearly varying height, see Fig. 2.

In this case the stress at element of length

$$h = \frac{W}{2A} = Sx$$

$$A = A_1 + \frac{Xl}{T}(h_2 - h_1) = A_1 + \frac{x}{T}(A_2 - A_1)$$

Let

$$\frac{A_2 - A_1}{T} = b$$

$$\therefore A = A_1 + bx$$

$$\text{Strain} = \phi = \frac{\text{stress}}{G} = \frac{W}{2G(A_1 + bx)}$$

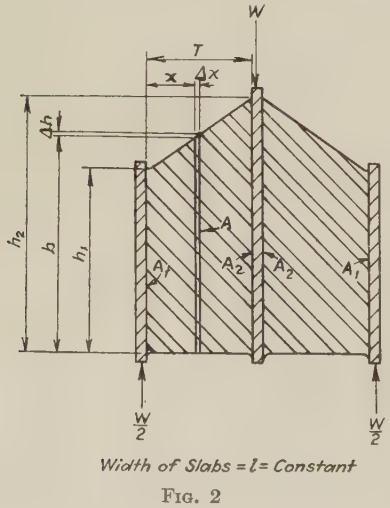

Fig. 2

If deflection in section $dx = dD$ and total deflection of $W = D$ then

$$\frac{dD}{dx} = \tan\phi = \tan\frac{W}{2G(A_1 + bx)}$$

when $x = 0, \quad \phi = \dfrac{W}{2GA_1}$

when $x = T, \quad \phi = \dfrac{W}{2GA_2}$

$$\frac{2\phi G}{W} = \frac{1}{A_1 + bx} \quad \therefore \frac{2G}{W}d\phi = -\frac{bdx}{(A_1 + bx)^2} = -\frac{4bG^2\phi^2 dx}{W^2}$$

$$\therefore dx = -\frac{Wd\phi}{2G\phi^2 b}$$

$$\therefore \tan\phi = \frac{dD}{dx} = -\frac{2G\phi^2 b\, dD}{Wd\phi}$$

$$\therefore dD = -\frac{W\tan\phi\, d\phi}{2Gb\phi^2}$$

or

$$\frac{2Gb}{W}dD = -\frac{\tan\phi}{\phi^2}d\phi$$

Integrating between limits, we get

$$\frac{2Gb}{W}D = \int_{\phi = \frac{W}{2A_2G}}^{\phi = \frac{W}{2A_1G}} \frac{\tan\phi}{\phi^2}d\phi$$

$$= \log_e\left(\frac{A_2}{A_1}\right) + \frac{1}{24}\left(\frac{W}{G}\right)^2\left[\frac{1}{A_1^2} - \frac{1}{A_2^2}\right] + \frac{1}{480}\left(\frac{W}{G}\right)^4\left[\frac{1}{A_1^4} - \frac{1}{A_2^4}\right] + \frac{17}{120{,}960}\left(\frac{W}{G}\right)^6\left[\frac{1}{A_1^6} - \frac{1}{A_2^6}\right] + \ldots$$

$$\therefore D = \frac{WT}{2G(A_2 - A_1)}\left\{\log_e\left(\frac{A_2}{A_1}\right) + \frac{1}{24}\left(\frac{W}{G}\right)^2\left[\frac{1}{A_1^2} - \frac{1}{A_2^2}\right] + \frac{1}{480}\left(\frac{W}{G}\right)^4\left[\frac{1}{A_1^4} - \frac{1}{A_2^4}\right] + \frac{17}{120{,}960}\left(\frac{W}{G}\right)^6\left[\frac{1}{A_1^6} - \frac{1}{A_2^6}\right] + \ldots\right\} \ldots\ldots [4]$$

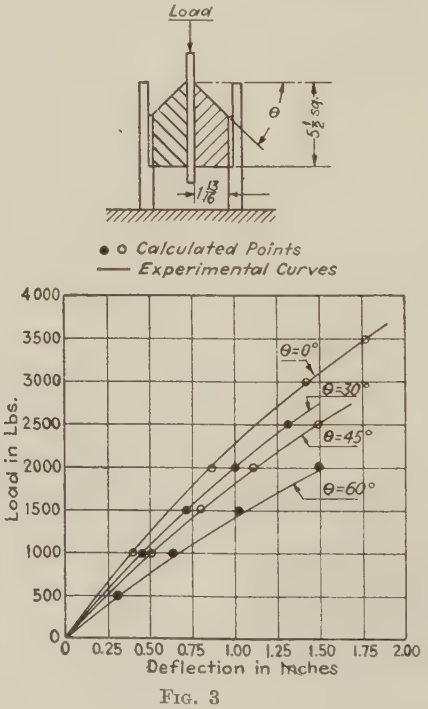

Fig. 3

Several samples with different shapes have been tested experimentally and the results are shown in Fig. 3. These show the agreement of theory and experiment. In this set of tests the modulus of elasticity in shear G was obtained from small deflections of a rectangular shear pad of the same material. This was found to be desirable, since the durometer and the relationship between durometer and shear modulus, previously given by the author,[2] while giving good results, in general, in this case would have introduced an error of 9.7 per cent.

Case 3 Cylindrical Disk Sandwiches

With Constant Radial Thickness. Refer to Fig. 4

$$A_1 = \pi(R_1^2 - r_1^2)$$

$$A_2 = \pi(R_2^2 - r_2^2)$$

$$A_x = \pi(R_x^2 - r_x^2)$$

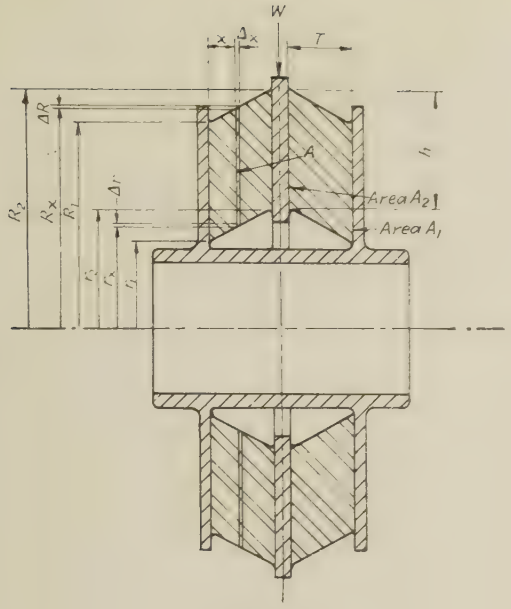

FIG. 4

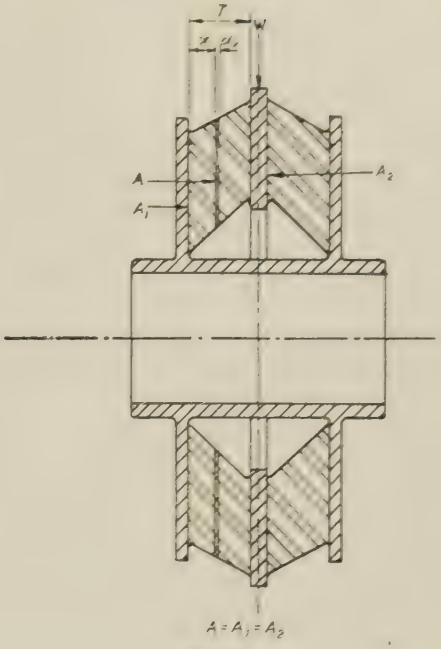

FIG. 5

$$R_x = R_1 + \frac{x}{T}(R_2 - R_1)$$

Let

$$\frac{R_2 - R_1}{T} = k = \frac{r_2 - r_1}{T}$$

$$r_x = r_1 + \frac{x}{T}(r_2 - r_1)$$

$$\therefore R_x = R_1 + kx$$

and

$$R_2 - r_2 = R_1 - r_1 = h$$

$$r_x = r_1 + kx$$

$$\begin{aligned} A_x &= \pi[(R_1 + kx)^2 - (r_1 + kx)^2] \\ &= \pi[R_1^2 + 2R_1kx + k^2x^2 - r_1^2 - 2r_1kx - k^2x^2] \\ &= \pi[(R_1^2 - r_1^2) + 2kx(R_1 - r_1)] \\ &= A_1 + x[2\pi k(R_1 - r_1)] = A_1 + 2\pi hkx = A_1 + bx \end{aligned}$$

where

$$b = 2\pi hk = \frac{2\pi}{T}(R_1 - r_1)(R_2 - R_1)$$

In this case the area varies linearly with distance from the smallest loading area, and is thus similar to the one previously discussed. Therefore in this case also .

$$D = \frac{WT}{2G(A_2 - A_1)}\left\{\log_e\left(\frac{A_2}{A_1}\right) + \frac{1}{24}\left(\frac{W}{G}\right)^2\left[\frac{1}{A_1^2} - \frac{1}{A_2^2}\right] + \frac{1}{480}\left(\frac{W}{G}\right)^4\left[\frac{1}{A_1^4} - \frac{1}{A_2^4}\right] + \frac{17}{120{,}960}\left(\frac{W}{G}\right)^6\left[\frac{1}{A_1^6} - \frac{1}{A_2^6}\right] + \right. \quad (5)$$

CASE 4 DOUBLE CYLINDRICAL DISK SANDWICHES

With Constant Area of Rubber. Refer to Fig. 5. This design is to be preferred over the one previously discussed because of the stress uniformity throughout the rubber.

In this case the strain

$$\phi = \frac{\text{stress}}{G} = \frac{W}{2AG}$$

If dD = deflection of section dx, and D = total deflection, then

$$\frac{dD}{dx} = \tan\phi = \tan\frac{W}{2AG}$$

$$\therefore D = \int_{x=0}^{x=T} \tan\frac{W}{2AG}\,dx = T\tan\frac{W}{2AG}$$

or

$$\frac{D}{T} = \tan\frac{W}{2AG} \quad (6)$$

In this instance $\frac{W}{2AG}$ is an angle in radians.

TORSION BUSHINGS

Torsional shear bushings are used extensively in practice, and equations have been developed[2] to show the connection between torque and angle of deflection for two cases; one with constant length of the rubber for large deflections, and the other for the coaxial tube of constant stress for both small and large deflections.

Because occasionally large deflections of the torsional tube of constant length are not necessary, an equation has been developed for small deflections. This simple development is as follows:

CASE 5 COAXIAL TUBE OF CONSTANT LENGTH IN TORSION

For Small Deflections. Refer to Fig. 6

$$\text{Torque} = T = 2\pi r^2 lS = 2\pi r^2 lG\phi$$

and approximately

$$\frac{r\,d\phi}{dr} = \phi$$

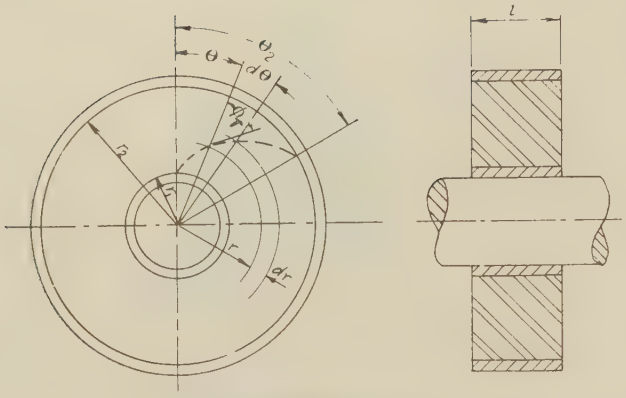

FIG. 6

$$\therefore \frac{T}{2\pi lG} = \frac{r^3 d\theta}{dr} \qquad \therefore d\theta = \frac{T}{2\pi lG}\frac{dr}{r^3}$$

$$\therefore \theta_2 = \frac{T}{2\pi lG}\int_{r_1}^{r_2}\frac{dr}{r^3} = \frac{T}{2\pi lG}\left[-\frac{r^{-2}}{2}\right]_{r_1}^{r_2}$$

$$= -\frac{T}{4\pi lG}\left[\frac{1}{r_2^2} - \frac{1}{r_1^2}\right] = \frac{T}{4\pi lG}\left[\frac{1}{r_1^2} - \frac{1}{r_2^2}\right] \quad \ldots\ldots\ldots [7]$$

The author's equation for "large deflections of a coaxial tube of constant length in torsion" is

$$\theta_2 = \frac{T}{4\pi lG}\left[\left(\frac{1}{r_1^2} - \frac{1}{r_2^2}\right) + \frac{1}{9}\left(\frac{T}{2\pi lG}\right)^2\left(\frac{1}{r_1^6} - \frac{1}{r_2^6}\right) + \ldots\ldots\right]$$

$$\ldots\ldots\ldots\ldots [8]$$

Thus the equation for "small" deflections is merely the first term of the equation for "large" deflections, as might have been expected.

CASE 6 COAXIAL TORSION BUSHING WITH LENGTH DECREASING LINEARLY WITH INCREASE IN RADIUS

A more difficult shear bushing to handle mathematically but one which is commonly met in practice is the case of the coaxial tube in torsion with the length of the rubber decreasing linearly with increasing radius. Such a bushing can be seen in Fig. 7. The development of the theory is as follows

$$T = 2\pi r^2 l s$$

$$r\frac{d\theta}{dr} = \tan\phi$$

$$\phi = \frac{S}{G}$$

$$\therefore \phi = \frac{T}{2\pi r^2 lG}$$

$$\therefore r\frac{d\theta}{dr} = \tan\frac{T}{2\pi r^2 lG}$$

and

$$d\theta = \frac{dr}{r}\tan\frac{T}{2\pi r^2 lG}$$

Now

$$\frac{l - l_2}{l_1 - l_2} = \frac{r_2 - r}{r_2 - r_1} \qquad \therefore l = l_2 + \left(\frac{l_1 - l_2}{r_2 - r_1}\right)(r_2 - r)$$

Let

$$l_2 + \left(\frac{l_1 - l_2}{r_2 - r_1}\right)r_2 = a = \frac{l_1 r_2 - l_2 r_1}{r_2 - r_1}$$

and

$$\left(\frac{l_1 - l_2}{r_2 - r_1}\right) = -b$$

$$\therefore l = a + br$$

$$\int_0^{\theta_2} d\theta = \int_{r_1}^{r_2}\frac{1}{r}\tan\frac{T}{2\pi G r^2(a + br)}\,dr$$

Let

$$\frac{T}{2\pi G} = k$$

$$\therefore \theta_2 = \int_{r_1}^{r_2}\frac{1}{r}\tan\frac{k}{ar^2 + br^3}\,dr$$

$$\tan x = x + \frac{x^3}{3} + \frac{2}{15}x^5 + \frac{17}{315}x^7 + \ldots. \text{ if } x^2 < \frac{\pi^2}{4}$$

which is generally true for this case.

$$\therefore \tan\left(\frac{k}{ar^2 + br^3}\right) = \left(\frac{k}{ar^2 + br^3}\right) + \frac{1}{3}\left(\frac{k}{ar^2 + br^3}\right)^3 + \frac{2}{15}\left(\frac{k}{ar^2 + br^3}\right)^5 + \ldots\ldots$$

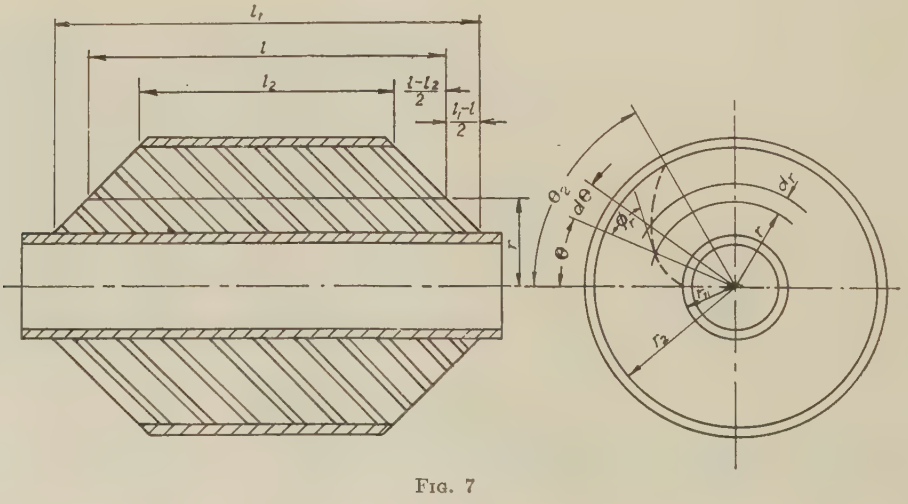

FIG. 7

$$\therefore \theta_2 = \int_{r_1}^{r_2}\left[\frac{k}{ar^3 + br^4}\right] + \frac{1}{3r}\left(\frac{k}{ar^2 + br^3}\right)^3 + \frac{2}{15r}\left(\frac{k}{ar^2 + br^3}\right)^5 + \ldots\ldots\right] dr$$

$$\therefore \theta_2 = k\int_{r_1}^{r_2}\frac{dr}{r^3(a + br)} + \frac{k^3}{3}\int^{r_2}\frac{dr}{r(ar^2 + br^3)^3} + \frac{2k^5}{15}\int_{r_1}^{r_2}\frac{dr}{r(ar^2 + br^3)^5} + \ldots\ldots\ldots [9]$$

Break the right side of Equation [9] into its several parts and integrate separately

$$A = k\int_{r_1}^{r_2}\frac{dr}{r^3(a + br)} = -\frac{1}{a^3}\left[\frac{(a + br)^2}{2r^2} - \frac{2b(a + br)}{r} + b^2\log_e\left(\frac{a + br}{r}\right)\right]_r^{r_2}$$

Refer to Dwight's tables of integrals[3] No. 103.1.

$$A = -\frac{k}{a^3}\left[\frac{(a + br_2)^2}{2r_2^2} - \frac{(a + br_1)^2}{2r_1^2} - \frac{2b(a + br_2)}{r_2} + \frac{2b(a + br_1)}{r_1} + b^2\log_e\frac{(a + br_2)}{r_2} - b^2\log_e\left(\frac{a + br_1}{r_1}\right)\right]$$

$$\therefore A = -\frac{k}{a^3}\left[\frac{l_2^2}{2r_2^2} - \frac{l_1^2}{2r_1^2} - \frac{2bl_2}{r_2} + \frac{2bl_1}{r_1} + b^2\log_e\left(\frac{l_2r_1}{r_2l_1}\right)\right]. \quad [10]$$

and

$$B = \frac{k^3}{3}\int_{r_1}^{r_2}\frac{dr}{r^7(a + br)^3}$$

Refer to Dwight's tables.[4]

$$\therefore B = \frac{k^3}{3}\left[\frac{-1}{a^9}\int_{r_1}^{r_2}\frac{\left(\frac{a + br}{r} - b\right)^8}{\left(\frac{a + br}{r}\right)^3}d\left(\frac{a + br}{r}\right)\right] \ldots [11]$$

Let

$$\frac{a + br}{r} = t$$

Where

$$r = r_1 \qquad t = \frac{l_1}{r_1}$$

Where

$$r = r_2 \qquad t = \frac{l_2}{r_2}$$

$$\therefore B = -\frac{k^3}{3a^9}\int_{r=r_1}^{r=r_2}\frac{(t - b)^8}{t^3}dt$$

$$= -\frac{k^3}{3a^9}\int_{t=\frac{l_1}{r_1}}^{t=\frac{l_2}{r_2}}\frac{b^8}{t^3}\left[1 - \frac{t}{b}\right]^8 dt = -\frac{k^3b^8}{3a^9}\int_{\frac{l_1}{r_1}}^{\frac{l_2}{r_2}}\frac{1}{t^3}\left[1 - 8\frac{t}{b} + 28\left(\frac{t}{b}\right)^2 - 56\left(\frac{t}{b}\right)^3 + 70\left(\frac{t}{b}\right)^4 - 56\left(\frac{t}{b}\right)^5 + 28\left(\frac{t}{b}\right)^6 - 8\left(\frac{t}{b}\right)^7 + \left(\frac{t}{b}\right)^8\right] dt$$

$$= -\frac{k^3b^8}{3a^9}\int_{\frac{l_1}{r_1}}^{\frac{l_2}{r_2}}\left[\frac{1}{t^3} - \frac{8}{bt^2} + \frac{28}{b^2t} - \frac{56}{b^3} + \frac{70t}{b^4} - \frac{56t^2}{b^5} + \frac{28t^3}{b^6} - \frac{8t^4}{b^7} + \frac{t^5}{b^8}\right] dt$$

$$= -\frac{k^3b^8}{3a^9}\left[\frac{t^{-2}}{-2} + \frac{8t^{-1}}{b} + \frac{28}{b^2}\log_e t - \frac{56}{b^3}t + \frac{70t^2}{2b^4} - \frac{56t^3}{3b^5} + \frac{28t^4}{4b^6} - \frac{8t^5}{5b^7} + \frac{t^6}{6b^8}\right]_{\frac{l_1}{r_1}}^{\frac{l_2}{r_2}}$$

$$= -\frac{k^3}{3a^9}\left[-\frac{b^8}{2t^2} + \frac{8b^7}{t} + 28b^6\log_e t - 56b^5t + 35b^4t^2 - \frac{56}{3}b^3t^3 + 7b^2t^4 - \frac{8}{5}bt^5 + \frac{t^6}{6}\right]_{\frac{l_1}{r_1}}^{\frac{l_2}{r_2}}$$

$$= -\frac{k^3}{3a^9}\left[-\frac{b^8}{2}\left\{\left(\frac{r_2}{l_2}\right)^2 - \left(\frac{r_1}{l_1}\right)^2\right\} + 8b^7\left\{\frac{r_2}{l_2} - \frac{r_1}{l_1}\right\} + 28b^6\log_e\left(\frac{l_2r_1}{r_2l_1}\right) - 56b^5\left(\frac{l_2}{r_2} - \frac{l_1}{r_1}\right) + 35b^4\times\left\{\left(\frac{l_2}{r_2}\right)^2 - \left(\frac{l_1}{r_1}\right)^2\right\} - \frac{56b^3}{3}\left\{\left(\frac{l_2}{r_2}\right)^3 - \left(\frac{l_1}{r_1}\right)^3\right\} + 7b^2\left\{\left(\frac{l_2}{r_2}\right)^4 - \left(\frac{l_1}{r_1}\right)^4\right\} - \frac{8b}{5}\left\{\left(\frac{l_2}{r_2}\right)^5 - \left(\frac{l_1}{r_1}\right)^5\right\} + \frac{1}{6}\left\{\left(\frac{l_2}{r_2}\right)^6 - \left(\frac{l_1}{r_1}\right)^6\right\} + \ldots\right] \ldots\ldots\ldots [12]$$

$$\therefore \theta_2 = \frac{k}{a^3}\left[\frac{l_1^2}{2r_1^2} - \frac{l_2^2}{2r_2^2} - \frac{2bl_1}{r_1} + \frac{2bl_2}{r_2} - b^2\log_e\left(\frac{l_2r_1}{l_1r_2}\right)\right] + \frac{k^3}{3a^9}\left[\frac{b^8}{2}\left\{\left(\frac{r_2}{l_2}\right)^2 - \left(\frac{r_1}{l_1}\right)^2\right\} + 8b^7\left(\frac{r_1}{l_1} - \frac{r_2}{l_2}\right) - 28b^6\log_e\left(\frac{l_2r_1}{l_1r_2}\right) + 56b^5\left(\frac{l_2}{r_2} - \frac{l_1}{r_1}\right) + 35b^4\left\{\left(\frac{l_1}{r_1}\right)^2 - \left(\frac{l_2}{r_2}\right)^2\right\} - \frac{56}{3}b^3\left\{\left(\frac{l_1}{r_1}\right)^3 - \left(\frac{l_2}{r_2}\right)^3\right\} + 7b^2\left\{\left(\frac{l_1}{r_1}\right)^4 - \left(\frac{l_2}{r_2}\right)^4\right\} - \frac{8b}{5}\left\{\left(\frac{l_1}{r_1}\right)^5 - \left(\frac{l_2}{r_2}\right)^5\right\} + \frac{1}{6}\left\{\left(\frac{l_1}{r_1}\right)^6 - \left(\frac{l_2}{r_2}\right)^6\right\}\right] \ldots\ldots\ldots [13]$$

If

$$\frac{l_1}{r_1} = u \text{ and } \frac{l_2}{r_2} = v$$

then

$$\theta_2 = \frac{k}{a^3}\left[\frac{1}{2}(u^2 - v^2) - 2b(u - v) + b^2\log_e\left(\frac{u}{v}\right)\right] + \frac{k^3}{3a^9}\left[\frac{b^8}{2}\left(\frac{1}{v^2} - \frac{1}{u^2}\right) - 8b^7\left(\frac{1}{v} - \frac{1}{u}\right) + 28b^6\log_e\left(\frac{u}{v}\right) - 56b^5(u - v) + 35b^4(u^2 - v^2) - \frac{56}{3}b^3(u^3 - v^3)\right.$$

[3] "Tables of Integrals and Other Mathematical Data," by Herbert B. Dwight, revised edition, The Macmillan Company, New York, N. Y., 1947, No. 103.1.

[4] Ibid., No. 100.

$$+ 7b^2(u^4 - v^4) - \frac{8b}{5}(u^5 - v^5) + \frac{1}{6}(u^6 - v^6)\Bigg] \ldots [14]$$

For a given set of dimensions this equation reduces to

$$\theta_2 = \frac{C_1 T}{G} + C_2\left(\frac{T}{G}\right)^3 + \ldots\ldots\ldots [15]$$

Discussion

Louis Marick.[5] The calculus integrations performed by the author for the several rubber shapes loaded in shear are of course of interest to anyone concerned with the structural design of rubber parts. Some of the shapes considered are quite common and load-deflection expressions for them have no doubt been used by many in the rubber industries. The author has given some other expressions which are special cases that have not been used frequently and will be found useful when these cases arise.

Developing the original load-deflection equations for these shapes by defining the shear strain as the angle of movement rather than the tangent of the angle is good practice as this agreement over the range of the more common deflections is close. Just how many terms in the derived expressions will be used in computing deflections or loads will depend upon the magnitude of the deflection, and the production tolerances permitted in the shear modulus of the rubber compound. It is likely that experience will show that by far the greater number of calculations will be made using the first term only in the expressions derived. It would be interesting to know the contribution to the calculated deflection by the first three terms in the experimental check which he made on one of the equations. The writer has not had the opportunity to do this from his data but perhaps he has the values at hand.

We assume that the parts shown in Figs. 4 and 5 are represented diagrammatically, as the practical construction of such a single part would present some molding difficulties.

[5] United States Rubber Company, Detroit, Mich.

Author's Closure

Dr. Marick would like to know the contribution to the calculated deflection by each of the terms in the expression for load deflection in the case of trapezoidal pads. This contribution of course varies both with load and with the angle of cutoff in the trapezoid. Typical figures have been chosen. In each case, only three terms were calculated.

For $\theta = 30$ deg and $W = 2500$ lb:
First term contributes 86.6 per cent
Second term contributes 11.5 per cent
Third term contributes 1.9 per cent

It should be noted that this load is considerably higher than is ordinarily met in practice and the contribution of terms after the first is also high.

For $\theta = 30$ deg and $W = 1000$ lb:
First term contributes 97.8 per cent
Second term contributes 2.1 per cent
Third term contributes 0.05 per cent

For normal loads, the third term is negligible, and the second term small.

For $\theta = 60$ deg and $W = 2000$ lb:
First term contributes 81.6 per cent
Second term contributes 14.6 per cent
Third term contributes 3.8 per cent

In this case both load and angle of cut are excessive and these values are given to show what might be expected in an extreme case.

For $\theta = 60$ deg and $W = 500$ lb:
First term contributes 98.9 per cent
Second term contributes 1.1 per cent
Third term contributes 0.0 per cent

Summarizing, it might be stated that the first two terms, in general, would give all the accuracy necessary and, if loads are light and angle θ is reasonable, the first term would give fair accuracy.

Dr. Marick is correct in assuming that Figs. 4 and 5 are diagrammatic. In each case the rubber parts were vulcanized to steel plates which in turn were fastened to the wheel and supporting frame.

Effect of Some Processing Variables on the Stress Required to Draw Tubular Parts[1]

By GEORGE ESPEY[2] AND GEORGE SACHS,[3] CLEVELAND, OHIO

Tubular brass parts were drawn to determine the effects of a number of variables upon the draw forces and stresses. The variations were in the tube dimensions, the contour and finish of the die and punch, the temper and surface condition of the tubular parts, and the lubricant. The draw stress for a given reduction increased with decreasing die angle, this being the most important die variable. Radiused dies behaved in a manner similar to conical dies of the same contact area. Other die variables investigated had little effect upon the draw stress, these being various lengths of the cylindrical portion of the die at the exit (bearing or land), the die material, and the die finish. Tests with tapered punches yielded results similar to those obtained with cylindrical punches. Experimentation with punches of various degree of finish revealed that rough punches gave higher draw forces than polished punches, particularly when used in conjunction with small-angle dies. A number of lubricants were investigated, none of which excelled the performance of a 2 per cent aqueous solution of soap. The draw stresses were found to decrease with increasing time of immersion in soap solution.

Introduction

THE force and power consumption required to deform a metal by a given type of forming theoretically depends upon a number of factors. In any forming process, the force increases roughly proportional to the average flow stress of the metal and the reduction in cross-sectional area (or any other decisive strain occurring in the process). The shape of the product exerts an effect which is determined by the state of stress[4] and which differs by only 15 per cent between the two extreme stress states, which are plane strain where strain occurs in only two directions (such as in drawing thin-walled tube), and where two principal stresses are equal (such as in the drawing of rod) (1).[5]

The experimental data now available confirm the conception that these factors almost completely determine the force and power consumption, if friction is absent or very low (3).

However, in the presence of friction, various other factors also become significant. It appears generally satisfactory to assume that the friction is of the ideal solid type, i.e., proportional to the pressure at the interface between metal and tool. The respective friction coefficient is directly dependent upon the two materials in contact, upon the nature of the lubricant, and probably also upon the condition of the metal surfaces. Little quantitative information is available at present regarding variations in frictional conditions and their effects upon the forces for any forming process.

The shape of the tools affects the forming force, according to the simplified analysis, only in so far as it determines the surface area subjected to frictional forces. In general, the larger this area, the larger is the contribution of the frictional forces to the forming force and power consumption, other conditions being identical.

Results on a number of variables were obtained from an experimental investigation of the process of cartridge-case drawing which extended over a number of years. As a part of this investigation, numerous tubular parts in both 70/30 brass (4) and spheroidized 1035 steel (5) were subjected to redrawing operations, in order to determine the effects of variables which might affect the performance during production. A number of these variables were studied to a sufficient extent to yield fundamentally significant relations between the forces required to reduce the tubular section and such variables as the dimensions, the temper, and the surface condition of the tubular part, the contours and the finishes of die and punch, and different lubricants. These data have been reanalyzed, and the conclusions derived regarding the draw stress are presented herewith.

In this investigation, either short pieces cut from tube, or tubular specimens (drawpieces) formed by blanking and deep drawing (cupping and redrawing) were pushed by means of a punch through various circular dies of approximately 0.500 in. diam. The punch was either cylindrical or tapered. In the case of a cylindrical punch, only one value of reduction and corresponding draw stress was obtained in each test. Therefore a set of cylindrical punches of various diameters was necessary to obtain different reductions.

The number of tests was considerably reduced by using tapered punches. The diameter and taper of these punches were such as to cover a range from 20 to 90 per cent wall reduction. This "tapered-punch test" yielded a force-stroke curve; from this curve and accurate measurements of the resulting drawpiece with tapered walls, the draw-stress versus reduction curve was calculated.

The tapered-punch test was also found of great value for determining the effects of various factors on the maximum reduction obtainable in drawing (drawability). To obtain the "drawability" by means of cylindrical punches, an excessive number of tools and tests are necessary, because of the large scattering (6). The tapered-punch tests can be continued until fracturing occurs, yielding the drawability directly. This value is accurately obtained by averaging the results from a sufficient number of tests, (4, 5). While the significance of this value

---

[1] This paper contains some results of experimentation conducted at Case Institute of Technology (formerly Case School of Applied Science), Cleveland, Ohio, as part of an investigation sponsored by Frankford Arsenal, Philadelphia, Pa. This work has been re-evaluated under the auspices of the ASME Research Committee on Plastic Flow of Metals, and assisted by a grant in aid from the Engineering Foundation.

[2] Formerly Department of Metallurgical Engineering, Case Institute of Technology; at present, Metallurgical Engineer, Lee Wilson Engineering Company.

[3] Research Laboratory for Mechanical Metallurgy, Case Institute of Technology. Mem. ASME.

[4] A complete analysis necessitates considering the variations of the stress state over the metal volume deformed in all directions; see Orowan (2).

[5] Numbers in parentheses refer to the Bibliography at the end of the paper.

Contributed by the Metals Engineering Division and presented at the Annual Meeting, Atlantic City, N. J., December 1–5, 1947, of THE AMERICAN SOCIETY OF MECHANICAL ENGINEERS.

NOTE: Statements and opinions advanced in papers are to be understood as individual expressions of their authors, and not those of the Society. Paper No. 47—A-10.

is not quite clear, it was observed on drawing cartridge cases that surfaces and lubricants which increased the drawability in tapered-punch tests, also definitely reduced the percentage of breakage during the experimental production (4, 5).

Force-Stroke Relations

The tests yielded directly force-versus-reduction curves of the general shape illustrated in Fig. 1. If such a curve extended to

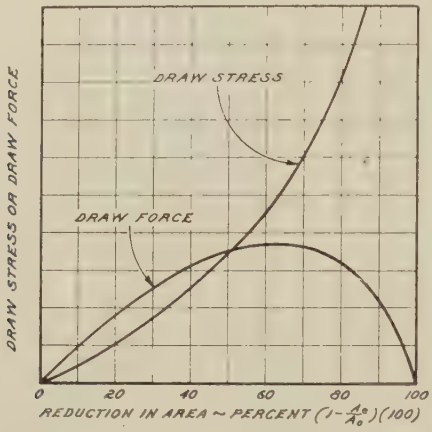

Fig. 1 General Shape of Force-Versus-Reduction and Stress-Versus-Reduction Curves for Metal With Constant Flow Stress

reductions larger than 60 per cent, it frequently showed a tendency to flatten out or to go through a maximum. This is apparently a purely mechanical phenomenon, as the draw stresses derived from such a curve increased with the reduction at the expected rate.

The peculiar shape of the force-versus-reduction curve can be readily explained. Assuming that no friction is present and that the metal is an ideal plastic metal, i.e., possesses a constant flow stress k, the "draw stress" on the final area s_1, is given by the equation

$$s_1 = k \ln A_0/A_e$$

where A_0 is the original (or entrance) area of the tube, and A_e is the final (or exit) area of the tube. Consequently the draw force F, is

$$F = s_1 A_e = kA_0(1 - R) \ln A_0/A_e$$

where $R = 1 - A_e/A_0$. The general shape of these two curves is illustrated in Fig. 1.

Force-versus-reduction curves exhibiting a maximum are not observed in other drawing processes, because it is not possible to obtain sufficiently high reductions.

Material, Equipment, and Procedure

The tubular 70/30 brass test specimens were of two types, either cut from commercial seamless tube, or formed by blanking, cupping, and drawing from sheet. The first-type specimens were obtained by cutting lengths of 1 to $2^1/_2$ in. from hard-drawn brass tube having $^9/_{16}$ in. OD and various wall thicknesses (0.015, 0.027, and 0.047 in.). The specimens were then annealed and one end closed in by spinning on a lathe, Fig. 2. Tubular drawpieces were made from annealed brass strip by blanking, cupping, and several redraws (with intermediate anneals) to the desired size and temper. The drawpieces were mostly of two standard sizes, the one having 0.613 in. OD with a wall 0.049 in. thick and the other having 0.558 in. OD with a 0.020-in-thick wall.

Annealing was performed in an electrically heated air-convection furnace for 15 min at 1100 F, followed by a water quench. The resulting Rockwell 15T hardness was between 60 and 65.

All specimens were pickled 5 min in a 3 to 5 per cent H_2SO_4 aqueous solution at room temperature, followed by a cold- and hot-water rinse, and then permitted to dry in the atmosphere. The specimens were allowed to stand in contact with the atmosphere for at least 16 hr (overnight) before drawing.

The dies were of hardened and polished 1 per cent carbon steel, chromium-plated steel, graphitized steel, and cemented carbides. The die openings were 0.500 ±0.002 in. diam. These dies were, regarding the contour of their working surfaces, either conical or radiused, Fig. 3. Some of the conical dies had a fillet radius between the conical die surface and the cylindrical bearing surface.

The cylindrical punches, Fig. 3 were of hardened 1 per cent carbon steel, polished with 4/0 emery polishing paper, with different diameters between 0.400 and 0.480 in. Two different tapered punches were used, the one changing from a diameter of 0.465 to 0.495 in. in 3 in. (0.5 per cent taper), the other from 0.400 to 0.495 in. in 3 in. (1.5 per cent taper), Fig. 3. One additional tapered punch was chromium-plated and polished to study the effect of punch material.

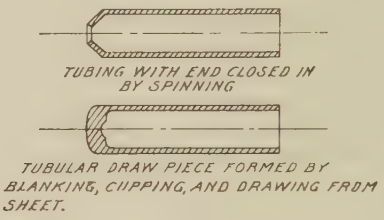

Fig. 2 Tubular Specimens

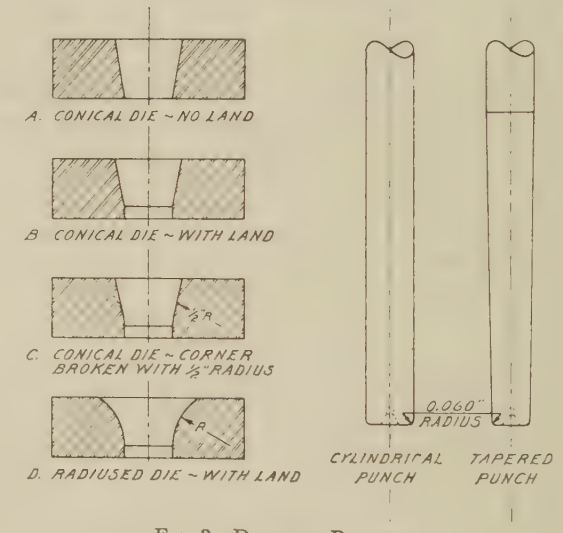

Fig. 3 Dies and Punches

A 2 per cent (by weight) aqueous soap solution was used for most tests as lubricant. For the major part of the investigation the method of lubrication was to dip the test specimens in the soap solution momentarily, or to immerse them for times varying between 1 and about 20 min. As experimentation progressed, it was found that time of immersion in the 2 per cent soap solution had a considerable effect on the draw forces (referred to later); therefore the specimens were immersed in the lubricant for at least 15 min before drawing. Several commercial lubricants were also investigated.

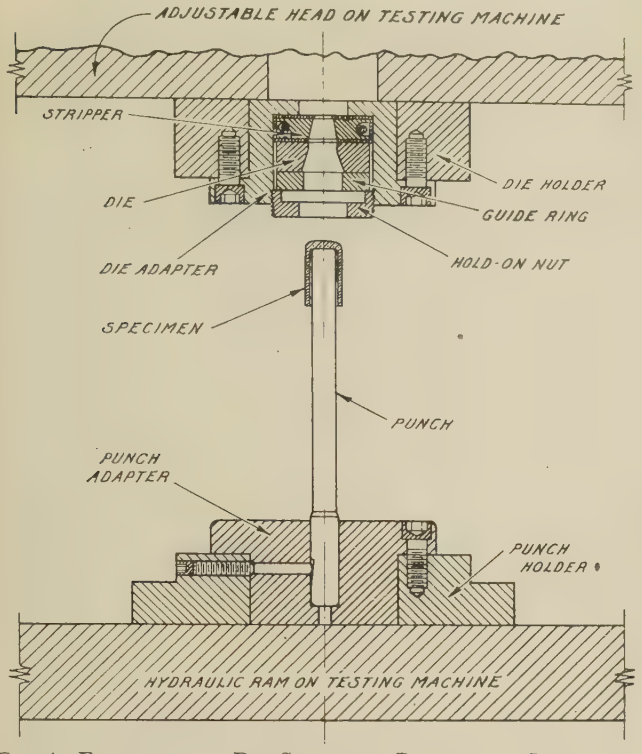

FIG. 4 EXPERIMENTAL DIE SETUP FOR DRAWING OR IRONING OF TUBULAR SPECIMENS

The tests were made on a 10,000/60,000-lb hydraulic testing machine with a maximum speed of $2^1/_2$ ipm. The tool assembly of die, punch, and specimen is shown in Fig. 4.

RESULTS OF TESTS

To determine the effect of a particular variable on the draw stress, it is common practice to determine the draw stress for a number of different decisive reductions. In the case of tube-drawing with a mandrel, the decisive reduction is that in cross-sectional area from the original to the final tube. The curves representing the draw stress versus this reduction in area closely follow the trend expected theoretically, as has been shown in a previous publication (3). This is somewhat surprising, as the actual conditions deviate considerably from the simplified condition subjected to theoretical analysis. In the theoretical analysis, the wall thickness is considered as infinitely thin in comparison to the diameter, rendering the problem one of plane strain. Also, the analysis disregards the fact that the drawing process actually consists of two components. The tube is first sunk to an inside diameter which is equal to the outside diameter of the mandrel, and then the process of true drawing with a mandrel begins.

This initial "reduction in diameter" depends upon two factors, i.e., the diameter of the tube specimen, and the mandrel diameter. The effect of the diameter reduction on the draw stress has been found to be negligible, according to Fig. 5. This is explained by the fact that the diameter reduction becomes smaller in comparison to the total reduction, as the total reduction increases. The two types of drawing, sinking and drawing with a mandrel, differ only in the contributions of friction. Therefore if the friction effect is as small as it has been found to be in the drawing of brass tube (3), the draw stress should be only slightly affected by the difference in the inside diameter of the tube and the outside diameter of the mandrel, if the over-all reduction in area is considered to be the decisive strain. The

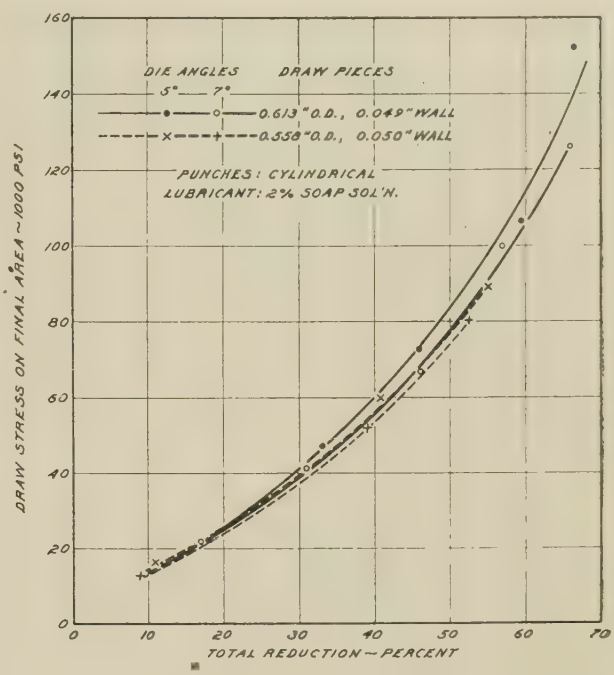

FIG. 5 EFFECT OF DIAMETER REDUCTION ON DRAW STRESS AT VARIOUS TOTAL REDUCTIONS

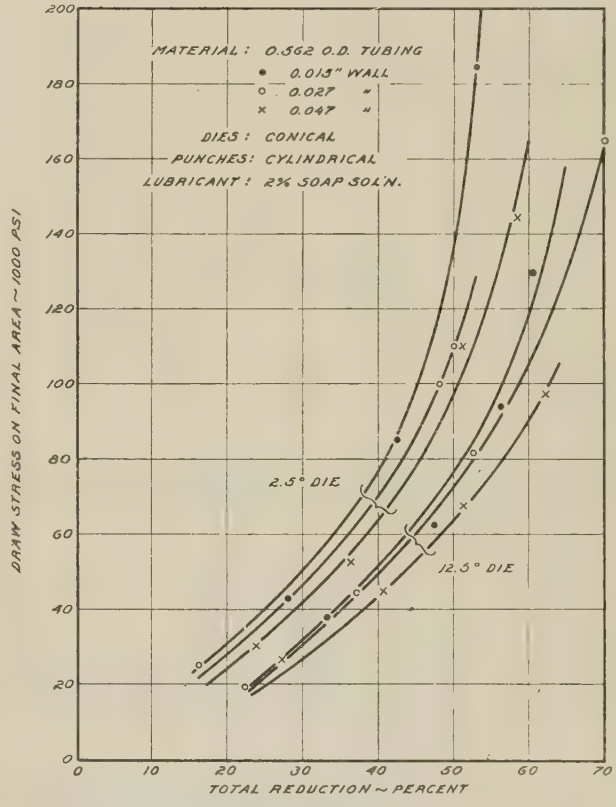

FIG. 6 EFFECT OF WALL THICKNESS AND DIE ANGLE ON DRAW STRESS

different positions of the trend curves in Fig. 5 can be attributed to slight variations in the hardness and grain size of the specimens, rather than to the direct effect of the specimen diameter.

The "wall thickness" of the tube, however, appears according

to Fig. 6 to affect the draw stress to an extent which exceeds that of the variations in the condition of the metal. If the wall becomes thicker in comparison to the diameter, the stress state increasingly deviates from the condition of plane strain and approaches that of balanced triaxiality present in a solid bar or wire (i.e., two principal stresses being equal). This change in stress state should cause the flow stress and, consequently, also the draw stress to decrease gradually to a maximum decrease of 10 to 15 per cent (3). The curves in Fig. 6 show this trend, the decrease in draw stress with increasing wall thickness being, however, larger than expected. However, this can again be explained partially by variations in hardness. On the other hand, the experimental data indicate that the wall-thickness effect becomes rather large at very high reductions. This fact cannot be explained by any simple conception; it would indicate that the frictional contribution increases considerably when the wall thickness becomes very small in comparison to the diameter.

The "surface condition" of the metal was found to affect the process of tube-drawing considerably. Previous qualitative observations (8), and some measurements clearly showed that freshly pickled specimens required greater draw forces and were more liable to rupture[6] than specimens which were drawn some time after pickling. For this reason the general procedure was adopted to expose the specimens to air for at least 16 hr (i.e., overnight) after pickling before drawing.

Surface conditions other than those obtained by exposure to air may considerably affect the draw stress, Table 1. A sulphide coating, created by the reaction of hydrogen sulphide, was found to reduce the draw force slightly. On the contrary, some cups slightly oxidized by heating in air at a temperature of 400 F gave slightly increased drawing forces. Unpickled cups (not listed in Table 1) covered with a heavy oxide layer, formed by annealing 15 min at 1100 F, required very high drawing forces, associated with immediate fouling of the die, and breakage of the cups.

TABLE 1 EFFECT OF SURFACE CONDITION OF DRAWPIECES ON WALL-DRAWING FORCE IN TWO DRAWS OF A TANDEM DRAW OF UNANNEALED CUPS[a]

(Std. 2% soap solution: 5–15 minutes' immersion)

Surface condition of drawpieces	Number of tests	—Average, draw force, lb— 0.705-in. die	0.610-in. die
Standard (16 hr in room atmos)	61	4150	9160
Freshly pickled	18	4490	9250
Oxidized	10	4280	9120
Sulphurized	10	4170	9120

[a] Hard cups 0.763 in. OD × 0.102 in. wall thickness drawn in preparation of standard drawpieces to a drawpiece 0.613 in. OD × 0.049 in. wall thickness through two dies in tandem, the dies being 0.705 in. and 0.610 in. diam. (Individual reductions equal 31 and 40 per cent; total reduction equals 58.5 per cent.)

Because of "metallurgical and processing" variations, the hardness and grain size of 70/30 brass may vary considerably.[7] In general, the hardness decreases and the grain size increases with increasing annealing temperature and with decreasing reduction prior to the final anneal. In this investigation the draw stress was found generally to conform approximately to the hardness of the specimen.

[6] In a very heavy single draw of 61 per cent on annealed drawpieces, the breakage of a lot of 17 freshly pickled cups was 85 per cent, while the normal breakage of lots varied between 5 and 20 per cent.

[7] The tube was softer than any of the drawpieces, and yielded correspondingly lower draw stresses, other conditions being identical. In the course of this investigation, the hardness of 70/30 brass after annealing at a given temperature was found to increase with increasing reduction prior to annealing, the grain size being practically constant (4). This does not agree with the frequently expressed opinion that the hardness of annealed 70/30 brass is determined by the grain size (9).

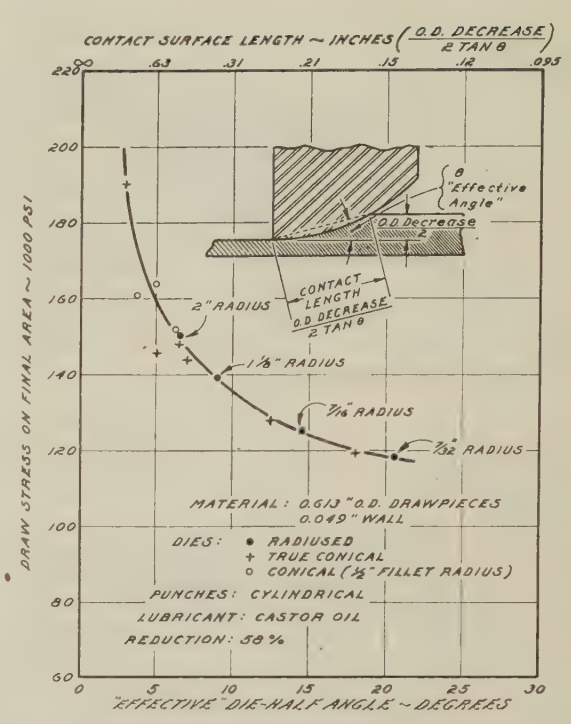

FIG. 7 COMPARISON OF DRAW STRESSES REQUIRED FOR RADIUSED DIES AND CONICAL DIES, SHOWING THE SAME RESULTS WHEN DRAW STRESS IS PLOTTED AGAINST "EFFECTIVE" DIE ANGLE

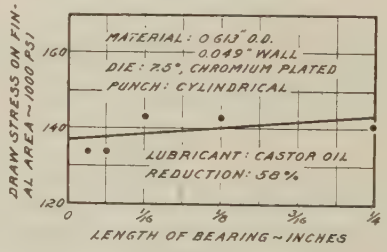

FIG. 8 EFFECT OF LENGTH OF DIE BEARING OR LAND ON DRAW STRESS

The effects of "die contour" are known from various publications. The stress required to draw tube, by any method, increases with decreasing die taper (1, 3, 8), Fig. 7. This relation can be generalized, stating that the draw force should increase with increasing length of the contact surface between metal and die, other conditions being identical. As an approximate inverse measure of this contact length, the angle between the axis and the chord drawn between the points of contact at the entrance and exit, respectively, can be taken. This angle may be termed " effective angle," Fig. 7. For a true tapered die, this effective angle is identical with the half-die angle. For a bell-shaped die, the effective angle increases with the reduction. If this effective die angle is used as variable, the draw force is found to be a function of this angle (for a given reduction) and practically independent of the die contour,[8] Fig. 7.

However, the presence of a cylindrical section at the exit, called land or die bearing, increases the draw stress in proportion to its length, Fig. 8. This land is rather short in conventional dies, and its contribution is therefore considered immaterial.

[8] Minor variations in the die shape, such as the radiused blending of the taper at the exit, Fig. 3, also do not noticeably affect the draw force; therefore, although conical dies of both types I and II are used for the experiments reported, no distinction has been made throughout the rest of the paper.

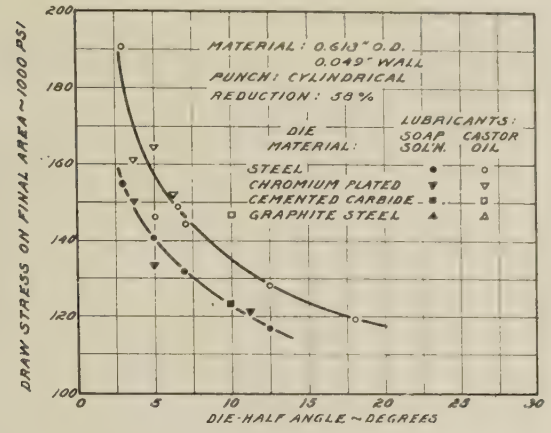

FIG. 9 EFFECT OF DIE MATERIAL AND LUBRICANT ON DRAW STRESS

The "die material" also did not noticeably influence the draw force, Fig. 9. The experimental data obtained with cemented-carbide dies, chromium-plated steel dies, and graphitized steel dies were within the limits of experimental error, identical to those obtained with the common hardened (high-carbon) tool-steel dies of equal contour.[9] This result does not agree with those obtained in previous investigations. The friction coefficients for cemented-carbide dies were usually found to be lower than those for steel dies (8). However, the friction coefficients for steel dies under conditions similar to those used in the present investigation were found to be exceptionally low (3). It appears therefore that the die (surface) material influences the draw forces to a significant extent only if the lubricant used does not reduce the coefficient of friction to a small value, and possibly also if the die is worn.

The "die-surface" condition influences the draw force to a slight extent. It has been observed that when using soap as a lubricant the first one or two specimens drawn through a die gave slightly higher draw forces than subsequent specimens gave.

This was particularly true for a newly polished die. Also, if a rough-ground (unpolished) die is used, the draw force increases gradually, and this was found to be associated with pickup.

The "punch contour" did not materially affect the draw stress, Figs. 10 and 11. The curves representing the draw force as a function of the reduction were almost identical, if a tapered punch or if cylindrical punches were used in combination with tapered dies having large angles (12.5 and 27.5 deg). However, with decreasing die angle, the curves obtained with tapered punches deviated increasingly to higher values from the curves obtained with cylindrical punches. This may readily be explained by the decrease of the actual working angle by an angle equal to the taper of the punch (0.9 deg half-angle), the effect of this being appreciable only for the small die angles where the draw stress is sensitive to variations in die angle, Fig. 9.

No influence of "punch material" could be detected. Tapered punches of steel and of chromium-plated steel yielded practically identical force-stroke curves for either smooth punches or for rough punches.

The "punch surface" had only a slight effect on the draw stress

[9] As there was no apparent difference in the draw stresses for unplated and chromium-plated steel dies, no distinction has been made in this respect throughout the rest of the paper, although a number of the dies were chromium-plated.

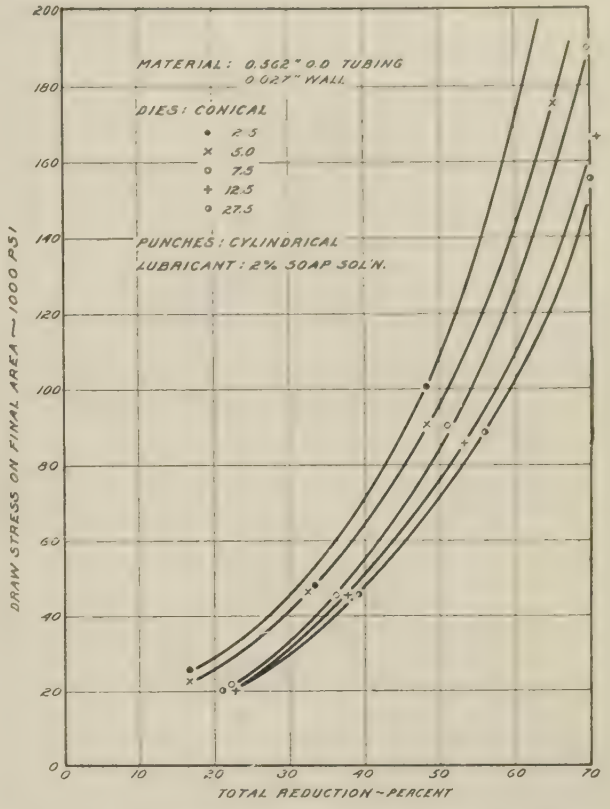

FIG. 10 DRAW STRESS-VERSUS-REDUCTION CURVES FOR CONICAL DIES OF DIFFERENT ANGLES AND CYLINDRICAL PUNCHES

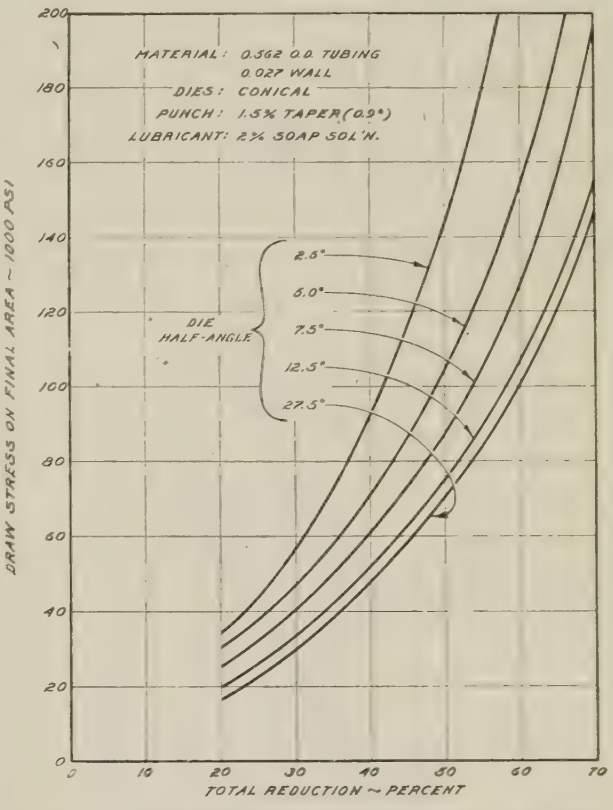

FIG. 11 DRAW STRESS-VERSUS-REDUCTION CURVES FOR CONICAL DIES OF DIFFERENT ANGLES AND A TAPERED PUNCH

TABLE 2 EFFECT OF VARIOUS LUBRICANTS ON DRAW FORCES IN TWO DRAWS OF A TANDEM DRAW ON HARD-DRAWN CUPS[a]

Lubricant	Number of tests	Average draw force, lb — 0.705-in. die	0.610-in. die	Remarks
Standard soap solution:				
5–10 min immersion	61	4150	9160	Satisfactory
2 hr immersion	25	3835	8850	Satisfactory
Castor oil	5	5160	10440	100 per cent breakage
Commercial lubricants:[b]				
No. 1 soap, oil, high-pressure lubricant	36	4000	9105	Satisfactory
No. 2 animal fat, emulsifying agent	14	4550	9750	Scoring and high breakage
No. 3 palm-oil base	25	4450	9530	Scoring
No. 4 (unknown composition)	10	4580	9650	Scoring
No. 5 animal and vegetable fats	6	5080	9600	Satisfactory
Standard soap solution plus 0.1 per cent stearin (10 sec immersion)	14	3980	9170	Satisfactory
Dry stearin (applied in ether)	10	4220	9560	Satisfactory
Dry stearin surface plus normal soap solution (10 sec immersion)	10	4100	9360	Satisfactory

[a] Hard cups 0.763 in. OD × 0.102 in. wall thickness drawn in preparation of standard drawpieces to a drawpiece 0.613 in. OD × 0.049 in. wall thickness through two dies in tandem, the dies being 0.705 in. and 0.610 in. diam. (Individual reductions equal 31 and 40 per cent; total reduction equals 58.5 per cent.)
[b] Dilutions were as recommended and varied between ratios of 1 to 6 and 1 to 4 parts lubricant to water.

TABLE 3 EFFECT OF DIE CONDITION AND VARIOUS LUBRICANTS ON DRAWING ANNEALED DRAWPIECES[a]

Lubricant	Highly polished die — No. of tests	Average draw force, lb	Breakage, per cent	Worn die — No. of tests	Average draw force, lb	Breakage, per cent
Standard soap solution:						
5–15 min immersion	350	3600	13	25	3660	12
24 hr immersion, plus 1.5 per cent lard oil	10	3210	20	15	3280	0
Castor oil	23	3410	0	10	3920	70
Tallow	7	3630	43			

[a] Annealed drawpieces 0.613 in. OD × 0.049 in. wall thickness drawn to 0.558 in. OD × 0.020 in. wall thickness (61 per cent reduction).

up to reductions of 50 per cent.[10] With further increasing reductions, however, the draw stress using a rough-ground punch became increasingly greater than that using a polished punch, Fig. 12. No appreciable differences in draw stress could be observed for punches polished with 4/0 emery polishing paper and punches with a Chrysler superfinish. The magnified outlines of these three surfaces are shown in Fig. 13.

[10] Tests on unannealed specimens showed considerably greater differences in draw stresses with rough and polished punches than did the annealed specimens, Fig. 12. The reason for this difference in behavior between soft and hard brass is not clear but indicates that a particularly high friction exists between hard brass and a rough punch.

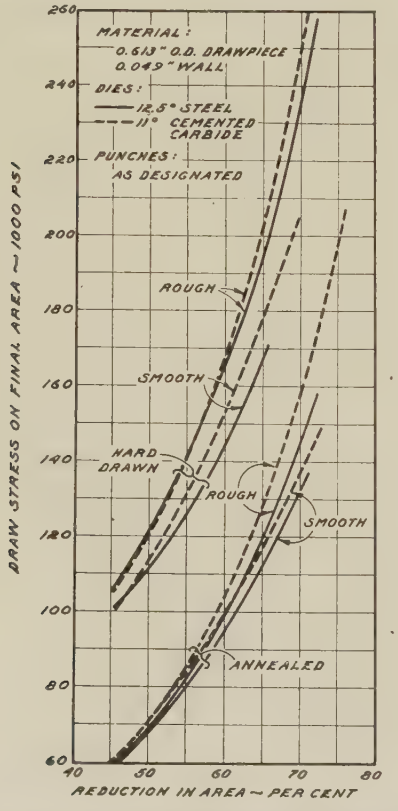

FIG. 12 EFFECT OF SURFACE CONDITION OF PUNCH AND HARDNESS OF BRASS UPON DRAW STRESS AT VARIOUS REDUCTIONS

To investigate the effects of lubricants, a large number of specimens were subjected to high reductions. In addition to measurements of the draw force, the breakage was determined and the specimens were inspected for scoring. The lubricants investigated comprised a number of specially prepared drawing compounds and, in addition, castor oil, tallow, aqueous soap solutions of various concentrations with and without additions of stearin or lard oil. The results of some of the tests are assembled in Tables 2 and 3.

Of the commercial lubricants investigated, none excelled the lubricating action of soap solution. This was observed particularly in the preparation of the drawpieces, involving several draws in the hard condition, Table 2. Only one of the proprietary lubricants (No. 1) which, significantly, also had a soap base, yielded approximately the low draw force of soap solution; and various water-soluble lubricants required 5 to 10 per cent higher draw forces than did soap solution.

Castor oil in combination with annealed drawpieces and polished dies (any material) yielded slightly lower draw forces than when immersed for a short time in soap solution (5 to 15 min), Tables 2 and 3, and Fig. 13.

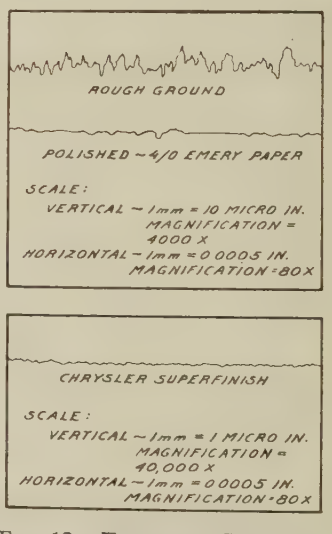

FIG. 13 EFFECT OF DIFFERENT FINISHING TECHNIQUES ON SURFACE FINISH OF PUNCHES

However, any condition deviating from optimum resulted in fouling of the tools, this causing considerable increase in the draw forces. The drawing of hard brass caused particularly heavy fouling of the die, scoring of the brass, high draw forces, and breakage, see Table 2.

The lubricant used as standard throughout these tests was a 2 per cent aqueous soap solution (chip soap) which is rather widely employed in the deep-drawing of cartridge cases. As the investigation progressed, a considerable portion of the scatter of the draw forces was traced to the short time of immersion in the lubricant, being usually between 1 and 15 min. A study of the effect of time of immersion of the specimens[11] in soap solution

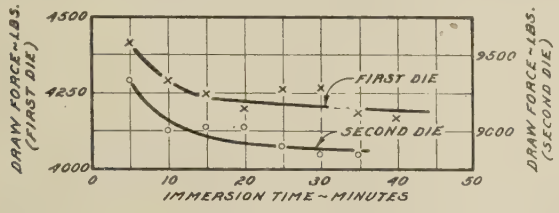

Fig. 14 Effect of Immersion Time in a 2 Per Cent Soap Solution on Draw Force in Individual Draws of Tandem Draw

yielded a decrease in draw force by approximately 5 per cent if immersed in the lubricant for at least 20 min,[12] Fig. 14. It is believed that this improvement in the lubricating action of soap solution is caused by the formation of a film of stearate which adheres to the metal surface (7). This film could be partially removed by rubbing the drawpiece with the hand or washing it in water prior to drawing, these precedures resulting in an increase in draw force. No differences were observed between the draw force obtained with freshly made and with aged soap solutions. A few tests on the effect of soap concentrations showed noticeably decreased draw forces if the concentration was less than $^1/_4$ per cent.

[11] The major portion of the investigation on lubricants was done during the drawing of the unannealed cups down to the standard-size tubular drawpieces. This explains the specimen sizes given in footnotes to Tables 1 and 2. All tests regarding effect of lubricants were made with cylindrical punches.

[12] Observation of the maximum load reached as the base of the drawpieces was pushed through the die showed this value also to decrease from about 3900 for a few seconds' immersion to 3200 for approximately 2 minutes' immersion, or a decrease of 18 per cent.

Additions of stearin, Table 2, or lard oil, Table 3, to a 2 per cent soap solution resulted in insignificant changes in draw force. It appears, however, that they stabilize the soap solution, greatly decreasing the time of immersion required to obtain consistent (and low) draw forces. A dry stearin coating on the test pieces, obtained by dipping them in a solution of stearin in ether, also gave approximately the same performance as the soap solution, Table 2.

Acknowledgments

We are indebted to the War Department for permission to publish this paper, also to Lieut. Col. L. S. Fletcher, previous director, C. C. Fawcett, Assistant Director, and other members of the Ordnance Laboratory, Frankford Arsenal, for technical support and co-operation. We also acknowledge the co-operation and assistance of Messrs. S. M. Clark, D. T. Doll, J. M. Taub, L. J. Ebert, and G. B. Kasik, who were co-authors of the various reports from which this paper was abstracted, and of Mr. F. J. Miller who assisted in the designing and making of the various equipment used.

BIBLIOGRAPHY

1 "Stress Analysis of Tube Sinking," by G. Sachs and W. M. Baldwin, Jr., Trans. ASME, vol. 68, 1946, pp. 655–662.

2 "The Calculation of Roll Pressure in Hot and Cold Flat Rolling," by E. Orowan, Proceedings of The Institution of Mechanical Engineers, vol. 150, 1944, pp. 140–167.

3 "Experimentation on Tube Drawing With a Moving Mandrel," by G. Espey and G. Sachs, *Journal of Applied Mechanics*, Trans. ASME, vol. 69, 1947, p. A-81.

4 "The Factors Influencing the Deep Drawing and Corrosion Cracking of 70/30 Brass Cartridge Cases," by G. Sachs, et al, Frankford Arsenal, Reports Nos. R-119, 1941, R-123, and R-125, 1942.

5 "Research Covering the Factors Influencing the Deep Drawing of Steel and 70/30 Brass Cartridge Cases," by G. Sachs, et al, Frankford Arsenal, Reports Nos. R-128, R-129, 1942, and R-284, 1943.

6 "Effect of Spacing Between Dies in the Tandem Drawing of Tubular Parts," by G. Sachs and G. Espey, Trans. ASME, vol. 69, 1947, pp. 139–143.

7 "Lubricants for Drawing Cartridge Cases," by S. Spring and H. Gisser, Frankford Arsenal Report No. 63-A, 1941.

8 "Experiments on the Properties of Drawn Wires and the Power Requirements in Wire Drawing," by W. Linicus and G. Sachs, Spanlose Formung, J. Springer, Berlin, Germany, 1931, pp. 38–67

9 "A Comparison of Grain Size Measurements and Brinell Hardness of Cartridge Brass," by W. H. Bassett and C. H. Davis, Trans. American Institute of Mining and Metallurgical Engineers, vol. 60, 1919, p. 428.

Strength and Failure Characteristics of Thin Circular Membranes

By W. F. BROWN, JR.,[1] and GEORGE SACHS,[2] CLEVELAND, OHIO

The problem treated in this paper concerns the deformation and failure characteristics of thin circular metal membranes. The problem originated in a research project on the elevated-temperature bulging of aluminum alloys, conducted at Case Institute of Technology under contract with the Office of Production Research and Development of the War Production Board. Commercially the problem relates to the design of safety diaphragms used for the protection of pressure vessels. Also, similar conditions of loading and geometry are present in certain structures subjected to underwater explosion or high hydrostatic pressure. The circular bulging of metal membranes also offers the possibility of investigating the fundamental properties of metal in biaxial stress and strain states.

In this paper the instability phenomena encountered in the deformation of such shapes is analyzed in terms of strain distribution and also by previously developed equations relating the stress-strain and radius-strain functions. The paper also develops the fact that the circular bulge test appears particularly suitable for determining basic stress-strain relations to much higher strain values than are obtainable by conventional methods.

Introduction

A thin membrane restricted at its periphery and subjected to hydraulic pressure offers a possible method of investigating the fundamental properties of metals under biaxial stress and strain states.

Problems of this nature are encountered commercially in the design of safety diaphragms used for the protection of pressure vessels. Also, similar conditions may be present in structures subjected to underwater explosion.

Bulging investigations on aluminum alloys were sponsored by various Government agencies during the war period (1, 2, 3,).[3] However, the fundamentals of the bulging process are not sufficiently understood at this time to permit a clear evaluation of all these results. In general the strains were found to be nonuniformly distributed over the surface of the bulge, increasing from a small value at the periphery to a maximum value at the pole. This can be explained by the restraint caused by clamping the blank at the periphery. The restraint gradually decreases with increasing distance from the edge. In these initial investigations a narrow region was observed in ductile metals in the vicinity of the fracture (usually occurring at the pole) where there was a rapid decrease in thickness. This was assumed to comprise a "neck" analogous to that observed in a tensile test. Disregarding this very localized strain peak, the strain exhibited a rather flat maximum in the surface area containing the fracture. To the value of this maximum strain measured after fracture, the same significance was ascribed as to the uniform strain in uniaxial tension. However, it was later found that it was related to the ductility (reduction in thickness at failure) in some obscure manner (2).*

In a previous publication by Sachs and Lubahn (4), a theory of tensional "instability" occurring in ductile metals subjected to various load conditions was developed, which included hydraulic bulging of thin circular membranes. This theory assumes that instability occurs when an increase in strain takes place without an increase or with a decrease either in an external load, such as the tensile load, or the internal pressure.

These concepts have been verified previously for pure tension (5). They also explain the beginning of necking at maximum load encountered in a flat sheet under conditions of plane-strain (6), and the maximum load strains observed in tubing subjected to combinations of internal pressure and longitudinal tension (7).

The purpose of the present investigation was to analyze experimentally and theoretically the hydraulic bulging of a thin circular membrane. Because of its high uniformity, pure copper was considered as the most suitable material. Three different conditions of the metal were selected, differing regarding (*a*) instability strain (necking strain), and (*b*) the ductility in uniaxial tension.

A complete analysis was made (*a*) for annealed electrolytic copper, this being representative of a material with a high uniform elongation and ductility, and (*b*) for hard-rolled electrolytic copper which has a low uniform elongation but a high ductility. In addition, several tests were made (*c*) on oxygen-free high-conductivity copper, a material possessing a high uniform elongation and a particularly high ductility. This problem required accurate measurement of the pressure, the strains, and the radii of curvature during the forming process. It was attempted to demonstrate the following relations:

1 The pressure should pass through a maximum with progressive straining at a certain "maximum load strain."

2 The strain distribution should exhibit an increase in strain gradient at the maximum load. The "experimental instability strain" derived from this strain distribution should agree with the maximum load strain.

3 The analysis of the stress-strain curve should yield a "theoretical instability strain" identical to both the maximum load strain and the experimental instability strain.

4 In addition, the stress-strain curve obtained in bulging should be identical to that in uniaxial tension, if the largest true stress for either case is plotted as a function of the greatest natural strain.

Theoretical Analysis

The theory of instability for various geometrical shapes subjected to a pressure normal to their surface, reported pre-

[1] Research Laboratory for Mechanical Metallurgy, Case Institute of Technology.

[2] Research Laboratory for Mechanical Metallurgy, Case Institute of Technology. Mem. ASME.

[3] Numbers in parentheses refer to the Bibliography at the end of the paper.

Contributed by the Metals Engineering Division and presented at the Annual Meeting, Atlantic City, N. J., December 1–5, 1947, of The American Society of Mechanical Engineers.

Note: Statements and opinions advanced in papers are to be understood as individual expressions of their authors and not those of the Society. Paper No. 47—A-20.

* A considerable amount of experimental and theoretical work on the deformation of large circular diaphragms was carried out at the David Taylor Model Basin of the U. S. Navy during the war period. These results have been described in Navy reports by Gleyzal (16,17), Greenfield (18), and Mostow (19), which were declassified too late for discussion of their results in this publication.

viously (4), may be developed more generally in terms of any one of the stresses or strains desired. However, since the equations may be solved graphically from the stress-versus-strain curve, it is desirable that the theory for a given shape be in terms of those "decisive" stresses and strains which are involved in one of the universal stress-strain relationships.[4]

Thus for cases of balanced biaxial tension arising from the application of pressure to various thin-walled geometrical shapes, $s_3 = 0$ and the decisive stress is twice the maximum shear stress, $s_1 = s_2$. The decisive strain is the normal strain, $\epsilon_3 = -2\epsilon_1 = -2\epsilon_2$.[5] Therefore the desired function of stress and strain will be

$$s_1 = f(\epsilon_3) \quad \ldots\ldots [1]$$

The maximum load condition for instability may then be developed in terms of these stresses and strains as follows, for balanced biaxial tension in a tube, sphere, or circular bulge:

The relation between the internal pressure p, in terms of the circumferential (true) stress s_1, the radius of curvature R, and the metal thickness h, for a thin-walled tube, is

$$p = \frac{s_1 h}{R} \quad \ldots\ldots [2]$$

For a sphere or circular bulge (the latter subject to certain assumptions discussed later) correspondingly

$$p = \frac{2 s_1 h}{R} \quad \ldots\ldots [2a]$$

where s_1 is now the meridional stress.[6]

The instability condition

$$dp = 0 \quad \ldots\ldots [3]$$

then yields the following relation

$$\frac{ds_1}{s_1} - \frac{dR}{R} + \frac{dh}{h} = 0 \quad \ldots\ldots [4]$$

which applies to all three of these shapes. The thickness h, for any of these cases may be expressed in terms of the initial thickness h_0, and the normal strain, e_3

$$h = h_0(1 + e_3)$$
$$dh = h_0 de_3$$

For the thin-walled tube, the radius is related to the circumferential strain (e_1) and for a sphere to the meridional strain (e_1) as follows

$$R = R_0(1 + e_1)$$
$$dR = R_0 de_1$$

However, for a circular bulge the radius is an unknown function of the strains.

The instability equation may now be rewritten for the tube and sphere in terms of the strains, as follows

$$\frac{ds_1}{s_1} - \frac{de_1}{1 + e_1} + \frac{de_3}{1 + e_3} = d \log_e s_1 - d\epsilon_1 + d\epsilon_3 = 0 \ldots [5]$$

or, considering that $\epsilon_1 = -\epsilon_3/2$

$$\frac{d \log_e s_1}{d\epsilon_3} + \frac{3}{2} = \frac{1}{s_1}\frac{ds_1}{d\epsilon_3} + \frac{3}{2} = 0 \ldots\ldots [5a]$$

For the analysis of a circular bulge the following assumptions are made: (*a*) any deviation of the stress and strain states from uniformity is neglected,[7] and (*b*) the contour of the bulge is considered as spherical in the region of the pole. However, in this case the stresses and strains are not uniformly distributed across the contour. Therefore the instability equation must be written in terms of the maximum values of s_1 and ϵ_3. These of course are those at the pole of the bulge and in the subsequent discussion will be referred to as the "maximum meridional" stress or strain, respectively. Therefore, from Equatian [4]

$$\frac{ds_1}{s_1} - \frac{dR}{R} + \frac{de_3}{1 + e_3} = 0 \ldots\ldots [6]$$

or

$$\frac{d \log_e s_1}{d\epsilon_3} - \frac{d \log_e R}{d\epsilon_3} + 1 = \frac{1}{s_1}\frac{ds_1}{d\epsilon_3} - \frac{1}{R}\frac{dR}{d\epsilon_3} + 1 = 0 \ldots [6a]$$

In order to solve Equation [6*a*] it is necessary to obtain experimentally the two functions

$$\frac{d \log_e s_1}{d\epsilon_3} = \frac{1}{s_1}\frac{ds_1}{d\epsilon_3}, \text{ and } \frac{d \log_e R}{d\epsilon_3} = \frac{1}{R}\frac{dR}{d\epsilon_3}$$

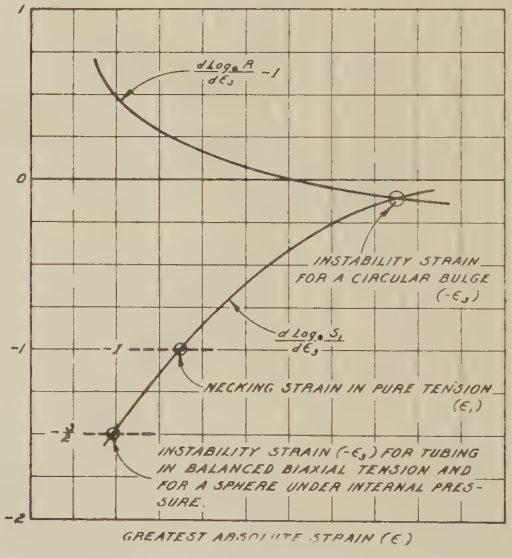

FIG. 1 EXAMPLE OF GRAPHICAL SOLUTION OF INSTABILITY EQUATIONS FOR VARIOUS SHAPES

It is interesting to compare these solutions with the maximum-load condition in pure tension

$$dF = 0$$

where F is the tensile load. The resulting equation in terms of the decisive stress s_1, and the decisive strain ϵ_1 is then

[4] The representation of the greatest absolute natural strain (ϵ_{max}) (referred to as the decisive strain) as a function of twice the maximum shear stress $(s_1 - s_2)/2$ (referred to as the decisive stress) has been chosen for this purpose. The use of the maximum-shear criterion may lead to stress values in error as much as 15 per cent. However, it has been shown (13) that the selected representation does yield stress-strain curves for the various stress states which are of nearly identical slope. Since the instability strain is dependent only upon the slope of the stress-strain curve, this relation should be satisfactory.

[5] ϵ is the natural strain $= \log_e(1 + e)$.

[6] The intersection of a plane passing through the pole and perpendicular to the base plane of the bulge or perpendicular to the diametral plane of a sphere defines a "meridian line" on the surface. The meridian lines parallel and perpendicular to the grain direction are referred to as the "major axes." The principal stresses or strains measured on and in the direction of these axes are referred to as "meridional stresses or strains."

[7] A previous analysis of a 24SO circular bulge formed to failure indicates the stress state to not deviate more than ±5 per cent from unity (balanced biaxiality) in the area enclosed by a circle (with its center at the pole) having a 4½ in. diam on the undeformed sheet.

$$\frac{d \log_e s_1}{d\epsilon_1} + 1 = 0$$

Fig. 1 shows a hypothetical graphical solution of the instability equations for these various cases. It can be seen that the instability strain in circular bulging should be considerably higher than that for either a tube in balanced biaxial tension, or a sphere.

Material and Procedure

Hard-rolled copper sheet of 0.040 in. thickness was available in two different compositions, electrolytic copper and "OFHC" (oxygen-free high-conductivity) copper. The electrolytic copper was subjected to bulging in both the hard-rolled and the annealed (1000 F for 45 min) conditions. The OFHC copper was investigated in the annealed condition only. The reduction in cold-rolling was kept sufficiently small so as to yield a low degree of directionality after annealing (8).

Before testing, the tensile and the bulge specimens were photogridded (9) with a 20-line to the inch net.

Tensile tests ($^1/_2$ in. in width and possessing 8-in. gage length) on all three experimental materials were made in the rolling direction, transverse, and at 45 deg to the rolling direction. The rate of straining in these tests was adjusted to be comparable with that encountered in bulging, i.e., the total time of testing was adjusted to be between 20 and 30 min. The stress-strain curves in these various directions were found to be practically identical for the annealed coppers. Tensile tests on the hard copper, however, revealed an anisotropy, evidenced by a difference in stress between the rolling and transverse directions (at maximum load) of approximately 2500 psi.

The bulging equipment consisted of a head supporting the die, and an oil-displacement cylinder capable of furnishing oil at pressures up to 3000 psi (3). The bulging die had a 6-in-diam circular opening in a 1-in-thick steel plate. The die edge was radiused to $^1/_2$ in. to prevent the specimen from fracturing at the periphery. The surface of the die contacting the specimen was serrated with four buttress teeth to the inch ($^1/_8$ in. deep $\times$ $^1/_4$ in. long). Six 1-in-diam studs extended upward from the bulging head passing through the metal sheet and the die. The specimen was clamped into place by tightening bolts on these studs.

A complete experimental analysis consisted of determining the pressures, the meridional strain distributions, and the contours (from which the radii were derived), for appropriate intervals of strain (at the pole), up to fracturing.

Such an analysis was made for one annealed electrolytic-copper bulge (test A1) and for one hard electrolytic-copper bulge (test H4). In these tests both the strain distribution and the contour were determined along the transverse (at 90 deg to rolling direction) major axis.[8] The strains were measured with a tape (3, 9) provided with squares identical to those on the undeformed grid. Strain measurements were made over $^1/_2$ in. gage lengths every $^1/_4$ in. along the axis.

Contours were determined with a specially designed profilometer, Fig. 2, which consisted of an Ames dial traveling on parallel bars, one of which carried a steel scale graduated in 0.01 in. A pointer, the direction of which coincides with the vertical axis of the Ames dial spindle, served as an index on the horizontal scale. The dial spindle was equipped with a tip having approximately 0.02 in. radius. Proper alignment of

[8] These measurements were limited in their extent (distance from pole) by the inner wall of the bulging die. Consequently, the complete surface area could not be covered, the meridional distance of the strain measurements and the total travel of the profile gage being, on the average, 2 in. arc length on either side of the pole.

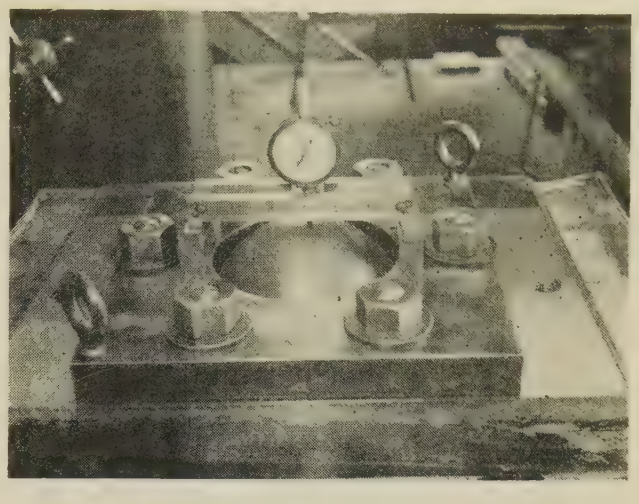

Fig. 2 Bulging Head With Profilometer in Place

this apparatus was insured by having three lines scribed on the upper die surface, two coinciding with and a third at an angle of 45 deg to the major axes of the bulge. Vertical reference lines were also scribed at the center on each end surface of the profilometer.

Before measuring the contour and strain distribution, the pressure was removed. The total time of testing was about 6 hr, the metal being under gradually increasing strain for 20 to 30 min.

For the two complete tests the contour was determined also in the rolling direction and at 45 deg to the rolling direction for a strain at the pole somewhat greater than that at maximum load, Figs. 3 and 4.

The annealed electrolytic copper, Fig. 3, exhibited identical contours in different directions. Slight but consistent variations in contour were observed for a hard-copper bulge, Fig. 4. Thus, according to these measurements, the anisotropy (of shape) for either the annealed or the hard material was insignificant.

In order to check the results and to investigate possible material variations, additional pressure-versus-strain curves were also recorded for both a hard (test H7) and an annealed electrolytic-copper bulge (test A2). These data and those obtained for tests A1 and H4 are in good agreement (see Figs. 9 and 10).

A further test (test OA6) was made on annealed OFHC copper sheet. In this test no contour measurements were made, but meridional strain distributions were determined at appropriate strain intervals.

The second annealed electrolytic-copper bulge (test A2) was not fractured but removed from the fixture after being formed to a maximum meridional strain somewhat beyond that at maximum load. This specimen was subjected to more detailed and accurate determination of the contour which could be compared with that obtained with the profilometer. To accomplish this, a comparator was constructed, consisting of a flat plate which could be moved in a horizontal direction by means of a micrometer screw graduated in 0.001 in. An Ames dial (0.001 in. per division) was mounted stationary in such a manner that its spindle (having as its tip a ball of known diameter) was perpendicular to this plate. Thus by clamping a bulge to the plate the horizontal and vertical co-ordinates of a point on its surface were easily determined by varying the horizontal position and reading the corresponding vertical displacements from the Ames dial. Data obtained with this comparator were then corrected for the spindle-ball diameter and replotted (see Fig. 6).

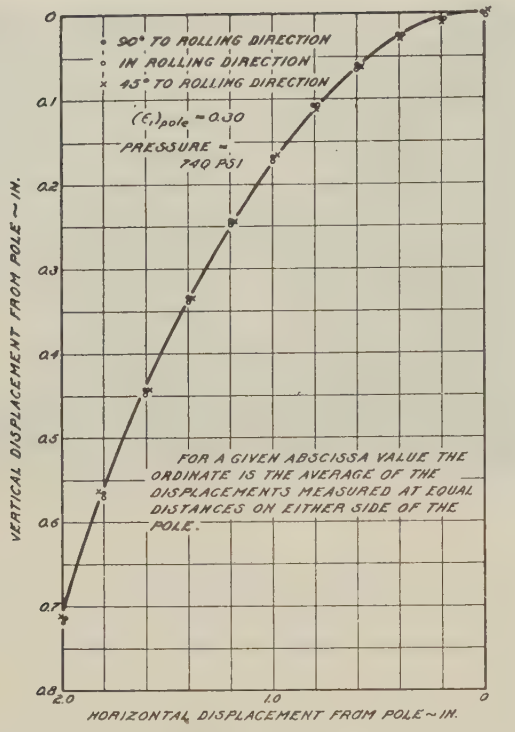

FIG. 3 ONE HALF THE CONTOUR OF AN ANNEALED ELECTROLYTIC-COPPER BULGE AS DETERMINED WITH PROFILOMETER IN THREE MERIDIONAL DIRECTIONS; TEST A1

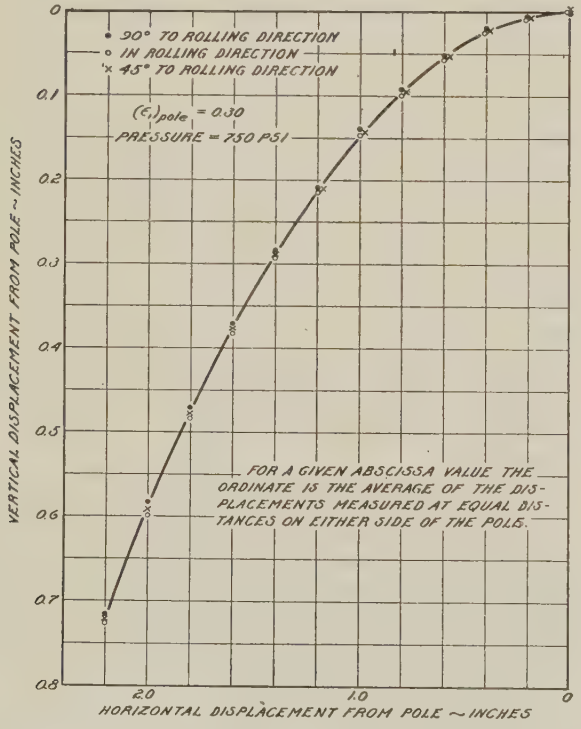

FIG. 4 ONE HALF THE CONTOUR OF A HARD ELECTROLYTIC-COPPER BULGE AS DETERMINED WITH PROFILOMETER IN THREE MERIDIONAL DIRECTIONS; TEST H4

DETERMINATION OF THE CURVATURE

It was desired to devise some method which would allow the determination of the curvature over a large portion of the contour and particularly at the pole. The technique selected,

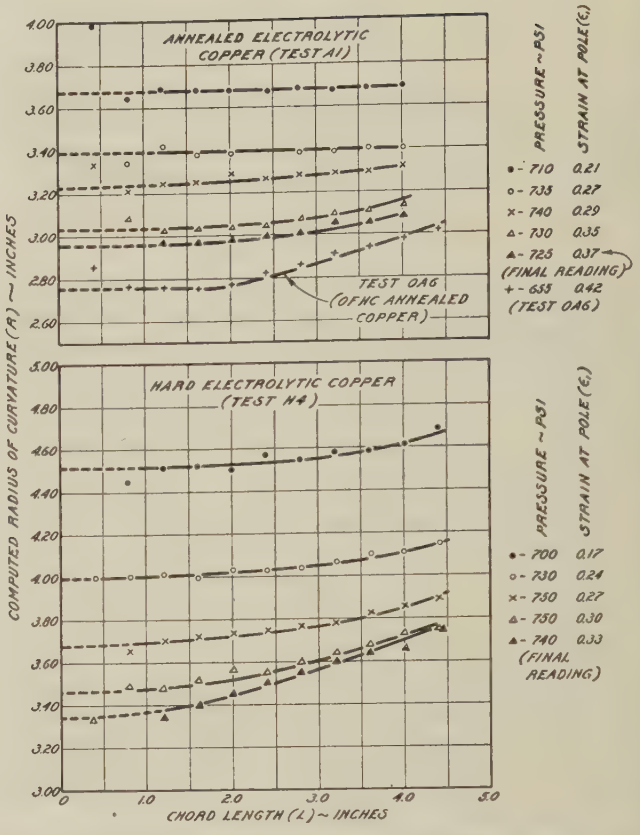

FIG. 5 EXAMPLES OF DETERMINATION OF RADIUS OF CURVATURE AT POLE FROM RADII OF CURVATURE CALCULATED FOR VARIOUS CHORD LENGTHS

using the previously described profilometer, yielded average radii for various chord lengths from which that at the pole was obtained by extrapolation. These radii were calculated from each chord length and its corresponding sagitta, neglecting the deviation of the arc from a circle.

Fig. 5 illustrates several examples of the results obtained by this method, for both an annealed- and a hard-copper bulge. The curves would be straight lines parallel to the abscissas if the entire contour had a constant radius of curvature, i.e., was spherical. Apparently the curvature is not constant, but differs slightly over the contour, the variations being more pronounced for the hard material. The change in curvature also increases with increasing strain, particularly after the maximum-load strain is passed.

However, such deviations from a constant curvature should not prohibit the use of the extrapolated value (for zero chord length) in the solution of the instability equation, since the theory is concerned only with the curvature in the vicinity of the pole.

In order to check the accuracy of this technique and to investigate possible variations in curvature for chord lengths less than 1 in., the contour of an annealed-copper bulge (test A2), bulged beyond the maximum-load strain, was determined by the previously described comparator. Fig. 6 shows one half of the contour obtained in this manner. From this curve the slopes for various abscissas values were determined graphically. In Fig. 7 the resulting experimental slope values are compared with values calculated theoretically on the assumption of several constant radii of curvature. The curve calculated for a radius of 3.06 in. fits the experimental data closely; and this indicates the contour over the range investigated to be very close to a

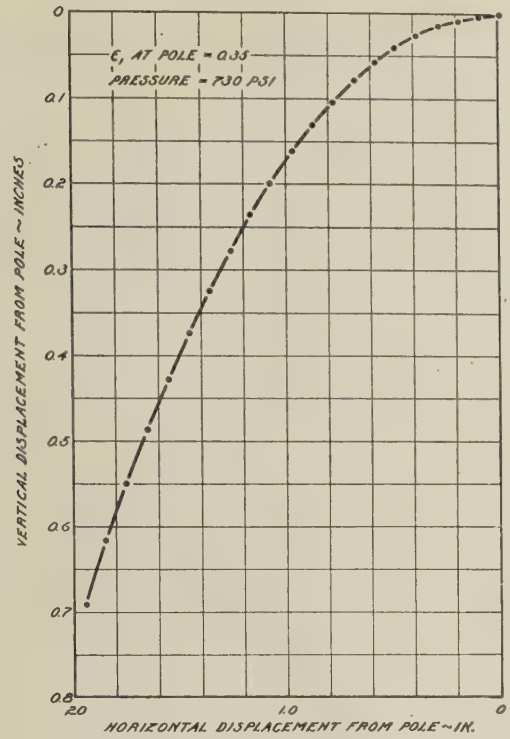

FIG. 6 CONTOUR OF ANNEALED ELECTROLYTIC-COPPER BULGE DETERMINED WITH COMPARATOR, TEST A2

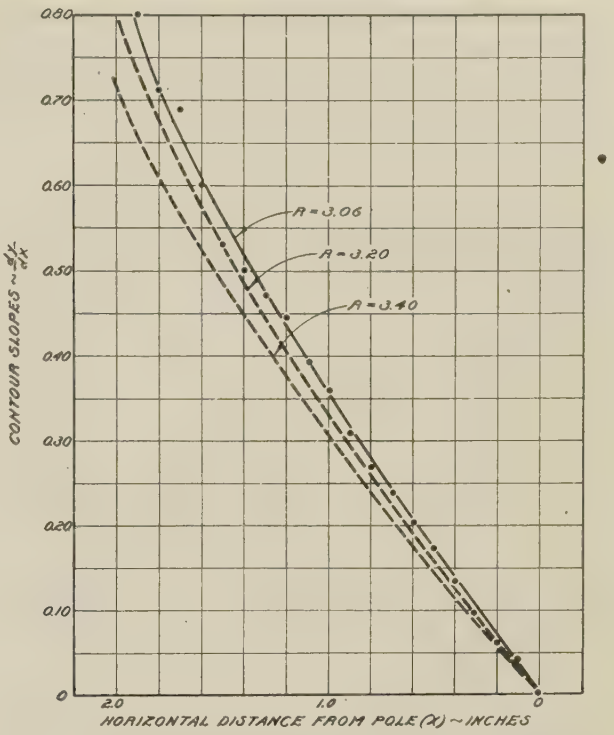

FIG. 7 SLOPES DETERMINED GRAPHICALLY FROM COMPARATOR MEASUREMENTS ON AN ANNEALED ELECTROLYTIC-COPPER BULGE, COMPARED WITH THOSE CALCULATED FOR SEVERAL CONSTANT RADII OF CURVATURE

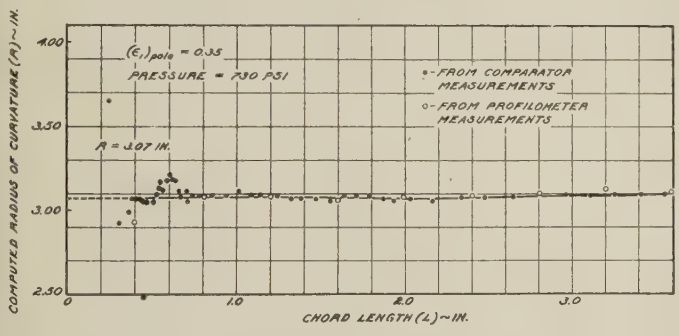

FIG. 8 RADII OF CURVATURE FOR VARIOUS CHORD LENGTHS AS COMPUTED FROM MEASUREMENTS MADE WITH COMPARATOR AND PROFILOMETER

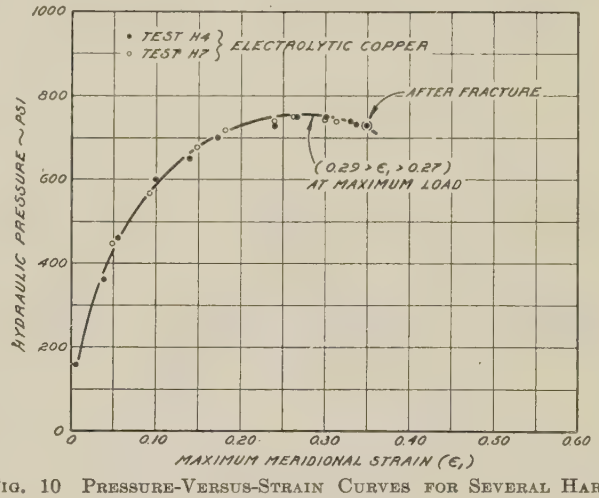

FIG. 10 PRESSURE-VERSUS-STRAIN CURVES FOR SEVERAL HARD-COPPER BULGES

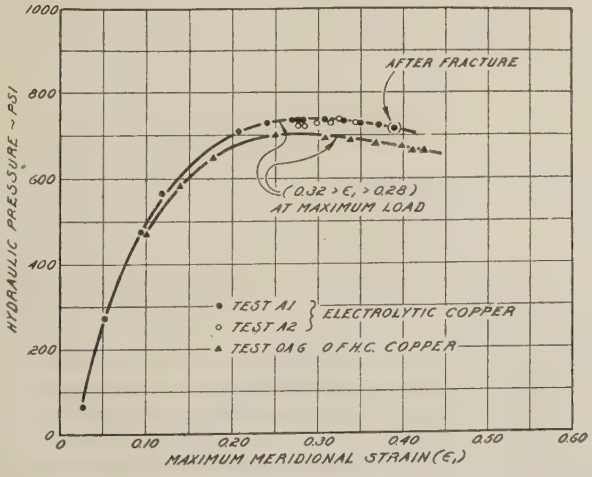

FIG. 9 PRESSURE-VERSUS-STRAIN CURVES FOR SEVERAL ANNEALED-COPPER BULGES

circle arc possessing this radius. This procedure is still not sensitive to small variations in radius near the immediate vicinity of the pole, as is shown by the convergence of the several curves in this region.

However, the same data permit a more accurate analysis of the contour of this bulge for short chord lengths. Fig. 8 shows the radii of curvature determined for various chord lengths as calculated from both the comparator measurements and from those made with the profilometer. The more elaborate method appears to yield reliable values (±1 per cent) of the curvature for chord lengths greater than 0.4 in.[9]

[9] A hump appears in the curve for a chord length of about 0.6 in. This would indicate a rapid but small decrease in the curvature in this region. Such a phenomenon cannot be explained, but may be associated with a "hard spot" in the metal.

Radii determined from profilometer data fit well on this curve for chord lengths greater than one inch, the scattering being only slightly larger. Below this value, small errors in the chord lengths measured by means of the profilometer, however, resulted in large errors in the calculated radius of curvature.

Analysis of the Instability

The theory of instability developed applies to ductile metals for which the bulging pressure should pass through a maximum before failure. The presence of such a maximum is shown by the pressure versus maximum meridional strain curves obtained for both annealed-copper, Fig. 9, and hard-copper bulges, Fig. 10.

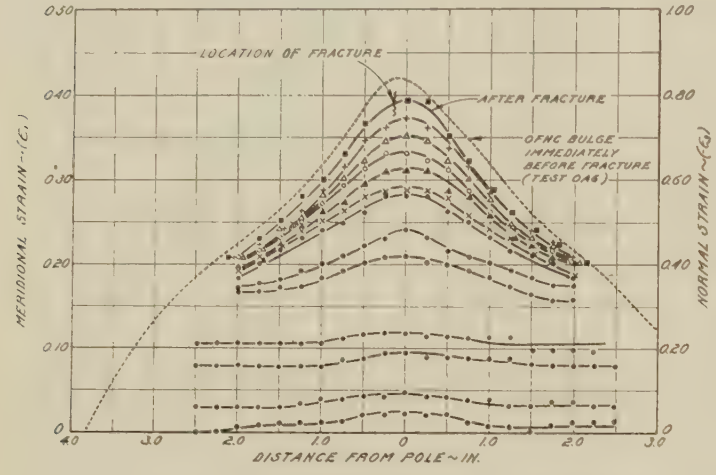

Fig. 11 Distribution of Meridional Strains at Various Loads and After Fracture for an Annealed-Copper Bulge; Test A1

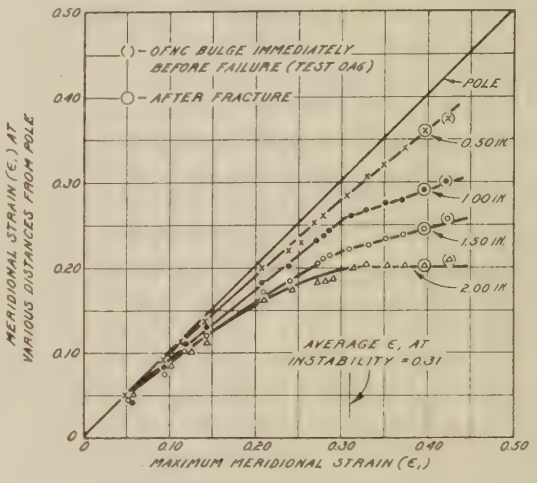

Fig. 13 Relation Between the Meridional Strain at the Pole and That at Various Distances From the Pole for an Annealed Electrolytic-Copper Bulge; Test A1

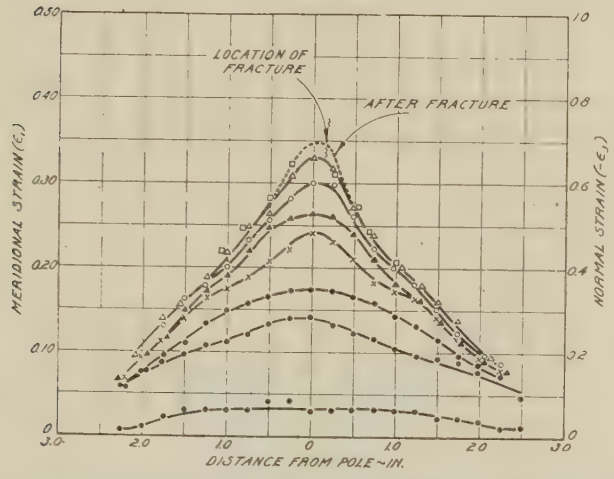

Fig. 12 Distribution of Meridional Strains at Various Loads and After Fracture for a Hard Electrolytic-Copper Bulge; Test H4

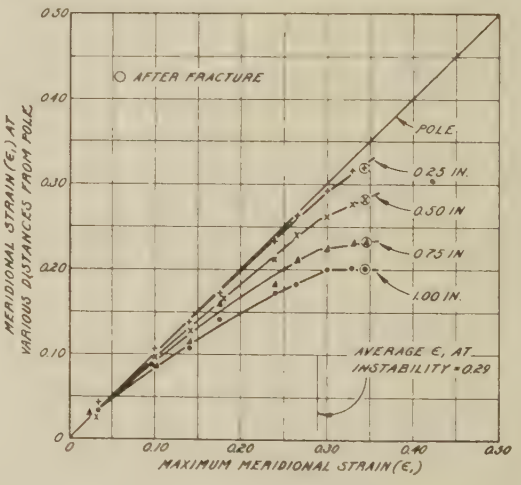

Fig. 14 Relation Between the Meridional Strain at the Pole and That at Various Distances From the Pole for a Hard Electrolytic-Copper Bulge; Test H4

The flatness of these curves prevents an accurate determination of the maximum load strain, but it appears that this value is between $\epsilon_1 = 0.28$ and 0.32 for both annealed coppers and between 0.27 and 0.29 for hard copper.

Figs. 11 and 12 illustrate the meridional strain distributions for annealed and hard electrolytic copper, respectively, at various selected pressures. Also, the final strain distribution obtained immediately before fracture for an annealed OFHC copper bulge has been added to Fig. 11. In each of these curves the strains at a given point are plotted against the position of this point on the undeformed sheet. While the distribution curves for the annealed and hard copper are similar in appearance, the strain gradient across the hard copper was found to be considerably higher.

As previously mentioned, the resulting distributions do not extend over the entire sheet surface. However, the strain must decrease to zero at some point determined by the die radius. This is confirmed by a complete strain distribution obtained for the OFHC copper bulge, Fig. 11. For hard copper, after a certain rather low strain is reached, the distribution curves exhibit a slight inflection at approximately $1^1/_4$ in. from the pole, which is not noted for the annealed copper.

It would be expected from the instability theory for the case of a uniform stress distribution, such as in a tensile test, that the strain should discontinue in all but a localized area after the maximum load has been reached, resulting in a "local neck." However, in the circular bulge, both stress and strain gradients exist from the outset of deformation, as can be seen from Figs. 11 and 12. Consequently, any necking if present does not create a strain distribution fundamentally different from that before necking. However, this cannot be taken as a proof that the

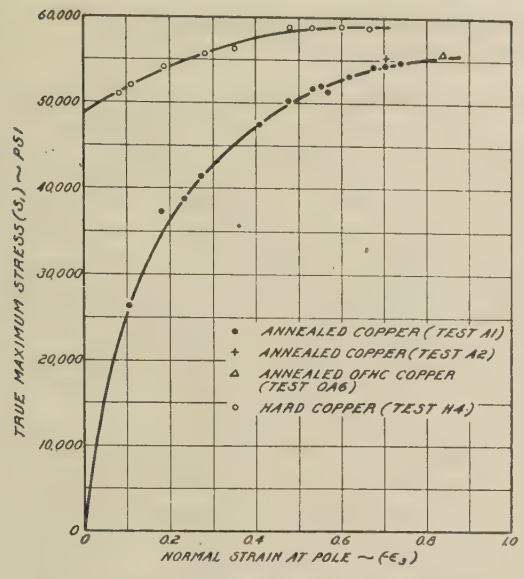

FIG. 15 TRUE MAXIMUM STRESS VERSUS NORMAL STRAIN AT THE POLE FOR ANNEALED AND HARD ELECTROLYTIC COPPER IN BULGING

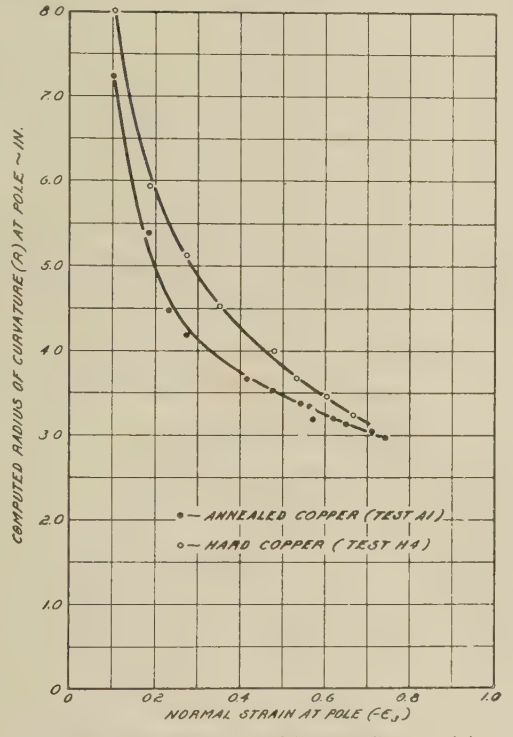

FIG. 16 RELATION BETWEEN THE NORMAL STRAIN (ϵ_3) AND THE RADIUS OF CURVATURE AT THE POLE FOR AN ANNEALED AND A HARD ELECTROLYTIC-COPPER BULGE

maximum-load condition has no significance for the strain distribution of a circular bulge, or that such a shape is not subject to a mechanical instability.

To extend the analysis, the experimental instability strain was determined by plotting the meridional strains at several given distances from the pole as functions of the maximum meridional strains for the annealed- and hard-copper bulges represented in Figs. 11 and 12. It can be seen from such a representation that any one of the curves thus obtained for the annealed copper, Fig. 13, exhibits a break at a maximum meridional strain value of $\epsilon_1 = 0.31$, approximately. Data obtained for the more ductile

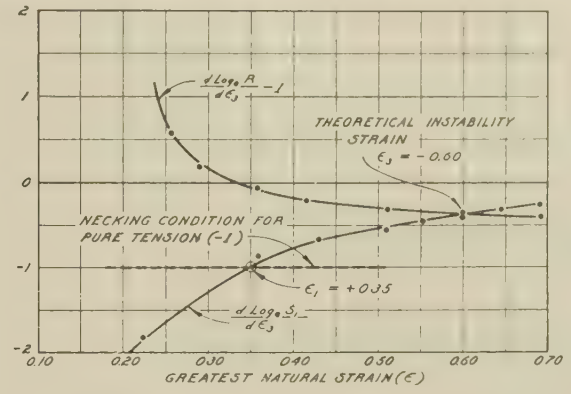

FIG. 17 GRAPHICAL SOLUTION FOR INSTABILITY STRAIN IN AN ANNEALED ELECTROLYTIC-COPPER BULGE; TEST A1

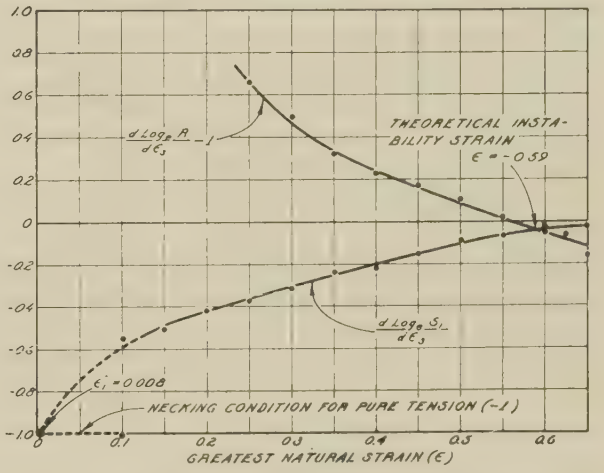

FIG. 18 GRAPHICAL SOLUTION FOR INSTABILITY STRAIN IN A HARD ELECTROLYTIC-COPPER BULGE; TEST H4

annealed OFHC copper bulge (points in parentheses) also fit well on these curves. In the corresponding series of curves for hard electrolytic copper,[10] Fig. 14, such a break appears at approximately $\epsilon_1 = 0.29$.

In order to obtain the theoretical instability strain, the true tensile stress s_1, at the pole must be known. It is determined from the various measured quantities by Equation [2a]

$$s_1 = \frac{pR}{2h} = \frac{pR}{2h_0(1 + e_3)} = \frac{pR(1 + e_1)^2}{2h_0}$$

Fig. 15 shows this stress s_1, as a function of the decisive strain ϵ_3, (normal strain at the pole) for both an annealed- and a hard-copper bulge. Also added to this graph are several points derived from tests on other annealed specimens.

The second required relation is that between the computed radii of curvature at the pole R, and the normal strain ϵ_3. This relation is shown in Fig. 16 for both annealed and hard copper.

The solution of the differential equation of instability, Equation [6a], is given in Fig. 17 for the annealed-copper bulge, and in Fig. 18 for the hard-copper bulge. The values of the theoretical instability strains thus obtained were $\epsilon_3 = -0.60$, or $\epsilon_1 = 0.30$, for the annealed copper and $\epsilon_3 = -0.59$, or $\epsilon_1 = 29.5$, for the hard copper.

Thus both the experimentation and the theoretical analysis

[10] For this material only those strains are considered at distances less than that at which the previously mentioned inflection in the strain distribution occurs (less than 1 in., see Fig. 12).

yield the result that an initially flat circular shape bulged by means of hydraulic pressure will exhibit very large strains at the pole before it becomes unstable. This apparently applies not only to a soft metal which is known to exhibit large strains when subjected to plane uniaxial tension, but also to a hard (rolled) metal which necks in tension after very small strains. This surprising difference between uniaxial tension and biaxial tension in an almost spherical shape obtained by bulging is explained by the pronounced change in curvature during bulging, which delays the occurrence of instability.

The theory shows that the instability strain in bulging depends upon two factors, the strain-hardening and the radius change. It will be shown in the Appendix that the strain-hardening of the metal during bulging follows the general laws of plasticity. The stress-strain relation is a function of the stress state, but independent of the geometry of the bulge.

On the contrary, the dependence of the radius (and radius change) upon the strain has not been analyzed as yet. It is definitely influenced by the stress-strain characteristics. Thus for a metal exhibiting high strain-hardening, the bulge contour is very close to a sphere, while the curvature may vary considerably for a metal with a low strain-hardening rate. These relations will be made the subject of further studies on materials widely varying in their stress-strain characteristics.

The significance of the meridional strain, measured after fracturing has not yet been discussed. This quantity is definitely not identical with the instability strain. In the case of the ductile metals investigated, this maximum strain has been found to exceed considerably the instability strain, see Figs. 13 and 14. Furthermore, OFHC copper, which is known to be more ductile than electrolytic copper, exhibited a considerably larger maximum strain. On the other hand, the magnitude of these strains, $\epsilon_1 = 0.43$, $\epsilon_3 = -0.86$ (corresponding to approximately 60 per cent contraction in area), for the annealed OFHC copper, and $\epsilon_1 = 0.40$, $\epsilon_3 = -0.80$ (corresponding to approximately 50 per cent contraction in area) for annealed electrolytic copper is considerably less than the expected fracturing strains or ductilities (from tensile tests). The maximum strain comprises apparently a strain value somewhere between the instability and fracturing strains. This confirms the results of previous investigations on aluminum alloys (2) in which a dependence of the maximum strains upon the ductilities was observed.

The decisive necking strain for annealed copper subjected to a tensile test was $\epsilon_1 = 0.35$. This value is also obtained for uniaxial tension from the stress-strain curve in bulging (see Fig. 17). It compares with a decisive instability strain in bulging, of $\epsilon_3 = -0.60$. For hard copper the necking strain in a tensile test was approximately $\epsilon_1 = 0.008$, while the decisive instability strain in bulging was $\epsilon_3 = -0.60$ (see Fig. 18).

Conclusions

1 The investigation confirms that an instability occurs in the hydraulic bulging of a thin ductile circular metal membrane.

2 This instability is associated with a maximum in the pressure–strain curve, which has been found to occur in a ductile metal, such as copper.

3 Apparently, the geometry of a (circular) bulge will not allow necking in a small area. However, the strain gradient increases after the maximum-load point is reached. This may possibly be explained by the fact that a region of severely localized strain would result in a decreased radius at this point which, in turn, would lessen the stress. Consequently, the strain would then stop at this location and then move to regions which had been subjected to less strain hardening.

4 The instability strain for a circular bulge predicted from the maximum-load theory is in good agreement with both the maximum-load strain and the experimental instability strain as shown in Table 1.

TABLE 1 INSTABILITY STRAINS FOR CIRCULAR BULGE

Material	Maximum-load strain	Experimental instability strain	Theoretical instability strain
Annealed copper.....	Approx $\epsilon_1 = 0.30$	$\epsilon_1 = 0.31$	$\epsilon_1 = 0.30$
Hard copper.....	Approx $\epsilon_1 = 0.28$	$\epsilon_1 = 0.29$	$\epsilon_1 = 0.295$

Appendix

One of the requirements for solution of metal-flow problems comprises the accurate determination of the stress-strain curve for a particular metal, over a wide range of strains. Generally, this basic stress-strain curve is determined for the simplest stress state, i.e., uniaxial tension or compression.

A large number of investigations have confirmed Ludwik's (10) conception that for a uniform metal, such as copper, the stress-strain curves for tension and compression become identical if the (true) stresses are related to the greatest (decisive) natural strains. However, the range of strain covered by these tests is rather small. The true stresses cannot be readily determined in tension after necking has occurred. In compression, with increasing strain the progressively increasing effect of friction between metal and compression plates limits the useful range of this test.

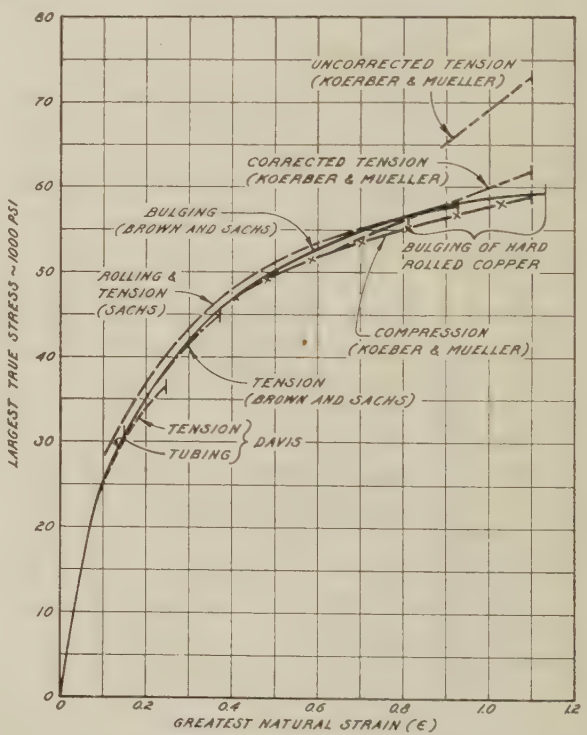

Fig. 19 Largest True Stress Versus Greatest Natural Strain Curves Obtained for Copper by Several Different Methods

Therefore considerable attention has been paid to the elimination of these effects by means of rather elaborate experimental techniques. A number of such corrected true stress versus decisive strain curves have been reported for copper. In both compression and tension the natural strain values have been extended to slightly beyond $\epsilon_1 = 1$, (11, 12). Such curves obtained by Koerber and Mueller (11), for a copper possessing practically the same properties in tension as that used in this investigation, are shown in Fig. 19. The two curves for tension and compression, respectively, agree up to a (decisive) strain

value of $\epsilon = 0.70$. At still higher strain values, the corrected tensile-stress values were slightly higher than the corrected compressive-stress values.

Furthermore, it is generally accepted that the effect of a moderate superimposed hydrostatic (or mean) stress on the maximum shear stress can be neglected. This means that balanced biaxial tension and compression should yield identical stress-strain relations and these, in turn, should conform to that obtained in tension. This has been confirmed for copper by Davis (13) with tests on tubes subjected to longitudinal and circumferential tensions, as shown in Fig. 19. The slight difference between the curves for uniaxial and biaxial tension, respectively, is explained by anisotropy of the tube investigated. However, the biaxial-stress state obtained with a tube supplies a stress-strain curve not distorted by instability to strain values even less than those obtained from tensile or compression tests.

On the contrary, a comparatively simple procedure to obtain stress-strain curves up to very high strains consists of extending the stress-strain curve in tension by means of tensile tests on rolled (14) or drawn specimens (15). Such a curve is also included in Fig. 19.

The process of bulging yields the stress-strain curve for annealed copper directly up to a decisive strain of almost $\epsilon_3 = -0.80$. This curve can be further extended to particularly high strain values by adding the stress values obtained on cold-rolled material. Using the natural normal strain as abscissas, the stress-strain curve for the investigated cold-rolled copper can be simply transposed to that of the annealed copper by a shift of $\epsilon_3 = -0.45$, as illustrated in Fig. 19.

The stress-strain curve thus obtained from the bulge tests agrees within ± 3 per cent with the various curves determined by other methods, up to a decisive strain value of $\epsilon = 0.80$. Beyond that limit, straining by rolling yields practically the same stress values as bulging. However, the corrected tension and, to a lesser degree, the corrected compression data deviate from the bulging curve to higher stress values.

Thus circular bulge tests appear particularly suitable for determining basic stress-strain relations of very ductile metals, to very high strain values.

Acknowledgments

The problem treated in this paper originated in the work carried out during a research project on the hot-forming of aluminum alloys conducted at Case Institute of Technology under contract with the Office of Production Research and Development of the War Production Board. The phenomena occurring in bulging were the subject of repeated discussions with Prof. M. Gensamer, Prof. J. E. Dorn, Mr. O. A. Wheelon, and Mr. L. L. Wyman, during committee meetings on this and related projects. An extension of this work into a fundamental analysis was made possible by the Frederick Gardner Cottrell grant from the Research Corporation, for which we are highly indebted. We are further indebted to Mr. M. H. Jones for assistance in the tests, and to Dr. H. P. Croft, Dr. W. M. Baldwin, Jr., and the Chase Brass and Copper Company for supplying the specially processed copper sheet.

BIBLIOGRAPHY

1 "Reports on the Plastic Flow of Aluminum Aircraft Sheet Under Combined Loads," by M. Gensamer, et al, War Metallurgy Division (NDRC) Reports, Serial Nos. M86, M141, M191, M270, M468, M527, M528, M529, M530.

2 "War Metallurgy Committee Reports," by G. Sachs, et al, Serial Nos. W-105 (1944) and W-125 (1945); and Office of Production Research and Development (WPB) Reports Nos. W-167, W-169, W-195, and W-199 (1945).

3 "Circular Bulging of Aluminum-Alloy Sheet at Room and Elevated Temperatures," by G. Sachs, G. Espey, and G. B. Kasik, Trans. ASME, vol. 68, 1946, pp. 161–173.

4 "Failure of Ductile Metals in Tension," by G. Sachs and J. D. Lubahn, Trans. ASME, vol. 68, 1946, pp. 271–276.

5 "The Necking of Tensile-Test Specimens," by J. D. Lubahn, Trans. A.S.M.E., vol. 68, 1946, pp. 277–279.

6 "Tensile Tests Under Plane Strain," by G. Baranski, *Zeitschrift Metallkunde*, vol. 26, 1934, pp. 173–180.

7 "Instability of Thin-Walled Tubes Subjected to Internal Pressure," by G. Espey, Trans. ASME, vol. 68, 1946, pp. 281–285.

8 "Relative Triaxial Deformation Rates," by W. M. Baldwin, T. S. Howald, and A. W. Ross, Trans. American Institute of Mining and Metallurgical Engineers, Institute Metals Division, vol. 166, 1946, pp. 86–109.

9 "Strain Analysis by Photogrid Method," by W. F. Brown, Jr., and M. H. Jones, *Iron Age*, vol. 158, Sept. 12, 1946, pp. 50–55.

10 "Comparison of Tensile, Compression, Torsion, and Rolling Tests," by P. Ludwik and R. Scheu, *Stahl und Eisen*, vol. 45, 1925, pp. 373–381.

11 "The Strain Hardening of Metallic Materials in Tensile and Compression Tests," by F. Koerber and H. Mueller, Mitteilungen Kaiser-Wilhelm Institut Eisenforschung, Düsseldorf, vol. 8, 1926, pp. 181–199.

12 "Resistance of Copper and Copper Alloys to Homogeneous Deformation in Compression," by M. Cook and E. C. Larke, *Journal of the Institute of Metals*, London, England, vol. 71, 1945, pp. 371–390.

13 "Increase of Stress with Permanent Strain and Stress-Strain Relations in the Plastic State for Copper Under Combined Stresses," by E. A. Davis, Trans. ASME, vol. 65, 1943, pp. 187–188.

14 "Investigations on Deep Drawing," by G. Sachs, *Spanlose Formung*, Julius Springer Verlag, Berlin, Germany, 1931, pp. 11–38.

15 "Stress Analysis of Tube Sinking," by G. Sachs and W. M. Baldwin, Jr., Trans. ASME, vol. 68, 1946, pp. 655–662.

16 "Plastic Strain and Deflection Tests on Clamped Circular Steel Plates 20 Inches in Diameter," by A. N. Gleyzal, U. S. Navy Department, TMB Report R-142, May, 1944.

17 "Progress Report on Underwater Explosion Research," by A. N. Gleyzal, Bureau of Ships Symbol E139, Part 14, U. S. Navy Department, TMB Report R-248, May, 1944.

18 "Progress Report on Underwater Explosion Research," by M. A. Greenfield, Bureau of Ships Symbol E139, Part 10, U. S. Navy Department, TMB Report R-248, May, 1944.

19 "Plastic Deformation of Thin Plates Under Hydrostatic Pressure," by W. Mostow, U. S. Navy Department, Bureau of Ships, Report No. 1946-1 (NAVSHIPS-250-424-1), 1946.

Discussion

W. P. Roop.[11] The main features of this paper are mentioned in the authors' summary in the order of increasing importance. In reverse order, beginning with the most significant, they are as follows:

The circular membrane (1) permits following the stress-strain curve to high strains without serious necking or localization; (2) offers the simplest experimental method for straining metal in sheet form under uniform equal biaxial load; (3) simulates a rather numerous class of service structures.

In order to make use of bulge data for obtaining stress-strain curves, however, a more explicit theory of the plastically bulged diaphragm is needed. This has been given by the writer.[12]

It might appear from the authors' Equation [4] that pressure is a function of three independent variables; stress, radius, and thickness. This, however, is not the case, since all three of these stand in rather simple relations to the meridional strain, as shown in the paper mentioned.[12] The pressure is thus a function of strain only; or it might be written as a function of any of the three variables, stress, radius, or thickness, singly.

For a reasonable approximation, the writer has fitted linear curves of the form $S = S_0 + k\epsilon$ to the data given in the authors' Fig. 15, as follows:

For hard copper: $S_1 = 51 + 28\,\epsilon$

[11] Swarthmore College, Swarthmore, Pa.

[12] "Stress and Strain in Plastic Flow," by W. P. Roop, *Welding Journal*, vol. 25, 1946, pp. 799–823.

For annealed copper: $S_1 = 30 + 76\epsilon$

Pressure has been calculated as in Reference 12, in terms of meridional strain.

The data cited in the authors' Figs. 9 and 10, generally confirm the result, but the deviation of calculated from observed pressures is somewhat greater than that between the two curves in Fig. 9.

It should be rather simple to reverse the process and derive a stress-strain curve directly from the observed pressure-strain curve, but the writer has not had opportunity to do this.

The theory cited assumes meridional profiles of circular form. The authors' Fig. 8 demonstrates that this condition is met with precision, although Fig. 5 shows that some departure from it occurs near the rim in the later stages of the test.

Some comment will now be made on the matter of instability. This is understood simply to refer to the maximum on the pressure-strain curve. If the experimental arrangements were such that pressure was automatically maintained regardless of deformation, as in the case of dead-weight load on a tensile specimen, failure would be catastrophic at this point.

The maximum is to be located by the usual process of equating to zero the derivative of the pressure as a function of strain.

The "instability strain" calculated in this way from the stress-strain data of Fig. 15, is found to be 0.23 for soft copper and 0.19 for hard. At these strain values the calculated pressure is 654 psi for soft copper and 843 psi for hard copper.

Authors' Closure

As the authors understand the argument, Captain Roop proposes a strain distribution which is dependent on purely geometrical quantities, namely, the dimensions of the bulge at some particular phase of the deformation, and is independent of the material.

Such an assumption permits the expression of the radius in terms of strain alone and yields the same radius strain function for any material. The relation between radius and strain, according to Captain Roop[12] is as follows

$$\epsilon_1 = a^2/4R^2$$

where a is the radius of the circular die and ϵ_1 is the natural meridional strain at the pole. Using this function it should be possible (1) to calculate the stress-strain curve directly from the pressure strain curve and (2) to determine the instability strain directly from the stress-strain curve in bulging. We have calculated the stress-strain curves accordingly from the pressure-strain data shown in Figs. 9 and 10 of this paper. The resulting curves shown in Fig. 20 of this closure are compared with those obtained experimentally. It is seen that the calculated stresses are considerably too low (approximately 20 to 25 per cent) for the hard copper, while those for the annealed copper agree more closely, particularly at low strain values. These errors in stress are explained by the fact that at a given strain the calculated radius values are too small, the difference being greatest for the hard copper.

An attempt also has been made to obtain the instability strain from the stress-strain curve in bulging and the relation between the radius and strain proposed by Captain Roop. This was done graphically by the manner outlined in the paper, and the results are shown in Fig. 21 of this closure, for the coppers and also for the aluminum alloy 75SO. This solution yields for hard copper $\epsilon_3 = -0.55$, which is close to the true value. However, for annealed copper, ϵ_3 at instability is —0.68, approximately 15 per cent too high. According to Fig. 21, 75SO would not be sufficiently ductile to exhibit instability. This is contrary to the experimental evidence,[13] which shows 75SO to become unstable at $\epsilon_3 = -0.47$, before fracture.

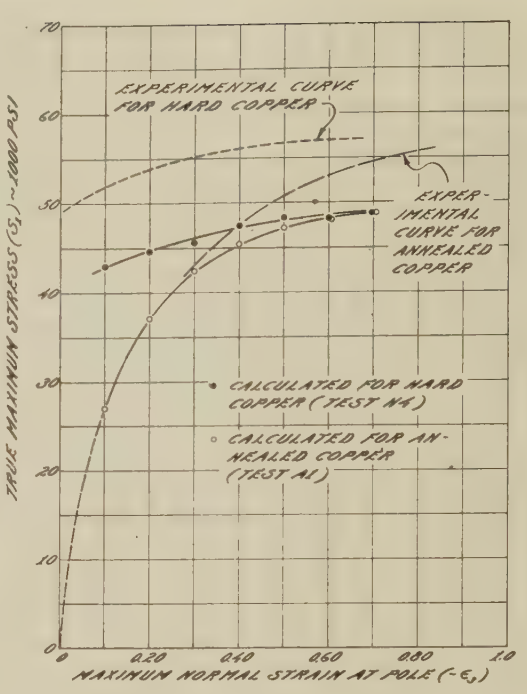

Fig. 20 Stress-Strain Curves Calculated From Pressure-Strain Data Using Roop's Relation Between Radius and Strain, Compared With Those Obtained Using the Experimentally Determined Radius-Strain Relation

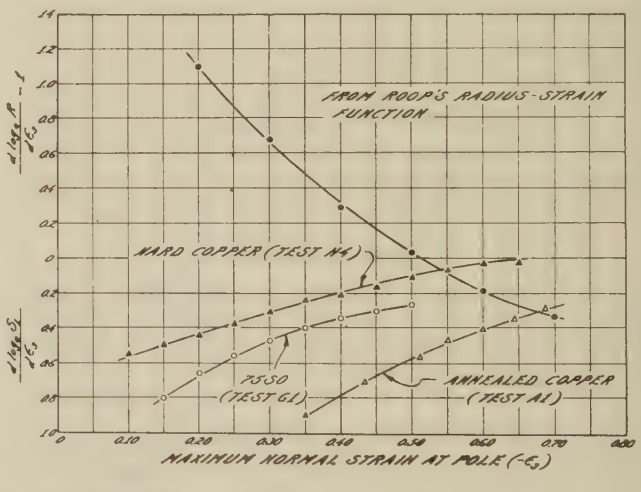

Fig. 21 Graphical Solution of Instability Equation for Several Materials Using Roop's Relation Between Radius and Strain

If, in addition to the assumed relation between radius and strain, the following two assumptions are also made: (1) by plotting suitable functions of the stress and strain, balanced biaxial tension and uniaxial tension may be represented by the same stress-strain curve, and (2) the stress-strain function may be satisfactorily approximated by a parabola of the form

$$S = K_1\epsilon_3^n$$

[13] "Deformation and Failure Characteristics of Circular Membranes," by W. F. Brown, Jr., and F. C. Thompson, ASME, 1948, (in preparation).

then it should be possible to calculate the pressure-strain curve in bulging from the stress-strain curve in uniaxial tension.

As yet, this has not been tried. However, the calculated pressures will certainly be in error, depending on the error in the radius values, as was stated previously. How much the error will be increased by assuming the stress-strain relation to be a parabola will depend on the material.

It may be concluded that any theory of the plastic deformation of a membrane, such as that proposed by Captain Roop and also by Lankford and Saibel,[14] must consider the effect of the strain-hardening on the strain distribution. An experimental investigation of this effect will be presented in a paper which has been submitted to the ASME for publication. Whether or not the parabola can be used successfully to approximate the stress-strain curve in such problems in plasticity is the subject of a paper now being prepared. Whether or not the known universal stress-strain relations yield the same functions between stress and strain for isotropic materials in uniaxial tension, compression, and balanced biaxial tension, the one author intends to investigate at the Cleveland aboratory of the NACA.

---

[14] "Some Problems in Unstable Plastic Flow Under Biaxial Tension," by W. T. Lankford and E. Saibel, AIME, Metals Technology, TP no. 2238, August, 1947.

The Statistics of Boiler Embrittlement

By C. D. WEIR,[1] GLASGOW, SCOTLAND

This paper describes the application of the methods of mathematical statistics to field data on boiler embrittlement, based upon the results of experiments carried out with Schroeder detector units.

Introduction

SINCE the introduction of the detector unit devised by Dr. Schroeder,[2] it has become possible to conduct field tests on boiler embrittlement on an extensive scale. In common with most other corrosion tests of this nature, the data obtained are subject to a considerable amount of experimental scatter, rendering it virtually impossible to grasp their full significance by mere inspection. Dot diagrams, or other methods of systematic tabulation, provide a useful summary of the results in that they bring any tendency toward regularity clearly to the eye. In the two extreme cases, when a definite functional relationship is obeyed by the data and when complete randomness prevails, it is possible to assess the results with some confidence. Many sets of data lie between these two extremes, however, and if they are assessed on the basis of the systematic tabulation alone, their assignment to one or other of the two classes becomes largely a matter of personal bias. Clearly this is an unsatisfactory procedure, and if erroneous conclusions are to be avoided some criterion of significance must be established. This is the task of mathematical statistics.

Within fairly recent years, analytical procedures have been developed which permit the drawing of reliable conclusions from comparatively restricted sets of data. This "technique of small samples" is of particular importance in assessing the results of experiments of the type under consideration. An example of the application of such methods to embrittlement data will be found in a recent paper by the author.[3] In this case, a regression line was fitted to the data and its coefficients tested for significance by "Student's" t-test. Such a procedure is not, however, generally applicable, and the more extensive treatment of the present paper requires a more versatile method.

The paper presents a fairly complete analysis of the data considered; but its main object is to bring to the notice of investigators in this field the statistical methods at their disposal, and to emphasize the dangers of drawing inferences from data whose significance has either been tested by unsuitable methods or not at all.

Contingency Tables

Perhaps the most general method of analysis supplied by mathematical statistics is that embodied in the construction of a contingency table. A contingency table may be constructed in almost every case where it is desired to test for agreement between the frequency distribution of a set of observed data and the distribution of some hypothetical infinite "population" of which the observed set is assumed to be a sample. From such a table a statistic may be computed which is characteristic of the sample as a whole, and which provides a reliable indication of the significance of the sample with regard to the assumed hypothetical distribution. The derivation of such a statistic is outlined in the next paragraph.

Let a sample S of N members be drawn from a population I. If it is now found possible to classify the members of S in two ways, either according to a characteristic A, or according to another characteristic B, we may construct a contingency table whose columns represent the values[4] assumed by A, and whose rows represent the values[4] assumed by B. If A can assume the m values, $A_1, A_2, \ldots A_m$ and B can assume the n values $B_1, B_2 \ldots . B_n$, then we shall have an $m \times n$ contingency table among whose cells the members of S are distributed as shown in the following:

	A_1	A_2	.	.	.	.	A_m
B_1	m_{11}	m_{12}	.	.	.	.	m_{1m}
B_2	m_{21}	m_{22}	.	.	.	.	m_{2m}
.	.	.	.	.	.	.	.
.	.	.	.	.	.	.	.
.	.	.	.	.	.	.	.
B_n	m_{n1}	m_{n2}	.	.	.	.	m_{nm}

If we suppose that in the population, I, from which S is drawn no linkage exists between A and B, then the cell frequencies should be proportional to the corresponding marginal totals, that is, the expected frequency in the kth column and lth now will be

$$\mu_{lk} = \frac{\sum_{i=1}^{n} m_{ik} \cdot \sum_{j=1}^{m} m_{lj}}{N},$$

where of course

$$N = \sum_i \sum_j m_{ij}$$

The deviations of the m_{ij} from the corresponding μ_{ij} are then given by

$$x_{ij} = m_{ij} - \mu_{ij}$$

We require, however, a statistic which will provide a measure of the significance of the derivations of the sample as a whole.

Such a statistic is given by the relationship

$$\chi^2 = \sum_i \sum_j \frac{x_{ij}^2}{\mu_{ij}}$$

The sampling distribution of χ^2 was found by Pearson to be

$$dF = \frac{2^{\frac{1}{2}(2-\nu)}}{\Gamma\left(\frac{\nu}{2}\right)} \cdot e^{-\frac{1}{2}\chi^2} \cdot \chi^{\nu-1}\, d\chi,$$

where ν is the number of degrees of freedom of the table, that is, the number of cells which can be filled arbitrarily without altering the marginal totals. From this distribution may be computed the probability, $P(\chi^2)$, that the value χ^2 found in any particular case may be ascribed to sampling variance. A table of values of χ^2 has been constructed by Fisher[5] for $P = 0.01$ to $P = 0.99$ and $\nu = 1$ to $\nu = 30$. The selection of the value of $P(\chi^2)$ above which the deviations cannot be regarded as significant is to some extent a matter of choice. In biological and actuarial work,

---

[1] Engineering Department, The University of Glasgow.

[2] "Embrittlement Detector," by W. C. Schroeder, A. A. Berk, and R. A. O'Brien, *Combustion*, vol. 12, August, 1940, pp. 19–21.

[3] "Intercrystalline Cracking," by C. D. Weir, *Mechanical Engineering*, vol. 67, 1945, pp. 834–835.

[4] It is to be noted that these "values" need not be of a numerical character.

[5] "Statistical Methods for Research Workers," by R. A. Fisher, Oliver & Boyd, London, England, 1944.

a value of $P = 0.05$ is conventionally regarded as the limit of significance, but for the practical purposes of boiler control the somewhat more stringent value of 0.02 is probably to be preferred. The particular value chosen is not, however, of any great moment, provided it is within reasonable limits.

The conditions which the data must fulfill in order that the χ^2-test may be applicable are not at all onerous. The assumption of continuity in deriving the sampling distribution of χ renders the method somewhat inexact when the cell frequencies are low, however, and it is advisable to arrange the data in such a way that the cell frequencies always exceed 5. Otherwise the nature and sequence of the groups are quite immaterial.

Origin and Tabulation of the Data

Before applying the statistical method outlined in the preceding section to a particular sample, it is convenient to insert here a brief description of the tests in which the sample originated, and of the tabulation of its data.

In a paper published in 1942, Partridge, Kaufman, and Hall[6] described a series of tests conducted by Hall Laboratories on a large number of boilers distributed widely throughout the United States and other countries. Schroeder detectors were fitted to the boilers and kept under careful observation, being adjusted whenever necessary, and the number of days required to produce cracking of the specimens noted. If failure did not occur within a certain period (usually 30 days) the test was discontinued. The result of each test, together with the analyses of the feedwaters and some supplementary data (rolling treatment, type of feedwater pretreatment, and so on) were recorded in an extensive series of tables. These were made available to the author through the courtesy of Hall Laboratories, and constitute the sample of the present paper.

Since the tables are arranged according to an arbitrary system of serial numbers, some rearrangement is necessary before statistical tests can be conveniently applied. The data are first divided into groups according to the values assumed by the characteristic whose influence it is desired to assess, care being taken to insure that a sufficient number of members are included in each group to assure the validity of the χ^2-test.

The number of cracked and the number of uncracked specimens in each group are then counted and their frequencies entered in the appropriate cells of the table.

In cases such as the present where a large number of counts have to be made, it is advantageous to record the result of each test on a separate card. This procedure enables the counts to be made much more quickly, since it is only necessary to arrange the cards according to the values of the characteristic under consideration, and then divide them into suitable groups. Moreover, on account of the ease with which the card grouping may be checked the method is much less liable to error than counting from a table. In many cases it should be possible to record the data directly onto the cards, thus avoiding the labor involved in transferring them from a list or table.

Application of the χ^2-test to the Data

Influence of Constituents of Feedwater. Almost every common constituent of boiler feedwater has been regarded at one time or another as having some influence on the incidence of embrittlement. Very often precisely opposite effects were attributed to the same component by different investigators. Recent research has done much to clarify the position, but the remnants of controversy have not altogether disappeared. In the author's submission, many cases of disagreement are due to personal bias in assessing data whose significance, were they submitted to a sufficiently critical statistical examination, could be determined with complete certainty.

Table 1 summarizes the results obtained by applying the χ^2-test to various constituents of the feed. Variations in the concentrations of hydroxide, chloride, oxide (R_2O_3), silica, and phosphates exert no influence on the relative frequency of cracking, for the analysis shows that the value of P exceeds the stipulated limit of 0.02 by a comfortable margin in each case. Therefore we may reject such variations as being of no significance with complete confidence. Whether the "absence" of any of these substances would alter materially the relative frequency of cracking is a question to which the data cannot supply an answer,[7] since each is present to some extent in every member of the sample. The matter is properly the subject of an extensive and carefully controlled laboratory investigation.

TABLE 1 RESULTS OF APPLYING χ^2-TESTS TO CONSTITUENTS OF FEEDWATER

Constituent	χ^2	ν	P
OH	0.114	3	0.90
SO_4	6.925	3	0.02–0.05
Cl	0.507	3	0.90–0.95
R_2O_3	4.325	2	0.10–0.20
SiO_2	4.058	3	0.20–0.30
PO_4	1.167	3	0.98–0.99
Tannin	11.021	1	< 0.01

Referring again to Table 1, it will be observed that the foregoing remarks do not apply to the constituents sulphate and tannin. With regard to sulphate, the value of P lies sufficiently close to 0.02 to merit a more detailed examination of the characteristics of the distribution, while the value of P, corresponding to tannin, places the significance of this constituent beyond all doubt.

The distribution of the data with regard to sulphate is shown in Table 2. At low concentrations some protective action is

TABLE 2 DISTRIBUTION OF DATA WITH REGARD TO SULPHATE

SO_4 ppm	Uncracked	Cracked	Totals
0	37 (32.52)	12 (16.48)	49
200	43 (48.45)	30 (24.55)	73
400	26 (29.87)	19 (15.13)	45
600	44 (39.16)	15 (19.84)	59
Totals	150	76	226

$\chi^2 = 6.925$

$\nu = 3$

$0.02 < P < 0.05.$

apparent, while, at intermediate values (200–600 ppm), there appears to be a stimulation of cracking; inhibition again becomes apparent at values exceeding 600 ppm. However, the deviations are sufficiently slight to engender some doubt of their reality; a doubt which finds quantitative expression in the value of P.

In the past, considerable importance has been attached to the maintenance of a high sulphate-hydroxide ratio. Lately, however, it has been suggested that this will be effective only in preventing failure when combined with a high chloride-hydroxide ratio. The support offered by the data to these two statements is examined in Tables 3 and 4. In neither case does the observed distribution differ significantly from the expected, so that no benefit can be derived from the fulfillment of either of these conditions. Indeed, in so far as Table 4 is concerned, the significance of the deviations has probably been overestimated, for the expected value in the right bottom cell is rather low; a situa-

[6] "Field Data From the Embrittlement Detector," by E. P. Partridge, C. E. Kaufman, and R. E. Hall, Trans. ASME, vol. 64, 1942, pp. 417–425.

[7] These remarks do not apply to phosphate, for in numerous members of the sample the concentration of this substance is zero.

TABLE 3 DISTRIBUTION OF DATA WITH REGARD TO SULPHATE-HYDROXIDE RATIO

$\frac{Na_2SO_4}{NaOH}$	Uncracked	Cracked	Totals
0	43 (42.76)	23 (23.24)	66
2	40 (39.52)	21 (21.48)	61
4	29 (27.86)	14 (15.14)	43
6	26 (27.86)	17 (15.14)	43
Totals	138	75	213

$\chi^2 = 0.506$
$\nu = 3$
$0.90 < P < 0.95$

TABLE 4 DISTRIBUTION OF DATA WHEN HIGH CHLORIDE-HYDROXIDE RATIO IS COMBINED WITH HIGH SULPHATE-HYDROXIDE RATIO

		$Na_2SO_4/NaOH$ = 0		$Na_2SO_4/NaOH$ = 4		
		Cracked	Uncracked	Cracked	Uncracked	Totals
$\frac{NaCl}{NaOH}$	0	73 (72.03)	39 (38.65)	54 (57.09)	29 (27.23)	195
	2	9 (9.97)	5 (5.35)	11 (7.91)	2 (3.77)	27
Totals		82	44	65	31	222

$\chi^2 = 2.454$
$\nu = 3$
$0.30 < P < 0.50$

TABLE 5 DATA SHOWING INFLUENCE OF TANNIN

Tannin	Uncracked	Cracked	Totals
Added	69 (57.46)	17 (28.54)	86
Not added	88 (99.54)	61 (49.46)	149
Totals	157	78	235

$\chi^2 = 11.021$
$\nu = 1$
$P < 0.01$

TABLE 6 CLASSIFICATION OF TESTS ACCORDING TO PRETREATMENT

Treatment	Uncracked	Cracked	Totals
Raw	60 (48.72)	14 (25.28)	74
Lime-soda	32 (42.80)	33 (22.20)	65
Zeolite	30 (30.29)	16 (15.71)	46
Evaporated	11 (11.19)	6 (5.81)	17
Totals	133	69	202

$\chi^2 = 15.633$
$\nu = 3$
$P < 0.01$

tion which tends to give a value of $P(\chi^2)$ which is less than the true one.

The analysis of the influence of tannin is shown in Table 5. In the original tables this constituent is characterized as being "added" or "not added" in many cases; therefore a 2×2 contingency table has been constructed on this basis. The large value of χ^2 (corresponding to a $P < 0.01$) is clearly to be adduced significant. Inspection of the table indicates that it is due to the low observed frequency in the "added-cracked" cell. Therefore tannin must be regarded as a definite inhibitor of embrittlement and is, in fact, the only determined constituent of the feedwaters which can be classified as such.

Further tests, in which the tannin content is determined quantitatively, are necessary before the amount of tannin required to reduce the relative frequency of cracking to zero can be determined with precision.

Influence of Type of Pretreatment. When the tests are classified according to the type of pretreatment employed, as in Table 6, some curious and highly significant deviations become apparent. Tests in which the feedwater is treated by the lime-soda process show a relative frequency of cracking greatly in excess of that expected, while tests in which raw water is employed evince a marked deficit in cracked specimens. The relative frequencies in cases where the feed is zeolite-treated or evaporated do not differ much from their expected values.

It is quite clear that these deviations cannot be ascribed to differences in feedwater composition (in so far as it is analyzed), since such variations have been shown to be without effect. The only exception to this statement is tannin, and it might be thought that some relationship exists between the amount of tannin present in the feed and the type of pretreatment employed. That this is not the case, however, is clearly shown by the analysis of Table 7. The cause of the deviations therefore

TABLE 7 SHOWING LACK OF RELATIONSHIP BETWEEN TANNIN IN FEEDWATER AND PRETREATMENT

Tannin	Raw	Lime-soda	Totals
Added	29 (30.06)	32 (32.94)	61
Not added	39 (37.94)	38 (39.06)	77
Totals	68	70	138

$\chi^2 = 0.312$
$\nu = 1$
$0.70 < P < 0.80$

remains obscure. Possibly complete analyses of the feedwaters of each group, in which particular attention was paid to organic components, would have revealed significant variations to which these results could be attributed.

Influence of Rolling Treatment. Table 8 illustrates the distribution assumed by the data when classified according to whether the specimens are hot- or cold-rolled. The value of χ^2 can scarcely be adduced significant; but if it is accepted as being so, it represents an extremely slight preponderance of cracking in hot-rolled specimens. The effect is obviously of a secondary nature, due possibly to the different surface conditions produced by the two treatments.

TABLE 8 CLASSIFICATION OF DATA ACCORDING TO ROLLING TREATMENT

	Uncracked	Cracked	Totals
Cold-rolled	146 (141.70)	67 (71.30)	213
Hot-rolled	13 (17.30)	13 (8.70)	26
Totals	159	80	239

$\chi^2 = 3.584$
$\nu = 1$
$0.05 < P < 0.10$

Summary

In the foregoing the methods of mathematical statistics have been applied to the results of experiments carried out with Schroeder detector units.

It has been shown that differences in composition of the feedwaters with regard to hydroxide, chloride, silica, oxide, and phosphate do not influence materially the susceptibility of the specimens to cracking.

Sulphate has been found to stimulate cracking somewhat when present at concentrations in the region 200–600 ppm. At concentrations outside this range it offers a certain amount of protection. However, the variations, though significant, are slight and no undue importance should be attached to them.

The data offer no evidence which might be adduced as sustaining the supposedly beneficial effect of a high $Na_2SO_4/NaOH$ ratio. Nor do they support the view that the association of a high value of this ratio with a high value of the NaCl/NaOH ratio will reduce the incidence of cracking to a significant extent.

Specimens subjected to the action of water containing appreciable amounts of tannin are shown to be remarkably immune from attack.

Tests in which feedwaters pretreated by the lime-soda process were employed show a remarkable preponderance of cracking, while tests employing raw waters exhibit an equally marked immunity. Zeolite-treated and evaporated feeds are not found to influence the frequency of cracking to a significant extent.

The influence of differences in rolling treatment is of a secondary nature. Hot-rolled specimens are found to be slightly more susceptible to cracking than cold-rolled.

Acknowledgment

The author wishes to express his gratitude to Prof. James Small of the Chair of the Theory and Practice of Heat Engines in the University of Glasgow for much useful advice and kindly encouragement, and to Mr. C. E. Kaufman of Hall Laboratories, Inc., Pittsburgh, Pa., who so kindly supplied the data for the analysis. He also wishes to record his indebtedness to the University Authorities for facilities afforded in carrying out the work.

Oil Flow and Temperature Relations in Lightly Loaded Journal Bearings

By JOHN BOYD[1] and B. P. ROBERTSON[2]

The trend toward higher speeds for certain types of apparatus and the decrease in weight of the moving parts which usually accompanies such a change has resulted in the application of an increasingly large number of bearings which operate at relatively high speeds and comparatively light loads. Many of these applications use sleeve-type bearings which are supplied with force-feed lubrication. In order to obtain data which may be used in designing bearings for such use, the oil flows and running temperatures of two common types of sleeve bearings have been investigated and the results compared with theoretical predictions.

Nomenclature

The following nomenclature is used in the paper:

C = diametral clearance
D = bearing diameter
H_f = heat loss due to viscous friction
H_h = heat carried away by shaft and housing
H_0 = heat carried away by oil
K = coefficient of heat loss from bearing
m = radiation exponent
l = axial length of bearing land (circumferentially grooved bearing) or one half over-all length (single-oil-hole bearing)
N = journal speed
Δp = inlet oil pressure minus ambient pressure
Q = total oil flow per bearing
R = ratio, flow with eccentricity/flow without eccentricity
ΔT = bearing temperature minus ambient temperature
$\overline{\Delta T}$ = temperature rise of oil
β = ratio, flow type B bearing/flow type A bearing
c = specific heat of oil
η = eccentricity ratio, journal eccentricity/radial clearance
μ = absolute viscosity
γ = density of oil

Subscripts A and B denote bearing types, Fig. 2.

Introduction

The trend toward higher speeds in certain types of apparatus and the decrease in weight of the moving parts which usually accompanies such a change has resulted in the application of an increasingly large number of relatively high-speed and comparatively lightly loaded bearings. In many cases, pressure-lubricated journal bearings are employed.

Since shaft-rigidity requirements and practical considerations frequently dictate bearing size, the design of bearings for such applications is principally concerned with determining oil flow and running temperature rather than choosing proportions which will give maximum load-carrying capacity.

A fortunate consequence of light loading and high speed is that they permit the journal to run with negligible eccentricity.[3] Thus for many practical purposes, the journal and the bearing may be considered as operating concentrically, a condition which greatly simplifies flow and loss calculations.

An important factor in determining the oil flow through a bearing is the type and distribution of the oil holes and oil grooves. The number of possible groove arrangements is of course infinite and much has been written on some of the various types. Several papers, which are of interest in the present case, are given in references (1–7),[4] inclusive.

The references mentioned include theoretical treatments and experimental results. Although the former should be applicable to the case at hand, the published data are restricted to relatively low speeds so that no satisfactory check of their validity may be made.

In order to obtain data for designing bearings for such service, tests were carried out on the following two common types of journal bearings (see Fig. 2):

Type A—360-deg plain bearing with circumferential groove at mid-length.

Type B—360-deg plain bearing with a single oil-supply hole on top at mid-length.

The results of the tests have been compared with the theoretical values obtained by Muskat and Morgan (3), for bearings of the foregoing types. The comparison indicates the extent to which the assumption of concentricity is applicable.

Test Apparatus and Procedure

The test apparatus is shown in Fig. 1. It consisted of a test shaft mounted in two accurately aligned bearings and driven through a light flexible shaft by a variable-frequency drive. The test shaft weighed 20 lb and constituted the only load on the bearings. The flexible shaft was $^3/_8$ in. diam × 8 in. long and was rigidly bolted to the test shaft and the drive unit.

The bearings were made from an aluminum alloy and were in the form of inserts (2 in. ID, $2^1/_4$ in. OD and $1^7/_{16}$ in. long), which were pressed into the housings. Bearing diameters and alignment were measured to ±0.00005 in. with pneumatic gaging equipment made especially for the tests. The shaft diameter was measured to comparable accuracy with an optical comparator.

The type A bearing had two lands each 0.593 in. long and a 0.250-in-wide × 0.020-in-deep circumferential groove. The edges of the groove were chamfered approximately 0.003 in. The oil-inlet hole was $^1/_4$ in. diam and opened directly into the groove. The diametral clearance at 85 F was 5.3 mils.

The type B bearing had a $^1/_4$-in-diam oil-inlet hole with ap-

---

[1] Section Engineer, Westinghouse Research Laboratories, East Pittsburgh, Pa.

[2] Technical Service Engineer, Humble Oil & Refinery Company, Houston, Tex. Formerly with Westinghouse Research Laboratories. Jun. ASME.

Contributed by the Research Committee on Lubrication and presented at the Annual Meeting, Atlantic City, N. J., December 1–5, 1947, of The American Society of Mechanical Engineers.

 Paper No. 47—A-62.

[3] For the tests described in this paper, maximum value of $\mu N/p$ = 43,000, where μ is in centipoises (cp), N is in rpm, and p is in psi.

[4] Numbers in parentheses refer to the Bibliography at the end of the paper.

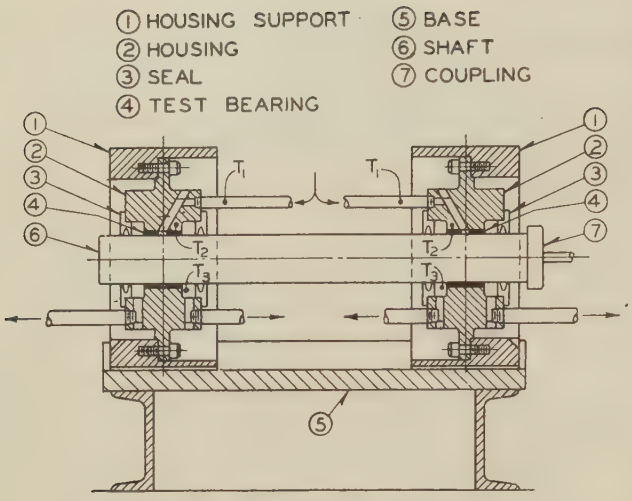

FIG. 1 TEST MACHINE FOR JOURNAL BEARINGS

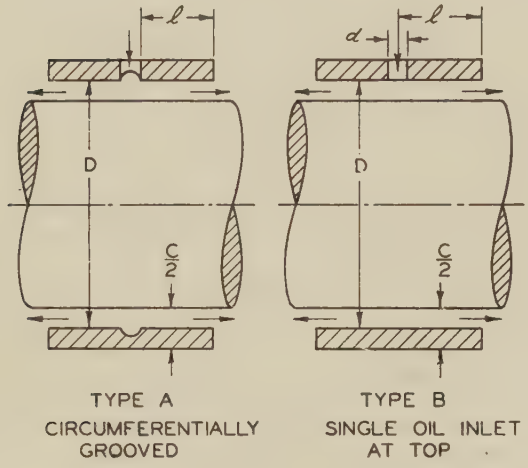

FIG. 2 TEST BEARINGS

proximately 0.003-in. chamfer. The diametral clearance at 85 F was 5.1 mils.

The temperature of the inlet oil, T_1, Fig. 1, was measured by a thermocouple inserted in the inlet oil line, near the bearing housing. The temperature of each bearing, T_2, was measured in two positions, each about 3/4 in. from the end of the bearing and about 1/8 in. from the outer diameter of the bearing insert. Readings for the two positions agreed within 1 deg F throughout the tests.

The oil-outlet temperature, T_3, was measured by a thermocouple arranged to contact the oil as it was thrown off by the bearing.

The oil used in the tests was bought under Army-Navy specification AN06. Its viscosity at 100 F and 210 F was as follows:

	Centipoises	Saybolt seconds
Viscosity at 100 F	14	85
Viscosity at 210 F	3	38

Oil flows were measured by determining the time required to pass a given volume of lubricant.

Tests were run by keeping the speed and oil-inlet temperature constant and varying the oil-inlet pressure. Sufficient time was allowed under each test condition to assure that a steady state had been reached. Speed was varied from 0–18000 rpm and oil-inlet pressure from 10–20 psig. The oil-inlet temperature was kept at 100 F throughout all of the tests.

Flow. In the case of the circumferentially grooved bearing (type A), Muskat and Morgan,[5] Orloff, and others have shown that the total flow Q_A, through the bearing is given by

$$Q_A = \frac{(2 + 3\eta^2)\,\pi\,\Delta p\,C^3}{96\,\mu\,(l/D)} \quad \ldots\ldots [1]$$

where

η = eccentricity ratio = journal eccentricity/radial clearance
Δp = inlet oil pressure minus ambient pressure
C = diametral clearance
μ = absolute viscosity
l = axial length of bearing land
D = bearing diameter

If η is put equal to zero and if more convenient units are substituted, the equation of flow for the concentric condition becomes

$$Q_A = 1.175 \times 10^{-4}\,\frac{\Delta p\,D\,C^3}{\mu l} \quad \ldots\ldots [2]$$

where

Q_A = total flow, gpm
Δp = inlet pressure-ambient pressure, psi
D = bearing diameter, in.
C = diametral clearance, mils
μ = absolute viscosity, cp
l = axial length bearing land, in.

The ratio R_A, of the flow with eccentricity ratio η, to the flow with zero eccentricity is found by division to be

$$R_A = 1 + \frac{3}{2}\eta^2 \quad \ldots\ldots [3]$$

A curve of R_A versus η is shown in Fig. 6, from which it will be noted that the flow with maximum eccentricity is 2.5 times the flow for concentric conditions.

For the case of a bearing with a single-inlet oil hole located on the top (type B), rearrangement of the expressions given by Muskat and Morgan[6] shows that the total flow Q_B, for the bearing operating with zero eccentricity is given by

$$Q_B = \frac{\Delta p \pi C^3}{3\mu\left[\frac{l}{D} - 2\log_e\frac{d}{D} - 4\sum_1^\infty \frac{1}{n(1 + e^{2nl/D})}\right]} \quad \ldots [4]$$

where Δp, C, μ, and D represent the same quantities as previously and

l = one half total axial-bearing length
d = diameter of oil inlet hole
n = an integer with values 1, 2, 3, 4 .... ∞
(usually it is not necessary to use n greater than 4)

Reducing to more convenient units

$$Q_B = 1.875 \times 10^{-3}\,\frac{\Delta p C^3}{\mu\left[\frac{l}{D} - 2\log_e\frac{d}{D} - 4\sum_1^\infty \frac{1}{n(1 + e^{2nl/D})}\right]} \quad \ldots\ldots [5]$$

where

Q_B = total flow, gpm
Δp = inlet pressure − ambient pressure, psi

[5] Reference 3(*b*), Equation [28], p. 406.
[6] Reference 3(*a*), Equation [21], p. 51; Equation [37], p. 60.

C = diametral clearance, mils
D = bearing diameter, in.
d = hole diameter, in.
μ = absolute viscosity, cp

Other conditions being equal, the flow through a type B bearing is less than the flow through a type A bearing. The ratio β, of the former over the latter may be found by substituting numerical values in Equations [2] and [5]. For bearings of the test proportions

$$\beta = 0.276$$

In order to find the ratio R_B, for the type B bearing, the approximate expression for the feed pressure must be used.[7] When this

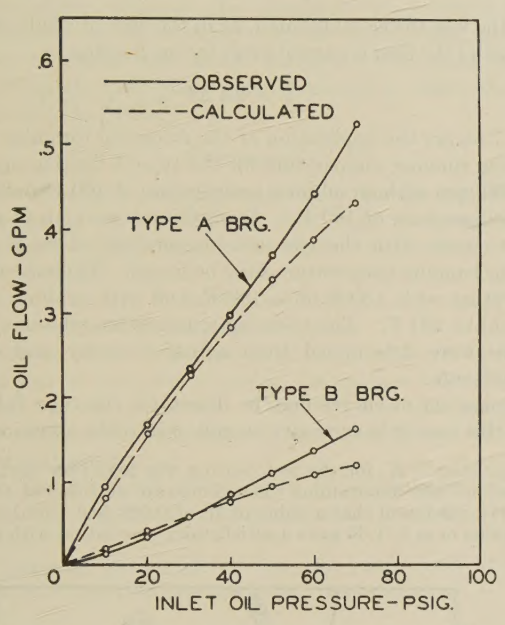

Fig. 3 Effect of Oil Pressure on Oil Flow for Types A and B Bearings Operating at 12,000 RPM

is combined with Equation [21],[8] R_B becomes

$$R_B = \frac{(1+\eta)^3\left(\frac{l}{D} - 2\log_e\frac{d}{D}\right)}{\left[\frac{l}{D} - 2\log_e\frac{d}{D} + 3\eta\left(\frac{l}{D} + 2 - \log_e 16\right)\right]} \quad \ldots [6]$$

Although this equation is approximate, the introduction of numerical values shows that the increase in flow due to eccentricity is more pronounced with the type B bearing than with the type A, Fig. 6. The equation is not intended to be used for values of $\eta > 0.5$.

Fig. 3 shows the effect of oil pressure on oil flow for the two bearings at 12,000 rpm. The agreement between theory and experiment is fairly close when one considers the different factors involved. The relative slope of the two sets of curves shows that the flow for the type B bearing is approximately equal to the theoretical value of 0.276 times the flows for the type A bearing. A superficial glance at the flow equations might lead one to suppose that the calculated curve should be straight if the inlet pressure remains constant. Actually, however, the temperature of the oil film falls as more oil is supplied so that the viscosity rises instead of remaining constant.

[7] Reference 3(a), Equation [36], p. 60.
[8] Ibid., p. 51.

Changes in temperature within the bearing also affect the clearance. It was found from calculation and from measurements that the clearance decreased approximately $^1/_2$ mil as the bearing temperature increased from 85 F to 185 F. The effect is largely due to the expansion of the journal which heats up uniformly whereas the bearing housing, being cool at the surface, does not expand in the same proportion. Because the clearance enters the flow equation as a cube, corrections for clearance were made for all calculations. The average film temperature was taken equal to the outlet temperature.

Fig. 4 shows the effect of speed on the oil flow for the type A

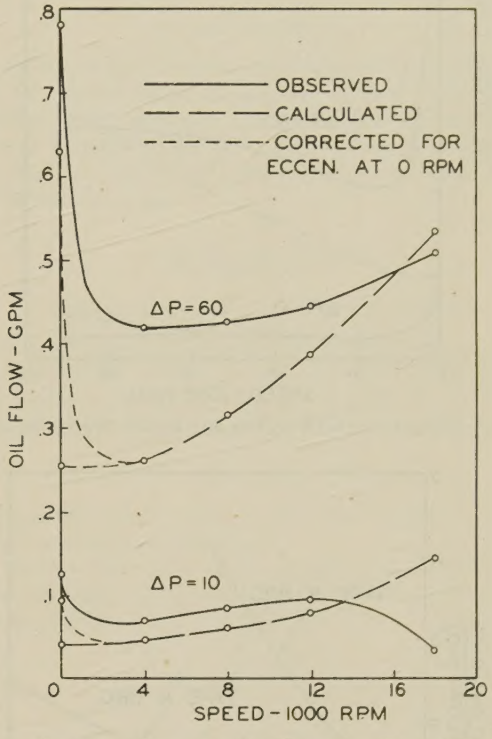

Fig. 4 Effect of Speed on Oil Flow for Type A Bearing

bearing. At 60 psi gage pressure, the agreement at the higher speeds is quite satisfactory. At the lower speed, however, the observed flows are considerably greater than the calculated flows. Most of this difference is probably due to eccentricity with a somewhat smaller portion due to errors in temperature and clearance measurements. Most of the slope of the calculated curve is due to changes in temperature. Correcting the calculated flow at zero rpm by multiplying by the R_A ratio of 2.5, agrees fairly well with the observed results.

Although the proportionate error at 10 psig is somewhat higher than the error at 60 psig, the principal point of interest is the drop in flow above 12,000 rpm. This is believed to be due to the centrifugal pressure built up by oil in the circumferential groove which tends to offset the low supply pressure.

Fig. 5 shows the effect of speed on the oil flow through the type B bearing. In general, the results are similar to those for the type A bearing, except for the smaller flow. Because of the absence of the circumferential groove, however, the flow does not drop off at the lower pressures and higher speeds.

Comparison of observed and calculated flows at 0 rpm indicate the greater effect of eccentricity for the type B bearing.

Running Temperature. The running temperature is most easily determined by graphical means. This is done by solving the heat-balance equations for the viscosity in terms of the tem-

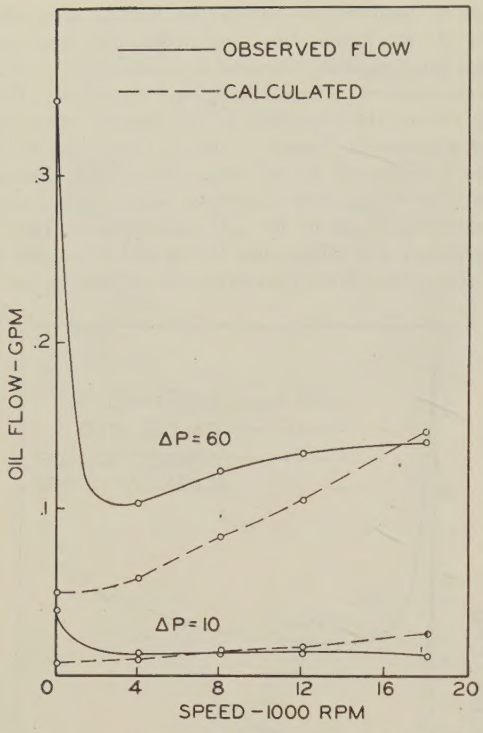

FIG. 5 EFFECT OF SPEED ON OIL FLOW FOR TYPE B BEARING

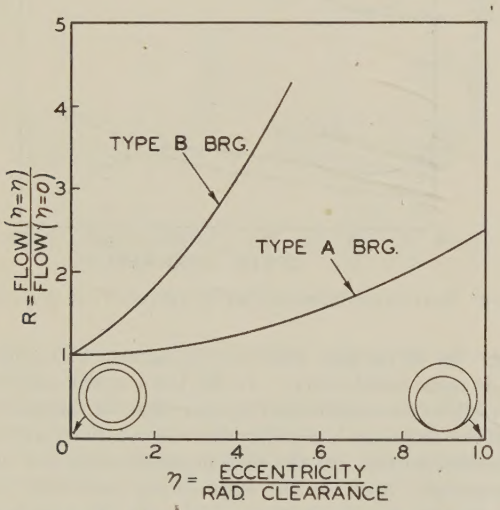

FIG. 6 EFFECT OF ECCENTRICITY ON THEORETICAL OIL FLOW

perature rise, and plotting the resulting relation on viscosity-temperature co-ordinates. The intersection of this curve with the viscosity-temperature relation for the lubricant plotted on the same co-ordinates gives the running temperature, Fig. 7.

From Equation [6a] of the Appendix, the viscosity in terms of the temperature rise is given by

$$\mu = A\,\Delta T^m + \sqrt{(A\,\Delta T^m)^2 + B\overline{\Delta T}} \quad \ldots\ldots [7]$$

where

$$A = 1.55 \times 10^7 \frac{CK}{lN^2D^3}$$

$$B = 3.64 \times 10^4 \frac{\Delta p \gamma c C^4}{l^2N^2D^2}$$

μ = viscosity, cp
C = diametral clearance, in.
D = bearing diameter, in.
l = axial length of bearing land, in.
N = journal speed, rpm
K = radiation coefficient, Btu/min/deg F^m
m = radiation exponent
Δp = inlet oil pressure — ambient pressure, psi
c = specific heat
γ = density, lb per gal
ΔT = temperature rise bearing above ambient, deg F
$\overline{\Delta T}$ = temperature rise of lubricant

For the case when the housing loss is negligible and the oil removes most of the heat

$$\mu = \sqrt{B\overline{\Delta T}} \quad \ldots\ldots [8]$$

When the loss to the oil is small, as in the case of small oil flows, and most of the heat is carried away by the housing,

$$\mu = 2A\,\Delta T^m \quad \ldots\ldots [9]$$

Fig. 7 shows the application of the foregoing formulas for determining running temperature for the type A bearing operating at 18,000 rpm with an oil inlet temperature at 100 F and an ambient temperature of 100 F.[9] From the intersection of the calculated curves with the viscosity-temperature curve of the oil used, the running temperature may be found. Thus the running temperature with ANO6 oil is 180 F, and with medium turbine oil would be 234 F. The viscosity-temperature relations for the two oils were determined from actual viscosity and density measurements.

A similar set of curves may be drawn for the type B bearing but in this case it is necessary to put β into the equation for B

[9] The constant K, for the test bearing was found by shutting off the machine and determining the cooling rate at different temperatures. It was found that a value of K of 0.028 Btu/(min)(deg F^m) and a value of m of 1.35 gave a satisfactory correlation with the test results.

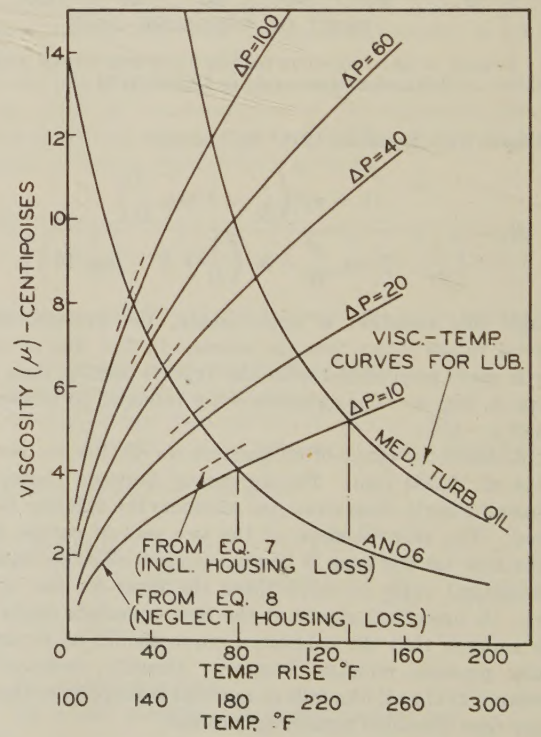

FIG. 7 SOLUTION OF EQUATIONS FOR RUNNING TEMPERATURE (Operating at 18,000 rpm; ambient temperature = 100 F; inlet oil temperature = 100 F.)

in order to take care of the reduced flow through this type bearing, thus

$$B = 3.64 \times 10^4 \frac{\beta \Delta p \gamma c C^4}{l^2 N^2 D^2}$$

Fig. 8 shows the calculated and observed running temperatures for the type A and type B bearings plotted as a function of the inlet oil pressure. As is to be expected, the latter-type bearing operates at a higher temperature because of the lower flow rate.

It will be noted that, in the case of the test-bearing setup, the housing loss was negligible. Thus the simpler equation, Equation [8], may be used in this case without introducing an appreciable difference.

At the higher pressures, the calculated temperatures are on the safe side as may be expected since the eccentricity, and hence the flow, increases with higher pressure. The effect is more noticeable in the case of the type B bearing in which the effect of eccentricity is greater.

Conclusions

1 The flow and running-temperature curves indicate that good agreement between the test results and the predictions of the Muskat-Morgan equations is obtained at the higher speeds where eccentricity is small. It should be kept in mind that the relations for the type B bearing are approximate, except in the case of $\eta = 0$, where the solution is rigorous.

2 Because of the centrifugal effect of the oil in the circumferential groove of the type A bearing, the oil flow falls off at high speed and low inlet pressures. The effect is of sufficient magnitude to warrant its consideration in the design of high-speed bearings of this type.

3 At lower speeds, the observed flows are considerably in excess of the calculated values primarily because of journal eccentricity.

4 Correcting the calculated flows for eccentricity at 0 rpm gives results which compare favorably with experiment.

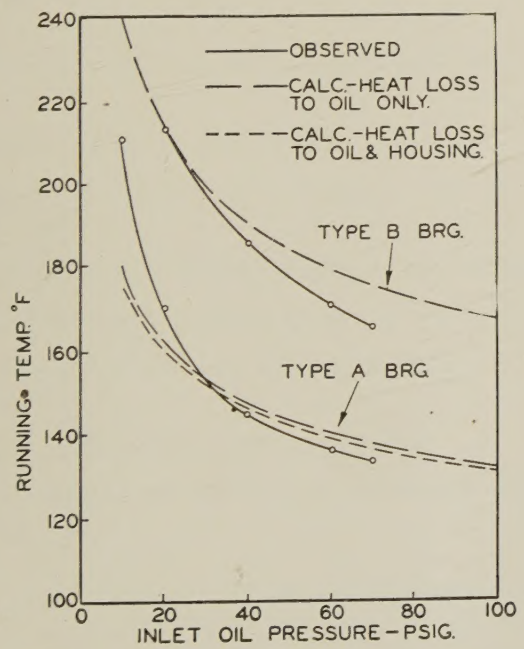

Fig. 8 Effect of Oil Pressure on Running Temperature for Types A and B Bearings
(Operating at 10,000 rpm; inlet oil temperature = 100 F; ambient temperature = 100 F.)

5 Other conditions being equal, the flow through a type B bearing is approximately 0.28 times the flow through the corresponding type A bearing. Because of this fact, the type B bearing will, in general, operate at a higher temperature.

6 For many practical applications, the heat loss through the housing is negligible compared to the heat carried away by the oil. Neglecting the housing loss simplifies the running-temperature calculations.

7 In general, the application of the foregoing analysis to relatively lightly loaded and comparatively high-speed bearings may be considered satisfactory, at least for a first approximation, if the limitations outlined above are kept in mind.

Acknowledgments

The authors wish to express their appreciation to Mr. M. D. Hersey for many helpful suggestions in connection with the preparation of the paper; to Dr. M. Muskat for his comments concerning the application of the formulas to the experimental results; and to Mr. R. E. Peterson for his interest in and sponsorship of the investigation.

Appendix

Equations for Running Temperature

Under equilibrium conditions, the rate of heat generation due to fluid friction within the oil film is equal to the sum of the rates at which it is being carried away by the oil and dissipated by the shaft and housing. This may be expressed by

$$H_f = H_0 + H_h \quad \ldots\ldots\ldots\ldots\ldots\ldots [1a]$$

where H_0 and H_h are the rates at which heat is being taken away by the oil and housing, respectively.

The rate at which heat is developed by fluid friction may readily be calculated from the viscous properties of the lubricant. For the concentric case, it is found to be

$$H_f = \frac{4\pi^3 \mu l N^2 D^3}{CJ} \quad \ldots\ldots\ldots\ldots\ldots\ldots [2a]$$

where μ, l, N, D, and C are as previously defined and J is the mechanical equivalent of heat.

The rate at which heat is carried away by the oil is given by

$$H_0 = Q\overline{\Delta T}\gamma c \quad \ldots\ldots\ldots\ldots\ldots\ldots [3a]$$

where Q is the oil flow, $\overline{\Delta T}$ is the temperature rise of the oil, and c and γ are the specific heat and the density of the oil, respectively.

The rate at which heat is carried away by the housing may be expressed with sufficient accuracy by a relation of the form (8)

$$H_h = K \Delta T^m \quad \ldots\ldots\ldots\ldots\ldots\ldots [4a]$$

where K and m are constants and ΔT is the temperature rise of the bearing above ambient.

Substituting Equations [1], [2a], [3a], and [4a] in Equation [1a] and solving for μ for the case $\eta = 0$ gives

$$\mu = A^1 \Delta T^m + \sqrt{(A^1 \Delta T^m)^2 + B^1 \overline{\Delta T}} \quad \ldots\ldots\ldots [5a]$$

where

$$A^1 = \frac{CKJ}{8\pi^3 N^2 D^3}$$

$$B^1 = \frac{\Delta p \gamma c C^4}{192\pi^2 l^2 N^2 D^2}$$

Expressing Equation [5a] in more convenient units gives

$$\mu = A\,\Delta T^m + \sqrt{(A\,\Delta T^m)^2 + B\overline{\Delta T}} \quad \ldots\ldots\ldots\ldots [6a]$$

where

$$A = 1.55 \times 10^7 \frac{CK}{lN^2D^3}$$

$$B = 3.64 \times 10^4 \frac{\Delta p \gamma c C^4}{l^2 N^2 D^2}$$

μ = viscosity, cp
C = diametral clearance, in.
D = bearing diameter, in.
l = axial length of bearing land, in.
N = journal speed, rpm
K = radiation coefficient, Btu/min/deg F^m
m = radiation exponent
Δp = inlet oil pressure — ambient pressure, psi
c = specific heat
γ = density, lb/per gal
ΔT = temperature rise, bearing above ambient, deg F
$\overline{\Delta T}$ = temperature rise of lubricant, deg F

BIBLIOGRAPHY

1 "Oil Flow in Complete Journal Bearings," by D. P. Barnard, *SAE Journal*, vol. 17, 1925, p. 205.

"Oil Flow in Plain Bearings," by D. P. Barnard, *Industrial and Engineering Chemistry*, vol. 18, 1926, p. 460.

2 "Film-Lubrication Theory and Engine-Bearing Design," by E. S. Dennison, Trans. ASME, vol. 8, 1936, p. 25.

3 (*a*) "The Theory of Thick Film Lubrication of a Complete Journal Bearing, of Finite Length With Arbitrary Positions of the Lubricant Source," by M. Muskat and F. Morgan, *Journal of Applied Physics*, vol. 10, 1939, p. 46.

(*b*) "The Theory of Thick Film Lubrication of Flooded Journal Bearings and Bearings With Circumferential Grooves," by M. Muskat and F. Morgan, *Journal of Applied Physics*, vol. 10, 1939, p. 398.

4 "Coefficient of Friction, Oil Flow and Heat Balance in a Complete Cylindrical Bearing," by M. E. Orloff, *Aeronautical Engineering*, Moscow, January, 1935, p. 25.

5 "Oil Grooves in Plain Bearings," by D. Clayton, *Engineering*, vol. 159, p. 145.

6 "Performance Characteristics of Journal Bearings With Forced Feed Lubrication," by S. A. McKee, H. S. White, and J. F. Swindells, NACA Report ARR 4H15, August, 1944.

7 "Oil Flow Through Engine Bearings," by J. Spiers, *Journal, IAE*, vol. 9, 1941, p. 7.

8 "Theory of Lubrication," by M. D. Hersey, John Wiley & Sons, Inc., New York, N. Y., 1936, p. 101.